

The functional analysis of rare genetic variants in a familial neurodegenerative spectrum disorder

Søren Lejsted Færgeman, MD
Thesis submitted for Doctor of Philosophy in Clinical Neuroscience



Green Templeton College
University of Oxford
Trinity Term 2018

The functional analysis of rare genetic variants in a familial neurodegenerative spectrum disorder

Søren Lejsted Færgeman, MD

Green Templeton College, University of Oxford, Trinity Term 2018

Thesis submitted for Doctor of Philosophy in Clinical Neuroscience

Abstract

Whole genome sequencing can enable an unbiased approach to the diagnosis and to the understanding of genetic aetiology of neurodegenerative diseases, which are a clinically and genetically heterogeneous group of disorders. Two brothers, originally diagnosed with primary progressive multiple sclerosis (PPMS), displayed an atypical disease progression over a 30-year period with a clinical picture of paresis, ataxia, mental impairment and dysarthria. Late stage fasciculations, absence of sensory symptoms and a follow-up magnetic resonance imaging (MRI) scan showing severe atrophy of the cerebrum, cerebellum and brainstem, but no white matter lesions, called the original diagnosis into question. Given the familial nature and the rarity of this very similar clinical profile, we hypothesised that a rare variant could be contributing to disease. Whole genome sequencing identified three rare variants segregating with disease: a homozygous non-frameshift deletion in the fatty acid 2-hydroxylase (*FA2H*) gene, an X-bound non-synonymous single nucleotide variant in the adaptor protein-1 complex subunit sigma-2 (*AP1S2*) gene, and a homozygous frameshift deletion in the mixed lineage kinase domain-like protein (*MLKL*) gene. Lipidomic analysis using liquid chromatography-tandem mass spectrometry of FA2H variant-expressing cell lines demonstrated no detrimental impact of the deletion in *FA2H* on protein function. Bioinformatic and computational

structural analysis suggested the variant in *AP1S2* to be benign. In contrast, the frameshift deletion in *MLKL* prevents expression of MLKL protein as demonstrated in patient-derived primary cells. The absence of MLKL was shown *ex vivo* to cause complete deficiency in necroptosis, a recently identified form of programmed cell death that is involved in a spectrum of neurodegenerative diseases. This thesis provides the first clinical case report implicating MLKL and necroptosis deficiency in a neurodegenerative spectrum disorder. The results suggest that current strategies to pursue MLKL inhibition for human therapy should be approached with caution.

Table of contents

Abstract **2**

Acknowledgements **7**

Publications and presentations during DPhil **10**

Abbreviations **11**

Chapter 1 ..... **15**

1. Introduction **15**
1.1. Thesis outline **19**
1.2 Multiple sclerosis **20**
1.2.1 The clinical course of PPMS 21
1.2.2 Neuroradiological findings in PPMS 23
1.2.3 Diagnosing PPMS 24
1.2.4 MS Therapy 25
1.2.5 Pathology and pathogenesis of MS 26
1.2.6 The genetic component of MS. 29
1.3 Hereditary spastic paraplegia **32**
1.3.1 Pathology 33
1.3.2 Phenotype genotype relationships in HSP 34
1.4 MLKL **35**
1.4.1 MLKL structure 37
1.4.2 What is the function of necroptosis? 39
1.4.3 Non-necroptotic functions of MLKL 40
1.4.4 Necroptosis in disease 42
1.5 FA2H **50**
1.5.1 FA2H structure 53
1.5.2 FA2H in disease 54
1.5.3 Variants spanning FA2H and MLKL 57
1.6 AP1S2 ..... **59**
1.6.1 AP1S2 in disease 62
1.7 Using whole genome sequencing in diagnosis and research **64**
1.7.1 Assessing the impact of genetic variants 65
1.8 Hypothesis **67**

Chapter 2. Methods **70**

2.1 Sanger sequencing of family members **70**
2.2 Cloning **71**
2.2.1 Site-directed mutagenesis 71
2.2.2 MLKL 72
2.2.3 FA2H 73
2.3 Culturing of cell lines **75**

2.4 Transfections **76**
2.5 PI/Annexin staining of MLKL transfected HEK293 cells **76**
2.6 Cell death assayed by Incucyte **76**
2.7 Flow cytometry **77**
2.8 Lentiviral packaging **78**
2.9 Transduction of FA2H constructs **78**
2.10 Liquid chromatography-tandem mass spectrometry (LC-MS/MS) **79**
2.11 Western blotting **79**
2.12 Bioinformatics **82**
2.13 Family donor work **83**
2.13.1 Consent 83
2.13.2 Culturing of fibroblasts 83
2.13.3 Isolation of peripheral blood mononuclear cells 84
2.13.4 PBMC surface staining 85
2.13.5 qPCR of donor PBMCs and fibroblasts 86
2.13.6 Cytokine stimulation and pharmacological investigations 87
2.13.7 Assaying MLKL dependent TNF-recycling in donor fibroblasts 88
2.14. Statistical analyses. **88**
2.15 Other **89**

3. Clinical and genetic characterisation of a family with two brothers originally diagnosed with primary progressive MS **90**

3.1 Introduction **90**
3.2 Chapter aim **90**
3.3 Results **91**
3.3.1 Clinical summary 92
3.3.1.1 Brother B1 92
3.3.1.2 Brother B2 94
3.3.1.3 Common pattern of symptoms in B1 and B2 96
3.3.2 Magnetic resonance imaging in 2013 97
3.3.2.1 MRI of B1 97
3.3.2.2 MRI of B2 101
3.3.3 Whole genome sequencing (WGS) 102
3.3.3.1 Validation of genetic variants by Sanger sequencing in unaffected family members 103
3.3.3.2 Assessing allele frequency of identified variants 104
3.3.3.3 Predicted protein-level effects of identified variants 105
3.4 Discussion **107**
3.4.1 MLKL 108
3.4.2 FA2H 109
3.4.3 AP1S2 110
3.5 Chapter conclusions **111**

Chapter 4. Functional analysis of the disease-associated MLKL 369 variant in cell lines 112

4.1 Introduction 112
4.2 Chapter aim 114
4.3 Results 115
4.3.1 Assaying the effect of MLKL 369 overexpression on cell death using PI/annexin V staining 115
4.3.2 Assaying the effect of MLKL overexpression on cell death using live-cell imaging 119
4.3.3 MLKL 369 variant analysed by western blotting 123
4.3.4 MLKL 369 variant analysed by flow cytometry 125
4.3.4.1 Lower tolerable expression of MLKL 369 127
4.3.4.2 Reduced MLKL expression, reflecting cell death, is partly reversible by NSA 130
4.4 Discussion 131
4.4.1. Phenotypic implications of increased necroptosis 134
4.4.2 Limitations of the data 136
4.4.3 Conclusions and future work 136

Chapter 5. The functional analysis of MLKL 369 in patient primary cells 138

5.1 Introduction 138
5.2 Results 140
5.2.1 PBMCs of B1 and B2 do not express detectable levels of MLKL by western blotting 140
5.2.2 B1 and B2 do not have atypical frequencies of immune subpopulations 141
5.2.3 MLKL is not expressed in cultured fibroblasts of B1 and B2 143
5.2.4 Assessing the effect of the MLKL 369 variant at the mRNA level 144
5.2.5 No MLKL protein expression in patients despite IFNy-mediated mRNA upregulation. 147
5.2.6 Assaying the effect of the *MLKL 369* variant on cell death 152
5.2.7 Exploring effects of *MLKL* (rs561839347) on non-necroptotic functions 161
5.3 Discussion 164
5.4 Conclusions and future studies 166

Chapter 6. The functional analysis of the FA2H F11 deletion and *in silico* analysis of the K55R substitution in *AP1S2* 168

6.1 Introduction 168
6.2 Results FA2H 170
6.2.1 Validation of lentiviral FA2H transduction by flow cytometry and WB 170
6.2.2 FA2H enzyme activity analyses 172
6.2.3 In silico analysis of FA2H F11del variant 178
6.3 *In silico* characterisation of K55R substitution in AP1S2 179
6.4 Discussion 184
6.4.1 Discussion on FA2H lipidomics 184
6.4.2 Discussion on AP1S2 *in silico* analysis 186

Chapter 7. Discussion 188

7.1 Summary of results 188
7.2 Limitations of the study 192
7.3 Interpreting WGS findings 193
7.4 Which cells of the CNS are affected by the identified variants? 197
7.5 Implications of MLKL deficiency 198
7.6 Why would MLKL deficiency affect the CNS and not other organs? 203
7.7 Why do the brothers not have increased susceptibility to infections? 204
7.8 MLKL as a therapeutic target 205
7.9 Future studies summary 207
7.10 General conclusions 207

References 210

Acknowledgements

First and foremost, I want to thank Professor Lars Fugger for giving me the opportunity to do research in neurodegenerative mechanisms at the highest level, and for invaluable discussions and advise throughout my stay in the lab. I want to express my deepest gratitude to Dr. Calliope Dendrou for her daily guidance and support in all aspects of the project. She has taught me most of the methods I use, and my discussions with both Lars and Calliope have taught me most of what I think I know about attempts to answer important scientific questions.

Heartfelt thanks to the members of the family in question. They were generously willing to participate in the study and to provide unique samples for research. Special thanks to Dr. Mette Sommerlund and to Dr. Lise Torp Jensen for their help in the isolation and culturing of primary fibroblasts.

I would like to direct special thanks to Dr. Gurman Kaur for helping me in the process of cloning, to Dr. Kate Attfield and Dr. Hayley Evans for their help with basic laboratory techniques and cell line culturing and to Dr. Christiane Desel for her help and support with western blots. I would also like to thank all members of the Fugger lab, past and present, for their kind advice in the scientific process and for creating a pleasant working environment.

I thank Dr. Annette Oturai for her clinical characterisation of the family in question and many thanks goes to Dr. Paul Matthews, Dr. Wilhelm Kueker and Dr. Bodil Ginnerup Pedersen for their input on the MRI-scans of the family. Professor Britta Brügger at the University of Heidelberg, Germany conducted the lipidomic analysis and I am very grateful for her help and support in the process of data analysis. I

would also like to thank GP Per Gjessing for his help in clarifying the details of the patients' history.

Special thanks to my wife Lea Kirstine Hansen for loving support and supernatural patience, to my daughter Ingrid Kirstine Færgeman for her joyful spirit and to my parents for their relentless support.

I would also like to thank Professor Jørgen Frøkiær, who has supported me from the beginning of my research and enabled my stay at Nuffield Department of Clinical Neurosciences, University of Oxford.

Finally, I would like to thank Aarhus University, Alice and Torben Frimodts Foundation, A.P. Møller Foundation, Augustinus Foundation, Jascha Foundation, Karen Tholstrup Foundation and Louis-Hansen Foundation for the generous financial support.

Publications and presentations during DPhil

Publications:
Resolving TYK2 locus genotype-to-phenotype differences in autoimmunity.
Dendrou, Calliope A; Cortes, Adrian; Shipman, Lydia; Evans, Hayley G; Attfield, Kathrine E; Jostins, Luke; Barber, Thomas; Kaur, Gurman; Kuttikkatte, Subita Balaram; Leach, Oliver A; Desel, Christiane; **Faergeman, Soren L**; Cheeseman, Jane; Neville, Matt J; Sawcer, Stephen; Compston, Alastair; Johnson, Adam R; Everett, Christine; Bell, John I; Karpe, Fredrik; Ultsch, Mark; Eigenbrot, Charles; McVean, Gil; Fugger, Lars.

Science Translational Medicine, Vol. 8, Nr. 363, 02.11.2016, s. 363ra149.

Poster presentations:
The Genetic and Functional Analysis of Multiplex Multiple Sclerosis Families.
Soren L. Faergeman, Calliope A. Dendrou, Adrian Cortes, Jacqueline Palace, M. Isabel Leite, Gabriele C. DeLuca, Ruth Geraldes, Rosie Gore, Joy Hodder, George Tackley, Guðrið Andorsdóttir & Lars Fugger.

The functional analysis of an atypical MS family.
Soren L. Faergeman1, Calliope A. Dendrou, Hayley Evans, Annette Bang Oturai & Lars Fugger.

Lipidomic analysis of rare variant in an atypical MS family.
Soren L. Faergeman, Calliope A. Dendrou, Britta Brügger, Annette Bang Oturai & Lars Fugger.

Oral presentations:
Analysis of clinically atypical brothers originally diagnosed with primary progressive multiple sclerosis.
Presented at the WIMM, 22.2.2018.

Abbreviations

ACMG	American College of Medical Genetics and Genomics
ALS	amyotrophic lateral sclerosis
ANOVA	analysis of variance
AP	adaptor protein
AP1S2	adaptor protein-1 complex subunit sigma-2
bp	base pairs
BSA	bovine serum albumin
CDx	cluster of differentiation (x is a number)
CHO-K1	chinese hamster ovary K1
CNS	central nervous system
CO_2	carbon dioxide
CSF	cerebrospinal fluid
C_t	threshold cycle
dCt	delta threshold cycle
DMEM	Dulbecco´s Modified Eagle´s Medium
DMSO	dimethyl sulfoxide
DNA	deoxyribonucleic acid
EAE	experimental autoimmune encephalomyelitis
EDTA	Ethylenediaminetetraacetic acid
EDSS	Expanded disability status scale
FA2H	fatty acid 2-hydroxylase
FAM	6-carboxyfluorescein
FCS	fetal calf serum

FH	familial hypercholesterolemia
FITC	fluorescein isothiocyanate
FTD	frontotemporal dementia
GAPDH	glyceraldehyde-3-phosphate dehydrogenase
GP	general practitioner
GC	guanine-cytosine content
GFP	green fluorescent protein
GWAS	genome-wide association study
HA	human influenza hemagglutinin
HEK	human embryonic kidney cells
HLA	human leukocyte antigen
HSP	hereditary spastic paraplegia
IFN	interferon-
Ig	immunoglobulin
kDa	kilo-dalton
KO	knockout
LB	lysogeny broth
LC-MS/MS	liquid chromatography-tandem mass spectrometry
LDL	Low-density lipoprotein
MAF	minor allele frequency
MLKL	mixed-lineage kinase domain-like protein
MRI	magnetic resonance imaging
mRNA	messenger ribonucleic
MS	multiple sclerosis

MOI	multiplicity of infection
n	number of independent experiments
NADH	nicotinamide adenine dinucleotide hydrogen
NFκB	nuclear factor kappa B
NK	natural killer
ns	not significant
NSA	necrosulfonamide
OH	hydroxyl group
PBMC	peripheral blood mononuclear cells
PBS	phosphate-buffered saline
PCR	polymerase chain reaction
pKa	acid dissociation constant
PTV	protein truncating variant
PI	propidium iodide
PPMS	primary progressive multiple sclerosis
qPCR	quantitative polymerase chain reaction
RIPK1	receptor-interacting serine/threonine-protein kinase 1
RIPK3	receptor-interacting serine/threonine-protein kinase 3
rpm	rotations per minute
RRMS	relapsing remitting multiple sclerosis
SEM	standard error of the mean
SNV	single nucleotide variant
SLE	systemic lupus erythematosus
TCR	T-cell receptor

TNF	tumour necrosis factor
WM	white matter
WT	wild type
WB	western blotting
WGS	whole genome sequencing

Chapter 1

1. Introduction

Neurodegenerative diseases encompass a spectrum of disorders characterised by a progressive loss of neurons resulting in chronic neurological deficits, such as cognitive, motor and sensory dysfunction. Common diseases such as Alzheimer´s dementia, Parkinson's disease, frontotemporal dementia (FTD), amyotrophic lateral sclerosis (ALS) and multiple sclerosis (MS) are all increasing in worldwide prevalence (1) and none of these diseases are curable.

Familial aggregation of neurodegenerative diseases has been observed for decades, which has provided important clues to the hereditary components of these diseases (2) and has shed light on key pathogenic pathways. Genetic variants in β amyloid precursor in familial Alzheimer´s disease (3), variants in *SNCA* (endocing α-synuclein) in familial forms of Parkinson's disease (4), variants in *TBK1* in FTD (5), and variants in *SOD1* in familial ALS (6) are prime examples of genetic factors thought to underpin the clustering of neurodegenerative diseases in families. The marked clinical heterogeneity of these conditions poses a challenge for clinicians, which is further complicated by the diverse array of genetic loci that promote predisposition to these diseases.

However, the majority of patients with neurodegenerative diseases occur sporadically. Efforts to characterise the hereditary component of neurodegenerative disease among these patients has relied on genome-wide association studies (GWAS) of thousands of cases and controls. Hundreds of common variants

conferring small increases in the risk to Alzheimer´s disease, ALS, Parkinson's disease and MS have been identified, though they only explain a proportion of the heritability of these conditions (7). Rare variants (allele frequency <0.5%) have been suggested to be the genetic basis for the missing heritability (8). These variants are not detectable in standard GWAS, but can be identified by the use of next generation sequencing. Figure 1.1.1 illustrates the rationale for researching complex disease genetics by combining GWAS of common genetic variants of low effect size with genetic studies using sequencing to detect rare variants that may have stronger effect sizes in families/isolated populations (7). Disease risk in each individual is most likely determined by common and rare variants that might also modify one another.

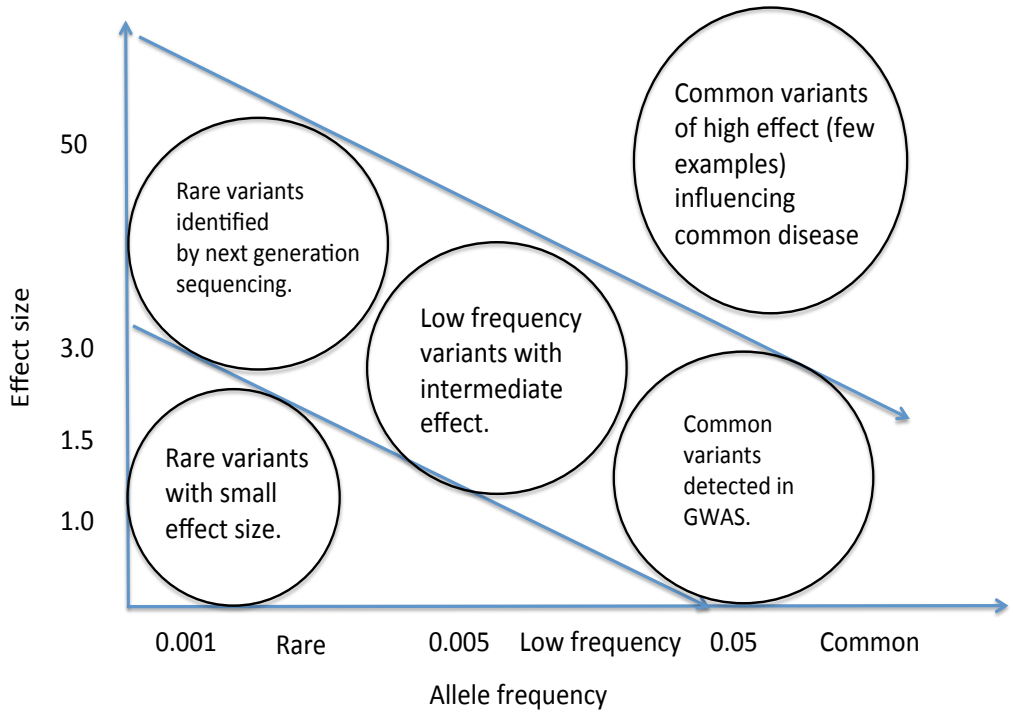


Figure 1.1 Researching the genetics of common diseases. Combining next generation sequencing of families and isolated populations with GWAS studies to analyse the genetic background of MS and complex diseases in general. Current emphasis lies on identifying genetic variants within the diagonal lines with variable effect sizes (odds ratio). Adapted and modified from Manolio *et al*. (7).

How can genetic variation affect the clinical phenotype and what are the clinical implications? One option is that rare variants are associated with complex diseases because they contribute to disease risk to a small or moderate extent. This possibility would be in keeping with the theory of rare variants being responsible for a part of the residual heritability in complex diseases. Indeed, complex diseases such as schizophrenia (9) and epilepsy (10) have been associated with rare structural variants, even in cases where no atypical clinical features have been reported upon diagnosis.

Another possibility is that rare variants cause a clinical phenotype that falls within the diagnostic criteria of complex diseases, but which is actually is a monogenic phenocopy. This option would be in keeping with the multiple case reports of monogenic disorders mimicking common diseases, such as MS (11).

Careful phenotypic characterisation of patients is therefore necessary, particularly in familial cases where the pedigree suggests a strong genetic component to their disease. Patients harbouring rare variants may in some cases reveal slightly atypical clinical features compared to the normal clinical presentation (10, 12), which most likely reflects the strong penetrance of the suspected rare variants. Family-based genetic studies may thus in some instances help to shed light on how genetic mechanisms affect different phenotypic aspects of the disease (for example early onset). Alternatively, genetic analysis of familial cases may reveal variants that affect pathways that are not implicated in the sporadic disease. In some cases these

may be pathways for which common variants have not been implicated, but which indeed contribute to the pathology of the common disease.

Finally, for some genes involved in complex diseases, common genetic variants with small effect sizes and rare genetic variants with stronger effects may occur in the same gene. For example, rare variants in *SNCA* and *LRRK2* (Leucine-rich repeat serine/threonine-protein kinase 2) are known to cause autosomal dominant forms of Parkinson's disease, while common variants in these genes have been associated with sporadic forms of Parkinson's disease (13). Another example is the *LDLR* gene encoding the low-density lipoprotein (LDL) receptor and *PCSK9* encoding proprotein convertase subtilisin–kexin type 9, which are reported in GWAS to harbour genetic variants associated with blood lipoprotein concentrations (14) - a complex trait known to influence the risk of developing atherosclerosis. Rare variants in the same genes are known to cause familial hypercholesterolemia (FH) (15, 16), which causes severely elevated levels of LDL leading to early onset cardiovascular death and death due to atherosclerosis. This observation contributed to the rationale for the development of statins that lower serum levels of LDL, thereby preventing the development of atherosclerosis and statins are today one of the main drugs used to treat cardiovascular disease (17). The story of FH exemplifies how family-based genetic analysis of a relatively extreme phenotype was used to identify a disease-associated pathway with broad therapeutic relevance to common complex diseases such as coronary artery disease and stroke.

1.1. Thesis outline

Motivated by a similar need to identify new therapeutic targets in neurodegenerative diseases, this DPhil project focuses on the role of rare variants identified by whole genome sequencing in a family with two brothers suffering from a severe neurodegenerative disease. The brothers were originally diagnosed with PPMS (18) in 1985 and 1990, but they have in retrospect developed clinically in a manner atypical for PPMS. Radiological and clinical follow-up has questioned the original diagnosis and suggested that hereditary spastic paraplegia (HSP) might be a more appropriate diagnosis. The principles of diagnosis and the pathology of MS and HSP are discussed in this chapter.

The clinical considerations relating to diagnosis necessitated genetic analysis for which WGS was used. These data along with the genetic analysis of the entire family, the pedigree and the clinical information on the brothers are presented in Chapter 3. Briefly, WGS identified two rare autosomal homozygous deletions in *MLKL* (Mixed-lineage kinase domain like protein) and *FA2H* (Fatty acid 2-hydroxylase) on chromosome 16. The genes are adjacent, located only 12 kb apart and the deletions were found to be inherited as a single haplotype, one from each heterozygous, unaffected parent. On the X chromosome we found one rare nonsynonymous variant in *AP1S2* (adaptor protein-1-complex subunit sigma-2). Each of these genes has been linked to different neurological diseases and functional studies were therefore needed to assess their relative biological impact. The functional analysis of the identified variants is presented and discussed in result Chapters 4-6. The genes

will be introduced in this first chapter, however, to provide the necessary background for the methodological approach employed in the project.

1.2 Multiple sclerosis

MS is the most common neuroinflammatory disease of the central nervous system (CNS) characterised by immune cell infiltration, progressive demyelination and neuronal loss (19). Over 2 million people are affected globally (1). Scandinavia and the UK have a relatively high prevalence of MS, being 100-150 cases per 100,000 individuals (20), with approximately three quarters of affected individuals being women (21). On average, patients have onset of symptoms around the age of 30, and MS therefore constitutes a major cause of neurological disease among young people.

Typically, the disease follows a relapsing pattern characterised by sudden attacks of neurological dysfunction, subsequent clinical remission (relapsing remitting (RR) MS). At onset patients will often report symptoms such as sudden asymmetrical weakness in limbs, altered sensation or monocular visual disturbances. On average, 50% of patients with RRMS will convert to secondary progressive MS (SPMS) 15 years after diagnosis.

However, 10-15% of patients are diagnosed with primary progressive MS (PPMS) who are distinguished clinically from RRMS patients in that they suffer a steady decline in neurological function from disease onset without phases of remission. Patients are generally older with a median age of onset of 40 years. As with RRMS, PPMS is still more prevalent in women, but the sex ratio is closer to 1:1. It is

important to note, however, that the disease course and presentation of RRMS, SPMS and PPMS are heterogeneous. Multiple borderline diseases of MS have been described, such as opticospinal MS and Marburg acute MS, which is characterised by very rapid neurological deterioration of the patient. These spectrum disorders of MS also underscore the challenges of diagnosing MS, despite the advances in magnetic resonance imaging over the last three decades.

It is currently unknown what causes MS, but it is generally acknowledged that MS is a complex disease in which disease risk is determined by genetic variation in combination with environmental risk factors such as Epstein-Barr virus infection and smoking (22) being the most well established risk factors. However, it is also worth noting that the incidence of MS increases with higher latitudes, which has been linked to lower vitamin D exposure in northern regions of the world. Approximately 30 % of disease risk is determined by genetic variation, making non-genetic factors the major determinants of disease risk.

1.2.1 The clinical course of PPMS

PPMS typically begins with a slowly progressive spastic paraparesis. The patient loses strength and coordination over a period of months to years, most often in the legs. PPMS patients often complain of asymmetrical stiffness, weakness and clumsiness, which are exacerbated during exercise. Urge incontinence, erectile dysfunction and sensory symptoms such as numbness and dysaesthesia may also be initial symptoms (23). The symptoms often reflect pathology in the spinal cord, which on examination presents as paresis with spasticity and hyperreflexia. In a

minority of cases (15%), the patients present with ataxia. Visual disturbance due to optic neuropathy may be present at the time of diagnosis. Patients with PPMS are typically also affected by a slowly developing decline in cognitive function, specifically with respect to attention, spatial reasoning, verbal memory and verbal fluency (24). The decline in neurological function may halt temporarily during the course of disease, but the patient will never gain neurological function after disease onset, as remission is not observed. The clinical course of the disease may vary considerably among PPMS patients and neurologists are therefore using the Expanded Disability Status Scale (EDSS) to quantify the progression of disability among MS patients (see Table 1.1) (25). A recent study (26) of the natural history of PPMS found a median time of 13.3 years to reach Expanded Disability Status Scale (EDSS) score 6, at which point the patient requires a walking aid (cane or crutch) to walk 100 m.

Table 1.1 Expanded Disability Status Scale (EDSS) used to quantify progression of disability in MS patients. FS = functional system (pyramidal, cerebellar, brainstem, sensory, bowel and bladder function, visual function).

Score	Description
1.0	No disability, minimal signs in one FS
1.5	No disability, minimal signs in more than one FS
2.0	Minimal disability in one FS
2.5	Mild disability in one FS or minimal disability in two FS
3.0	Moderate disability in one FS, or mild disability in three or four FS. No impairment to walking
3.5	Moderate disability in one FS and more than minimal disability in several others. No impairment to walking
4.0	Significant disability but self-sufficient and up and about some 12 hr a day. Able to walk without aid or rest for 500 m
4.5	Significant disability but up and about much of the day, able to work a full day, may otherwise have some limitation of full activity or require minimal assistance. Able to walk without aid or rest for 300 m
5.0	Disability severe enough to impair full daily activities and

	ability to work a full day without special provisions. Able to walk without aid or rest for 200 m
5.5	Disability severe enough to preclude full daily activities. Able to walk without aid or rest for 100 m
6.0	Requires a walking aid - cane, crutch, etc - to walk about 100 m with or without resting
6.5	Requires two walking aids - pair of canes, crutches, etc - to walk about 20 m without resting
7.0	Unable to walk beyond approximately 5 m even with aid. Essentially restricted to wheelchair; though wheels self in standard wheelchair and transfers alone. Up and about in wheelchair some 12 hr a day
7.5	Unable to take more than a few steps. Restricted to wheelchair and may need aid in transferring. Can wheel self but cannot carry on in standard wheelchair for a full day and may require a motorised wheelchair
8.0	Essentially restricted to bed or chair or pushed in wheelchair. May be out of bed itself much of the day. Retains many self-care functions. Generally has effective use of arms
8.5	Essentially restricted to bed much of day. Has some effective use of arms retains some self care functions
9.0	Confined to bed. Can still communicate and eat
9.5	Confined to bed and totally dependent. Unable to communicate effectively or eat/swallow
10	Death due to MS

1.2.2 Neuroradiological findings in PPMS

Magnetic resonance imaging (MRI) of the brain and spinal cord is the standard diagnostic procedure of patients suspected of having PPMS. In patients with PPMS, MRI typically shows lesions in the grey and white matter of the brain that are smaller and more scarcely distributed than normally observed in RRMS and SPMS (27). Gadolinium enhancing lesions that reflect active lesion formation and breakdown of the blood-brain barrier are often observed in the early stages of the disease, though less frequent compared to RRMS and SPMS (28). Atrophy, especially of the grey matter, is detectable already at the early stages of PPMS (29), which may develop to global atrophy. MRI of the spinal cord typically shows diffuse mild

hyperintensities in T2 weighted scans (23), and likewise one can observe spinal cord atrophy, as measured by decreased cord area.

1.2.3 Diagnosing PPMS

Even though none of the symptoms mentioned above are pathognomonic for PPMS or MS in general (11), the spectrum of symptoms reflects the damage to multiple areas in the CNS that is a key characteristic of the disease and central to diagnosis (dissemination in space). The revised 2017 McDonald criteria for MS state that patients with the following findings may be diagnosed with PPMS (30):

1. One year of disease progression (retrospectively or prospectively determined).
2. Plus at least 2 of the 3 following criteria:

a. Evidence of dissemination in space in the brain based on $\geq$ 1 T2 lesions in at least 1 area characteristic for MS (periventricular, cortical, juxtacortical, or infratentorial).

b. Evidence of dissemination in space in the spinal cord based on $\geq$ 2 T2 lesions in the cord.

c. Cerebrospinal fluid positive for oligoclonal bands and/or elevated IgG index.

However, despite the fact that the McDonald criteria are broadly accepted in the neurological community, setting a diagnosis of PPMS still remains a considerable challenge (31), which is specifically stressed in the 2017 revised McDonald Criteria. Many neurological diseases present with symptoms also observed in PPMS, which

poses a risk for misdiagnosis and thereby mismanagement. Therefore, careful consideration of metabolic, infectious, inflammatory, vascular and hereditary diseases is a vital part of the diagnostic process, as it determines treatment and prognosis (23).

Single gene disorders constitute a substantial diagnostic pitfall as several diseases display a progressive phenotype with continual, slow neurological decline from disease onset, which may also share radiological characteristics with PPMS such as cerebral atrophy (11). For example, Warshawsky *et al*. reported a 49-year-old female patient diagnosed with PPMS whose son died at the age of 10 from a severe neurodevelopmental disorder. Subsequent genetic analysis of the mother and son identified a novel X-bound point mutation in the proteolipid protein 1 gene (*PLP1*) known to cause Pelizaeus-Merzbacher disease, in which one mutant allele is enough to contribute to disease in women due to skewed X inactivation (32). Similarly, genetic analysis revealed a mitochondrial variant known to cause Leber´s hereditary optic neuropathy in a family with six patients originally diagnosed with MS (33).

1.2.4 MS Therapy

MS attacks are treated in the acute phase with steroids that effectively inhibit the immune infiltration. When the disease is stabilised, MS patients are treated with disease modifying therapy that aims at preventing lymphocyte activation and infiltration into the CNS. The US Food and Drug Administration has currently approved 15 disease-modifying drugs for the treatment of MS (21). Drugs such as

natalizumab and fingolimod effectively prevent T cells from migrating into the CNS, however, with the risk of instigating opportunistic infections such as JC-virus causing natalizumab-associated progressive multifocal leukoencephalopathy (34).

Despite the therapeutic success of being able to reduce relapses, there has been less success in slowing disease progression and brain atrophy (35), which might reflect a lack of understanding of the mechanisms driving progression. In addition, PPMS patients do not respond to the drugs used in the treatment of RRMS and SPMS, with the exception of ocrelizumab (monoclonal antibody depleting CD20-expressing B cells) that became available to PPMS patients with early signs of disease in 2017 (36). In this phase 3 trial, ocrelizumab was, compared to placebo, shown to be efficacious in PPMS patients with early disease, by reducing clinical progression and reducing the volume of T_2-weighted brain lesions. The efficacy suggests that PPMS patients might have subclinical inflammatory attacks, in which limiting the antigen-presenting capacity and/or autoantibody production of B cell is beneficial. Nevertheless, ocrelizumab is only licensed for patients with early disease with evidence of inflammatory activity identified by MRI.

1.2.5 Pathology and pathogenesis of MS

The pathological cornerstone of MS is the dissemination in time and space of lesions formed by infiltrating immune cells in the parenchyma of the CNS, which causes inflammation and tissue damage. MS lesions can be identified by MRI and may appear in all regions of the CNS, but are often found in the white and grey matter of the cerebrum (particularly in the corpus callosum), brain stem, optic nerve and

spinal cord (37). The lesions gradually develop in normal appearing white matter with ensuing inflammation, demyelination, neuronal degeneration and gliosis.

The disease process begins with the activation of auto reactive lymphocytes (19). It is currently debated whether this detrimental, autoimmune process is initiated inside or outside the CNS. According to the extrinsic model, break down of central immunological tolerance, possibly due lower numbers and activity of T regulatory cells (38), promotes the activation of autoreactive T cells in the peripheral lymph nodes. This process might occur through molecular mimicry whereby an alien antigen is taken up by an antigen presenting cells and presented to a T cell recognising the peptide as a self-antigen, which mounts an immune response against the individual. If activated against CNS-autoantigens, T-cells with monocytes and B-cells may cross the blood brain barrier (BBB) and initiate an inflammatory response. Accordingly, approximately half of all cortical MS-lesions are perivascular(21).

This influx and presence of activated $CD4^+$ and $CD8^+$ cells in cortical lesions has been shown to strongly correlate with neuronal loss (39), and indeed brain atrophy is a strong predictor of disability in MS patients (40). The infiltrating immune cells further promote inflammation by activation of CNS resident cells such as microglia and astrocytes, which release pro-inflammatory cytokines and chemokines causing additional demyelination, neurodegeneration and plaque formation (41). However, the degenerative processes in neurons and oligodendrocytes are not necessarily interdependent as there is only little correlation between plaque formation and

neuronal loss, suggesting that parallel neurodegenerative disease mechanisms may occur simultaneously (42). Regions in the white matter may subsequently undergo remyelination, which is visible on MRI scans as disappearance of previously identified T1 weighted hypointensities, so called “black holes” (43).

The white matter of PPMS patients is generally characterised by fewer signs of inflammatory white matter lesions compared to RRMS and SPMS, but clear signs of atrophy and prominent cortical demyelination are often present (23) (44). At later stages in PPMS, the lesions become inactive plaques that are surrounded by a rim of active macrophages and microglia. The centre is characterised by complete demyelination and astrogliosis, as well as loss of axons and oligodendrocytes (44). The surrounding normal appearing white matter may also be affected by demyelination, as well as a reduction in axonal density. Diffuse meningeal inflammation is often observed in PPMS, but unlike SPMS, tertiary lymphoid structures in the meninges are not observed (45).

The inflammatory insult to the CNS often fades out over time or is partly alleviated with the use of anti-inflammatory drugs targeting the peripheral immune system. However, a chronic state of neurodegeneration, possibly driven by pro-inflammatory CNS-resident cells, may still continue as observed in patients with SPMS and PPMS, with ensuing clinical deficits. The chronic inflammation can induce an oxidative burst in activated microglia and macrophages resulting in the release of reactive oxygen and nitrogen species. This oxidative stress in the surrounding tissue causes mitochondrial damage, which has been shown to correlate with

demyelination (46). In this context, it is worth noting that several mitochondrial disorders, such as the MELAS syndrome (Mitochondrial encephalopathy, lactic acidosis and stroke-like episodes) and Leigh disease has the potential to clinically mimic MS, which underscores the involvement of mitochondria in neurodegenerative processes (11).

The mitochondrial damage in MS may further lead to energy deficiency in cells. Neurological activity is highly energy demanding due to need of neuroaxonal transport of neurotransmitters and maintenance of ion homeostasis, etc., which makes neurons highly vulnerable to alterations in energy supply (41). To compensate for this damage, dying and demyelinated axon redistribute ion channels such as voltage-gated sodium channels $Na_v1.6$ and $Na_v1.2$ in an effort to maintain ion homeostasis (47). Similarly has the acidic conditions in EAE lesions been shown to activate voltage-insensitive acid sensing ion channel-1 (ASIC1), which allow for a toxic influx of sodium and calcium ions and thereby contributes to neuronal cell death (48). Accordingly, ASIC1 is up regulated in lesions of MS patients, which has been shown to correlate with axonal damage and blocking ASIC1 in EAE has been shown to ameliorate the disease course (49). The MS-SMART trial, testing the effects of the ASIC1 inhibitor amiloride in SPMS patients, is expected to finish in 2018.

1.2.6 The genetic component of MS.

For well over a century researchers and clinicians have observed that MS tends to aggregate in families, suggesting a genetic component in the aetiology of the disease (50). Accordingly, the overall lifetime age adjusted risk of developing MS is 18.4%

for monozygotic twins, 4.6% for dizygotic twins and 2.7% for siblings (51), giving rise to a familial recurrence rate of roughly 20%. In addition, epidemiological studies have suggested that familial genetic factors affect not only the risk of developing MS, but also the disease course of MS. Specifically, clinical traits such as age of onset and disease course are more likely to be similar between siblings, which is observed for all MS clinical subgroups (52).

Much research effort have been directed towards characterising the variants, common and rare, that drive genetic risk with the view that this can provide insight into molecular pathways implicated in disease aetiology. The heritable component of MS risk has been studied in non-related MS patients with the identification and delineation of allelic variance in the human leucocyte antigen (HLA) locus initially using serological testing and subsequently using genome-wide association studies (GWAS). MS is associated with the class II risk allele *HLA-DRB1*1501*, which is the strongest genetic risk factor in MS with an odds ratio of approximately 3 (53) and is particularly dominant in populations of northern European descent. Additional effects have been observed for other class II alleles such as *HLA-DRB1*13:0*3 (odd ratio of 2.62), whereas a class I HLA allele such as *HLA-A*02:01* is protective conferring an odds ratio of approximately 0.67 (54).

GWAS of MS have revealed 110 independent, non-HLA association signals in 103 genomic regions (53, 55, 56). Fine-mapping of MS-associated loci combined with downstream functional analyses have helped to pin-point the precise genetic variants driving associations to reveal their mode of action. For example, studies on

the tyrosine kinase 2 gene (*TYK2)* (57) and the *TNFRSF1A* gene (58) encoding tumor necrosis factor receptor 1 (TNFR1), have shed light on key disease mechanisms and have suggested that genotype-to-phenotype analyses in MS can have therapeutic implications.

The associated genetic variants identified in GWAS of MS primarily affect genes that are implicated in immune regulation, and there is considerable overlap of the genomic regions with other autoimmune diseases. GWAS of MS do not indicate any differences in the variants conferring genetic pre-disposition between RRMS and PPMS. These observations are in keeping with the present understanding that non-HLA variants determine the threshold at which the immune system is activated, whereas HLA-peptide-TCR interactions likely determines the CNS specificity (59).

The genetic variants identified by GWAS are all common, having a minor allele frequency in the general UK population of ~5% or more, noting that the genotyping strategy utilised in GWAS to date has a relatively limited power to detect low frequency variants (allele frequency = ~0.5-5%) and practically no power to identify rare variants (allele frequency = <0.5%) (60). The lack of sensitivity stems from the fact that the typing strategy relies on the use of tag single nucleotide polymorphisms (SNP) that delineate genomic regions in linkage disequilibrium (LD), which allows for screening of thousands of cases and controls, as opposed to querying all genetic variation across the genome.

The variants identified in MS GWAS, moreover, account for only about 30% (60) of the heritability of MS. The missing heritability might reflect the fact that GWAS identifies tag SNPs rather than truly causative SNPs. Another possibility is that disease risk is affected by functional epistasis between loci, in which the effect of one variant is dependent on other genetic variants acting as modifiers (61). Finally, the genetic component of disease risk may be governed by common variants, as well as rare variants with stronger impact on disease risk (7).

Rare genetic variants are known to be enriched in genetically isolated populations (62). Studies of isolated populations with strong genetic founder effects have enabled the identification of disease associated genetic variation such as the C7-FLJ40243 risk locus identified in a cohort of related Finish MS patients (63). Similarly, genetic analyses performed on the island of Sardinia have identified genetic variation in *CBLB* to be associated with MS (64). These approaches to MS genetics exploit the phenomenon that genetic isolation allows for the enrichment of rare and more penetrant genetic variants with a strong impact on disease risk, which can provide clues to disease mechanisms.

1.3 Hereditary spastic paraplegia

HSP constitutes a clinically heterogeneous group of neurodegenerative diseases characterised by progressive, symmetric gait disturbance, muscle weakness and spasticity in the lower limbs with a prevalence of 3-10 per 100,000 individuals (65). Patients presenting with these symptoms in isolation are considered to have pure HSP, whereas patients with additional symptoms such as urinary incontinence,

seizures, visual disturbances and ataxia are considered to have complex HSP (66). The rate of progression and age of onset varies considerably among HSP patients. The diagnosis is based on (67):

1) Clinical history of spastic gait impairment and neurological findings of lower limb spasticity and weakness.
2) Often (though not always) a family history of similarly affected first-degree relative(s).
3) Exclusion of other disorders.

The diagnosis can be confirmed using genetic testing of variants in genes known to cause HSP, of which 68 genes have currently been identified (68). Genetic variants have shown autosomal dominant, autosomal recessive, X-linked and mitochondrial inheritance. Rather than pointing to a shared, affected pathway, the recognised "HSP genes" identified so far seem to be involved in different cellular processes such as axonal transport (for example *KIF1A* and *KIF5A*)(69), endoplasmic reticulum (ER) morphology (*ATL1*) (70), mitochondrial functions (*HSPD1*)(71), myelination (*GJA12/GJC2*)(72) and lipid metabolism (*CYP2U1*)(73).

1.3.1 Pathology

The consistent pathological finding in HSP is the ascending degeneration of axons in the lateral corticospinal tract, affecting motor control of limbs and digits, as well as degeneration of axons in the gracile fasciculus, carrying sensory input from the trunk and lower limbs (74). These observations have led to the understanding that

long axons are particularly vulnerable to the metabolic impacts of HSP associated variants. However neuropathological studies have also reported degeneration of shorter neurons in the thalamus, corpus callosum and substantia nigra (75), which has challenged the neuropathological understanding of HSP (74). MRI of the brain and spinal cord are often normal at the time of diagnosis (67), but may later show atrophy, as well as white matter lesions (76).

1.3.2 Phenotype genotype relationships in HSP

The list of genes implicated in HSP continues to expand, fuelled by the advent of whole genome and exome sequencing (77). The technology further substantiates the genetic heterogeneity of HSP, but also points to the relevance of HSP of our understanding of neurodegenerative diseases more broadly. For example, variants in *EIF2B5*, *CLN8*, *ARG1* and *ALS2,* which are known to cause other neurodegenerative diseases (Leukoencephalopathy with vanishing white matter, Ceroid lipofuscinosis and Arginase deficiency and Juvenile ALS, respectively) were recently identified by exome sequencing in a cohort of 55 families with members affected by autosomal recessive HSP (65). These observations may either reflect that rare variants in these genes have variable phenotypic impacts, which might relate to differences in allelic expression or other modifying genes. Another possibility is that genetic heterogeneity of HSP and the relatively non-specific diagnostic clinical criteria of HSP set the stage for misdiagnosis.

Patients with HSP and PPMS both present with symptoms of the lower extremities and may present with white matter lesions on MRI of the brain and spinal cord.

Indeed, families with patients fulfilling the criteria for both HSP and MS have been described (78) (79), which underscores the close clinical resemblance of these diseases. However, there is no evidence to suggest that common genetic factors in HSP and MS are at play (80).

1.4 MLKL

MLKL variants have not previously been associated with HSP or MS, neither in GWAS studies (MS) nor in case reports. MLKL is the effector molecule of necroptosis, a recently discovered form of programmed cell death (81). Until about two decades ago, cell death was thought to occur either by apoptosis or as ”accidental” cell death, termed necrosis caused for example by trauma, chemical or ischaemic insult. Necroptosis shares morphology with necrosis to the extent that the cell swells and the cell membrane ruptures during cell death, but the molecular processes leading to cell death are highly regulated, as is the case in apoptosis. The rupture of the membrane causes release of cellular contents, including damage-associated molecular patterns, which can activate pattern recognition receptors in cells of the innate immune system. Necroptosis is therefore considered a relatively proinflammatory form of cell death in contrast to apoptosis, which is characterised by cell shrinkage, condensation of the nucleus and sustained integrity of the cell membrane prior to undergoing phagocytosis (82).

Despite these morphological differences, however, the cellular pathways leading to apoptosis and necroptosis are intricately linked as shown in Figure 1.2.

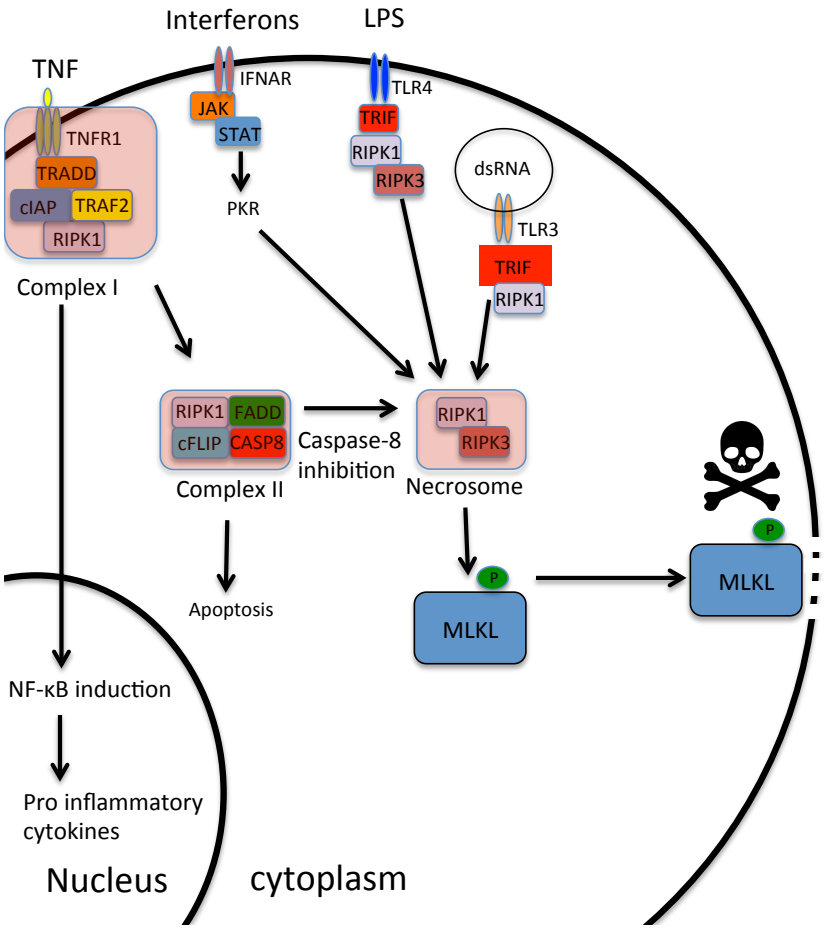


Figure 1.2. The molecular machinery of necroptosis. The effector molecule of necroptosis, MLKL, is activated through the association of RIPK1 and RIPK3, which may be induced by interferon signalling, Toll-like receptors (TLR) upon lipopolysaccharide (LPS), cytoplasmic sensing of viral DNA (DAI) and tumor necrosis factor (TNF). Upon activation of the membrane bound TNFR1 receptor by TNF, a protein complex called complex I is formed with the recruitment of TRADD (TNFR1-associated death domain protein), TRAF2 (TNF receptor associated factor 2) and RIPK1 (Receptor-interacting serine/threonine-protein kinase 1). Polyubiquitylation of RIPK1 by cIAP1 and cIAP2 stabilizes the complex and enables TAK1 (TGF-activated kinase 1) to dock to complex 1 together with TAB (TAK1-binding protein), thus promoting proinflammatory signals and inhibition of cell death by activation of NF-κB (83, 84). Deubiquitylation of complex 1 by Cylindromatosis (CYLD) (not shown) or cIAP-inhibition by SMAC mimetics destabilizes Complex 1, allowing the formation of cytosolic pro-apoptotic complex II. In situations where caspase-8 is inhibited (for example by virally encoded proteins) or pharmacologically inhibited by pan-caspase inhibitor zVAD-FMK, RIPK1 and RIPK3 are allowed to interact through their RHIM (RIP homotypic interaction motif) whereby the molecules autotransphosphorylate one another thus forming the necrosome. RIPK3 mediates the phosphorylation of MLKL at Thr 357 and Ser358, which activates MLKL and causes it to translocate to the cell membrane where pore formation occurs. Modified from Silke *et al*. (85).

Both modes of cell death can be activated downstream of toll-like receptor signalling, interferon stimulation and other stimuli, but TNF-mediated cell death has so far been the best characterised (85). TNFR1 signalling may either promote cell survival or cell death depending on the cellular activity of key regulating molecules (see Figure 1.2 legend). Receptor-interacting serine/threonine protein kinase 1 (RIPK1) plays a key role as a part of the NF-kappa B activation machinery, since RIPK1 can activate both pathways downstream of TNFR1 signalling depending on the cellular context. Another key player is caspase-8 which promotes the activation apoptosis, whereas its absence or inactivation leads to RIPK1 forming an activated complex with receptor-interacting serine/threonine protein kinase 3 (RIPK3) called the necrosome. MLKL is phosphorylated by RIPK3 in this context leading to its translocation from the cytosol to the cell membrane. At the cell membrane MLKL causes primary necroptosis either through calcium ion influx through its interaction with transient receptor potential melastatin related 7 (TRPM7) (86), sodium ion influx (87) or through induction of liposome leakage (88). These different mechanisms are not necessarily mutually exclusive, though further work needs to be carried out to fully resolve the action of MLKL at the cell membrane (89).

1.4.1 MLKL structure

During the delineation of the pathways leading to apoptosis, researchers discovered that lack of caspase activity in the presence of TNF signalling leads to necrosis, and that this form of cell death was dependent on RIPK1 and RIPK3 (82). In 2012, MLKL was discovered as the substrate of RIPK3 phosphorylation and the target of necrosulfonamide (NSA) using a chemical screening approach (81). In the following

year the crystal structure of murine Mlkl was solved, which revealed that Mlkl is a pseudokinase, which can bind adenosine triphosphate (ATP), but without displaying any kinase activity (90). Human MLKL is 471 amino acids (aa) in length and consists of a N-terminal helical bundle (N-bundle), bound to the C-terminal pseudokinase domain through a brace region as shown in Figure 1.3.

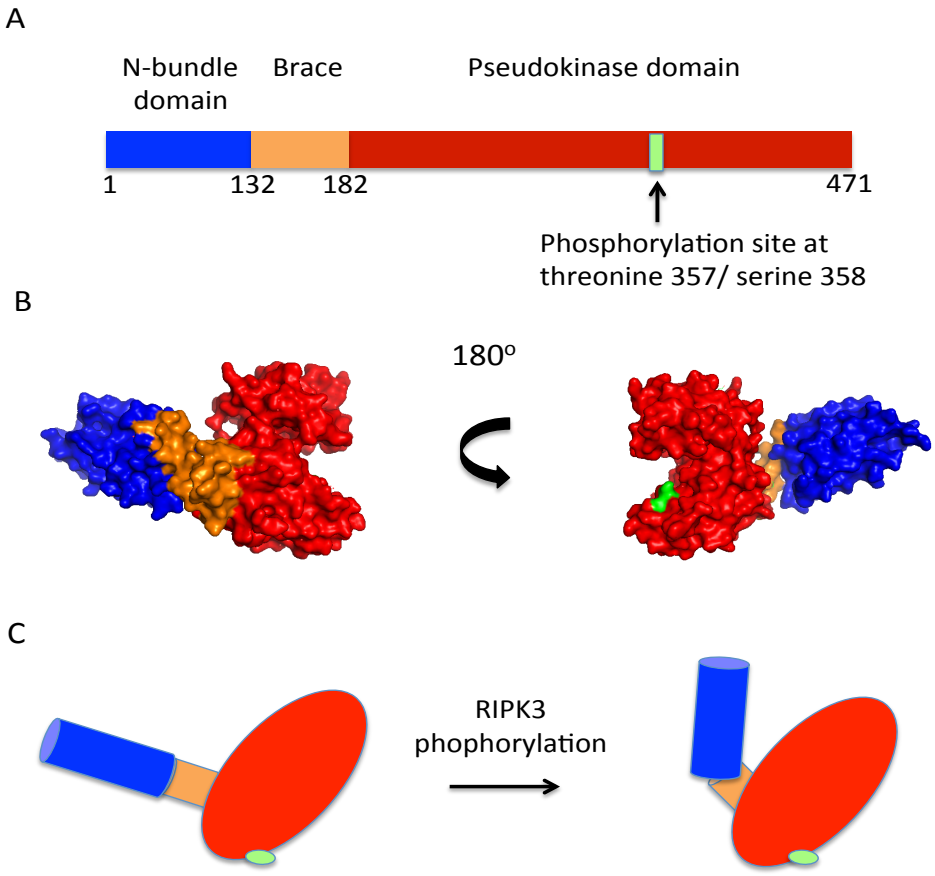


Figure 1.3. Molecular structure of MLKL. A. Schematic representation of human MLKL structure. Protein domain boundaries are based on analysis of mouse MLKL structure (91). **B**. Crystal structure of mouse MLKL (Protein ID 4BTF). RIPK3 phosphorylation site is shown in green in the figure on the right (90). **C**. Cartoon depicting the molecular switch mechanism by which autoinhibition of the N terminal helix bundle domain by the pseudokinase domain is released upon RIPK3 phosphorylation.

Phosphorylation by RIPK3 induces a conformational shift in the pseudokinase domain, whereby the inhibitory function on the N-bundle is cancelled (92). The brace region allows MLKL to oligomerise prior to translocation to the cell membrane, where the N-bundle domain causes pore formation in the plasma membrane (91).

1.4.2 What is the function of necroptosis?

Studies in mice and cell lines have suggested that necroptosis plays a role in innate immunity during viral infections by eliminating the virally infected cells and hence viral replication during infection. HSV-1 infection, for example, triggers RIPK3 and MLKL dependent necroptosis and RIPK3 deficient mice show reduced control of HSV-1 infection(93). Furthermore, HSV-1 and HSV-2 have evolved mechanisms to counteract necroptosis by encoding proteins that prevent the RHIM (RIP homotypic interaction motif)-dependent binding between RIPK1 and RIPK3 (94). Similarly, human cytomegalovirus (CMV) has been reported to block TNF-mediated necroptosis downstream of MLKL (95). However, viruses (including HSV and CMV) are also known to have evolved inhibitors of apoptosis, for example caspase-8 inhibitors (96). These observations have led to the hypothesis that necroptosis participates in an "arms race" between mammals and viruses and has evolved as an alternative system that is activated to clear the viral niche, and hence viral replication, when apoptosis is inhibited by virally encoded proteins and vice versa (97).

Two lines of evidence suggest that MLKL is also involved in combating bacterial infection. First, *Escherichia coli* has been reported to express proteases that inhibit RIPK3 and MLKL activity (98). Secondly, in a model of cutaneous and systemic bacterial infection using *Staphylococcus aureus*, *Mlkl -/-* mice were less able to clear the bacterial infection, had higher rates of sepsis-induced lethality, and exhibited an exaggerated cytokine response compared to their wildtype littermates (99). These data suggest that necroptosis benefits the host by mediating an appropriate and controlled level of inflammation necessary to combat the bacterial infection and by killing damaged cells in a controlled fashion.

Necroptosis does not seem to play role during development, as *Mlkl -/-* mice are viable and demonstrate a normal immune cell and haematopoietic development (90, 100). This finding is in stark contrast to apoptosis, in which mice lacking apoptotic regulators, such as caspase-8, die in utero(101). Collectively, cell line and mouse studies suggest that necroptosis seems to be functional solely during adulthood by participating in the clearance of infections and controlling the inflammatory response.

1.4.3 Non-necroptotic functions of MLKL

In addition to mediating the clearance of infected cells, MLKL is also reported to activate nucleotide-binding oligomerization domain (NOD)-like receptor protein 3 (NLRP3) inflammasome, which again induces caspase-1-mediated cleavage and release of IL-1β. (102). This additional proinflammatory capacity of MLKL was explored in bone marrow-derived macrophages (BMDM) upon lipopolysaccharide

(LPS) treatment, in which *Mlkl-/-* cells were deficient in IL-1β release. Importantly, the NLRP3 activation and release of IL-1β is a cell-intrinsic mechanism and not caused by mere release of cellular contents upon plasma membrane disruption. These *in vitro* studies stand in contrast to *in vivo* data on *S. aureus* challenged *Mlkl -/-* mice, which showed increased IL-1β release compared to wild type littermates. These apparently inconsistent findings may reflect tissue-specific differences in the regulation of necroptosis, or possibly counter regulatory mechanisms in the *in vivo* scenario, whereby the net effect is increased cytokine release despite the absence of Mlkl. In this context, It is also noteworthy that cell type/tissue-specific differences have been observed with respect to the relative importance of necroptosis: for example, RIPK1 deficiency in the gut causes excessive caspase-8-mediated apoptosis (103), whereas mice lacking RIPK1 in the skin suffer from severe RIPK3-mediated necroptosis and inflammation (104).

The severe phenotypes observed in mouse studies demonstrate the potent nature of the necroptosis pathway, and by implication a necessity for tight regulation. In addition to the previously mentioned inhibitory capacity at the level of caspase-8, RIPK3 oligomerization and intrinsically by the MLKL pseudokinase domain, MLKL-induced necroptosis was recently shown to be antagonized by the endosomal sorting complexes required for transport (ESCRT) III machinery (105). By promoting and controlling plasma membrane repair, the ESCRT III complex delays the onset of necroptosis and thereby allows for pro-inflammatory chemokine production and antigenic cross-priming of $CD8^+$ T cells. This pro-survival repair mechanism relies on the shedding from the plasma membrane of MLKL-

permeabilised membrane sites, which form so-called membrane blebs. Yoon *et al*. (106) recently reported a similar mechanism by which MLKL bound ESCRT III proteins and thereby facilitated the release of extracellular vesicles containing phosphorylated MLKL (p-MLKL). In addition, MLKL was reported to play a housekeeping role by facilitating the formation of early endosomes, and thereby controlling the uptake of receptors and ligands from the cell surface that are destined for lysosomal degradation.

1.4.4 Necroptosis in disease

Since the discovery of necroptosis, further interest into the pathway has been sparked by reports implicating necroptosis in a large spectrum of human diseases. Although MLKL has been mostly studied in the context of the immune system the breadth of diseases in which necroptosis is implicated could reflect that necroptosis is implicated in other cell types. Consistent with this, MLKL is ubiquitously expressed, although the highest expression is nonetheless in immune cells as shown in Figure 1.4. With respect to the MLKL mRNA data, it is important to remember that relatively high tissue MLKL expression, for example in lung tissue, may reflect the presence of MLKL-expressing immune cells.

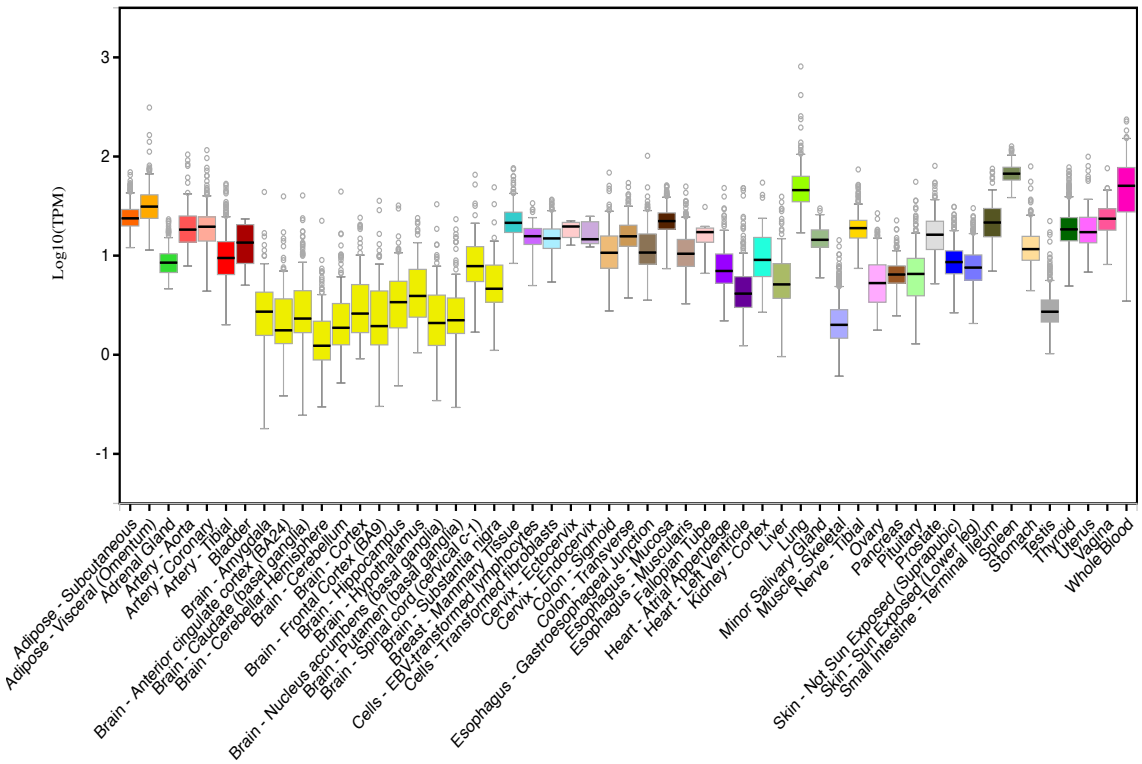


Figure 1.4. MLKL mRNA expression across tissues in healthy individuals. TPM (transcripts per million). Data extracted from gtexportal.org (107).

In the absence of established *in vivo* biomarkers of necroptosis, most studies have explored the disease relevance of necroptosis using antibodies against p-MLKL in post-mortem human tissue, pharmacological inhibitors against necroptosis such as necrostatin-1 (RIPK1 inhibitor) and NSA (MLKL inhibitor), and cell lines and mice deficient in MLKL. For example, p-MLKL is strongly upregulated in liver biopsies from patients with autoimmune hepatitis (108) and atherosclerotic lesions of coronary arteries (109), inhibition of necroptosis using necrostatin-1 lowers infarct size in a guinea pig model of cardiac ischaemia (110), and delays ischaemic brain injury in a mouse model of stroke (111), and *Mlkl -/-* mice are protected in cerulean-induced pancreatitis (100). The common denominator in these studies is that the disease pathology involves a degree of cell death that was previously thought to be

solely mediated by apoptosis, but now, with varying degrees of evidence, seems to also be mediated by necroptosis.

Necroptosis has also been reported to play a key role in several CNS diseases, despite the fact that MLKL is lowly expressed in the CNS. In 2015, necroptosis was shown to be involved in MS pathology as p-MLKL was observed by immunohistochemistry in the cerebral white matter lesions of MS patients (112). Ripk1 was upregulated in the spinal cord of mice with induced experimental autoimmune encephalomyelitis (EAE), a mouse model of MS, and the disease course was ameliorated when treating the mice with RIPK1 inhibitor 7N-1. In 2017, RIPK1 and p-MLKL were shown to be upregulated in brain tissue of patients with Alzheimer´s disease (113). In addition, inhibition of Mlkl activity in a mouse model of Alzheimer´s disease lowered disease severity. Necroptosis has also been shown to contribute to pathology in Gaucher´s disease (114), Niemann-Pick disease (115), Huntington´s chorea (116), ALS (117) retinal detachment (118), spinal cord injury (119), stroke (111, 120) and Japanese encephalitis (121). Table 1.2 provides a summary of these results. Necroptosis therefore seems to be playing a pathogenic role in CNS diseases with a wide range of different aetiologies, which fits well with the fact that MLKL functions downstream of multiple signalling pathways.

Table 1.2. Necroptosis in neurological diseases. Abbreviations: Optineurin (*Optn*), superoxide dismutase-1 (SOD1), Immunohistochemistry (IHC), Western blotting (WB), WM (White matter), Npc1 (Niemann-Pick disease, type 1), Necrostatin-1 (Nec-1).

Disease	Human tissue	Animal model	Cells	Pharma intervention in animal model.	Ref.
ALS	Spinal cord (WB): ↑RIPK1 ↑RIPK3 ↑p-MLKL	*Optn*$^{-/-}$ + SOD1^{G93A}: Spinal cord (WB): ↑Ripk1 ↑Ripk3 ↑p-Mlkl	L929 *Optn*$^{-/-}$ Sensitized to TNF induced necroptosis.	Nec-1 delayed onset of motor dysfunction in SOD1^{G93A}	(117, 122)
Alzheimer's disease	Brain (WB+IHC) ↑RIPK1 ↑p-MLKL	Viral activation of Mlkl exacerbates disease.	No data	Nec-1 treatment reduces p-Mlkl in neurons *in vivo.*	(113)
MS	Cortical WM-lesion ↑RIPK1 ↑RIPK3 ↑p-MLKL/MLKL	EAE-model: Spinal cord (WB) ↑Ripk1 (microglia + oligodendrocytes) -Cuprizone model: Protection from Ripk3$^{-/-}$	TNF stim. of cultured rat oligodendrocytes induces necroptosis sensitive to 7N-1 treatment.	EAE-model: - 7N-1 (RIPK1-inhibitor) reduced disease severity Cuprizone model - Protection from demyelination (oligodendrocytes) with 7N-1 (RIPK1-inhibitor)	(112)
Gaucher´s disease (type 2)	↑RIPK1 (n=1)	*Gba*flox/flox; nestin-Cre mice. ↑Ripk1 ↑Ripk3 *Ripk3*$^{-/-}$ mice protected from chemical induced Gaucher's disease.	No data	No data	(114)
Niemann-Pick disease, type C1	Cerebellum ↑RIPK1 ↑RIPK3	Npc1-mutant mice: Cerebellum ↑Ripk1 ↑Ripk3	Patient fibroblasts/ neuronal precursor ↑RIPK1 ↑RIPK3	Increased fibroblast viability by Nec-1 treatment. Delayed disease onset in Npc1-mutant mice treated with Nec-1:	(115)
Huntington´s chorea	No data	R6/2 model	Striatal neurons ↑Cleaved RIPK1 ↑Cell death from zVAD-fmk	Improved disease score from Nec-1 treatment.	(116)

Retinal detach-ment	No data	Surgical induction. Rat retina (WB+ IHC):↑Ripk1 ↑Ripk3 *Ripk3*$^{-/-}$ mice: ↓Cell death after retinal detachment	Photo-receptor loss due to necroptosis.	Reversible by Nec-1 in combination with zVAD-fmk	(118)
Spinal cord injury	No data	Spinal cord injury	No data	Nec-1 treatment: - Reduced lesion size - Improved clinical score	(119)
Stroke	No data	Mouse ischaemic brain injury	No data	Reduced infarction size with Nec-1 (RIPK-1 inhibitor)	(111)
	No data	Oxygen-glucose deprivation	Primary cortical neurons. ↑RIPK1 ↑RIPK3	MLKL inhibition by Nec-1 attenuated brain damage in induced hypoxia-ischemia.	(120)
Japanese encephalitis	No data	Virus infection in mice (i.p.) ↑Mlkl + p-Mlkl by IHC and WB in brain (neurons). *Mlkl -/-* mice demonstrate alleviated progression of JE and reduction of inflammatory cytokine.	Neuro2a ↑MLKL upon virus infection.		(121)

However, how can necroptosis contribute to disease development when the expression of MLKL mRNA is low in the CNS? A key paper that shed light on this conundrum was published in 2016, which examined the effect of variants in the optineurin gene (*OPTN)* that is associated with the amyotrophic lateral sclerosis (ALS) (122). Optineurin is a multidomain protein involved in numerous cellular pathways including autophagy, NF-κB signalling and antiviral responses through IFN type 1 responses. Variants in *OPTN* are also associated with other neurodegenerative diseases, such as normal-tension glaucoma and juvenile open-

angle glaucoma (123). The ALS associated variants affect the RIPK1 and Ubiquitin binding domains, as opposed to glaucoma associated variants that affect upstream domains. Optineurin was shown to facilitate the proteosomal degradation of Ripk1 through ubiquitination, and hence loss-of-function *Optn* variants cause reduced Ripk1 turnover and thus increased Ripk1 expression. The downstream implication was increased levels of Mlkl and p-Mlkl demonstrated in *Optn-/-* mice, which caused slowly progressive axonal degeneration and dysmyelination. The necroptosis machinery (RIPK1, RIPK3, MLKL and p-MLKL) was also shown to be upregulated in the spinal cord of ALS patients, compared to unaffected controls, though it was unfortunately not investigated in ALS patients with *OPTN* variants.

The example of *OPTN* variants in ALS points to the necessity of tight control of the necroptosis pathway and how the relative expression of the necroptotic machinery affects the sensitivity of cells to undergo necroptosis. Like MLKL, optineurin is ubiquitously expressed, yet ALS patients with *OPTN* variants are not reported to suffer from disease outside the CNS (124) suggesting CNS specificity of genetically dysregulated necroptosis.

Tank-binding kinase (TBK1) is a known regulator of optineurin in which mutations have been associated with ALS and FTD (125). ALS-associated missense *TBK1* variants (5) have been shown to disrupt the regulation of optineurin, which might suggest a common, dysregulated pathway contributing to these spectrum disorders. Thus, *TBK1* variants, via an impact on optineurin, could potentially have an impact on necroptosis, although studies formally addressing this hypothesis would need to

be performed. Likewise, variants in the ESCRTIII subunit CHMP2B have been functionally investigated in cases of FTD (126) and ALS (127).

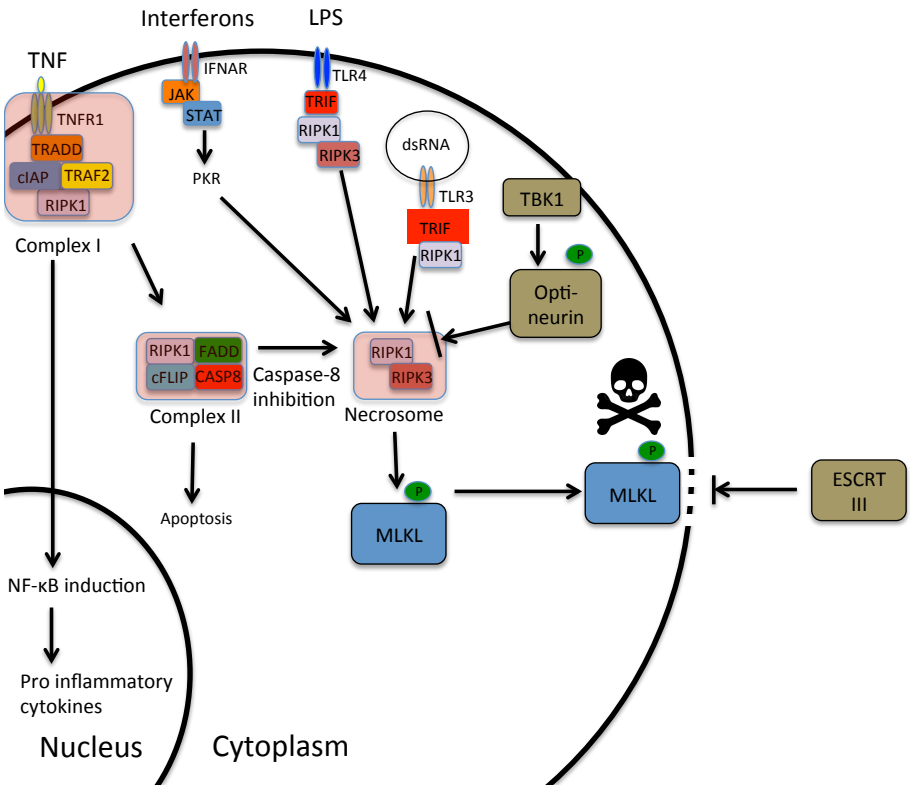


Figure 1.5. Genetic variants in regulators of necroptosis are associated with neurodegenerative disease. Loss of function variants in optineurin disrupts optineurin inhibition of RIPK1 thus initiating necroptosis in ALS. ESCRT III antagonises membrane permeabilisation caused by phosphorylated MLKL and variants in ESCRT III subunit CHMP2B are found to be pathogenic in ALS and FTD. Adapted and modified from Silke *et al.* (85)

Variants in the regulatory proteins upstream and downstream of MLKL are thus associated with neurodegenerative diseases as summarised in Figure 1.5**.** These observations support the notion that the necroptotic machinery must be very finely tuned to avoid disease, and that the CNS could to be particularly susceptible to genetically determined dysregulation of necroptosis. One can speculate that such sensitivity could be related to the relatively low turnover rate of cells in the CNS relative to other organs.

The extensive spectrum of neurological diseases with diverse aetiologies seems to suggest a fundamental mechanism whereby the CNS necroptotic machinery clears damaged cells as a secondary response to different pathogenic insults. The current available data in the literature would suggest that the activation of necroptosis is a contributing factor to disease severity. It is important to note, however, that the great majority of animal models of necroptosis rely on the application of Nec-1 to prove *in vivo* the contribution of necroptosis to disease. It is known that Nec-1 also targets other pathways, for example T-cell receptor activation, which complicates interpretation of the data, though this caveat is ignored in most studies (128).

At present, much research emphasis has been focused on delineating the necroptosis pathway downstream of TNF signalling in the context of innate immunity, most notably microbial clearance of infected cells. A broader disease relevance of necroptosis has been suggested, though these studies rely primarily on studies in animal models and cell lines, occasionally supported by human post-mortem tissue. The physiological relevance and function of necroptosis in humans is therefore still an open question. Indeed, the necroptotic machinery, with the exception of RIPK1, is not well conserved in the animal kingdom. For example, carnivores and metatheria do not express MLKL, which questions the notion of a universal role for necroptotic cell death in the animal kingdom (129).

Recently a heterozygous stop-gain variant affecting the N-terminal domain of MLKL was found to confer susceptibility of Alzheimer´s disease in a Chinese (Hong-Kong) cohort of late onset Alzheimer's disease, suggesting that reduced expression of

MLKL and hence reduced activation of necroptosis may cause disease (130). The paper does not address the controversy of necroptosis previously having been shown to be contributing factor in Alzheimer's as noted above (113), but the result would be in keeping with necroptosis serving role of cellular clearance as a counter regulatory measure during disease.

1.5 FA2H

The other variant on the haplotype segregating with disease in the brothers is located in the *FA2H* gene on chromosome 16. FA2H is a hydroxylase, highly expressed in brain, stomach, testis, kidney and skin (131). FA2H is located in the endoplasmic reticulum (ER), where it hydroxylates fatty acids prior to the incorporation into ceramides during *de novo* synthesis as shown in Figure 1.6. The formation of ceramides begins in the ER with the condensation of dihydrosphingosine from serine and palmitoyl CoA (Coenzyme A). Dihydrosphingosine condenses with fatty acids of variable carbon chain length to form ceramides. A variable proportion of these fatty acids are then hydroxylated by FA2H. Ceramides are subsequently further modified by galactosyltransferase to galactoceramides in the ER (132), or to sphingomyelin by sphingomyelin synthase in the Golgi apparatus (133). Ceramides thus serve as the common precursor of complex sphingolipids.

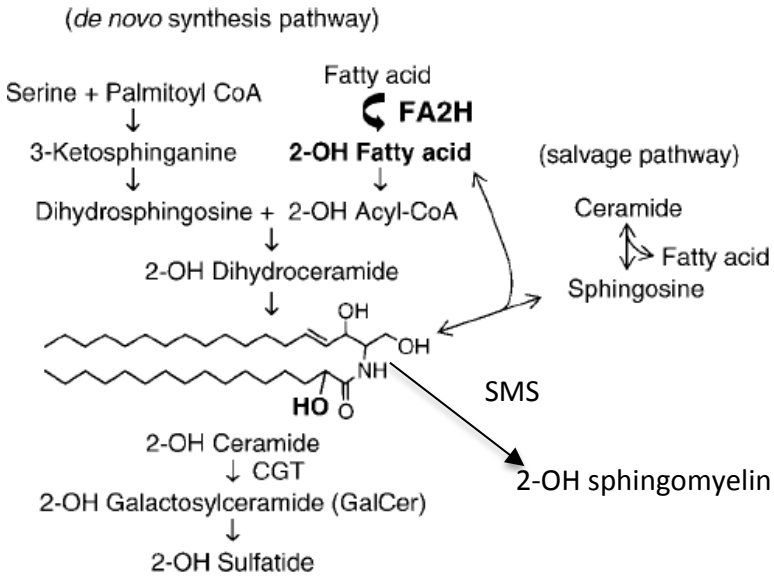


Figure 1.6 FA2H functions in the pathway leading to 2-hydroxy sphingolipids. FA2H hydroxylates fatty acids, which condense with dihydrosphingosine to form 2-OH dihydroceramide. Galactosyltransferase (CGT) catalysis the formation of Galactosylceramide (GalCer), which may be further sulfatated to sulfatides. 2-OH dihydroceramide may also be modified to sphingomyelin by sphingomyelin synthase (SMS), which adds a phosphocholine headgroup to the sphingosine backbone of ceramides. The formation of non-hydroxy sphingolipids occurs in an identical pathway. Adapted from Alderson *et al*. (134)

In the CNS, neurological function is highly dependent on oligodendrocyte-derived myelin that wraps around axons to provide insulation of salutatory nerve conduction, and 25-30% of the lipids that make up myelin are ceramide derivatives, including galactosylceramides and sulfatides (132). The myelin sheath is formed from the oligodendrocyte plasma membrane, which consists of lipids and proteolipid proteins (PLP), but it is highly enriched in glycosphingolipids compared to cell membranes of other cells (135). During development, the expression of myelin basic protein and PLP allows oligodendrocytes to manoeuvre the internal and external surfaces of the myelin bilayer into apposition thus forming insulating, compact myelin around the axon as shown in Figure 1.7.

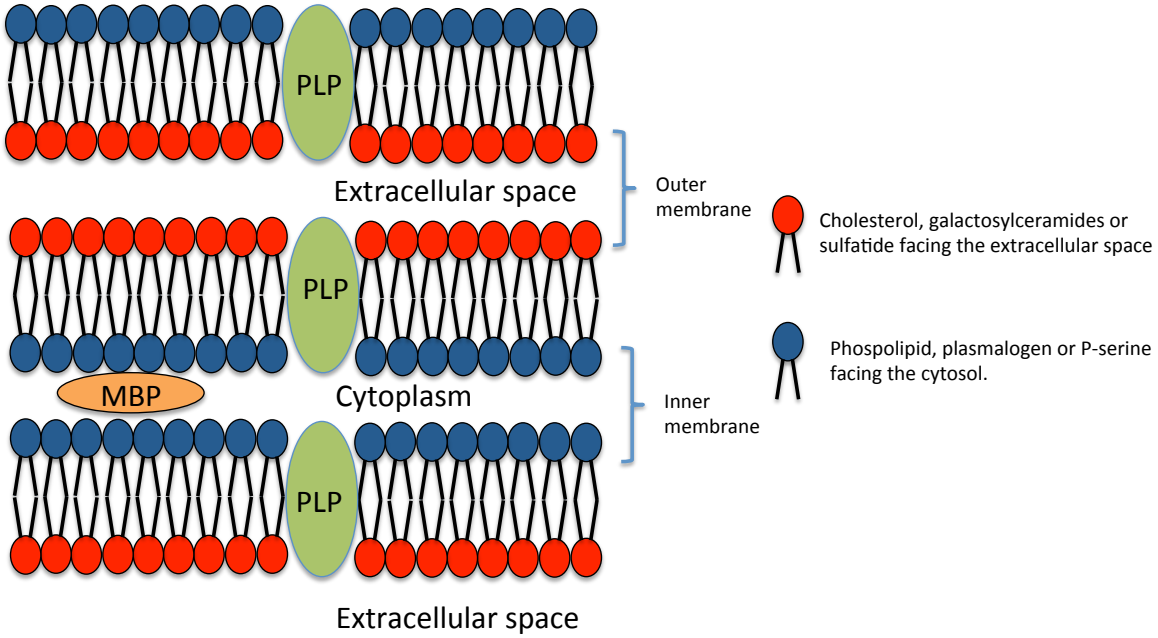


Figure 1.7. The structure of myelin. 2-hydroxylation of fatty acids in ceramides (shown in red) ensure the formation of hydrogen bonds necessary for repulsion of the hydrophilic extracellular space. Adapted from Aggerwal *et al*. (135).

The hydrophobic nature of lipids and PLP repels the aqueous environment in the cytosol and extracellular space. Crucially, the membrane is further tightened by intermolecular hydrogen bonds formed from free hydroxyl groups at the C2 position of the fatty acid chain of ceramides as shown in Figure 1.8 (135).

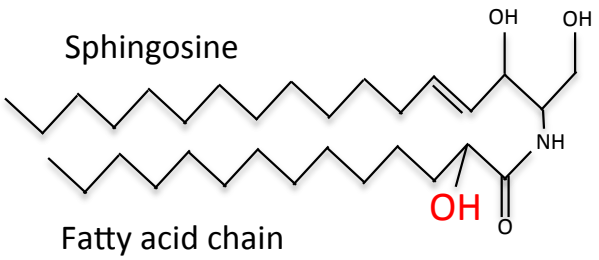


Figure 1.8. Molecular structure of ceramides. Hydroxyl group at the second carbon atom (shown in red) of the fatty acid chain is added by FA2H.

Studies in rats have shown that the ratio of hydroxylated fatty acids to non-hydroxylated fatty acids in galactosylceramides and sulfatides increases through development reaching 60% at 4 months post partum (136). The importance of fatty acid hydroxylation is demonstrated by *Fa2h -/-* mice, which suffer from severe demyelination, axonal enlargement and axonal loss within the CNS, whereas the peripheral nervous system is unaffected (137).

1.5.1 FA2H structure

FA2H is a 372 aa protein that consists of a N-terminal cytochrome b5 domain (aa 15-85) and a catalytic C-terminal domain containing 4 transmembrane domains (aa 210-367) (138) as shown in Figure 1.9. The catalytic domain contains a histidine motif, characteristic of hydroxylases, which is believed to mediate the transport of electrons from the cytochrome b5 domain to the substrate (131). Accordingly, removal of the cytochrome b5 domain abolishes hydroxylase activity (139).

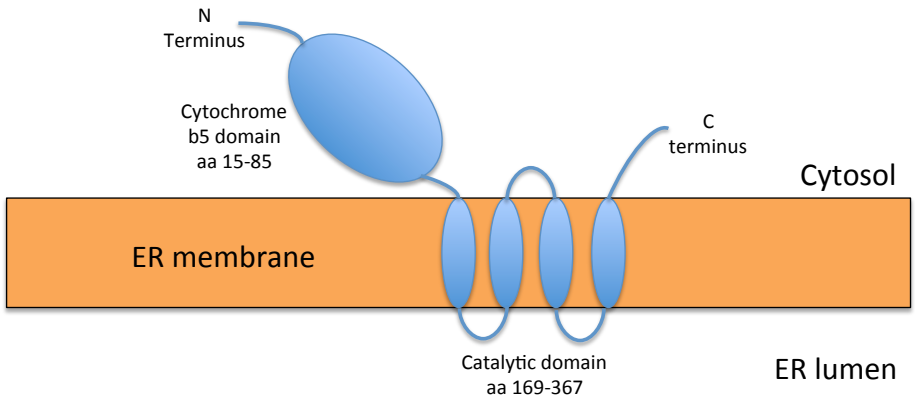


Figure 1.9. Domain structure of FA2H. Numbers indicate amino acid residue. The catalytic domain contains 8 conserved iron-binding histidine residues, which are directed towards to cytosol and mediates the hydroxylation of fatty acids. Adapted and modified from Tonelli *et al.* (140).

1.5.2 FA2H in disease

Variants in *FA2H* have been associated with three neurodegenerative disorders, specifically hereditary spastic paraplegia (HSP) (141), leukodystrophy with spastic paraparesis and dystonia (138), and neurodegeneration with brain iron accumulation (NBIA) (142). These neurological disorders overlap clinically, though the majority of cases are diagnosed with HSP. *FA2H* is one of currently 68 genes in which variants have been reported in individuals with HSP. Variants in *FA2H* have mainly been reported in a clinically heterogeneous subgroup of complex HSP patients termed spastic paraplegia form 35 (SPG35), in which patients tend to present during childhood with spastic paraparesis, ataxia, dysarthria and cognitive decline (141). Seizures and optic atrophy my also be present. Magnetic resonance imaging (MRI) often shows atrophy of the cerebrum, brainstem and cerebellum, T2 hyperintensity of the cerebral white matter and leukodystrophy. T2 hyperintensity is an unspecific MRI finding in itself, which may reflect demyelination and/or axonal loss.

Table 1.3 summarises the genetic variants and clinical characteristics of the current, independent reports on *FA2H* variants and associated phenotypes. The variants include amino acid substitutions, premature stop codons and splice site variants that affect the catalytic domain as well as the cytochrome b5 domain. However, based on the genetics there are no obvious correlations between the variants in question and clinical manifestations, age of onset, or the MRI findings. In the

majority of cases, the relative magnitude of the functional effect on FA2H-activity has not been investigated.

Table 1.3. Reported cases of patients with *FA2H* variants. Abbreviations: Cytochrome (Cyt). Gas chromatography–mass spectrometry (GC-MS). Thin-layer chromatography (TLC). Liquid chromatography-tandem mass spectrometry (LC-MS/MS).

***FA2H* variant**	**Protein domain location**	**Clinical features**	**MRI finding**	**Age of onset (years)**	**Functional analysis**	**Ref.**
Splice site variant c.786+1G>A, skipping of exon 5 and 6	Catalytic domain	Spastic paraparesis Dystonia Ataxia Seizures Cognitive decline	Atrophy of corpus callosum, cerebellum and pons.	4-6		(138)
c.103G>T D35Y	Cyt. b5 domain	Spasticity	Normal	4-6	GC-MS shows reduced hydroxylation in FA2H mutant transfected COS7 cells	(138)
c.703C>T p.R235C	Catalytic domain	Spastic paraparesis Dystonia Seizures Cognitive decline	T2 hyperintensity in WM periventricularly	6-11	TLC shows reduction in hydroxylation	(141)
c.157-174 del >p.Arg53_Ile58del	Cyt. b5 domain	Spastic paraparesis Dystonia Cognitive decline Seizures	Atrophy of cerebellum, Cerebrum and brainstem	4	-	(141)
c.460 C>T p R154C	Between domains	Spasticity Ataxia Seizures Dysmetrioptic atrophy	Pontocerebellar atrophy Hypointensity of globus pallidus consistent with brain iron accumulation	4-5	-	(142)
c.509_509delAC, p.Y170X	Truncation of catalytic domain	Spastic paraparesis Dystonia Ataxia Cognitive decline seizures	Pontocerebellar atrophy Hypointensity of globus pallidus consistent with brain iron	2-3	-	(142)

			accumulation			
Splice site variant c.270+3A>T. Loss of exon 2-7	Catalytic domain	Spastic paraparesis Cognitive impairment	White matter disease and atrophy of cerebellum, brainstem and spinal cord	4-7	-	(143)
Compound het (p.S70L/p.P323L)	Catalytic domain/ Cyt. b5 domain	Spastic paraparesis Cognitive decline	Periventricular dystrophy	3	-	(144)
c.509A>G p.Y170C	Between domains	Spastic paraplegia Dysarthria Nystagmus	Cerebral and cerebellar atrophy Iron deposit in cerebral peduncles and basal ganglia	40/38	-	(140)
p.Gln89stop	Truncation of catalytic domain	Spastic paraparesis Dysarthria Ataxia Dystonia Seizures	Cerebellar atrophy Leukodystrophy Hypointensity of basal ganglia indicating iron deposition	3	-	(145)
p.Trp176Cys	Between domains	Spastic paraparesis Dysarthria Ataxia Dystonia	Cerebellar atrophy Hypointensity of basal ganglia indicating iron deposition	6-11	-	(145)
p.Arg269Leu	Catalytic domain	Spastic paraparesis Dysarthria Nystagmus Ataxia Dystonia	Leukodystrophy Cerebellar atrophy Hypointensity of basal ganglia indicating iron deposition	9-14	-	(145)
(c.509_510 del) > (p.Y170X).	Truncation of catalytic domain.	Spastic diplegia Dysatrhia Tremor	Atrophy of cerebellum, pons, corpus callosum	2/3	-	(146)
Compound het. (c.388C>T/ p.L130F and splice donor site variant c.506+6C>G)	Catalytic domain	Spastic paraparesis Horizontal nystagmus Dysarthria Dysphagia	Cerebellar atrophy Hyperintensity of periventricular white matter	17	Verified in CHO-K1 cells by LC-MS/MS	(147)
(c.230T>G/ p.L77R)	Cyt b5 domain	Spastic quadri-paresis Cerebellar signs Dysarthria Seizures	-	4	Verified in CHO-K1 cells by LC-MS/MS	(147)

It has been suggested that the heterogeneity of clinical presentations of patients with different *FA2H* variants may be due to effects of other modifying genes, or to differential effects of the variants on hydroxylase activity (148). The latter possibility has been studied experimentally using transfection of cells deficient in endogenous FA2H, such as CHO-K1 (Chinese Hamster Ovary cells) or COS7 cells, followed by measurement of hydroxylase activity by thin-layer chromatography (TLC) or mass spectrometry (138, 141, 147). These studies have demonstrated that *FA2H* variants reduce 2-hydroxylation activity in vitro between 40-60%. Edvardson *et al*. (138) also attempted to measure fatty acid 2-hydroxylation activity in cultured fibroblasts from patients using deuterated tetracosanoic acid as a substrate. The results suggested, however, that additional fatty acid 2-hydroxylation activity occurs in the fibroblasts, which is independent of FA2H. Furthermore, fibroblasts are not reported to express FA2H (149).

1.5.3 Variants spanning FA2H and MLKL

As mentioned in the beginning of this chapter, *MLKL* and *FA2H* are adjacent genes, located on the long arm (q) of chromosome 16, only 12 kb apart, with transcription occurring off the reverse strand. Heterozygous deletions covering *MLKL* and *FA2H* have been associated in one case with spastic paraplegia, but interestingly also with the development of psychiatric disorders. A 167.1 kb deletion spanning *FA2H, MLKL* and the first exon of *RFWD3*, which is just downstream of *MLKL*, was identified in two brothers diagnosed with autism spectrum disorder (ASD). The brothers were diagnosed at the ages of 4 and 5, and MRI demonstrated hyperintensity in the T2 FLAIR (Fluid-attenuated inversion recovery) in the posterior periventricular region

(150) of the brain. The clinical neurological examination of both brothers was normal. Vu *et al*. (151) described a patient who was heterozygous for a 350 kb deletion covering *MLKL*, *FA2H* and *WDR59* and partly deleting *RFWD3* and *ZNRF1*. This patient was aged 18 years and was diagnosed with intermittent explosive disorder, which is characterised by impulsive episodes of aggression, rage and violence. No MRI had been performed. *RFWD3* and *ZNRF1* are not independently associated with CNS diseases, which suggest that it is variation region in the region encompassing *MLKL* and *FA2H* that somehow drives the disease. The described case reports summarised in Table 1.4 on genetic variants in *FA2H* and *MLKL* demonstrate that genetic variants involving these loci are associated with a wide spectrum of clinical phenotypes involving the CNS.

Table 1.4. Reported heterozygous deletions spanning at least part of both *FA2H* and *MLKL.*

Genetic variation	Clinical features	MRI finding	Age of onset (years)	Ref.
Compound het. 28 kb deletion spanning exons 3-7 of *FA2H*, plus 8 kb of *MLKL* including exon 1. Paternal missense variant in *FA2H* c.707. C>T; p. F236S	Spastic paraplegia Dystonia Ataxia Cognitive decline Sural axonal neuropathy	Demyelinating leukodystrophy Thinning of corpus callosum Atrophy of brainstem and cerebellum Borderline mineralization of globi pallidi	3	(148)
Rare copy number variant: 350 kb deletion on chromosome 16q22.3-q23.1 deleting *MLKL*, *FA2H* and *WDR59*, partly deleting *RFWD3* and *ZNRF1*.	Intermittent explosive disorder	No data	18	(151)
Rare copy number variant: Heterozygous 167.1 kb deletion including *FA2H, MLKL* and first exon of *RFWD3*	2 brothers with autism and intellectual disability	Mild T2-FLAIR hypersignal in posterior periventricular region	4/5	(150)

Very little functional work has been carried out to disentangle the mechanism by which variants in these neighbouring genes contribute to disease. Functional lipidomic assays on residual fatty acid 2-hydroxylase activity may help to clarify genotype-phenotype correlation in larger cohorts of HSP-patients with detrimental homozygous FA2H variants. However, the observation that the *FA2H* and *MLKL* heterozygous state is associated with ASD and intermittent explosive disorder suggest that FA2H 2-hydroxylase activity may not always explain the phenotype and other modifying genetic effects may be at play.

1.6 AP1S2

The final variant in the brothers identified by whole genome sequencing is located in the *AP1S2* gene. *AP1S2* encodes the σ1B subunit (157 aa) of the larger protein complex called Adapter Protein Complex-1 (AP-1), as shown in Figure 1.10, that also consists of a γ subunit, a β1 subunit and a μ1 subunit each of which can be expressed as different isoforms (152). AP1S2 is located in the cytosol of cells where it mediates the sorting and bidirectional transport of clathrin-coated vesicles between the *trans* Golgi network and endosomes (153). The sorting of vesicles containing protein cargo by AP-1 allows polarised cells (for example neurons) to transport and distribute proteins, such as ion channels and receptors from the soma to the target site. AP-1 is part of a larger adapter protein complex family, which also includes AP-2-AP-5, all of which function in mediating intracellular transport (154).

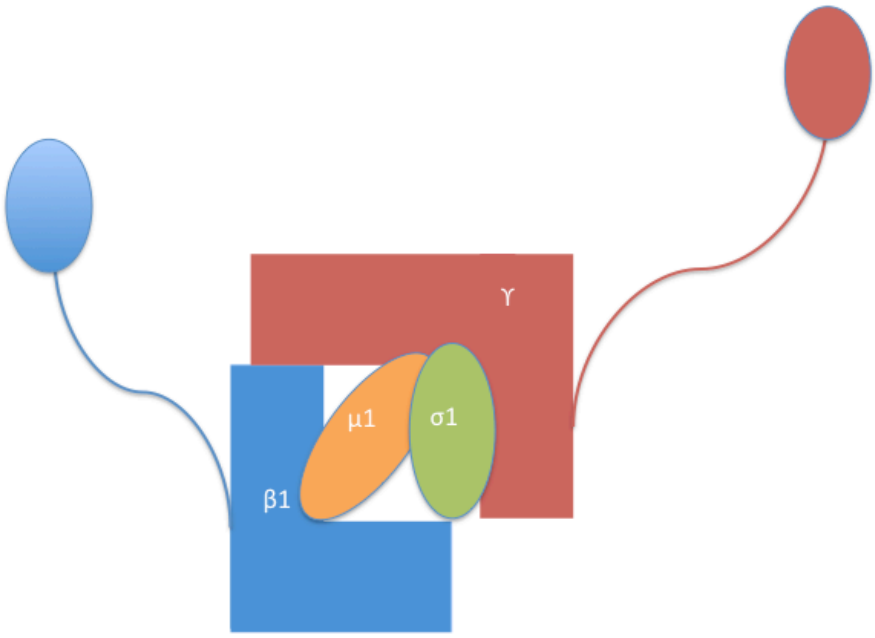


Figure 1.10. Schematic structure of the AP-1 complex.
AP1S2 encodes the σ1B subunit. σ1 exists in three subunit isoforms: σ1A, σ1B and σ1C. Adapted and modified from Janvier *et al.* (155).

Within the AP-1 complex, the γ and β1 subunits constitute the core which binds a lipid called phosphatidylinositol 4-phosphate PI(4)P on membranes after being unlocked by the GTPase Arf1(Exomer–ADP-ribosylation factor 1) (156). The σ1 and γ subunits contain conserved motifs that bind dileucine motif ((D/E)XXXL(L/I)) on the cytosolic tails of transmembrane cargo proteins, whereas the μ1 subunit binds tyrosine-based YØØX signals (where X is any amino acid and Ø is a bulky hydrophobic amino acid), allowing for specific sorting of proteins.

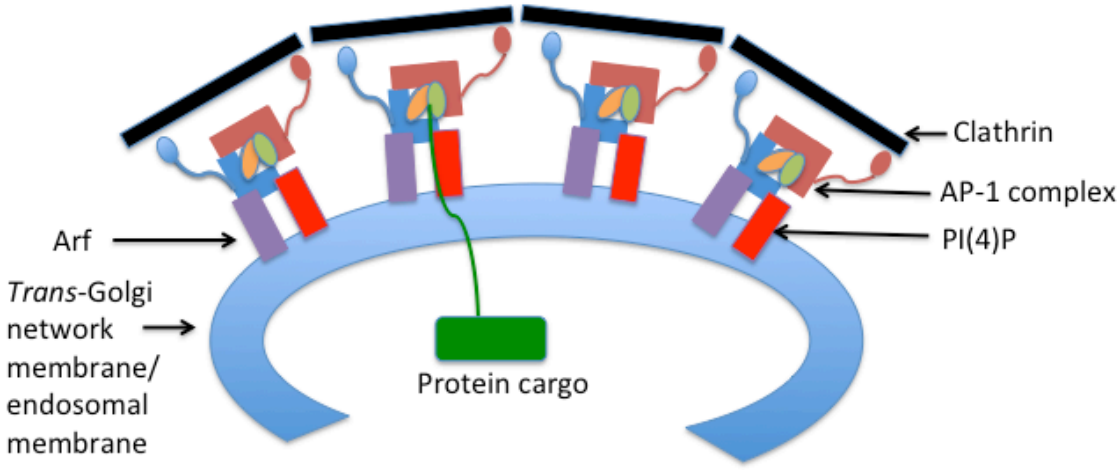


Figure 1.11. Sorting of vesicles by AP-1. AP-1 in complex with clathrin and vesicle membrane during protein sorting**.** Protein cargo may ion channels, neurotransmitters or any other protein destined for transport. Adapted from Canagarajah *et al.* (153).

The long "hinge-ear" domains of the γ and β1 subunits induce clathrin polymerisation thus making a scaffold that curves around the cargo-containing vesicle. Clathrin provides structural integrity to the vesicle prior to transport as shown in Figure 1.11. AP1S2 is ubiquitously expressed in all human tissues, though highly expressed in the brain. σ1B- deficient mice have compromised synaptic recycling of neurotransmitters in the hippocampus, as well as learning defects (157). Lipodystrophy and defective adipocyte signalling have also been reported (158). Further substantiating a role for AP-1 in the CNS, it was recently shown that sorting of copper transporter ATP7B from the soma to the somatodendritic domains in primary rat neurons is mediated by dileucine signals in the cytosolic domain of copper transporter ATP7B that binds to the σ1 subunit in AP-1 (159). As such, the AP-1 complex essentially facilitates the contact between transmembranous cargo proteins and the clathrin-coated vesicle.

1.6.1 AP1S2 in disease

Variants in *AP1S2* have been associated with the development of X-linked mental retardation (XLMR) (160). Since 2006, families formerly diagnosed clinically with Pettigrew syndrome and Fried syndrome have been genetically re-characterised using exome sequencing and were found to harbour variants in *AP1S2.* Pettigrew syndrome is characterised by mental retardation, seizures and cerebellar malformation, facial dysmorphism and inconstant choreoathetosis (161). Fried syndrome was initially described in 1972 in a Scottish family in which affected males presented with mental retardation, calcification of the basal ganglia and hydrocephalus. The overlapping clinical presentations of these syndromes are now thought to be caused by variants in *AP1S2*, although no functional assays on specific gene variants have been conducted. The identified variants introduce a premature stop codon, which causes a truncation of the protein. In addition, a 495 kb deletion that includes *AP1S2* has been described in a boy with psychomotor delay and hypotonia (162). Six different families have been reported to date as summarised in Table 1.5.

Table 1.5. Reported variants in *AP1S2* and the associated clinical phenotype.

***AP1S2* variant**	**Clinical features**	**Radiological findings**	**Age of onset (years)**	**Ref.**
Nonsense variant c.106C>T p.Q36X	Intellectual disability, hypotonia, delayed walking, aggressive behaviour, facial dysmorphism and microcephaly	-	2-3	(160, 163)
Nonsense variant c.154 C>T p.R52X	Mental retardation, hypotonia and developmental delay	-	6 months	(160, 164)
Splice site variant: c.180-5del4 causing skipping of exon 3 and termination at codon 64 (prediction)	Hypotonia at 6 months, seizures and no intelligible speech	.	6 months	(160)
Splice site variant: G>A transition at position+5 of splice donor site in intron 3 resulting in premature stop codon	Mental retardation, microcephaly, severe hypotonia and seizures	Calcification of basal ganglia. Hypoplasia of vermis in cerebellum	2	(165)
Splice site variant c.426 + 1G>T causing skipping of exon 4 and deletion of 46 aa (p. Val97-Glu142del)	Intellectual disability, developmental delay facial dysmorphism and inconstant choreoathetosis	Dandy-Walker malformation (Cerebellar vermis hypoplasia) Iron deposition in basal ganglia.	Developmental delay from first few months of life	(161)
495 kb deletion in *AP1S2*	Psychomotor delay, hypotonia, Hyperreplexia, and poor social interaction	CT scan: Normal	4	(162)

The common clinical picture is that the affected males develop hypotonia shortly after birth and delayed achievement of psychomotor milestones in the first year of life. Mental retardation becomes apparent in the first few years of life. Abusive

behaviour and poor social interaction may be present (161, 162) and seizures may appear in adolescence or adulthood. The calcifications and iron deposition in the basal ganglia as identified by MRI, computed tomography (CT) scanning, as well as in post-mortem pathology sections and seem to be a consistent finding in the few reported cases. Hypoplasia of the cerebellar vermis was also described in the two families in which the affected individuals underwent MRI scans (161, 165).

1.7 Using whole genome sequencing in diagnosis and research

With the advent of WGS the capacity to identify rare genetic variants has greatly improved making the technology useful in family-based studies. However, estimating the degree to which genetic variants are causal for disease is an on-going challenge when using WGS, as it identifies all genetic variants in the individual and the biological impact of these variants cannot always be directly inferred. Variant filtration and prioritisation are of crucial importance to the diagnostic utility of WGS. The clinical usage of WGS, outside of the cancer arena, is therefore currently limited to cases with disease of a likely genetic origin - either familial or rare conditions - especially if a candidate gene approach yields a negative result (166).

The interpretation of genetic variants takes into account allele frequency, predictive data based on computational analysis, segregation data combined with optional functional data when necessary as described in Chapter 1. The methods are constantly being improved to meet the growing needs of WGS data analysis (167) and will briefly be reviewed here.

1.7.1 Assessing the impact of genetic variants

Non-structural genetic variants in coding regions can include single nucleotide polymorphisms, deletions and insertions. They can alter protein function through missense substitutions, isoform alterations due to splicing changes or cause loss of protein due to mechanisms such as nonsense-mediated decay (NMD). Finally, they can lead to frameshifts that cause novel protein generation or protein truncation through the introduction of a premature stop codon (nonsense variant).

It is difficult to model and determine the impact of variants in which for example certain domains of the protein are missing. In contrast, the likelihood of a detrimental impact of small-scale variants, such as amino acid substitutions, can be assessed *in silico* by aligning the amino acid sequence of a given protein across species to compare the relative amino acid conservation, based on the hypothesis that the most functionally important residues will be highly conserved. The degree of conservation can be quantified using online tools such as Polyphen-2(168), which can thus provide a relative estimate of the impact of the variant in question. However, this approach cannot take into account protein tertiary structure, which is important when considering coding variants. Nor are the tools able to provide clues as to whether the variant causes a loss or gain of function.

A different approach used to assess the impact of genetic variants relies on estimating the allele frequency of a variant on a population basis. The approach is based on the hypothesis that disease-causing variants are under negative selective pressure as they reduce the reproductive fitness of carriers and are therefore rare.

The ability to evaluate the allele frequency increases as the whole genome and exome datasets expand. The Genome Aggregation Database (gnomAD) (169) contains the largest collection of 138,632 sequenced individuals (whole genome or exome), which facilitates allele frequency evaluation of genetic variants across populations. In general, genetic variants with an allele frequency >1% are considered less likely to be pathogenic. Ruling out any disease association is difficult, however, due to the possibility of incomplete penetrance and variant effects being dependent on genetic modifiers (169). It should also be noted that the gnomAD database consists of a mix of patients and healthy individuals and no phenotypic information on these individuals is available. It is therefore certain to contain disease-associated variants, which complicates the interpretation of impact of the allele frequency on human disease.

The database has, however, provided insight into the variability in tolerance and frequency of different categories of genetic variants. For example, for protein truncating variants (PTV), which is in a relatively rare category of variant, any given individual will on average harbour 85 heterozygous and 35 homozygous PTVs (169). The majority of PTVs have an allele frequency >5% and are therefore believed to be benign, but any given individual (regardless of disease status) will also harbour on average 2 singleton variants, which are variants only observed once in the data set of the gnomAD database. Thus, even very rare genetic variants with substantial consequences on the function of a protein do not necessarily result in disease. This could be explained by the relative importance of different proteins: loss of a protein acting in a redundant pathway where other proteins can

compensate for its loss is unlikely to have any substantial effect at the cellular or systemic levels.

Finally, regional and population specific differences in allele frequencies play into the equation of assessing the functional impact of genetic variants. For example, WGS of 2,636 Icelanders showed that stop-gain variants with a minor allele frequency of 0.1-1% in large outbred populations were found at a higher frequency in Iceland (56% enrichment) (62), which is most likely due to a strong founder effect. Such findings indicate that allele frequencies can vary depending on the population in question and ethnic background should be considered when assessing allele frequency for any given patient.

1.8 Hypothesis

MLKL, *FA2H* and *AP1S2* are, as described, all involved in CNS physiology and alterations of their expression or function have been directly or indirectly implicated in neurological disease. The genes were identified as a result of the choice of using whole genome sequencing rather a candidate gene or genome-wide typing approach to interrogate the genetic basis of two brothers diagnosed with PPMS. The candidate gene approach relies on the researcher/clinician to have an *a priori* hypothesis regarding the causal gene that may explain the phenotype or some knowledge of the likely variant or appropriate tagging variants in the case of genome-wide typing strategies. The power of whole genome or exome sequencing lies in its ability to identify novel disease-associated gene variants or larger scale variants that are not easily detected without the use of next generation sequencing.

However, whole genome/exome sequencing also generates the clinical and scientific problem of navigating in the vast number of genetic variants and gauging the relative evidence of pathogenicity among those identified. This challenge is a key issue in the medical genetics community, in which there is a justified concern that false positive assignment of pathogenicity can have detrimental implications for patients with respect to diagnosis and hence prognosis and therapeutic options (170). Distinguishing pathogenic variants from non-pathogenic genetic variants is therefore important in order for whole genome/exome sequencing to have a beneficial impact to the research and clinical community. It is in practise, however, extremely difficult to definitively prove that the presence of a genetic variant alone is necessary and sufficient to cause a rare disease given the very low number of patient cases that may have been recognised (170). Therefore, is it imperative to consider multiple levels of evidence for each genetic variant in question to support the likelihood of a pathogenic or benign effect. Such evidence includes allele frequency, *in silico* variant analysis, segregation data and when possible experimental data. In this project we have applied the guidelines on interpretation of sequence variants from the American College of Medical Genetic and Genomics (ACMG), as they provide relatively clear principles for assessing the impact of genetic variants (171), summarised in Table 1.6. The guidelines have primarily been designed for application in clinical genetics, but with caution they also form a useful framework for variant interpretation in research.

Using an example of WGS of a family with two brothers diagnosed with PPMS, I hypothesised that functional experiments could help to distinguish pathogenic

variant from non-pathogenic variants, while also shedding light on possibly new disease mechanisms. Without a functional understanding of the biological and clinical impact of rare variants identified by WGS, it may be difficult to harness the full potential of this technology.

Table 1.6. Summary of the ACMG guidelines on the interpretation of genetic variants. LoF, Loss of function. MAF, minor allele frequency. Adapted from Richards *et al*. (171).

	Benign		**Pathogenic**			
	Strong	**Supporting**	**Supporting**	**Moderate**	**Strong**	**Very strong**
Population data	MAF too high or observation in controls inconsistent with disease penetrance			Absent in population databases	Prevalence in affected increased over controls	
Computational data		Multiple lines of computational evidence suggest no impact on gene /gene product Missense variant in gene where only truncation causes disease	Multiple lines of computational evidence support a deleterious effect on the gene /gene product	Novel missense change at an amino acid residue where a different pathogenic missense change has been seen before Protein length changing variant	Same amino acid change as an established pathogenic variant	Predicted null variant in a gene where LoF is a known mechanism of disease
Functional data	Well-established functional studies show no deleterious effect		Missense variant in gene with low rate of benign missense variants and Pathogenic missense variants are common	Mutational hot spot or well-studied functional domain without benign variation	Well-established functional studies show a deleterious effect	
Segregation data	Non-segregation with disease		Co-segregation with disease in multiple affected family members			

Chapter 2. Methods

2.1 Sanger sequencing of family members

The family investigated in this thesis consists of two affected brothers, an unaffected sister and two unaffected parents, as described in detail in Chapter 3. The two brothers underwent whole genome sequencing as part of the WGS500 program(18), which identified two homozygous variants on chromosome 16 in *MLKL* and *FA2H*, as well as one X-bound variant in *AP1S2* that segregated with disease. To verify the inheritance pattern of each variant in the family, blood samples were taken from the father, mother and sister (see figure 3.1).

Genomic DNA was isolated from whole blood samples from the father, mother and sister of family 1 using the QIAamp DNA Blood Midi kit (Qiagen). The genomic regions spanning the variants of interest in *MLKL*, *FA2H* and *AP1S2* were amplified in a PCR reaction using primers shown in Table 2.1. Genomic regions in *MLKL* and *AP1S2* were amplified using NEB High-Fidelity DNA Polymerase according to the manufacturers' protocols. The PCR products were gel purified from a 1.2% agarose gel revealing more than one band for *MLKL*. Appearing just below the 400 bp sized marker band, the PCR products of the anticipated size for *MLKL* and *AP1S2* were gel extracted using the Qiagen Gel Extraction Kit and PCR purified using Qiagen PCR Purification Kit prior to Sanger sequencing. As the genomic region in the FA2H gene harbouring the variant has a GC content of 74%, a OneTaq DNA Polymerase (NEB) with a GC-enhancer buffer was used. Only one band was observed and consequently no gel extraction was performed. The PCR product was PCR purified, and Sanger sequencing was accomplished using deoxyguanosine triphosphate (dGTP)-

chemistry at Source Biosciences, Oxford UK. The *MLKL* and *AP1S2*-specific PCR products were sequenced using standard Sanger sequencing (Sanger sequencing facility, Weatherall Institute of Molecular Medicine).

Table 2.1. Primers used in validation of genomic variants

Gene	Left primer	Right primer	PCR-product size
MLKL	CCCTCTAGCCACTGCCAGAAA	CCCTGGCAATTGTGTGTAGCA	396 bp
FA2H	TCCCACGTAGTACTGCTCCA	GGTATGCAAATGAGCAGGTG	378 bp
AP1S2	TTCAAAGGATTTCCCTGCCTTT	GGGAAAGCTTCGACTGCAAAA	360 bp

2.2 Cloning

Untagged MLKL cDNA in pCMV-XL4 vector (cat. nr. SC108101) and a C-terminal MycDDK-tagged FA2H cDNA in a pCMV6-Entry vector (cat nr. RC202093) were purchased from Origene. The sequence of the MLKL and FA2H inserts was validated using the primers shown in Tables 2.2 and 2.3 using Sanger sequencing.

2.2.1 Site-directed mutagenesis

Site-directed mutagenesis was used to create the disease-associated genetic variants in FA2H and MLKL according to manufacturers' protocol (Quickchange II, Agilent). Primers were designed using www.agilent.com/genomics/qcpd**.** Final constructs were transformed into One Shot® MAX Efficiency® DH5α™-T1R Competent Cells (Thermo Fisher) and cultured overnight. In the morning, colonies were picked and cultured in 5 ml LB-broth. DNA was isolated using Miniprep Kit (Qiagen). The sequences of isolated constructs were confirmed by Sanger sequencing, whereby mutated clones were identified. Plasmids containing the

desired mutation in the construct were sequenced using Sanger sequencing to ensure that random mutations had not arisen during the amplification. All transformations were carried out with a parallel negative control plate.

2.2.2 MLKL

The MLKL insert was amplified in a PCR reaction using primers that introduced the *Afl*II and *Xho*l cut sites; all primers used for cloning are shown in Table 2.2. The MLKL 182 construct was made by introduction of a premature stop codon. All MLKL constructs were subcloned into the vector pcDNA3.1+ plasmid (Invitrogen) by digesting insert and vector with restriction enzymes *Afl*II and *Xho*I. Subsequently the vector was dephosphorylated using antarctic phosphatase (NEB), and the vector and insert were ligated using T4 ligase (NEB) in an overnight reaction according to the manufacturers' protocol.

Table 2.2. Primers used in MLKL cloning.

Cloning Primers	**Sequence**
F1 AflII-K-MLKL	GATGCGTCTTAAGGCCACCATGGAA AATTTGAAGCATATTATCACC
R1 XhoI_MLKL	GCCCTCTAGACTCGAGGTCGACCTA CTTAGAAAAGGTGGA
R1 MLKL180stop XhoI	GCGCGCCTCGAGCTATGGTGGTAAA TACTGC
Primers for site-directed mutagenesis	
MLKL SDM antisense for c.1107_1110del: p.369_370del	GAGATATGCTGTAGATTTGACTCTG TCTTTTCTCTCGTAGTT
MLKL SDM sense for c.1107_1110del: p.369_370del	AACTACGAGAGAAAAGACAGAGTC AAATCTACAGCATATCTC
Primers used for sequencing of final constructs	
pcDNA3.1_1F	CTGTGCCTTCTAGTTGCCAG
pcDNA3.1_1R	AATAGCTCAGAGGCAGAGGCG
pcDNA3.1_2F	GCCCCTAACTCCGCCCAGTTC
pcDNA3.1_2R	ACCCCAGAGTCCCGCTCAGAA

pcDNA3.1_3F	TTCGCAGCGCATCGCCTTCTA
pcDNA3.1_3R	CCTACACCGAACTGAGATACC
pcDNA3.1_F4	TTCCGACCCTGCCGCTTACC
pcDNA3.1_R4	AGTAAGAGAATTATGCAGTGC
pcDNA3.1_F5	AGTAAGTTGGCCGCAGTGTT
pcDNA3.1_R5	GCAGTTTACCGTAAATACTC
pcDNA3.1_F6	TAATGACGTATGTTCCCAT
pcDNA3.1_R6	TTCCTTGATTTCTTTCATGT
pcDNA3.1_F7	AGACGAAGACAGGCGAGCTT
pcDNA3.1_R7	GCTTCACAGCCACCAGCTTG
pcDNA3.1_F8	ACACAGACTTCCATGAGTTT
pcDNA3.1 F 1.1	TTAATTCTGTGGAATGTGTGT
pcDNA3.1 F 1.2	GTTCGCCAGGCTCAAGGCGCG
pcDNA3.1 F 1.3	GGATAACGCAGGAAAGAACAT
pcDNA3.1 F 1.4	GTCCTGCAACTTTATCCGCCT
pcDNA3.1 F 1.5	CTGCTTAGGGTTAGGCGTTTT
pcDNA3.1 F 1.6	GGAGATAGAAAAGTTCAGCAA

Ligation reactions were screened for successful insertion of the MLKL insert with a diagnostic PCR. Positive constructs were transformed into One Shot® MAX Efficiency® DH5α™-T1R Competent Cells (Thermo Fisher) and grown overnight on Lysogeny broth (LB) agar plates containing 100µg/ml of ampicillin. Clones containing the MLKL-pcDNA3.1+ constructs were identified by a diagnostic PCR and grown in a starter culture (5 ml) and subsequent large culture flask (200 ml) in LB containing 100 µg/ml of ampicillin. DNA was isolated using the High Speed Plasmid Midi Kit (Qiagen), and thereafter quantified and purity checked by NanoDrop™ spectrophotometry (Thermo Fisher Scientific).

2.2.3 FA2H

The FA2H insert was subcloned into pSIN-CSGW-UbEm plasmid (kindly given by Dr Jessica Boname/Prof. Paul Lehner, University of Cambridge, UK)(172, 173) (Figure 2.1) by PCR amplification of the FA2H insert using primers encoding restriction sites

*Bam*HI, *Not*I and a C-terminal Flag-tag. All primers used for cloning are shown in Table 2.3. The FA2H Y170X construct was made by introducing a premature stop codon, as described for the patient harbouring the mutation (146). The PCR products were gel extracted and purified as described for MLKL. The pSIN-CSGW-UbEm plasmid and FA2H inserts were then digested using *Bam*HI and *Not*I in NEB Cutsmart buffer, and subsequently gel purified and gel extracted using QIAEX II gel extraction kit (QIAGEN) due to the large size of the plasmid (10.7 kb). The pSIN-CSGW-UbEm plasmid was then dephosphorylated using antarctic phosphatase and ligated with the FA2H inserts using Blunt/TA Ligase Master Mix according to the manufactures' instructions. The ligation reaction was amplified using One Shot® MAX Efficiency® DH5α™-T1R Competent Cells (Thermo Fisher). Clones were screened for the presence of FA2H inserts using a double digestion (*Bam*HI and *Not*I). All FA2H constructs were validated using the Sanger sequencing facility at the Weatherall Institute of Molecular Medicine.

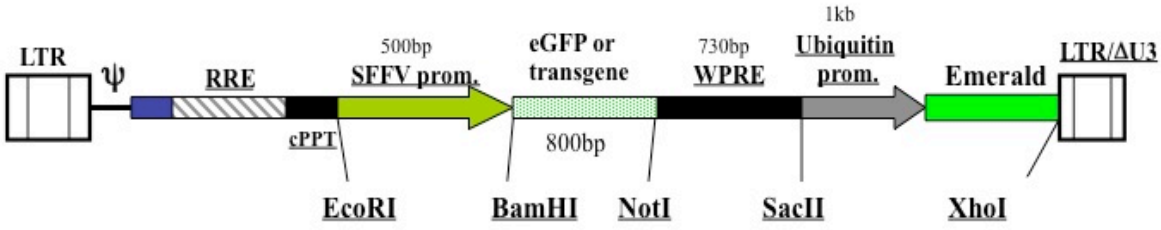


Figure 2.1. The pSIN-CSGW-UbEm plasmid. The FA2H constructs were inserted between the *Bam*HI and *Not*I cut sites. Emerald is a variant of GFP protein with improved photostability expressed under the control of the ubiquitin promoter (172, 173).

Table 2.3. Primers used in FA2H cloning.

Primer name	Sequence
Cloning primers	
F2lFA2HBamH1	TAATATAATTAATGGATCCGCCACCATGGC CCCCGCTCCGCCCCC
R3lFA2HFLAGnot1	ATATTAGCGGCCGCCTACTTGTCGTCATCG TCTTTGTAGTCACGCGTCTGCGTCTTCAGG
R3lFA2H170Flagnot1	ATATTAGCGGCCGCCTACTTGTCGTCATCG TCTTTGTAGTCCCAGACAGTCTTAGAGAGG
Sequencing primers	
F1pSIN-CSGW-UbEm primer	CTGTTCGCGCGCTTCTGCTTC
R1pSIN-CSGW-UbEm primer	CCACATAGCGTAAAAGGAGC
F3 FA2H	CCAAGTCCATGTTCCCCGGGC
R1 FA2H	TTCTCCATGGAGCCCTGCTGC
Primers for site-directed mutagenesis	
F1 FA2H SDM for L77R substitution	TAGTACTGCTCCCGCCAGCGGCGCG
R1 FA2H SDM for L77R substitution	CGCGCCGCTGGCGGGAGCAGTACTA
F1 FA2H SDM for R235C substitution	ATGTGGAACAGGAAGCAGTGGATGAGGTA CTCG
R1 FA2H SDM for R235C substitution	CGAGTACCTCATCCACTGCTTCCTGTTCCA CAT
F1 FA2H SDM for F11 deletion	GGAGGGCGAGGAGGCGGCGGG
R1 FA2H SDM for F11 deletion	CCCGCCGCCTCCTCGCCCTCC

2.3 Culturing of cell lines

All cell lines were cultured at 37°C at 5% CO_2 in Panasonic incubators. CHO-K1 cells were cultured in F12K media (ATCC) supplemented with 1% penicillin/streptomycin (Sigma) and 10% heat-inactivated and filter-sterilised foetal calf serum (FCS) (Sigma). HEK293 cells (ATCC) were cultured in Dulbecco's Modified Eagle Medium (DMEM) Lonza (BE12604F) with 10% FCS and 1% penicillin/streptomycin.

2.4 Transfections

HEK293 cells were seeded in a 24-well plate 24 hours prior to transfection at a concentration of 50,000 cells per well. Lipofectamine 3000 (Invitrogen) was used to transfect HEK293 cells according to the protocol of the manufacturer. Transfection efficiency was determined by flow cytometry.

2.5 PI/Annexin staining of MLKL transfected HEK293 cells

HEK293 cells were transfected using Lipofectamine 3000 as described above. 2-16 hours post transfection, the cells were washed in cold PBS containing 2 % FCS. The cells were then resuspended in 1x binding buffer and stained with FITC Annexin V and PI according to the protocol of the manufacturer (BD Biosciences). Cells were analysed 15 min. post staining using a Cyan™ ADP flow cytometer (Dako Cytomation).

2.6 Cell death assayed by Incucyte

Cell death in HEK293 cells and fibroblasts was measured by live cell imaging using the Incucyte Zoom (Essen Bioscience Ltd). Prior to transfection the media was supplemented with 250 nM IncuCyte™ Cytotox Red Reagent (Essen Bioscience Ltd). Each well was imaged every 2-3 hours using the red channel. For HEK293 cells, cell death was measured by red object area normalised to % confluence as advised by the Essen Bioscience (https://www.essenbioscience.com/hi/applications/cell-health-viability/apoptosis/). Red object area and confluence was measured automatically using mask settings based on the manufacturers' recommendations. This method of quantification was not applicable for primary human fibroblasts due

to morphological differences. Cell death quantification of fibroblasts was therefore conducted by terminating each experiment with 0.5% Triton X-100 (Sigma-Aldrich) to quantify and normalise to the total amount of cells in each well.

2.7 Flow cytometry

For intracellular staining of MLKL in MLKL transfected HEK293 cells, the cells were harvested from wells using trypsin (Gibco), resuspended in phosphate-buffered saline (PBS), and transferred to polystyrene FACS tubes. The cells were then centrifuged at 1400 rpm (Thermo Scientific, MegaFuge 16) for 5 min., and fixed and permeabilized in BD Cytofix/Cytoperm™ for 30 min. Cells were washed twice in BD Perm/Wash™ prior to staining for 20 min at 4°C using the rat anti-MLKL antibody (clone 3H1). Subsequently, cells were again washed in BD Perm/Wash™ and the goat anti-Rat IgG (H+L) Alexa Fluor® 647 conjugate (Life Technologies) was added to the cells for 20 min at 4°C for secondary stain. The cells were then washed again in BD Perm/Wash™ and fixed in 1x BD CellFIX™. Cells were analysed within 24 hours using a Cyan™ ADP flow cytometer (Dako Cytomation).

For the validation of the MLKL antibody (clone 3H1) for flow cytometry, HEK cells were transfected with MLKL expressing an N-terminal HA tag. Eight hours post transfection the cells were stained for MLKL and HA using the mouse anti-HA tag Alexa Fluor® 488 antibody. All data were analysed using FlowJo, LLC.

2.8 Lentiviral packaging

FA2H constructs were packaged using 2nd generation lentiviral packaging system by co-transfection of packaging plasmid psPAX2 (gift from Didier Trono (Addgene plasmid # 12260) and vesicular stomatitis virus –G envelop plasmid pMD2.G (also a gift from Didier Trono (Addgene plasmid # 12259)). The plasmids were transfected into HEK293T cells using Mirus TransIT 2020 reagent. Lentiviral particles released into the supernatant were harvested 48 hours and 72 hours post transfection and the pooled supernatants were centrifuged (Avanti J-301, Beckman Coulter) at 22,000 rpm at 4°C for 2.5 h. Viral titers were determined by serial dilution of packaged plasmid and transduction of HEK293T followed by measurement of Emerald (GFP) expression by flow cytometry.

RIPK3 expressed in pLenti-C-Myc-DDK-P2A-Puro vector (Origene, RC209549L3) was packaged into the same 2nd generation lentiviral packaging system as described for FA2H. Lentiviral titers were determined by flow cytometry by staining for the C-terminal Myc tag.

2.9 Transduction of FA2H constructs

100,000 CHO-K1 cells were seeded into each well of a 6-well plate. One hour later polybrene (Santa Cruz Biotechnology) was added to the medium at a final concentration of 8 µg/ml and viral particles were added at a multiplicity of infection (MOI) of 20. Cells were harvested 72 hours later with 3 washes of PBS and dissolved in 100 mM NH_4HCO_3 (pH adjusted to 7.8). Cells were scraped off and snap frozen in liquid nitrogen. Control samples for each construct were harvested simultaneously

and analyzed by western blotting and flow cytometry showing a transduction efficiency of 99.8-100% of all FA2H constructs.

2.10 Liquid chromatography-tandem mass spectrometry (LC-MS/MS)

Cell lysates were analysed in the laboratory of Professor Dr. Britta Brügger at Biochemie-Zentrum der Universität Heidelberg. Samples were analysed using the QTRAP6500+ System (Bio-Equip). Data was analysed using in house software ShinyLipids 2015 (by Mathias Gerl, Manuel Haußmann, Sebastian Bender Version: 1.0) and GraphPad Prism 7.

2.11 Western blotting

Cells were harvested by removal of culture media followed by rinsing in PBS. The cells were then removed from the surface using trypsin (Gibco) or by a cell scraper where indicated and centrifuged at 1400 rpm (Thermo Scientific, MegaFuge 16). The cell lysate was dissolved in RIPA (radio immuno precipitation assay) buffer (Sigma-Aldrich) with protease inhibitor (cOmplete™, Mini, EDTA-free Protease Inhibitor Cocktail from Roche, UK) according to the manufactures' instructions. Cell lysates were either used directly for western blotting or stored at -80°C. Protein concentration was determined using the Pierce™ BCA Protein Assay Kit.

All protein lysate samples were analysed using 12% polyacrylamide gels made in house (Table 2.4) in the Mini-Trans Blot® system (Bio-Rad Laboratories, UK). All gels were run with protein size markers (Precision Plus Protein™ Dual Color Standards). After gel electrophoresis, the gel was blotted onto a 0.45 µm

nitrocellulose membrane (GE Healthcare Life Sciences) for 1 hour at 100 volts in 1X transfer buffer (see Table 2.5 for all buffer recipes used). The membrane was then submerged in blocking buffer for 1 hour on a shaking device, speed 30 (Stuart Scientific). The primary antibodies (see Table 2.6) were then added to the blocking buffer and the blot was incubated over night at 4°C. The following morning the blot was washed 3x10 min in PBS 0.1% Tween (Sigma) and incubated with secondary antibody for 30 min protected from light. Subsequently, the blot was washed 3x10 min in PBS 0.1% Tween and 2x10 min in PBS. The blot was imaged using the Odyssey Infra-Red Imaging System (Software version 2.0 LI-COR Biosciences).

Table 2.4. 12% Polyacrylamide gel.

Chemical	Resolving gel	Stacking gel
MilliQ water	4.9 ml	2.2 ml
30% Acrylamide (Flowgen Bioscience)	6.0 ml	0.67 ml
1.5 M Tris HCl (pH 8.8) (Sigma-Aldrich)	3.8 ml	
0.5 M Tris Sigma-Aldrich (pH 6.8)		1 ml
10 % Sodium dodecyl sulphate (SDS) (Fisher Bioreagents)	150 µl	40 µl
10 % Ammonium persulfate (APS, Sigma Aldrich)	150 µl	40 µl
Tetramethylethylenediamine (TEMED, Sigma Aldrich).	6 µl	4 µl

Table 2.5. Buffers used in Western blotting.

2x Laemmli buffer	**Amount**
10% SDS (Fisher Bioreagents)	400 ul
Glycerol (Ultra Pure, MP Biomedicals)	200 ul
0.5 M Tris HCl pH 6.8 (Sigma Aldrich)	250 ul
Bromophenol blue (Bio-Rad Laboratories)	100 ul
β-Mercaptoethanol (MP Biomedicals)	50 ul
5X Running buffer (1 L)	
Tris Base (Sigma Aldrich)	15.1g
Glycine (Scientific Laboratory Supplies)	94 g
10% SDS (Fisher Bioreagents)	50 ml
MilliQ water	Up to 1 L.
10X Transfer buffer (1 L)	
Tris Base (Sigma Aldrich)	30.285 g (250 mM)
Glycine (Scientific Laboratory Supplies)	142.633 g (1.9M)
Tris-buffered saline, 0.1 % (TBST)	
Tween BSA 5%	
Bovine serum albumin (BSA) (Sigma Aldrich)	5%
TBS 10X (200 mM Tris, 1.5 M NaCl)	10 %
Tween (Sigma Aldrich)	0.1%
Milk blocking buffer (PBS)	
Milk skim powder (Oxoid)	5%
Tween (Sigma Aldrich)	0.1%

Table 2.6. Antibodies used for Western blotting

Antigen	Host	Clone	Company	Concentration	Blocking solution
Human N-terminal MLKL	Rat	3H1	Millipore	1:1000	5% Milk or 5% BSA
GAPDH	Rabbit	14C10	Cell Signalling	1:2000	5% BSA
FA2H	Mouse	OTI2C5	Origene	1:2000	5% Milk
TNFR1	Rabbit	C25C1	Cell Signaling	1:1000	5% BSA
TNFR2	Rabbit	EPR1653	Abcam	1:10.000	5% BSA
HA-Tag	Mouse	6E2	Cell Signaling	1:1000	5% BSA
Mouse IgG (secondary antibody; IRDye® 800 CW)	Goat		LI-COR	1:10.000	-
Rabbit IgG (secondary antibody; IRDye® 680LT conjugate)	Goat		LI-COR	1:10.000	-
Rat IgG (secondary antibody IRDye® 800 CW conjugate)	Goat		LI-COR	1:10.000	-

2.12 Bioinformatics

The rarity of each genetic variant was assessed using the ExAC Browser by searching the canonical transcript for each gene for the described mutations. PolyPhen-2 (Polymorphism Phenotyping v2) (168) was used to estimate the functional impact of the AP1S2 mutation. Pymol (174) software was used to visualise AP complexes. Sanger sequences were analysed using CLC DNA Workbench 7. Uniprot (175) and RCSB PDB (176) were used to access basic protein information. Ensembl (human genome assembly: GRCh38.p12) was used for downloading genomic and cDNA sequences (177). Primers for sequencing and PCR were designed using Primer3 (http://bioinfo.ut.ee/primer3-0.4.0/). NEBcutter V2.0

(http://nc2.neb.com/NEBcutter2/) was used to assess and pick restriction sites in constructs.

2.13 Family donor work

2.13.1 Consent

Permission to take blood samples and skin biopsies from affected and unaffected members of the family, following obtainment of informed consent to do so, was granted by The Research Ethical Committee II of Central Denmark Region (Case number 1-10-72-29-16) under the responsibility of the author. As the brothers were not in a mental capacity to provide informed consent, the sister and the general practitioner of the brothers provided consent on their behalf.

Informed consent from control donors of PBMCs was obtained through the project: "Studying the Molecular Mechanisms of action of genes with relevance to Multiple Sclerosis in Healthy Controls" (REC Ref. No.: 10/H0605/5; v.1).

2.13.2 Culturing of fibroblasts

Skin biopsies were obtained from the thigh of the sister and both brothers at Marselisborg Hospital, Aarhus University Hospital, Denmark under the responsibility of Consultant Dermatologist Mette Sommerlund. Briefly, the skin was cleaned with ethanol tissue and anesthetized using lidocain 5mg/ml with epinephrine 5µg/ml. A punch biopsy of 4 mm in diameter was then taken from the dermis. Skin biopsies were transported on ice in Advanced DMEM, 10% heat-

inactivated and filter sterilised FCS (PAA), 1X GlutaMax (Life Technologies) and 1X Antibiotic-Antimycotic (Life Technologies). Skin biopsies were washed in PBS and dissected into dermal samples with sharp edges of roughly 1 mm^3 with a Swan Morton scalpel size 23 in a petri dish, according to the standard operating procedure by StemBANCC, University of Oxford. Briefly, the dermal samples were then placed in a well of a 6-well plate containing Advanced DMEM, 10% heat-inactivated and filter sterilised FCS (PAA), 1X GlutaMax (Life Technologies) and 1X Antibiotic-Antimycotic (Life Technologies). In each well a sterile glass cover slip (22 mm) was placed on top of 5-6 dermal samples to ensure stabile adherence to the bottom of the well during fibroblasts outgrowth. When the wells were confluent from fibroblast outgrowth the cells were subcultured and expanded into T25 and T75 flasks prior to cryopreservation in liquid nitrogen. The author handled all skin samples at the Department of Clinical Immunology, Department of Clinical Medicine, Aarhus University, Denmark. Subsequent subculturing of all fibroblast lines, cryopreservation and shipment was managed by Associate Professor Lise Torp Jensen from the same department.

2.13.3 Isolation of peripheral blood mononuclear cells

Blood samples were obtained from the cubital vein in a 9 ml sodium heparin coated tube (Greiner Bio-One) and mixed with the anti-coagulant for 20 min on a rotator. Blood samples were then diluted 1:1 with sterile PBS (Gibco) and carefully loaded onto a layer of 15 ml Lymphoprep™ (Axis-Shield, UK) in a 50 ml Falcon tube. The blood samples were then subject to density gradient centrifugation at 800 × g for 20 min in a Hettich Rotanta 460 centrifuge with no brake. The white layer of PBMCs

was removed manually using a pasteur pipette. The isolated PBMCs were then centrifuged at 1350 rpm for 10 min with the full brake setting, re-suspended in cold PBS containing 2% FCS and then placed on ice. Cells were counted manually at this stage using a haemocytometer.

For subsequent analysis using western blotting, PBMCs were lysed in RIPA buffer (Sigma) containing protease inhibitor (Roche) according to the manufactures' instructions at a concentration of 20 million cells per ml and frozen at -80 degrees. A total of 20 million PBMCs were lysed in RLT buffer (Qiagen) for RNA analysis and frozen at -80. Remaining PBMCs from each donor were cryopreserved in FCS containing 10% dimethyl sulfoxide (DMSO) (Sigma) and cooled down overnight at-80°C in a Mr. Frosty container prior to storage in liquid nitrogen.

2.13.4 PBMC surface staining

For characterization of immune populations, one million fresh PBMCs per donor were aliquoted into polypropylene tubes and stained for surface markers shown in Table 2.7. The cells were then fixed and permeabilized using Fixation/Permeabilization solution (BD biosciences, UK) for 20 min. at 4 degrees and washed in BD Perm/Wash™ (BD biosciences, UK). Samples were analysed on a LSRFortessa at the FACS Core Facility at Aarhus University, Denmark.

Table 2.7. Surface antibodies used for the characterisation of immune cell populations.

Surface	Supplier	Cat nr.
Pacific Blue™ anti-human CD8 Antibody	Biolegend	344718
BV605 Mouse Anti-Human CD4	BD	562658
Brilliant Violet 785™ anti-human CD19 Antibody	Biolegend	302240
PE anti-human CD56 (NCAM) Antibody	Biolegend	318305
APC anti-human CD45RA Antibody	Biolegend	304111
Anti-Human CD14 APC-eFluor® 780	ebioscience	47-0149-41

2.13.5 qPCR of donor PBMCs and fibroblasts

Total RNA was isolated using RNAeasy Mini Kit (Qiagen) according to the kit protocol and quantified by NanoDrop™ spectrophotometry (Thermo Fisher Scientific). Synthesis of cDNA from 1 µg of RNA was conducted by reverse transcription using the QuantiTect Revese Transcription Kit (Qiagen) according to the protocol of the kit. Samples were analysed in a MicroAmp Optical 384-Well Reaction Plate covered with adhesive film (Applied Biosystems).

Each well contained 0.1 µg of cDNA per donor, TaqMan® Universal PCR Master Mix (Thermo Fisher Scientific) and one of the TaqMan® Gene Expression Assays shown in Table 2.8, also from Thermo Fisher Scientific. Samples were analysed on an Applied Biosystems 7900HT PCR machine using the PCR program shown in Table 2.9 and data were processed using SDS version 2.4.

Table 2.8. Gene expression probes used for quantification of MLKL gene expression.

Taqman gene expression assay	Product code
MLKL	Hs00930421_m1
GAPDH	Hs02758991_g1

Table 2.9. qPCR program used on Applied Biosystems 7900HT PCR machine.

Stage	Cycles	Temperature (°C)	Time (min.)
1	1	50	2 min.
2	1	95	10 min
3	40	95	15 seconds
		60	1 min

The relative gene expression was measured by using the number of PCR cycles (stage 3) necessary for amplification of the transcript as detected by the FAM reporter. The threshold for distinguishing background noise from signal was set automatically using the SDS2.4 software. At the threshold, the Ct (threshold cycle) was measured and imported for analysis into Microsoft excel and GraphPad Prism 7. Accordingly, lowly expressed transcripts require more cycles for amplification and they are thus detected at higher Ct values. Gene expression of *MLKL* was normalised to a housekeeping gene (*GAPDH*) by subtracting the Ct value of the housekeeping gene from the Ct value of MLKL, referred to a delta Ct. To obtain a measure of MLKL expression relative to the housekeeping gene, fold change was analysed as 2^{-dCt}. For MLKL the specificity of the probe MLKL_Hs00930421_m1 was verified by serial dilutions of MLKL pcDNA3.1+ plasmid.

2.13.6 Cytokine stimulation and pharmacological investigations

To induce MLKL expression, fibroblasts were stimulated with IFNγ (PeproTech) using 5ng/ml-1000 ng/ml. To examine any effect of MLKL inhibition and proteasome inhibition, fibroblasts were cultured in the presence of NSA (Millipore) 2μM and the proteasome inhibitor MG-132 (Sigma Aldrich) 25 μM.

2.13.7 Assaying MLKL dependent TNF-recycling in donor fibroblasts

The donor primary fibroblasts were washed twice in PBS and starved in serum free Advanced DMEM 24 hours prior TNF treatment in order to maximise surface TNF receptor surface expression, as described by Yoon et al. 2017(106). TNF (Peprotech, Cat. Number 300-01A) was biotinylated using EZ-Link™ Micro Sulfo-NHS-Biotinylation Kit (Thermo-Fisher Scientific) using 50 mM excess of biotin to TNF and incubated for 2 hours on ice according to the instructions of the manufacturer. Excess biotin was removed using the Zeba™ Spin Desalting Columns, 7K MWCO, 2 mL (Thermo-Fisher Scientific) according to the protocol of the manufacturer. The cells were cultured in TNF biotin 5ug/ml in CO2-independent medium (Thermo-Fisher Scientific, cat. number 18045054) 30 min on ice, washed twice in PBS and incubated at 37°C for 0 hours, 0.5 hour, 1 hour and 2 hours. The cells were harvested at indicated time points using a cell scraper, centrifuged at 1400 rpm (Thermo Scientific, MegaFuge 16) and dissolved in RIPA buffer (Sigma-Aldrich) with protease inhibitor (cOmplete™, Mini, EDTA-free Protease Inhibitor Cocktail from Roche, UK) according to the manufactures' instructions. Western blot analysis was conduced as described in section 2.11. TNF-biotin was visualised using IRDye® 680LT Streptavidin (Li-Cor), and quantified as described in section 2.11.

2.14. Statistical analyses.

All statistical analyses were conducted in GraphPad Prism 7. The experiments carried out in cell lines (Chapter 4 and 6) were repeated at least three times, in which a paired t-test (two-tailed) was used for the analysis of all flow cytometry data, western blotting and lipidomics data. The threshold for significance was set to

p-values < 0.05. For Incucyte experiments in Chapter 4 and Chapter 5, a two-way ANOVA Tukey´s multiple comparisons test was used as previously described (178). P-values < 0.05 were considered significant. In Chapter 5, optimisation experiments were only carried out once due to limited material of fibroblasts from the family. MLKL mRNA expression analysis in the fibroblast and cell death analysis was repeated in at least three experiments.

2.15 Other

MRI images were analysed and formatted using the Horos Dicom Viewer.

3. Clinical and genetic characterisation of a family with two brothers originally diagnosed with primary progressive MS

3.1 Introduction

The first step of exploring how genetic variation might contribute to disease development and progression involves first and foremost a characterisation of the clinical phenotype in affected and unaffected individuals through time. Second, whole genome sequencing of affected and unaffected family members allows for the identification of potential disease causing genetic variants. However, distinguishing pathogenic variants from non-pathogenic variants remains a considerable challenge, despite the widespread availability of bioinformatic tools designed to assess allele frequency and phylogenetic amino acid conservation.

3.2 Chapter aim

This chapter aims first and foremost to provide an overview of the clinical information from 1985 to 2017 collated by the author on the two patients studied in this project in order to build a coherent clinical picture, including clinical progression as quantified by EDSS. The description of the disease course is based on clinical records written by clinical consultants since the first admission to hospital and re-assessment of the patients by the author in 2017. Second, to interpret the findings of the MRI scans conducted in 2013 in the light of the clinical disease course of both patients. Third, the Chapter aims to present a summary of the WGS of the patients conducted at the Welcome Trust Centre for Human Genetics in 2013(18). Finally, it gives the results of the subsequent genetic validation of the identified variants in the extended family.

3.3 Results

MS is a clinical diagnosis supported by MRI demonstrating white matter lesions and by detection of oligoclonal bands in the cerebrospinal fluid (CSF). The two brothers were, however, diagnosed with PPMS in 1985 and 1990, at a time when MS was diagnosed based on the clinical judgement supported by the presence of oligoclonal bands in the CSF as defined by the Poser criteria (179). Hence, the diagnosis was made prior to the routine clinical usage of MRI scans, which today to a large extent defines the diagnosis of MS in combination with the clinical examination and history of the patient. Such changes in the diagnostic criteria of MS (and many other diseases) complicates diagnosis, especially in patients with chronic disease, who do not necessarily satisfy all diagnostic criteria throughout the course of the disease as defined at a particular point in time.

The following clinical description is based on the files from Consultant Neurologist Dr. Annette Bang Oturai, Rigshospitalet, Copenhagen, who examined the patients clinically in 1994 and 2013, as well as on the patient records from the Neurological Department of Aalborg Hospital. The clinicians referring, admitting and diagnosing the brothers are not identifiable, nor are the files concerning the diagnosis of B2 available. However, in the beginning of the 1990s, Professor of Neurology and MS, Nils Koch Henriksen described the clinical status of the two patients in detail using EDSS.

The family originates from the area around Aars in Jutland, Denmark (Figure 3.1.). Both parents were born in this region, but they are not known to be related. The

father passed away in 2015 at the age of 91, and he had lived a healthy life with the exception of a minor stroke at the age of 53.

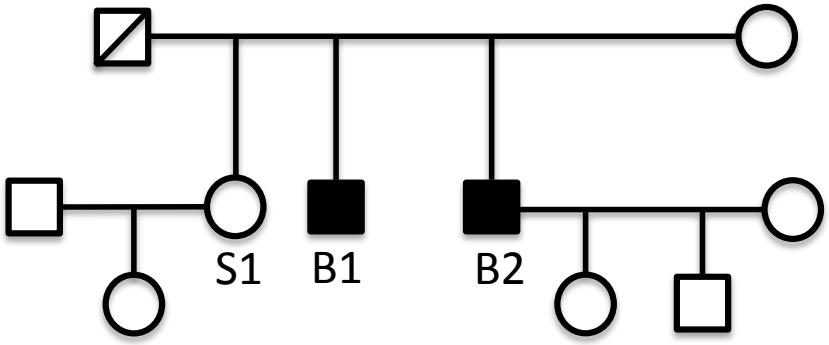


Figure 3.1. Family pedigree. B1 is the proband. ■: Affected male. □: Unaffected male. ○: Unaffected female. Filled boxes indicate affected individuals and box with strikethrough indicates deceased individual.

Their mother and sister are still alive and unaffected. B1 never married or had any children, whereas B2 has two children. Apart from the brothers no other family members have shown signs of neurodegenerative disease.

3.3.1 Clinical summary

3.3.1.1 Brother B1

3.3.1.1.1 Clinical history

B1, born 1963, was admitted to the Department of Neurology of Aalborg Hospital, Denmark in September 1985, referred from a private neurology clinic on the suspicion of MS. The patient's symptoms began to appear in 1982 at the age of 19 years with a feeling of an insecure gait and lack of coordination of the lower limbs. The patient´s left leg in particular displayed a marked stiffness and weakness, which

became apparent when playing football as he noticed that his left leg tired more quickly than the right leg. Alcohol exacerbated the symptoms. According to the family, he also complained of transient loss of vision though this is not confirmed in the original hospital records. The patient had no sphincter symptoms or symptoms from the upper limbs. At no point had the patient experienced any sensory symptoms and he was otherwise healthy up until diagnosis. At the time of diagnosis, the patient worked as a cabinetmaker, although he had no formal education as such.

3.3.1.1.2 Physical examination

At the time of admission, examination of his lower limbs demonstrated increased tone (which was most notable on the left side), hyperactive reflexes, bilateral ankle clonus and bilateral Babinski's sign. The gait was characterised by spasticity and ataxia. The admitting consultant also found saccadic eye movements and bilateral pale optic discs. The other cranial nerves were intact. All objective findings in the upper limbs were normal. All sensory modalities were normal.

Over the following 30 years the patient suffered a slow, progressive decline in gait function. In 2003 he became wheelchair-bound. During this time he also developed paresis, spasticity and ataxia of the upper limbs. From 1992 the patient began to have epileptic episodes, which have been well controlled on oxcarbazepin. From 1995 the patient developed dysarthria and mild mental impairment. In the beginning of 2000s, the patient developed urge incontinence, which was treated with tolterodine. Between 1995 and 2013 the patient´s clinical status worsened from EDSS 6.5 to 8.0. When this author assessed the patient in 2017, he had

developed fasciculations over the right thigh and had progressed to EDSS 8.5. At this time, the patient presented with quite severe ataxic dysarthria, but was still able to communicate simple words and sentences, and was clearly aware of his surroundings. The patient is in need of full-time care and he lives in a nursing home.

3.3.1.1.3 Investigations

Suspecting MS, a spinal tab was carried out at the time of diagnosis in 1985, which showed oligoclonal band positivity and increased IgG-index. Neurophysiological examination showed bilateral, prolonged visual evoked potentials. Sensory evoked potentials were normal. A thoracic myelography showed normal conditions around the spinal canal and nerve roots. The patient was diagnosed with PPMS based on the clinical history, the clinical objective findings and the oligoclonal band positivity.

3.3.1.2 Brother B2

3.3.1.2.1 Clinical history

B2**,** born 1955, was diagnosed with PPMS in 1990 at the age of 35 years. At the time of diagnosis he had experienced a disturbance in gait function progressing over a 5-year period. Specifically, he felt a stiffness and lack of coordination in the lower limbs, especially on the left side, causing him to stumble. Fatigue and alcohol exacerbated the symptoms. He had no symptoms in the upper limbs. He also had no visual problems and he had no bladder dysfunction. The patient had practised orienteering until 1980 and was at the time of diagnosis working as a cabinetmaker.

3.3.1.2.2 Physical examination

The patient presented in 1990 with bilateral spasticity of the lower limbs, most prominent on the left side and he had bilateral Babinski sign. There was no ataxia or paresis. The upper limbs were normal, except for mild hyperreflexia on the left side. Eye examination revealed mild ocular instability and bi-temporal pale discs, but there was no nystagmus.

The patient was diagnosed with PPMS based on his clinical history and the objective findings. The CSF, however, was not checked for oligoclonal band positivity and the diagnosis of PPMS seems to have been partly based on the clinical resemblance with B1, who was already diagnosed at the time.

The patient´s ability to walk deteriorated steadily after the diagnosis. In 1993 his maximal walking distance was reduced to 300 m without aid (EDSS 4.5), which declined further making him dependent on a wheelchair in 1999. During these years he developed ataxia of all extremities, foot clonus, urinary incontinence, ataxic dysarthria and mental impairment. All sensory modalities were normal. In 2013 the patient scored 7.0 on the EDSS scale and was living in a nursing home receiving full time care. In 2017 the patient had progressed to EDSS 8.0, as assessed by the author. The patient was still able to communicate simple phrases and was aware of his surrounding. The author did not confirm the previous observations of aggressive behaviour. The patient is treated for epilepsy with gabapentin.

3.3.1.3 Common pattern of symptoms in B1 and B2

The patient records of B1 and B2 over time thus reveal a strikingly similar course of disease. Based on the symptoms, their disease began in the pyramidal tract causing paraparesis, Babinski´s sign, hyperreflexia and spasticity, and then gradually affected the cerebellum (ataxia) and cerebrum causing mental reduction. Dysarthria may be caused by neuronal loss in all of those areas. Their disease development measured by EDSS is summarised in Figure 3.2. It is noteworthy that in both cases progression occurred relatively quickly during the first 10 years and later reached a plateau. It should be noted, however, that as the EDSS score is non-linear, the presence of a plateau at EDSS > 6 does not necessarily reflect lack of disease progression, but rather insensitivity of the EDSS scale to capture accumulation in disability. The progression in EDSS through time is nevertheless comparable to the general disease course of PPMS patients (26, 180), though the age of disease onset is relatively early for B1.

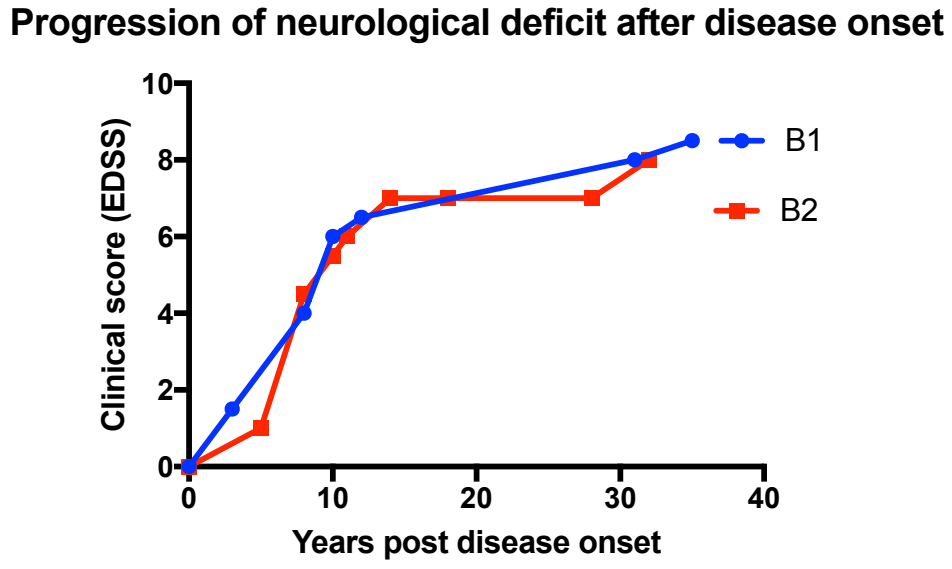


Figure 3.2. Progression of neurological deficit post disease onset. EDSS scores were collected from patient records of neurological consultants reviewing the patients during routine clinical follow-up.

3.3.2 Magnetic resonance imaging in 2013

The brothers were diagnosed at a the time when the Poser criteria (179) were used to diagnose MS and hence prior to the routine clinical usage of MRI. In addition, these criteria do not formally describe PPMS. Given the strict male predominance of disease in the family, the lack of sensory symptoms, the striking similarity of disease course and symptomology between the patients, as well as the lack of investigations in Brother B2, it was necessary to conduct a reaffirmation of their diagnosis using the McDonald criteria (181). Consequently, an MRI scan of the cerebrum, brainstem and spinal cord of each brother was carried out in 2013, organised by Dr. Annette Bang Oturai and Professor Jørgen Frøkiær, Aarhus University Hospital, Denmark.

3.3.2.1 MRI of B1

The MRI scan shown in Figure 3.3A demonstrated extensive atrophy of the cerebrum with dilated sulci, enlargement of the ventricles, atrophy of the corpus callosum and reduced white matter. Very discrete white matter lesions were observed in the periventricular areas. The cerebellum, the cortical cerebellar fibres, the pons (brainstem) and the middle cerebellar peduncles connecting the cerebellum to the pons were likewise atrophic (Figure 3.3B+C). There was no regional predominance indicating a distinct neurodegenerative disorder and there were no signs of cerebral ischaemia. There were no signs of iron deposition in the basal ganglia. The MRI scan of the spinal cord showed no obvious signs of pathology, but the scans were of low imaging quality due to movement artefacts (Figure 3.3D).

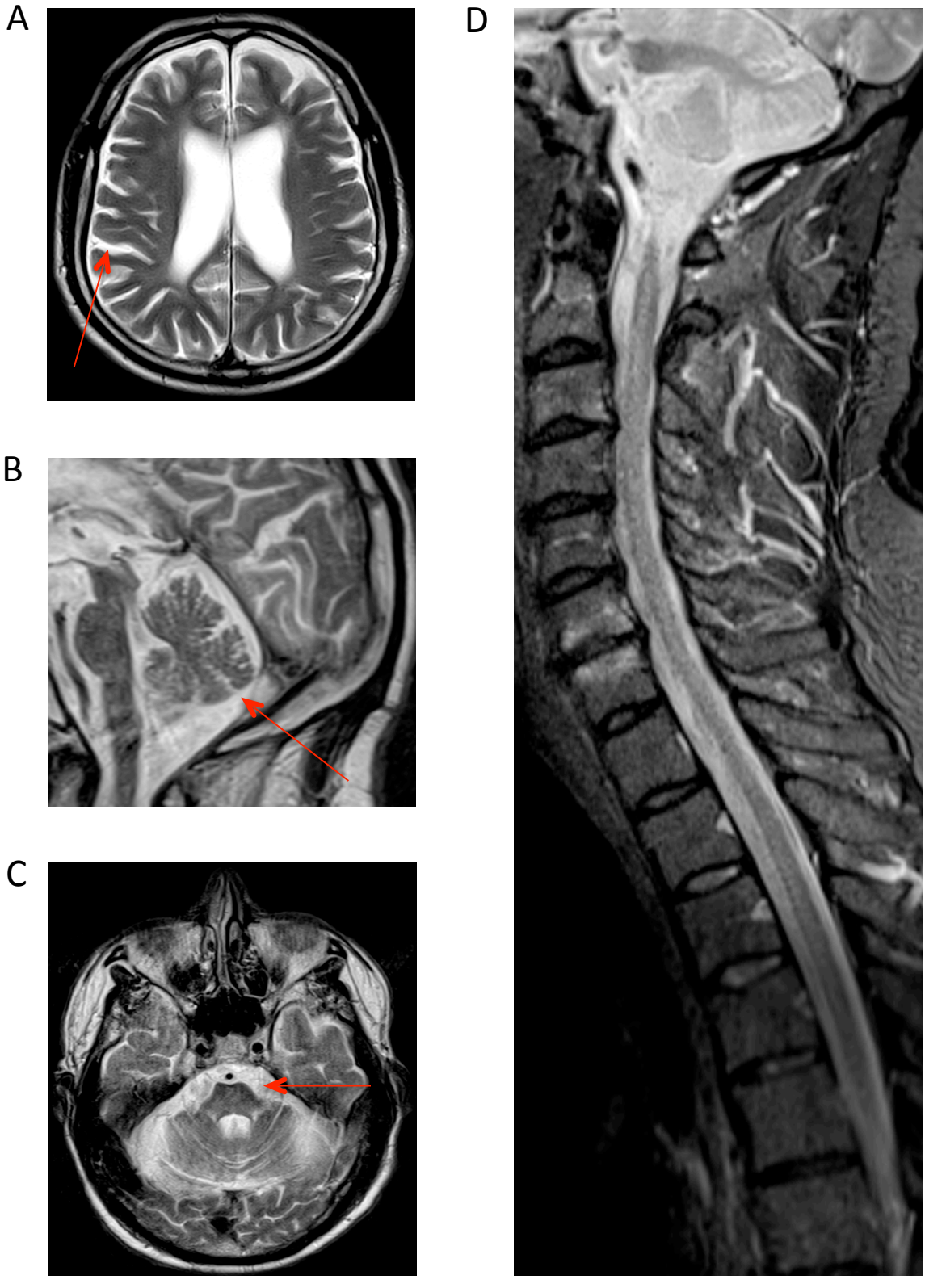


Figure 3.3. T2-weighted MRI of the neuroaxis of B1.
A. Axial image of the cerebrum showing extensive atrophy of the parenchyma indicated by distended internal and external CSF space (red arrow). Discrete white matter lesions were observed in the periventricular areas, as well as atrophy of the

corpus callosum **B**. Sagittal image of cerebellum showing proportional atrophy (red arrow) compared to cerebral atrophy shown in A. No signs of cerebellar vermis agenesis. **C**. Axial image of the pons and cerebellum demonstrating marked pontine atrophy (Red arrow)**. D**. Sagittal image of the spinal cord. No white matter (WM) lesions or myelopathy observed. There were clear degenerative changes of the discus (C2-C7) and discus protrusion, but no signs of spinal stenosis.

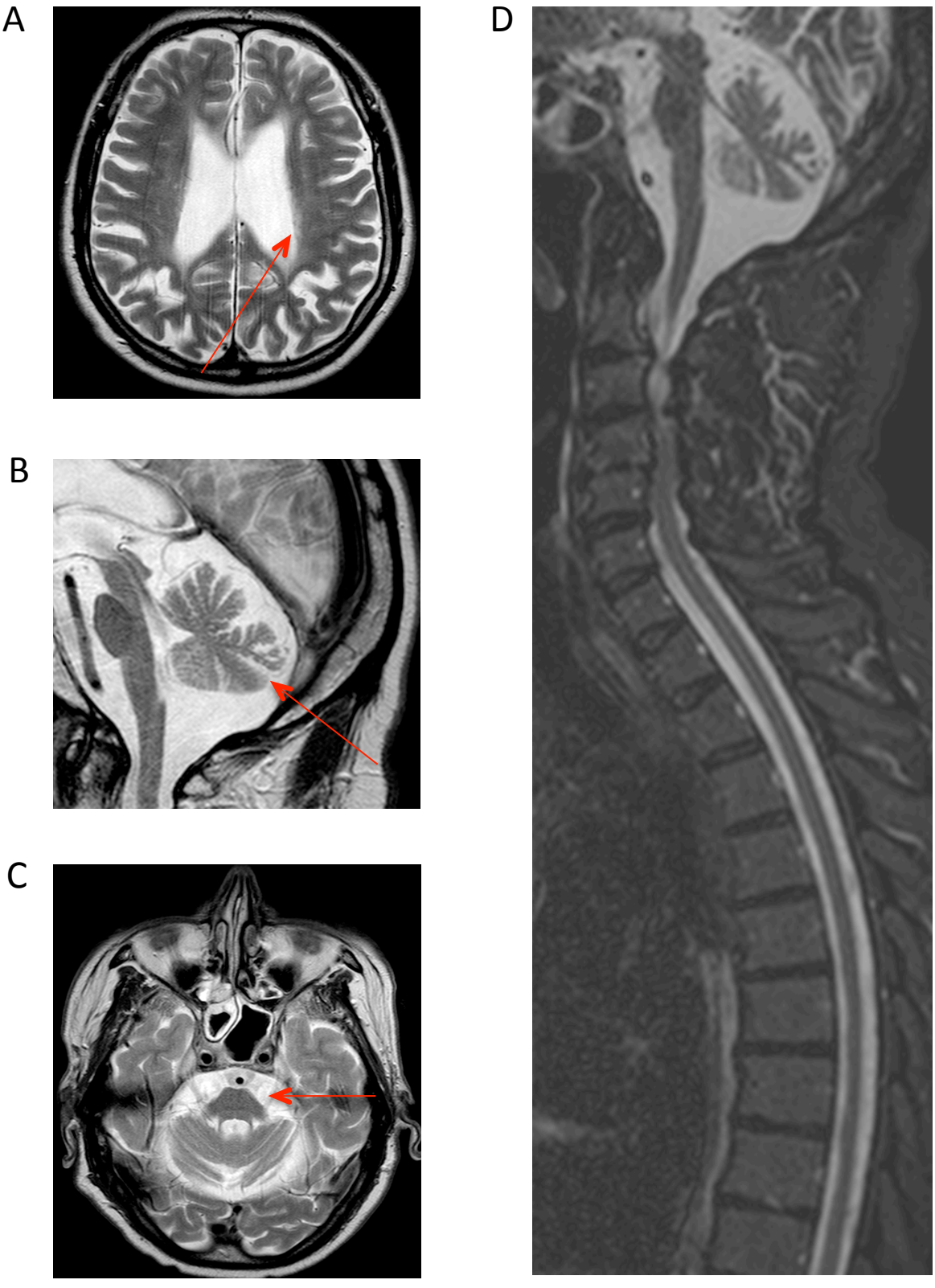


Figure 3.4. T2-weigthed MRI of the neuroaxis of B2. A. Axial image of the cerebrum showing extensive atrophy with marked enlargement of ventricles and the cerebral sulci. Discrete WM lesions were observed in left corpus callosum (red arrow), which was also atrophic. **B**. Sagittal image of the cerebellum showing

marked atrophy, but no signs of cerebellar vermis agenesis. **C**. Axial image of the pons and cerebellum showing extensive atrophy (red arrow). **D**. Sagittal image of the spinal cord in which no white matter lesions were observed. There is extensive disc protrusion at C5 and C6, but no signs of myelopathy.

3.3.2.2 MRI of B2

As in B1, the MRI of B2 shown in Figure 3.4A showed severe global cerebral volume loss that exceeded what was expected for the patient´s age. The atrophy equally involved the cerebellum, the brainstem, and the cortical cerebellar fibres with atrophy of the middle cerebellar peduncles, and there was clear distension of the lateral, third and fourth ventricles reflecting severe atrophy (Figure 3.4B+C). No signs of iron deposition in the basal ganglia were observed. Overall, there was no focal anatomic dominance of the atrophy to indicate a particular neurodegenerative disease. Discrete white matter lesions were observed in the cerebrum (Figure 3.4A). No white matter lesions were observed in the spinal cord (Figure 3.4D). Due to degenerative changes in the discs and vertebra, there was clear narrowing of the spinal canal, but there were no signs of stenosis or myelopathy.

The MRI scans of both brothers thus showed a strikingly similar pattern of severe global atrophy of the cerebrum, the cerebellum and the brainstem. Only very discrete white matter lesions were observed, which called the original diagnosis of PPMS into question. The extensive, global atrophy suggests a primary neurodegenerative disorder, but the MRI results are not in itself indicative of a particular disorder, which might reflect that the scans were conducted many years post disease onset. However, the extensive atrophy of the cerebrum, the cerebellum

and brainstem demonstrated by MRI is entirely consistent with the patients' clinical manifestations. It is noteworthy that no iron accumulation was observed as that has previously been described in patients with variants in *FA2H,* which is one of the genes affected in the brothers (142).

3.3.3 Whole genome sequencing (WGS)

To further clarify the diagnosis, the brothers were recruited to the WGS500 programme (18) in 2013, which was designed to assess how WGS could be used to aid diagnosis of diseases with a likely genetic component. The patients were specifically chosen for the study being related and being atypical for MS, as they are both male, were both diagnosed with PPMS and are negative for all MS-associated HLA class II risk alleles, including *HLA-DRB1*1501*. As the family tree is consistent with an autosomal recessive or X-linked recessive pattern of inheritance, the genomic analysis was specifically directed towards identifying autosomal homozygous, compound heterozygous and X-linked genetic variants. A rare autosomal homozygous frameshift deletion of four base pairs (c.1107_1110del:p.369_370del) in *MLKL* was identified, which causes an insertion of 21 novel amino acids followed by a premature stopcodon resulting in a truncation of the protein. 12.3 kb upstream on the same haplotype on chromosome 16, a homozygous non-frameshift deletion in the adjacent gene, *FA2H*, was identified, which causes a deletion at the 11th phenylalanine amino acid residue (c.32_34del:p.11_12del). Finally, on the X-chromosome, in *AP1S2* a nonsynonymous variant was identified causing a lysine to arginine substitution at residue 55 (c.A164G:p.K55R). Table 3.2 summarises the details of these genes and variants. No

other rare, coding variants were found that had the potential to be consistent with an autosomal recessive or X-linked recessive pattern of inheritance.

Table 3.2. Genes and their variants identified by WGS and their cellular function. SNV (single nucleotide variant).

Gene	*MLKL*	*FA2H*	*AP1S2*
Chromosome	16	16	X
Transcript ID	NM_152649	NM_024306	NM_003916
Variant	Homozygous frameshift deletion c.1107_1110del: > p.369_370del	Homozygous deletion c.32_34:> p.11_12del	Nonsynonymous SNV c.A164G: > p.K55R
Domain affected	Pseudokinase domain	Cytochrome B5 domain	Protein has one single domain
gnomAD	3 homozygous (European non-Finnish)	0	1 heterozygous female
Cellular expression	Ubiquitous (high expression in immune cells)	Ubiquitous (highly expressed in oligodendrocytes)	Ubiquitous
Cellular function	Effector molecule of necroptosis	Enzyme mediating hydroxylation of fatty acids important for myelination	Subunit of the AP1 complex. Transport of vesicles between the trans-Golgi network and endosomes

3.3.3.1 Validation of genetic variants by Sanger sequencing in unaffected family members

The genotype of the unaffected parents and sister was determined by Sanger sequencing to confirm that the genetic variants segregated with disease and to validate their mode of inheritance. Both parents were heterozygous carriers of the nucleotide deletions in the genes encoding *MLKL* and *FA2H,* as shown by the loss of synchronised traces after the deletion in *FA2H* and *MLKL* (Figure 3.5A). The sister was not a carrier, a finding consistent with the idea that the gene variants in the brothers were relevant for the disease. Also, given that the *MLKL and FA2H* genes are adjacent to each other on chromosome 16 and the parents are heterozygous,

whilst the brothers are homozygous, these two nucleotide deletions must be inherited as one haplotype from each parent. As expected, the mother was a carrier of the *AP1S2* variant. The sister was not a carrier of the *AP1S2* variant, and as anticipated the father did not harbour the variant (Figure 3.5B).

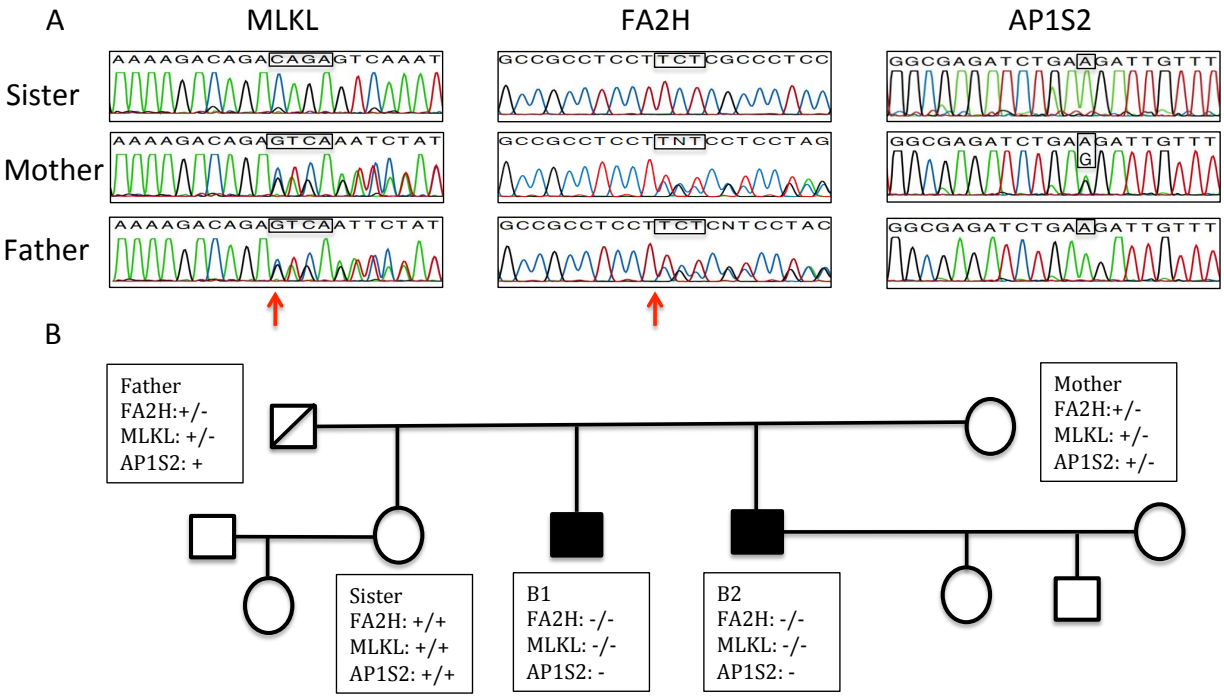


Figure 3.5. Validation of genetic variants in non-affected family members. A. Sanger sequencing of variant sites in *MLKL*, *FA2H* and *AP1S2*. Red arrows indicate loss of trace synchronisation demonstrating heterozygous genotype. **B.** Pedigree of family and genotype status for *MLKL*, *FA2H* and *AP1S2*. + common variant. **-** rare variant. ■: Affected male. □: Unaffected male. **O**: Unaffected female.

3.3.3.2 Assessing allele frequency of identified variants

In the WGS500 programme, rarity of genetic variants (rare variant = <0.5%) was based on filtering against variant frequencies determined by the 1000 Genomes Project. Since then, additional next generation sequencing studies have been launched and the summary data are available through gnomAD (182). Searching this database the homozygous variant in *MLKL* (rs561839347) was found to have an

allele frequency of 0.2724%, which confirmed it as being a rare variant. The variant was also found to be present in the homozygous state in three individuals (European non-finish). As the database does not contain information about the clinical phenotype of the sequenced individuals, it is unclear whether any of these individuals are affected by disease or not. Nor do we know anything about the degree of penetrance of the variant. The *FA2H* variant has not been registered previously, whereas the *AP1S2* variant (rs759073386) is present in heterozygous form in one female (allele frequency 0.0005668 %).

3.3.3.3 Predicted protein-level effects of identified variants

The four-nucleotide deletion (CAGA) in the *MLKL* gene causes a frameshift resulting in 21 novel amino acids followed by a pre-mature stop codon such that the last 102 amino acids of full-length MLKL are missing, as shown in Figure 3.6. Thus, the C-terminal pseudokinase domain is truncated, which is known to play an important regulatory role in the function of MLKL (92). Based on this structural information, the variant would be predicted to be a gain of function variant, however, as the protein is truncated the ultimate result could also be a loss of function.

The non-frameshift, three-nucleotide deletion (TCT) in *FA2H* causes the deletion of a phenylalanine amino acid (F11del) right before the start of the cytochrome b5 heme-binding domain that controls electron transport to the catalytic histidine domain of the hydroxylase(183). As the deletion is outside functional domains, one would not anticipate an effect on enzyme function, but obviously it could not be

ruled out. Finally, the lysine and arginine residues encoded by the common and rare alleles in *AP1S2*, respectively, have similar biochemical properties in that both are hydrophilic and have positively charged side chains, which suggested that the variant was most likely benign.

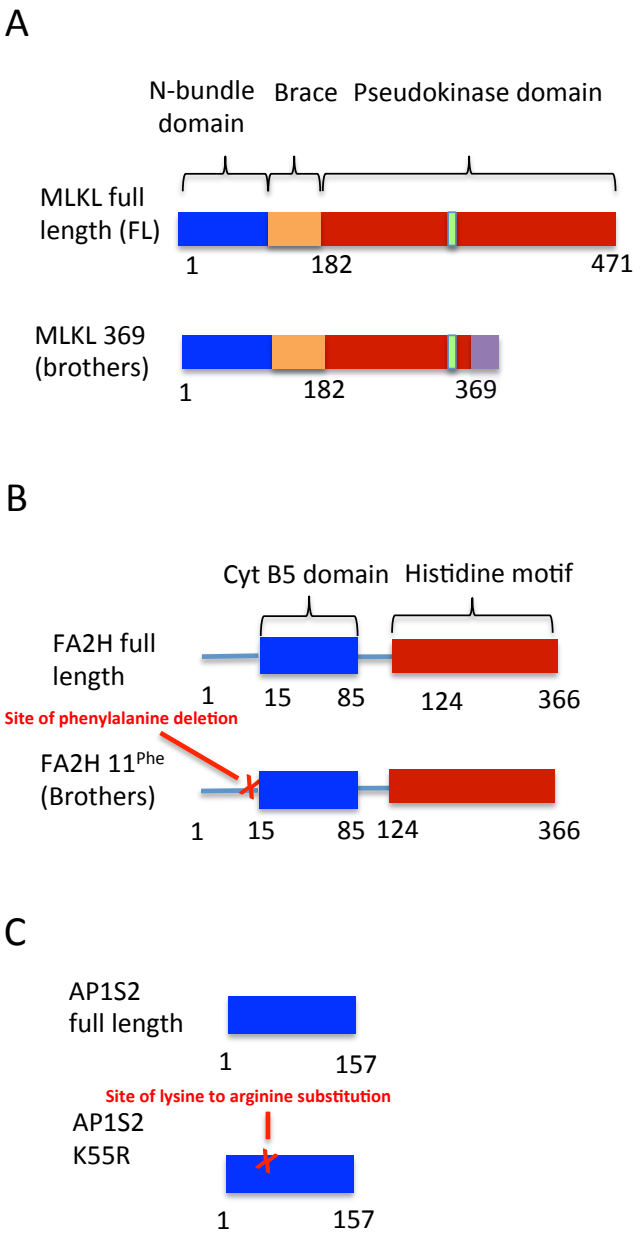


Figure 3.6. Schematic depiction of position of affected amino acids relative to protein domains. Numbers refer to amino acids. **A**. MLKL. **B.** FA2H. **C.** AP1S2.

3.4 Discussion

This chapter describes two brothers diagnosed with PPMS with a clinical presentation of progressive, ascending paralysis with spasticity, ataxia and mental impairment. Their disease course is strikingly similar despite an 11-year difference in disease onset. Even though the disease course is comparable to the average disease course of PPMS, which may vary considerably, the clinical presentation in these two patients has features that are atypical for MS. The lack of sensory symptoms as well as the presence of fasciculation's in B1 are not part of the clinical picture in MS, whereas they are often seen in patients with ALS, in whom they are due to degeneration of motor neurons. The initial presentation of slowly progressive, lower limbs spastic paresis could be suggestive of HSP, though HSP patients often present with symmetrical symptoms, and asymmetrical presentation would hint at a different aetiology. Finally, the striking similarity of symptoms and clinical findings between B1 and B2 is unusual in MS in which the heterogeneity of symptoms is more typical, because the anatomical sites of immune infiltration are disseminated as if due to a more random disease process.

The MRI scans showed severe global, atrophy, which is abnormal for the age of the patients. The white matter lesions observed by MRI in these patients were very discrete and hence neither of the brothers would fulfil the currently used McDonald criteria for diagnosing PPMS (30). This observation was surprising given that MS lesions are typically visible on MRI brain scans of PPMS patients, even at a late stage. The extensive brain atrophy is, however, not suggestive of a particular neurodegenerative disorder, and the MRI scans are thus not conclusive from a

diagnostic point of view. What thus a remains clear, is that whatever pathogenic process has caused their disease, has severely impacted the cerebrum, cerebellum and brainstem, which corresponds well to their clinical presentation.

Based on the atypical disease presentation, the similarity of the disease course and presentation between the patients, the lack of the strongest MS-associated genetic determinants, and the pedigree characterised by male predominance of disease it was suspected that a monogenic disorder might be an underlying factor in the disease of these two patients. WGS and segregation analysis could in that context possibly confirm the presence of pathogenic variants (in genes with a known disease mechanism) or identify variants in genes not previously known to be associated with disease.

3.4.1 MLKL

The four-nucleotide frameshift deletion (rs561839347) in *MLKL* shortens the protein by 102 amino acids and thereby causes a truncation of the MLKL pseudokinase domain. As a protein length-changing variant, the variant would be predicted to be pathogenic with a moderate level of evidence(171). If the variant causes degradation of the transcript by non-sense mediated decay or protein misfolding thus causing a protein knockout, the predicted level of pathogenicity would increase to very strong. *MLKL* is not a gene with a known disease mechanism, however, as there are currently no case reports of patients with *MLKL* variants, the level of evidence for pathogenicity could be considered to be somewhere between moderate and very strong (171). The presence of three individuals listed in the

gnomAD database, who are homozygous for the rare allele of rs561839347, has no formal implication for the level of evidence according to the ACMG guidelines as the allele frequency is <0.5 % and the variant is therefore defined as rare. Whilst it would have been informative to know the age and disease status of these three individuals to better gauge the impact of the variant, such information is currently not available through the gnomAD database.

As described in Chapter 1, MLKL plays a key role in necroptosis, which is known to be implicated in neurodegenerative diseases such as MS (112), ALS (122) and Alzheimer´s disease (113, 130) among others. Recognising that the brothers suffer from a neurodegenerative disease that to some extent overlaps clinically with these diseases led to the hypothesis that the variant in *MLKL* could contribute to disease pathology, thereby warranting an investigation of its functional consequences.

3.4.2 FA2H

The FA2H 11^{Phe} variant affects an amino acid located upstream of the cytochrome b5 domain. However, given its close proximity to the functional domain, it was difficult to gage whether the variant would impact 2-hydroxylase activity. The FA2H 11^{Phe} deletion has not been detected among the sequenced individuals in the gnomAD database, which would moderately support a pathogenic effect of the variant. Regarding this category of evidence, the ACMG notes two caveats: 1: Insertions and deletions may be poorly called by next-generation sequencing. 2: Many benign variants are unique to individuals and families and absence in a race-matched population will therefore not be considered sufficient evidence for

pathogenicity (171). Given the involvement of FA2H in HSP as described in Chapter 1, this variant looked intuitively like a good candidate to explain the disease. However, according to the ACMG guidelines (171), the clinical phenotype of the brothers is not in itself supporting a pathogenic effect of the variant in *FA2H*. Overall, a pathogenic effect of the FA2H 11^{Phe} deletion could not be ruled out based on the clinical and population data, and consequently functional studies were therefore needed, which are presented in Chapter 6.

3.4.3 AP1S2

Computational analysis of the K55R substitution in AP1S2 using the Polyphen-2 software program scored the variant as possibly damaging, also noting that the amino acid residues in question have similar biochemical properties. As explained in Chapter 1, all publically available patient cases with *AP1S2* variants have been reported to harbour either protein truncating variants or large deletions, in which a functional effect of the residual protein is highly unlikely, such that the patients are effectively AP1S2 knockouts. These observations would support the K55R substitution in AP1S2 as being benign according to the ACMG guidelines. In addition, the phenotypes of the reported cases with *AP1S2* variants are characterised by childhood onset intellectual disability, facial dysmorphism, basal ganglia disease and cerebellar vermis agenesis, none of which are clinical features consistent with the brothers' disease.

Mice deficient in *AP1S2* are phenotypically characterised by lipodystrophy (158) and hippocampal deficiencies, demonstrated by reduced spatial learning and memory when challenged with a Morris water maze (157). The brothers do not share these phenotypic characteristics. However, it should be noted that *AP1S2* KO mice represent the extreme phenotype. It could therefore not be ruled out that the K55R substitution in AP1S2 could exert a subtle effect on protein function, given that AP1S2 plays a role in the CNS. Consequently, a more in-depth *in silico* analysis was carried out based on amino acid conservation, the AP-1 crystal structure and known binding partners. This work is presented in Chapter 6.

3.5 Chapter conclusions

Overall, WGS in conjunction with bioinformatic analysis and population data could not definitely identify a single causal variant that could allow us to assign the two brothers to a particular monogenic disorder. Re-evaluation of the clinical data, the MRI scans and WGS suggested that the brothers suffer from a neurodegenerative condition that shares clinical characteristics with PPMS, HSP and ALS. Based on these results and considerations we hypothesised that the haplotype on chromosome 16 containing *MLKL* and *FA2H,* for which the brothers are homozygous, contributes to their disease. Based on the theoretical impact of the variants in *MLKL* and *FA2H* we therefore wanted to use *in vitro* experiments to detect possible effects of the amino acid deletion in *FA2H* and to delineate, if possible, new disease mechanisms in the case of *MLKL.*

Chapter 4. Functional analysis of the disease-associated MLKL 369 variant in cell lines

4.1 Introduction

In order to explore the effect of the 4-nucleotide deletion in *MLKL* of the brothers, it was necessary to study the variant and any downstream effects in isolation from the genetic background. A cell line transfection system would enable the examination of MLKL variant proteins as the single source of variation being tested. As described in Chapter 1, section 1.4.2, MLKL is the effector molecule in the necroptosis pathway. Indeed the mere overexpression of MLKL in cell lines causes cell death, indicating that MLKL can exert its function independently of upstream regulators (184). In 2014 it was shown that removing the MLKL pseudokinase domain causes the molecule to loose the autoinhibitory effect on N-bundle domain (92). This in turn causes the molecule to be in a constitutive open conformation, which leads to increased cell death compared to the native form of MLKL when the mutated constructs are expressed in cell lines (91).

As described in Chapter 3, the frameshift deletion in *MLKL* causes a truncation of the pseudokinase domain in MLKL, whereby 21 novel amino acids are introduced at the C-terminal end of amino acid 369, which is followed by a premature stop codon. The truncated MLKL protein of B1 and B2 (the brothers) is from here on onwards denoted as MLKL 369. The site of the variation begged the question of whether the remaining part of the MLKL pseudokinase domain in MLKL 369 would be able to exert adequate inhibition of the MLKL N-bundle domain to prevent cell death from occurring on a constitutive basis.

Given that the RIPK3 phosphorylation site at threonine 357/ serine 358 was intact it was possible that MLKL 369 was still regulatable and MLKL 369 would therefore function like MLKL-full length. Another possibility could be that the remaining part of the MLKL pseudokinase domain is not functional, which would cause increased necroptosis and thus increased cell death. No computational modelling would be able to convincingly answer this question, so we employed an *in vitro* approach that was based on constructs containing full-length MLKL (wild type) and the disease-associated MLKL 369. To specifically assay any residual function of the truncated pseudokinase domain in MLKL 369, a third construct was designed that lacked the pseudokinase domain completely. This construct is termed MLKL 182, as shown in Figure 4.1. The MLKL 182 construct has previously been shown to cause increased cell death compared to MLKL full-length and would thus be able to serve as a positive control (91).

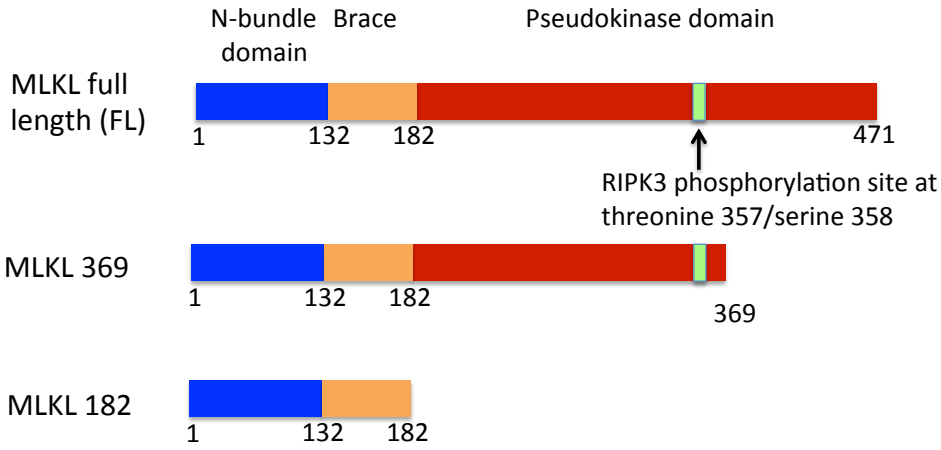


Figure 4.1 Schematic representations of MLKL constructs used to investigate the effect of MLKL 369 variant. Boundaries between domains were identified based on mouse crystal structure of mouse MLKL (PDB ID: 4BTF, 2.604 Å(91)). Numbers refer to amino acid.

There are currently no available cell death assays that specifically distinguish necroptosis from other forms of cell death, and necroptosis has therefore been studied using classical cell death assays such as PI staining or lactate dehydrogenase release. The specificity of necroptosis in cell death assays can be demonstrated by genetic or pharmacological manipulation of MLKL and by blocking apoptosis pharmacologically.

PI is an intercalating agent that emits fluorescence when it reacts with DNA, and it can thus function as a marker of nuclear permeabilization during cell death. In the experimental setup we chose to combine this dye with annexin V, which stains phosphatidylserine exposed on the cell membrane during the earlier stages of apoptosis or necroptosis (105). Depending on the stage of cell death, cells may be double positive for PI and annexin V. The fluorescence can be quantified using flow cytometry, which thus provides measure of cell death at a single time point. To capture the kinetics of cell death over time we therefore supplemented the experimental setup with the Incucyte Zoom live cell imaging system that relies on the IncuCyte® Cytotox Red Reagent to differentiate live cells from dead cells. In addition, it allows for the quantification of cell death directly inside the well and does not require any handling of the cells that may introduce artefacts.

4.2 Chapter aim

The purpose of this chapter is two investigate whether the frameshift deletion in *MLKL*, identified in the two brothers, has an impact on the known functions of

MLKL, specifically relating to cell death. Given the evidence suggesting that necroptosis is activated in the CNS during disease described in Chapter 1 (section 1.4.4), it was particularly important to investigate whether the variant in *MLKL* causes a loss or gain of function. Furthermore, it was important to experimentally determine whether the disease associated variant in *MLKL* confers an impact on the expression of the mutant form of MLKL. Finally, it aims to determine whether any downstream genotype dependent differences of MLKL 369 would be reversible by the MLKL inhibitor, necrosulfonamide (NSA).

4.3 Results

HEK293 cells were chosen for the *in vitro* analysis as they have previously been used to study the mechanisms of necroptosis (86) and this cell line functioned as a good transfection host, showing transfection efficiencies of MLKL FL of approximately 60% using Lipofectamin 3000.

4.3.1 Assaying the effect of MLKL 369 overexpression on cell death using PI/annexin V staining

To capture possible differences in the dynamics of cell death upon transfection with MLKL constructs, a time course experiment was conducted as shown in Figure 4.2. The cells were harvested with 2-4 hours intervals post transfection and stained with PI and annexin V. After 6 hours one could begin to observe a trend for increased cell death that could be differentiated from empty vector transfected cells. With respect

to PI stained cells, the increased degree of cell death was highest 8 hours post transfection, at which point approximately 60% of MLKL transfected cells were positive. At the 8-hour time point one could detect a trend of differential degrees of PI and annexin V % positivity between MLKL constructs. Consequently this time point was chosen to examine whether the MLKL 369 construct caused an altered degree of cell death.

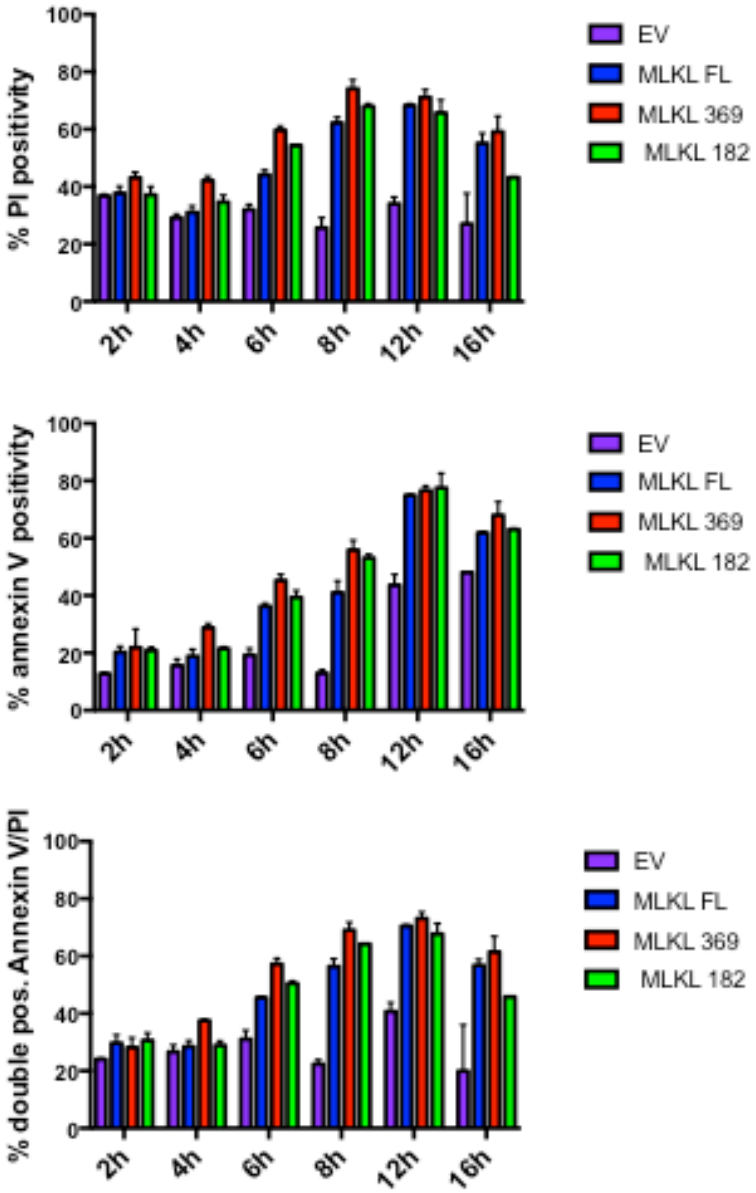


Figure 4.2. Time course experiment of PI/Annexin V stain. Annexin V and PI % positivity were measured for each time point in duplicates. EV, empty vector.

Figure 4.3 shows the degree of annexin V and PI positivity at 8 h post MLKL transfection measured in three independent experiments. The gating strategy is shown in Figure 4.3 A. HEK293 cells transfected with MLKL 369 showed a significant 10% increase in PI/annexin V % positivity compared to MLKL FL (Figure 4.3 B-D). No significant difference was observed between MLKL 369 and MLKL 182.

The majority (approximately 60%) of transfected cells were positive for PI and annexin V indicating that the cells were dying already at 8 hours after transfection. It should be noted that across the repeated experiments, the cells transfected with empty vector showed a roughly 40% positivity for annexin V and PI, indicating a relatively high degree of background cell death, which may have been related to manual handling of the cells required to perform the annexin V and PI staining.

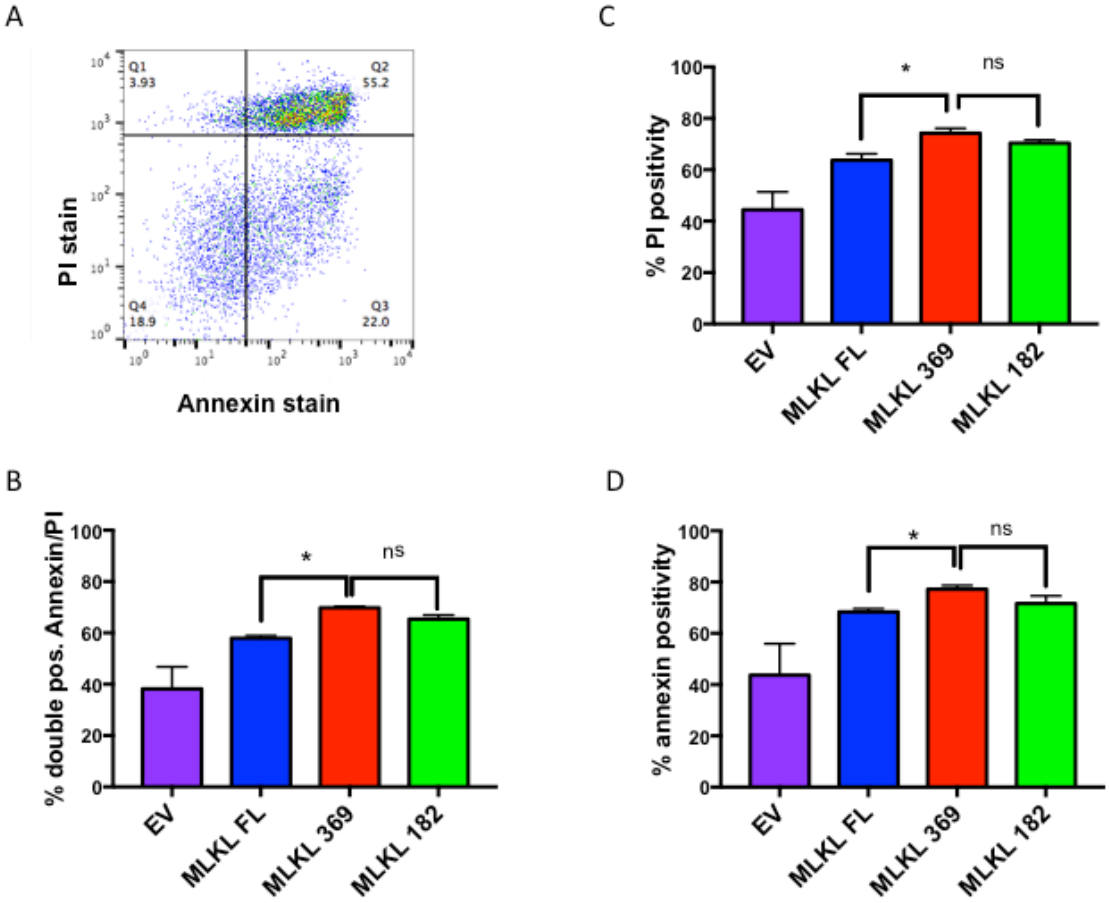


Figure 4.3. Cell death assayed by propidium iodide and annexin V staining 8 h post MLKL transfection. A. Representative plot showing gating strategy of HEK293 cells stained with PI and annexin V. Q2 corresponds to double positive annexin/PI positivity **(B)**, whereas Q2 +Q3 and Q1+Q2 relates to PI **(C)** and **(D)** annexin V % positivity, respectively. Shown are the mean results ± SEM of three independent experiments. Each experiment was carried out in quadruplicate wells. Paired t-test: * = $p < 0.05$.

Nevertheless, the overall results of MLKL-induced cell death in HEK293 cells using PI and annexin V suggested that the lack of a functional pseudokinase domain in MLKL 369 caused the molecule to be overactive with increased cell death as a result.

Inhibition of the cell death caused by MLKL transfection was also attempted by culturing the cells with the MLKL-inhibitor necrosulfonomide (NSA) during the cell death experiments using Incucyte and PI/Annexin staining. NSA prevents the oligomerisation of MLKL prior to pore formation in the cell membrane and hence cell death. As NSA thus targets the brace region of MLKL it should theoretically exert a similar effect on MLKL FL, MLKL 369 and MLKL 182. However, NSA increased the background cell death substantially indicating a toxic effect of the molecule, which limited its use in this cell death assay.

4.3.2 Assaying the effect of MLKL overexpression on cell death using live-cell imaging

To verify the result of an increased degree of cell death observed upon MLKL 369 transfection we used the Incucyte Zoom technology, as it allowed for the quantification of non-manipulated cells in real time. Like PI, the Incucyte Cytotox Red Reagent emits red fluorescence during the chemical reaction with DNA and thus provides a measure of permeabilised cells undergoing cell death. Figure 4.4 A-D shows representative images of HEK293 cells in a 24-well plate, 14 hours post transfection with the indicated MLKL constructs.

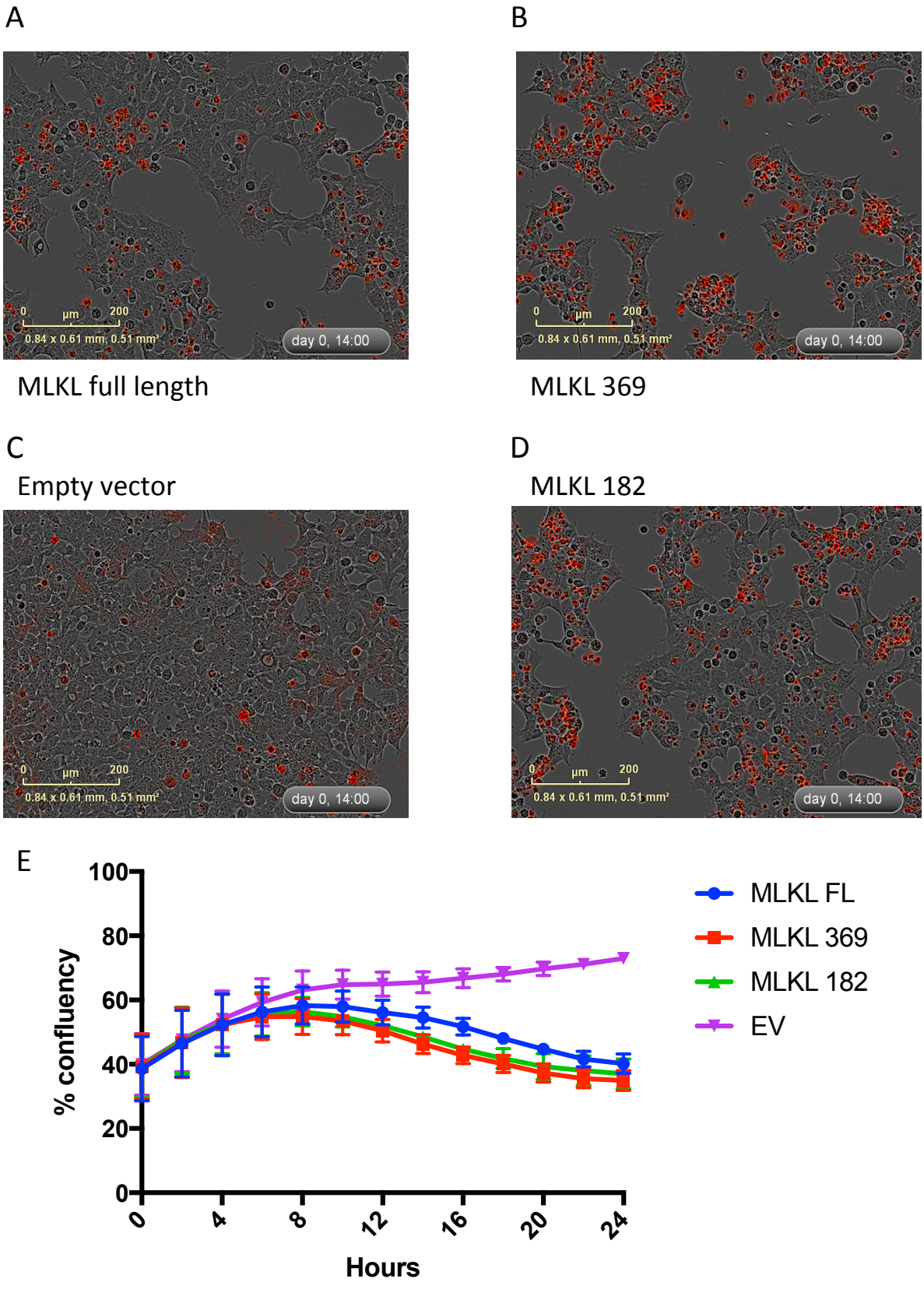


Figure 4.4. Incucyte analysis of cell death and confluency in real time upon MLKL transfection. A-D. Live-cell images (10x) of HEK293 cells transfected with MLKL full length (**A**), MLKL 369 (**B**), empty vector (**C**) and MLKL 182 (**D**) at 14 h

post transfection. Dead cells are stained with IncuCyte™ Cytotox Red. Scale denotes 200 μm **E.** Quantification of cell confluency upon MLKL transfection. Confluency was measured by Incucyte Zoom software. Experiment carried out in triplicate. Shown are the mean values of three independent experiments ± SEM.

The cells were imaged for confluence and red fluorescence every 2 hours over a 24-hour period immediately following transfection. In contrast to cells transfected with empty vector, we observed a clear decrease in confluency in wells with cells transfected with MLKL constructs as shown in Figure 4.4E. Similarly, the pseudopodia of cells transfected with any MLKL construct seemed to be retracted compared to empty vector-transfected cells.

The red fluorescence omitted from cells undergoing cell death was quantified by the Incucyte software as the total red object area of the well. To account for any potential differences in cell proliferation or cell number per well, each well measurement was normalised to the percentage confluency, as suggested by the manufacturer, Essence Bioscience. Transfection with any MLKL construct resulting in overexpression of MLKL protein caused a clear increase in cell death compared to cells transfected with empty vector (EV) as shown in Figure 4.5. From 16-22 hours post transfection one could observe a statistically significant increase of approximately 30% in the degree of cell death in cells transfected with MLKL 369 compared to MLKL full-length (MLKL FL) (p-values = 0.0231-0.0430). Similarly, there was a 30% increase in cell death of cells expressing MLKL 182 compared to MLKL FL from 18-24 hours, which was statistically significant (p-values = 0.0079 – 0.0201). The observed difference between MLKL 182 and MLKL FL was comparable to data from the literature (91) and indicated that the assay had an acceptable

sensitivity to detect differences in cell death dependent on the presence or absence of autoinhibition exerted by the MLKL pseudokinase domain. The MLKL 369 did not cause a significantly different degree of cell death compared to MLKL 182 throughout the experiment (P >0.7898). This observation suggested that the frameshift deletion in the MLKL pseudokinase domain of B1 and B2 prevents autoinhibition of the N-bundle domain, a failure that ultimately causes necroptosis to be increased.

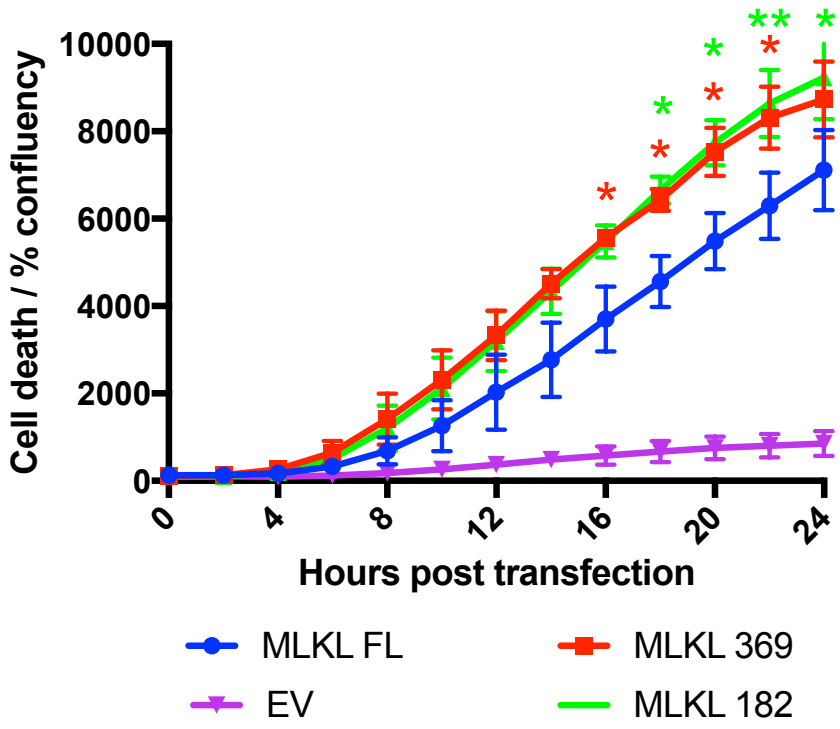


Figure 4.5. Cell death upon MLKL transfection. Cell death measured in HEK293 cells upon transfection with indicated constructs over 24 h using Incucyte. Each experiment was carried out in triplicate wells. Shown are the results ± SEM, n=3. Two-way ANOVA with Tukey's multiple comparisons test* = $p < 0.05$ and ** = $p < 0.005$. p-values relate to the statistical comparison of MLKL 369 and MLKL 182 relative to MLKL FL. MLKL FL = full-length, EV = empty vector.

4.3.3 MLKL 369 variant analysed by western blotting

The increased cell death observed for MLKL 369 suggested that the protein was functional in mediating necroptosis, which was expected given the sustained integrity of the N-bundle domain. To further examine the integrity of the MLKL 369 protein mediating the increased cell death, we characterised the protein in transfected HEK293 cells by western blotting using a monoclonal MLKL antibody clone (3H1). The antibody was raised against the murine aa sequence CQPASWQQEDRQDAEED of the MLKL N-bundle domain. The corresponding human peptide sequence is SQGASWAQEDQQDADED (aa 127-144) located at the N-bundle domain of MLKL and the antibody would thus theoretically recognise MLKL FL, MLKL 369 as well as MLKL 182. The HEK293 cells were harvested for analysis 16 h post transfection as cell death was occurring at this time point based on the Incucyte data (Figure 4.5). MLKL FL was identified as expected at 54 kDa, and MLKL 369 and MLKL 182 were observed around 40 kDa and 20 kDa, respectively, as expected from the amino acid length and as shown in Figure 4.6A. The blot also revealed an approximately 2/3 reduction in the band intensity of MLKL 369 compared to MLKL FL ($p = 0.0049$) (Figure 4.6B). The band intensity of MLKL 182, was significantly lower than that of MLKL 369 ($p = 0.0283$), which was unexpected given the equal degree of cell death observed in the Incucyte experiments. This finding could suggest that the MLKL 182 construct might have a slightly stronger effect on cell death, which may not be detectable with other assays. Overall, these results are consistent with the results of other investigators using the same MLKL antibody clone showing reduced band intensity of MLKL 182 compared to MLKL FL (91) in the lysates of transfected cells.

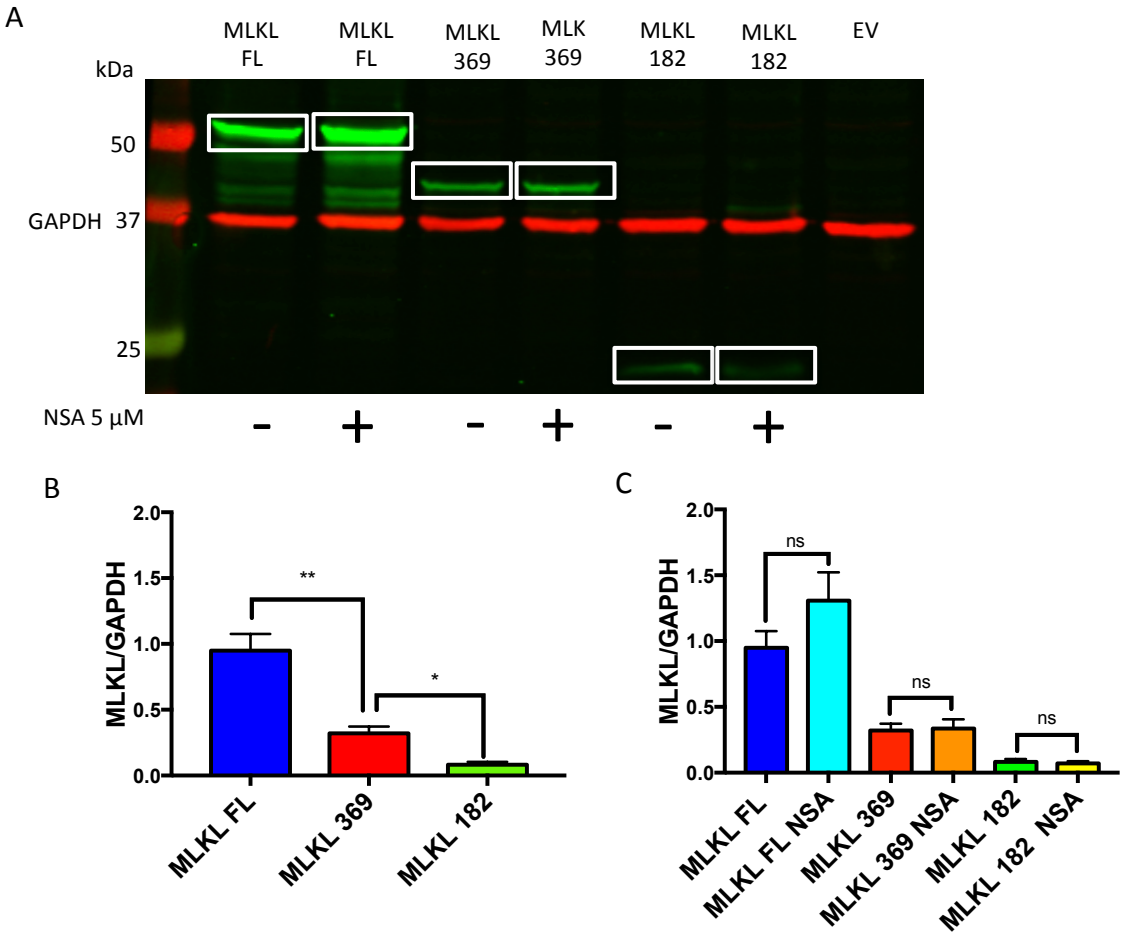


Figure 4.6. MLKL constructs analysed by western blotting A: Western blot of MLKL transfected HEK293 cells 16 h post transfection. **B** Densitometry of fluorescence intensity of MLKL bands from MLKL transfected HEK293 cells in white boxes quantified by LI-COR software. Shown is the mean intensity of MLKL normalised to GAPDH in three independent experiments ± SEM. The band intensity of MLKL 369 was significantly lower compared to MLKL full-length. MLKL 182 was significantly lower compared to MLKL 369, n= 3. Paired t-test. **C.** Densitometry of MLKL bands normalised to GAPDH from HEK293 cells treated with NSA 5µM.

These genotype-dependent differences in the apparent expression of MLKL could be due to the differential effects of MLKL FL, MLKL 369 and MLKL 182 on cell death. Cells expressing these constructs would undergo cell death and would thus not be detected by western blotting. The increased cell death caused by MLKL 369 and MLKL 182 would thus result in fewer MLKL expressing cells detectable by the MLKL antibody. To further explore this possible explanation, a rescue experiment was

used based on the usage of the MLKL inhibitor NSA. Even though this compound resulted in increased background cell death, it could possibly have a specific effect on MLKL mediated cell death. By inhibiting MLKL induced cell death one would expect an increased MLKL expression in cells treated with NSA.

No significant effect of increased MLKL expression upon culturing in 5 μM NSA (81) during transfection could be observed for any MLKL construct, however, though a trend for increased band intensity was observed for MLKL FL (Figure 4.6C). The result could either reflect a genuine incapability of NSA in inhibiting MLKL during transfection or a limited sensitivity western blotting in capturing subtle differences in MLKL expression. The latter option would be consistent with the subtle trend of increased expression observed for MLKL FL cultured in NSA (Figure 4.6C).

4.3.4 MLKL 369 variant analysed by flow cytometry

Combining the observation of increased cell death as a function of MLKL 369 expression with the reduced band intensity observed by western blotting suggested that there might be a relative difference in the tolerable expression of MLKL FL and MLKL 369 before a cell would undergo necroptosis. To further assay a possible differential tolerance to the expression of MLKL constructs we turned to flow cytometry as it could provide a relative measure of expression on a per cell basis rather than average expression in the cell lysate as measured by western blotting. As an N-terminal tag has been reported to interfere with capacity of MLKL to induce cell death(92), we attempted to use the monoclonal MLKL antibody (clone 3H1) to evaluate MLKL expression by flow cytometry.

The monoclonal MLKL antibody (clone 3H1) has previously been used only in western blotting and immunocytochemistry, whereas its application in flow cytometry has not been described. To validate the utilisation of the MLKL monoclonal antibody clone for flow cytometry we used an MLKL construct containing N-terminal HA tag. Figure 4.7 shows a plot of an intracellular co-staining using an anti-HA-tag fluorescent antibody and the MLKL monoclonal antibody (clone 3H1) of HEK293 cells 8 hours post transfection. From the plot, one can observe that cells expressing the HA-MLKL construct were positive for HA as well as MLKL expression, indicating that the monoclonal MLKL antibody recognised the epitope in the brace region of MLKL when used in flow cytometry.

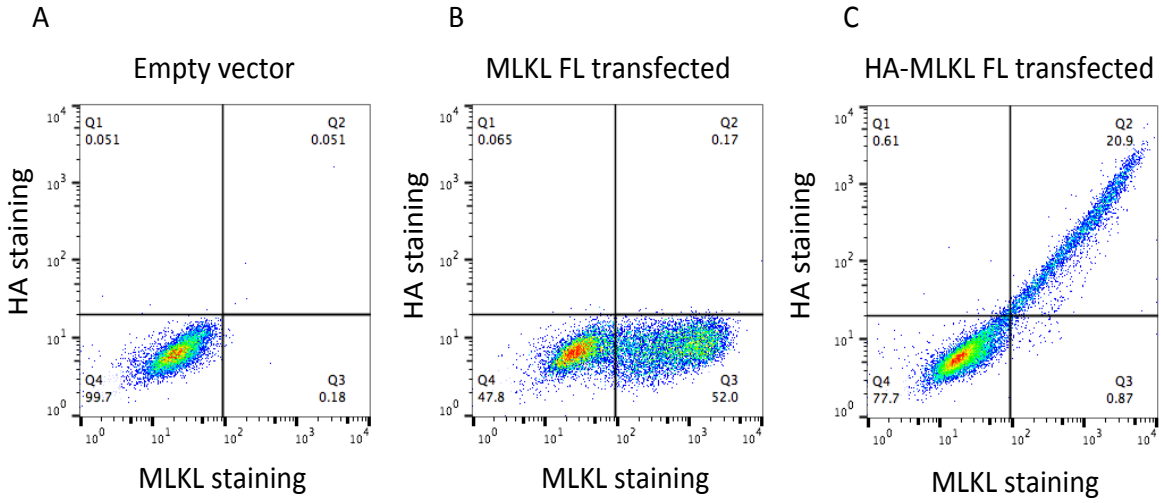


Figure 4.7. Validation of monoclonal MLKL antibody (clone 3H1) for use in flow cytometry. HEK293 cells were transfected with empty vector (**A**), FL MLKL construct (**B**) and MLKL FL containing an N-terminal HA tag (**C**). The plot in **C** demonstrates double positivity of MLKL and HA indicating that the MLKL antibody recognises the N-terminal human epitope at the N-bundle domain aa 127-144.

4.3.4.1 Lower tolerable expression of MLKL 369

Given that the MLKL antibody was working well for flow cytometry it was possible to conduct the subsequent analyses using untagged constructs. The 8 hour time point was chosen to compare the results of MLKL staining to the PI/annexin V data. From the initial plot of MLKL FL transfected cells (Figure 4.8B) one could observe a clear positive population of roughly 50%, and an additional population of cells expressing a higher degree of MLKL, approximately 9% of total cells. The gating strategy shown in Figure 4.8A was used to capture these two populations and focussed on the percentage total positive cells and the high expressing cells, denoted MLKL ++ subset gate positive cells. The MLKL negative gate was set according to the brightness of the empty vector transfected HEK293 cells.

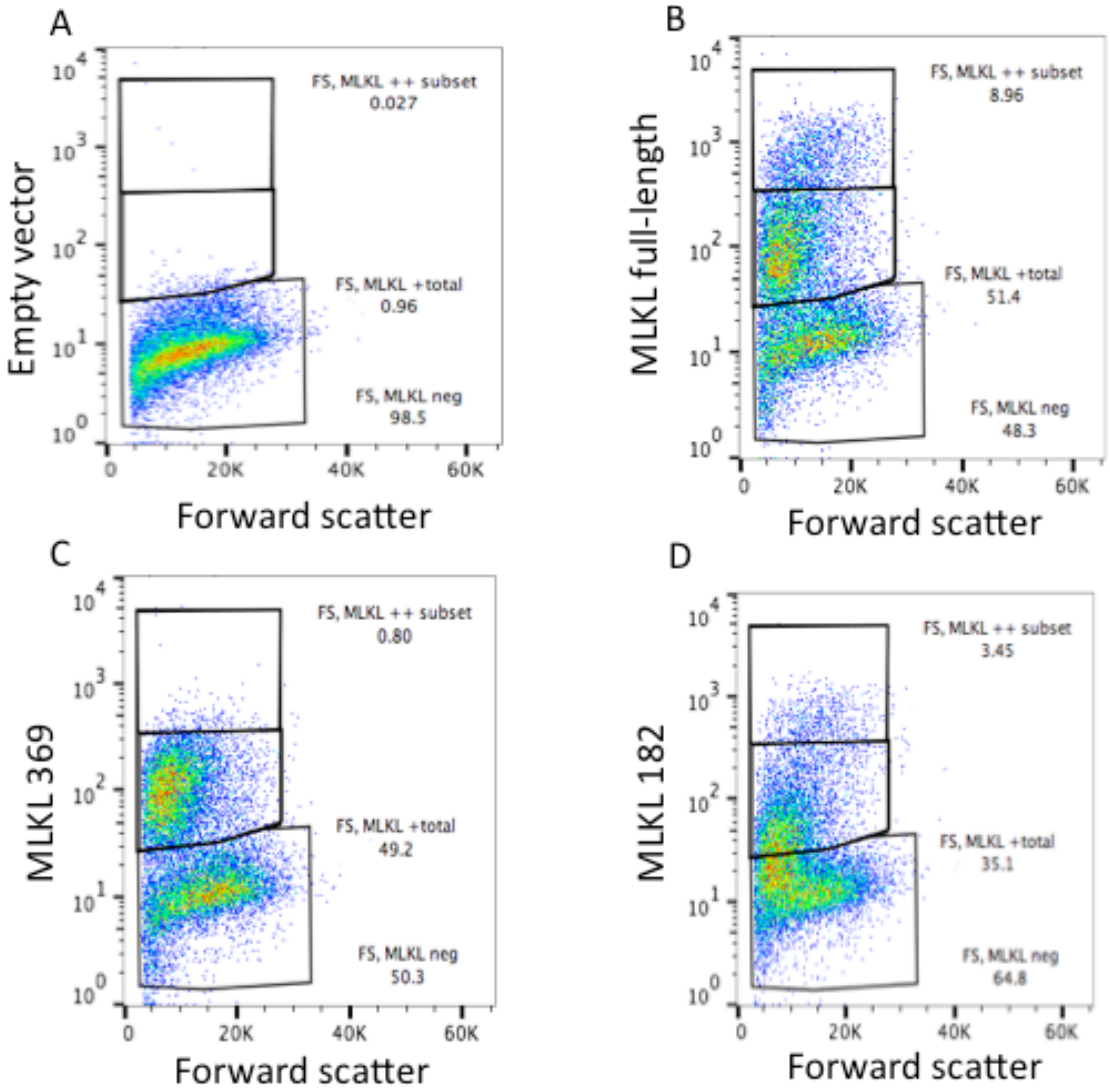


Figure 4.8 Gating strategy for analysing MLKL transfected HEK293 cells. A: HEK293 cells transfected with empty vector. **B-D:** plots showing representative staining patterns of MLKL expression 8 hours post transfection.

The percentage of total cells expressing MLKL was significantly reduced in cells expressing MLKL 369 compared to MLKL FL (Figure 4.9A), with approximately 60% of cells being MLKL FL positive and roughly 50% being positive for MLKL 369. The reduction in MLKL 369 expression was primarily caused by a marked and significant reduction in cells expressing high amounts of MLKL 369 (MLKL ++ cells <1%) as shown in the diagram in Figure 4.9B. Similarly, one could observe a marked

reduction in total % of cells expressing MLKL 182 compared to MLKL FL and MLKL 369. The majority of MLKL 369 expressing cells were located as a relatively well defined population in the lower quadrant of MLKL positive cells, similar to MLKL FL. In contrast, cells transfected with MLKL 182 were more diffusely expressed, though clearly reduced in expression.

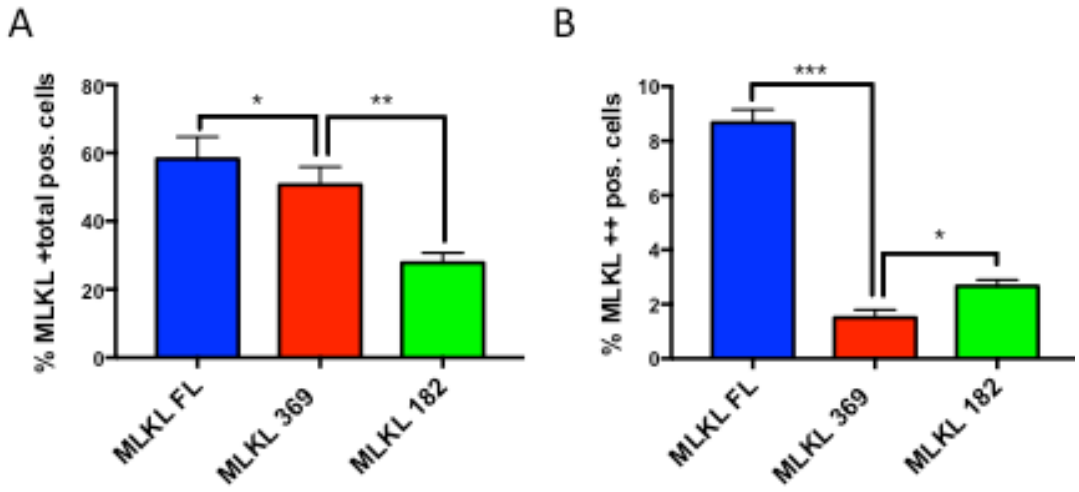


Figure 4.9. Flow cytometry analysis of MLKL transfected HEK293 cells 8 hours post transfection. A: Relative MLKL % positivity of total positive cells. **B**: % of positive cells in MLKL++ subset gate. Experiment carried out in duplictes. Shown is the mean % positivity ± SEM. n = 5. Paired t-test.

Overall, the flow cytometry data on MLKL expression were consistent with the western blot data, showing that upon transfection of MLKL 369 and MLKL 182 into HEK293 cells, the MLKL protein was significantly less expressed. However, flow cytometry also proved to be a more sensitive method for assaying which cell populations were driving relative differences in MLKL expression. Importantly, the method revealed a reduced level of MLKL 369 expression, as <1% of cells were present in MLKL++ subset gate. Given that MLKL 369 and MLKL 182 causes increased cell death, this marked reduction in expression most likely reflects that

cells have a reduced tolerability of MLKL 369 and MLKL 182 expression vs. MLKL FL expression, i.e. cells expressing MLKL 369 and MLKL 182 are more prone to undergo necroptosis and will therefore no be able to reach high MLKL expression.

4.3.4.2 Reduced MLKL expression, reflecting cell death, is partly reversible by NSA

The increased sensitivity of flow cytometry to measure tolerable MLKL expression levels begged the question of whether the method would allow for the detection of a protective effect of MLKL inhibitor NSA (5 μM) in the culture medium during MLKL transfection. One could therefore hypothesise that a protective effect of NSA would result in higher degree of MLKL percentage positivity in cells, as translated MLKL would be prevented from the oligomerisation necessary to induce necroptosis. If NSA would be effective, MLKL could potentially accumulate in cells upon transfection, but without causing cell death.

The gating strategy shown in Figure 4.8 was also applied for this experiment. As shown in figure 4.10A, NSA treatment during MLKL transfection did not cause increased percentage positivity in the total amount of MLKL FL transfected cells. However, one could detect a significant 5% increased expression in MLKL ++ subset population (Figure 4.10B), thus confirming the trend observed in western blot analysis of NSA treated MLKL FL transfected cells (Figure 4.6C). A more pronounced effect of NSA was detected in MLKL 369 and MLKL 182 transfected cells, as the percentage of cells in the total positive gate was significantly increased when compared to untreated cells. No significant differences in total MLKL

expression between MLKL FL, MLKL 369 and MLKL 182, could be detected upon NSA treatment in which all MLKL showed an approximate 50% total positivity. This finding indicated that NSA was able to inhibit MLKL induced cell death and thus equalise the MLKL expression, independently of the presence of a functional MLKL pseudokinsase domain (Figure 4.10A). The inhibitory effect of NSA on MLKL induced cell death was most prominent for MLKL 182 in which NSA treatment also resulted in a significant increase from 2.5% to 5% of cells present in the MLKL++ subset, as shown in Figure 4.10B.

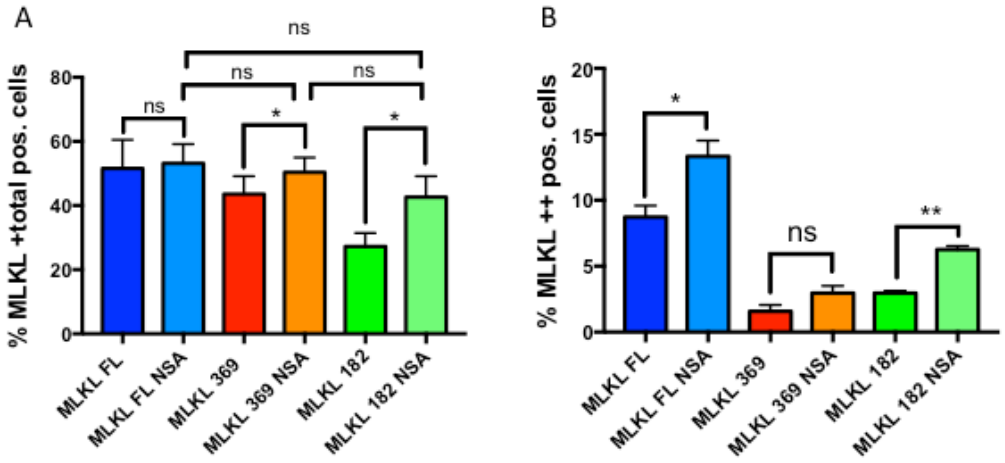


Figure 4.10. Tolerable MLKL expression is increased by MLKL inhibitor NSA. **A**: The effect of NSA in the culture medium on the total percentage of MLKL positive cells. **B**: The effect of NSA in the culture medium on the ++ subset positive gate of MLKL positive cells. Shown are the mean % positivity ± SEM. Experiment carried out in duplicate. n=3. Statistical analysis was performed using a paired t-test.

4.4 Discussion

The experiments described in this chapter were designed to detect whether the homozygous frameshift deletion in *MLKL* identified in the two brothers had an impact on the cellular expression and the known function of MLKL as the effector

molecule of necroptosis. Transfection of the HEK293 cell line with variant forms of MLKL using equal amounts of plasmid was used to address these questions. This cell line has previously been used to study necroptosis and serves as a good transfection hosts. It was deliberately decided to avoid using a tagged MLKL construct, as an N-terminal tag has been reported to interfere with the capacity of MLKL to induce cell death. A C-terminal tag was not an option as it could potentially affect the function of the residual pseudokinase domain, which we aimed to assay. In other situations where the gene of interest does not cause cell death these issues could be resolved using bicistronic vectors in which a reporter protein is expressed along with protein of interest. However, as MLKL induces cell death, the question of transfection efficiency becomes slightly more complex, as the cells expressing MLKL are not detected if they undergo necroptosis. The ability of the MLKL antibody to detect MLKL using flow cytometry enabled the quantification of expression. This assay also allowed us to examine how the MLKL inhibitor reversed expression differences between MLKL FL, MLKL 369 and MLKL 182, which indicate that there is no difference in MLKL transfection efficiency when cancelling the effect of MLKL induced cell death (Figure 4.10A).

As the variant affects the pseudokinase domain of MLKL, the experiments were set up to specifically assay whether the residual part of the MLKL pseudokinase domain (MLKL 369) enabled function analogous to the full-length protein or not. MLKL 182 was therefore included in the assay as a positive control, since it completely lacks a pseudokinase domain. Expression of MLKL 369 causes increased cell death compared to MLKL FL, and this is likely due to lack of autoinhibition from a fully

functional pseudokinase domain, which is required to inhibit the active N-terminal bundle domain. Cell death, assayed by PI/annexin V staining and Incucyte showed that MLKL 369 caused a similar extent of cell death as MLKL 182, indicating that the residual pseudokinase domain in MLKL 369 is not functional in repressing the MLKL N-terminal bundle domain that induces necroptosis.

Visualisation of the MLKL 369 using the monoclonal MLKL antibody (3H1) using western blotting revealed MLKL 369 to be significantly less abundant than MLKL FL. Flow cytometry was used to establish that the difference in band intensity was related to a specific subset of cells (MLKL++ subset), which was capable of expressing high amounts of MLKL FL but not MLKL 369 or 182. The increased cell death observed in cells transfected with MLKL 369 and MLKL 182 compared to MLKL FL indicated that these shorter MLKL constructs were indeed functional.

It should be noted, however, that cells transfected with MLKL 182 demonstrated significantly higher MLKL expression in the MLKL ++ subset gate compared to MLKL 369, as shown in figure 4.8D and figure 4.9B. The most likely explanation for this observation is that this degree of truncation of MLKL prevents the molecule from adequate oligomerisation, which is necessary for the translocation to the cell membrane and induction of necroptosis. Consequently, a subset of transfected cells is capable of expressing relatively high amounts of MLKL 182 compared to MLKL 369. This possibility could possibly be formerly tested using fluorescence resonance energy transfer, which can detect interactions between proteins and thus indirectly the cellular location. A different approach could rely on immunocytochemistry using

the MLKL 3H1 antibody to detect MLKL 182 expressing cells and possibly the subcellular location of MLKL 182. This approach has previously been used to demonstrate that MLKL, upon activation, translocates to the cell nucleus before being transported to the cell membrane (185).

All in all, the reduced expression of MLKL 369 observed by western blotting and flow cytometry may reflect a lower cellular expression tolerance to MLKL 369 compared to MLKL FL. Indeed, inhibition of the necroptotic activity of MLKL by NSA resulted in increased and equalised expression of all MLKL constructs, when assayed by flow cytometry. These observations support the concept that the tolerable expression of MLKL is determined by the relative degree of cell death, which can be amended either by genetic variants in the MLKL pseudokinase domain or by pharmacological inhibition, in this case by NSA. This intricate relationship between cell death and cellular expression of MLKL observed *in vitro* has not previously been described in the literature.

4.4.1. Phenotypic implications of increased necroptosis

Overall, the results generated *in vitro* suggested that the frameshift deletion in *MLKL* causes a gain of function of MLKL 369, which would theoretically lead to a cellular shift towards increased levels of necroptosis in the brothers. At this stage of the project, it was unclear why increased necroptosis would lead to disease solely in the CNS, and one could speculate that the low level of turnover of cells in the CNS might make them more susceptible to altered levels of necroptosis. This interpretation

was supported by the observation from the literature showing that variants in genes encoding regulators of necroptosis upstream and downstream of MLKL have been linked to neurodegenerative diseases. As mentioned in Chapter 1, loss of function variants in *OPTN,* identified in patients with ALS, have been shown to increase the activity of RIPK1 and thus the necroptotic pathway, which is also demonstrated by increased levels of phosphorylated MLKL (122). These findings would suggest that motor neurons might be particularly vulnerable to altered levels of necroptosis, possibly due to the high metabolic activity or length of the axons. Furthermore, variants in *TBK1*, a known regulator of optineurin, have been demonstrated in patients with ALS and FTD (5). Finally, ESCRT III was recently shown to antagonise MLKL activity by preserving cell membrane integrity (105), and variants in an ESCRT III subunit called *CHMP2B* are associated with ALS and FTD (126, 186). It is important to note that patients with variants in the mentioned necroptotic regulators have no other organ malfunctions other than those in the CNS. This finding could suggest that dysregulated necroptosis, due to genetic variants in the necroptotic machinery, causes a selective vulnerability to necroptosis in the CNS or particularly the motor neurons, depending on what signalling protein in the necroptotic pathway is affected. However, the cellular mechanisms that control necroptosis are still far from fully elucidated at the cellular level, and the function of necroptosis in the CNS is likewise not understood. For example, it remains an open question whether the necroptosis pathway is activated by different molecules in the CNS compared to other organs. Equally are the cellular events downstream of MLKL mediated pore formation and thus necrotic cell death in the CNS far from understood.

The clinical presentation, however, of B1 and B2 overlaps partly with ALS and frontotemporal dementia, most notably in the severe atrophy identified by MRI in the cortex, as well as the fasciculations observed clinically in B1. The progression of disability in B1 and B2 is substantially slower than that typically observed in ALS and FTD, however, patients with ALS and *OPTN* variants have been reported to have a particular slow progression of disease (187).

4.4.2 Limitations of the data

Most of the current knowledge of human necroptosis is derived from work in cell lines, which warrants caution when extrapolating to physiological settings. Likewise, as the results presented in this chapter were generated in cell lines, they should therefore be interpreted with caution with respect to their relevance to disease. Most important is the question of whether MLKL 369 would cause a similar effect *in vivo* as observed *in vitro*. The *in vitro* experiments were all conducted within a 24 hours period due to the strong impact on cell death upon MLKL transfection. We can therefore not know whether counter-regulatory cellular mechanisms could come into play *in vivo* to prevent cell death beyond this time point.

4.4.3 Conclusions and future work

The genotype-dependent differences in necroptosis and expression observed upon transfection of MLKL 369 into cell lines suggested that the variant in *MLKL* might be implicated in the disease of the B1 and B2. The increased degree of necroptosis,

caused by the lack of autoinhibition from the truncated MLKL pseudokinase domain in MLKL 369 could be rationalised as a possible contributing factor to the clinical phenotype described in Chapter 3. In support of this possibility it is worth noting that variants in regulators of necroptosis had been described in patients with amyotrophic lateral sclerosis and frontrotemporal dementia.

Almost all of the current understanding of necroptosis has been generated in cell lines and animal models. Indeed the experiments described in this chapter were based on this understanding. Recognising this limitation necessitated data on necroptosis and MLKL 369 based on *ex vivo* samples from the family in question. The results of this work are described in Chapter 5.

Chapter 5. The functional analysis of MLKL 369 in patient primary cells

5.1 Introduction

The genotype dependent differences observed for the *MLKL* variant (rs561839347) demonstrated that MLKL 369 *in vitro* causes increased cell death. This finding indicated that rs561839347 would result in dysregulated necroptosis in the patients. Furthermore, the evidence to suggest that necroptosis is activated in neurodegenerative diseases such as MS(112), Niemann-Pick disease (115), Alzheimer´s disease(113) and ALS(122), supported that the variant in *MLKL* could be implicated in the disease of brothers. The observed activation of necroptosis in the mentioned neurological diseases, as well as in autoimmune hepatitis (108), cardiac ischaemia (110), pancreatitis (100) and atherosclerosis (109, 188) have led to MLKL being pursued as drug target for inhibition (89, 189, 190). Much of this data supporting a pathogenic effect of necroptosis is based, however, to a large extent on experiments carried out in animal models and immortalised cell lines, which can display differences in biological processes when compared with human primary cells.

Given the limitations of cell lines and animal models, it was necessary to further explore how the variant in *MLKL* could contribute to disease using primary cells derived from the affected family members. As the functional impact of rs561839347 in primary cells has not been previously characterised, cellular samples obtained from the family could potentially offer a unique insight into how dysregulated necroptosis might contribute to disease in humans and thus have potential implications for the therapeutic targeting of MLKL.

Four questions that needed to be addressed were:

1. Does the rs561839347 have any impact on MLKL expression?

2. Given the role of MLKL in the immune system, does rs561839347 have an impact on peripheral blood immune cell frequencies?

3. Does rs561839347 confer a gain of MLKL function and thus an increased tendency for necroptosis *ex vivo* as observed *in vitro*?

4. Does the rs561839347 affect the non-necroptotic function of MLKL?

In order to address these questions, primary cells were obtained in the form of fibroblasts and PBMCs (peripheral blood mononuclear cells) from the two brothers, as well as from their unaffected sister. Additional blood samples were taken from unaffected, unrelated individuals as controls. The samples were taken upon obtainment of informed consent as described in methods Chapter 2.

5.2 Results

5.2.1 PBMCs of B1 and B2 do not express detectable levels of MLKL by western blotting

Figure 6.1 shows a western blot of the relative expression of MLKL protein in the PBMCs of all donors, including the sister of the two brothers, S1, as well as B1 and B2. MLKL was detectable in all unaffected individuals at 54 kDa, as highlighted in the yellow box. MLKL 369 should appear around 40 kDa, but no band could be observed at this size, indicating that B1 and B2 do not express MLKL in the PBMC compartment.

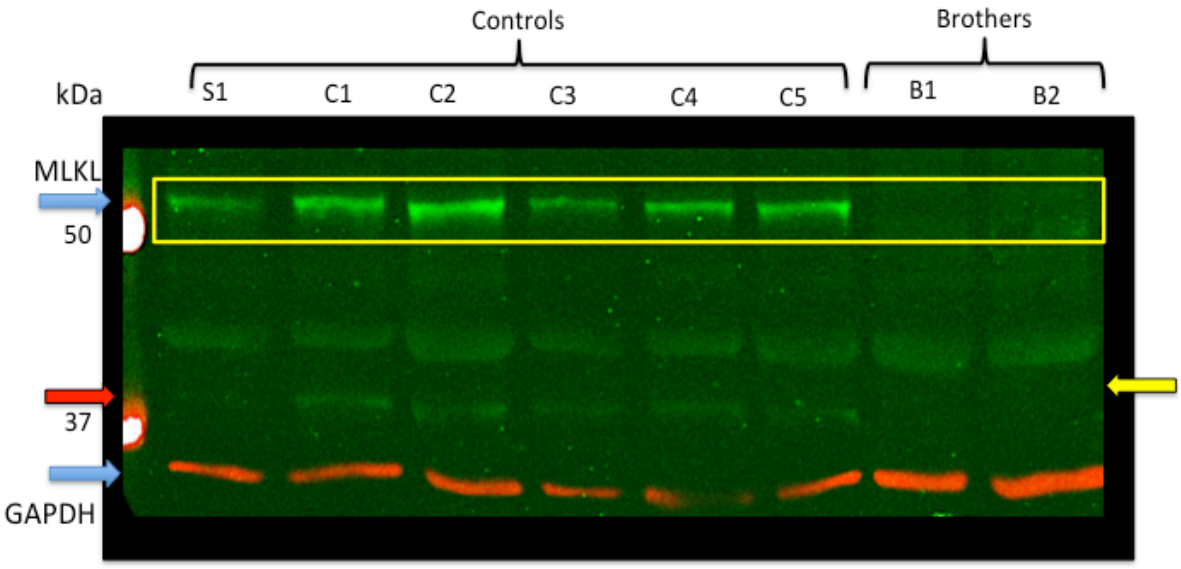


Figure 5.1. MLKL expression in PBMCs isolated from B1, B2 and non-affected controls. 300.000 cells loaded per lane. C1-C5 indicates non-affected male controls. S1 is the sister of B1 and B2. MLKL was detected at 54 kDa as expected (top blue arrow). The yellow arrow indicates the expected size of MLKL 369. The red arrow indicates a band around 39 kDa, which was observed in non-affected individuals though not in B1 and B2. Glyceraldehyde 3 phosphate dehydrogenase (GAPDH)(bottom blue arrow) was used as the loading control.

The blot also revealed an unexpected band around 39 kDa in PBMCs of unaffected individuals, but this was not observed in B1 and B2. The band could be an isoform of

MLKL that is rendered absent by the *MLKL* variant rs561839347. MLKL is also reported by Ensembl (191) to exist as a second isoform termed MLKL-2 around 28 kDa, but this isoform was not observed in western blots of human PBMCs in our study.

5.2.2 B1 and B2 do not have atypical frequencies of immune subpopulations

The absence of MLKL 369 in the PBMCs of B1 and B2 was surprising given that MLKL was expressed and detectable *in vitro*, as demonstrated in Chapter 4. As discussed in Chapter 1, necroptosis is thought to be important for the mammalian host defence against viral and bacterial infections(95, 99). Absence of MLKL in PBMCs would therefore be expected to increase susceptibility to infections, but the clinical history of B1 and B2, as described more fully in Chapter 3, indicates no such susceptibility. According to available hospital records, the brothers have not been hospitalised due to infections. The general practitioner, who has cared for the brothers since 1991, also confirmed to the author, moreover, that the patients are not particularly prone to infections.

Based on the *in vitro* data on MLKL 369, showing reduced expression of MLKL 369 likely as a function of its pro-necroptotic capacity, we therefore hypothesised that rs561839347 was exerting a similar, constitutive and pro-necroptotic effect on the patient immune cells. The impact for the immune system of the brothers would be that necroptosis would occur on a more frequent basis than in normal individuals enabling more effective clearance of microbe infected immune cells, which could explain why B1 and B2 do not show an increased susceptibility to infections. If this

hypothesis was true, one could therefore expect a negative selective pressure against PBMC subsets that express MLKL 369. Necroptosis has been implicated in the regulation of T cell survival and proliferation as demonstrated in mice (192), and from this perspective it was also necessary to examine whether rs561839347 would affect the frequencies of T cells and other immune subsets.

Table 5.1. Characterisation of immune cell populations in the B1, B2 and non-affected controls in freshly isolated PBMCs. Numbers refer to percentage values. The brothers have normal immune population frequencies. Lymphocyte subsets are expressed as a percentage of the total lymphocyte population. Monocytes are defined as a percentage out of total live PBMCs. CD4+ naïve T-cells and CD8+ naïve T-cells are defined by the co-expression of CD45RA. Memory T-cells are defined by the CD45RA negative population. NK-cells are defined by CD56 positivity. B-cells are defined by expression of CD19 and monocytes are defined as CD14 positivity.

Donor	CD4 + T-cells	CD4+ naive T-cells	CD4+ memory T-cells	CD8+ T-cells	CD8+ naive T-cells	CD8+ memory T-cells	NK-cells	B-cells	Monocytes
B1	**59.3**	**46.4**	**37.1**	**4.7**	**74.2**	**15.0**	**25.3**	**6.1**	**16.7**
B2	**47.8**	**17.0**	**68.1**	**13.3**	**55.2**	**12.9**	**25.7**	**9.6**	**9.9**
C1	54.9	38.6	48.0	21.8	55.7	20.7	16.8	2.6	8.2
C2	60.8	19.7	63.1	5.9	39.8	32.1	29.8	2.6	3.7
S1	58.6	43.1	41.1	7.8	59.1	17.3	20.6	6.0	10.4

The major subpopulations of the immune compartment were therefore quantified in freshly isolated cells from blood and assayed by flow cytometry. Total PBMC counts between donors were comparable. Table 5.1 shows the percentages of immune cells in B1, B2 and S1, as well as two unrelated controls. The percentages of immune cells of B1 and B2 were all within the normal range, which did not support the hypothesis that MLKL 369 exerts a constitutive pro-necroptotic and thus detrimental effect on the cells of the immune compartment.

5.2.3 MLKL is not expressed in cultured fibroblasts of B1 and B2

To further substantiate the observed lack of MLKL in B1 and B2 in PBMCs and to ensure that this was not a cell lineage-specific effect, fibroblasts isolated from each of the three siblings were also analysed. A western blot of MLKL, shown in Figure 5.2, confirmed that MLKL 369 was not expressed in the patient fibroblasts either. In contrast, a clear band at 54 kDa was observed in S1, who is homozygous for the rs561839347 major allele. The weak band around 39 kDa observed in PBMCs of unaffected individuals (Figure 5.1, red arrow), was not detected in the cultured fibroblasts of S1, which might suggest a cell type specific expression differences of this MLKL isoform.

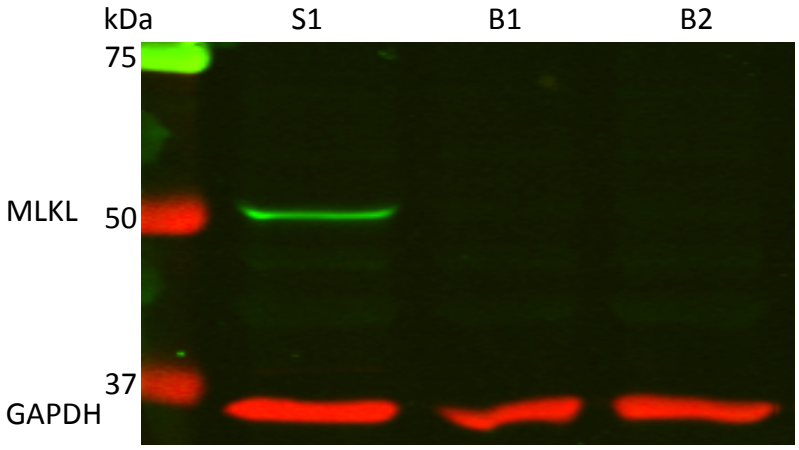


Figure 5.2. MLKL expression in cultured fibroblasts of the three siblings. MLKL is detectable in the fibroblasts of S1 at 54 kDa. MLKL 369 would be expected to appear around 40 kDa. No unique band could be detected at this size in B1 and B2.

Western blot analysis of MLKL in PBMCs and cultured fibroblasts could thus demonstrate that the variant in *MLKL* of B1 and B2 resulted in lack of MLKL expression, which most likely reflects an MLKL deficiency across all cell types.

5.2.4 Assessing the effect of the MLKL 369 variant at the mRNA level

In order to explore the underlying mechanism for the observed lack of MLKL expression in B1 and B2, we aimed to characterise the mRNA level expression of MLKL. RNA was isolated from cultured fibroblasts and amplified in a PCR reaction using primers centred approximately 394 base pairs around the 4-nucleotide deletion. Figure 5.3A shows an image of the gel in which the amplified PCR product is visible at 394 base pairs. A plasmid encoding full-length MLKL was used as a positive control. Though this method does not allow for statistical quantification, it was noteworthy that the 394 base pair band appeared to be less bright in B1 and B2 compared to S1. To verify the *MLKL* variant at the mRNA level, the band was excised, purified and sequenced, which confirmed the presence of the 4-nucleotide (CAGA) deletion in the B1 and B2 cDNA as shown in Figure 5.3 B.

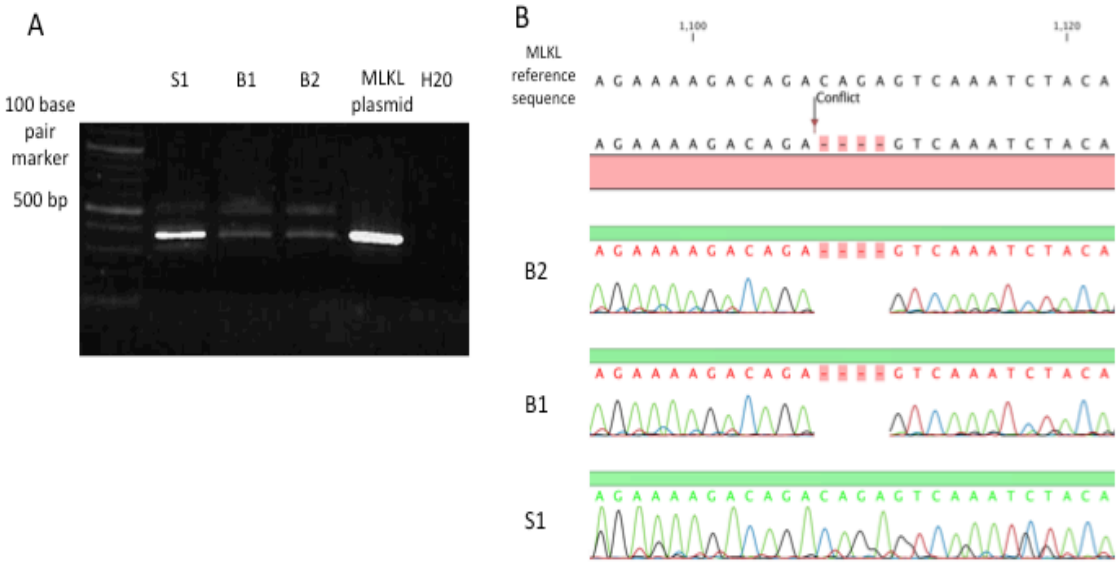


Figure 5.3. Verification of 4-nucleotide deletion in MLKL at the mRNA level. A. Image of gel showing amplified PCR product from 100 ng cDNA of S1, B1 and B2. Primers were centred around the 4-nucleotide deletion in exon 8 of *MLKL*. **B.** Sanger sequencing of isolated PCR product verifying the 4-nucleotide (CAGA) deletion in *MLKL* of B1 and B2.

To confirm the apparent reduction in MLKL mRNA in the patient fibroblasts, a qPCR assay was set up to quantify MLKL mRNA expression. The MLKL Taqman gene expression assay used targets the MLKL NM_15264 transcript encoding full-length MLKL. The probe binds to the exon 4-5 boundary and should therefore not be affected by the 4-nucleotide deletion (rs561839347) in *MLKL*, which is located in exon 8. qPCR analysis of cultured fibroblasts confirmed a lower expression of B1 and B2 MLKL mRNA relative to S1, with the patients having approximately 1/3 of the level in S1, as shown in Figure 5.4A. B2 expressed slightly higher levels compared to B1.

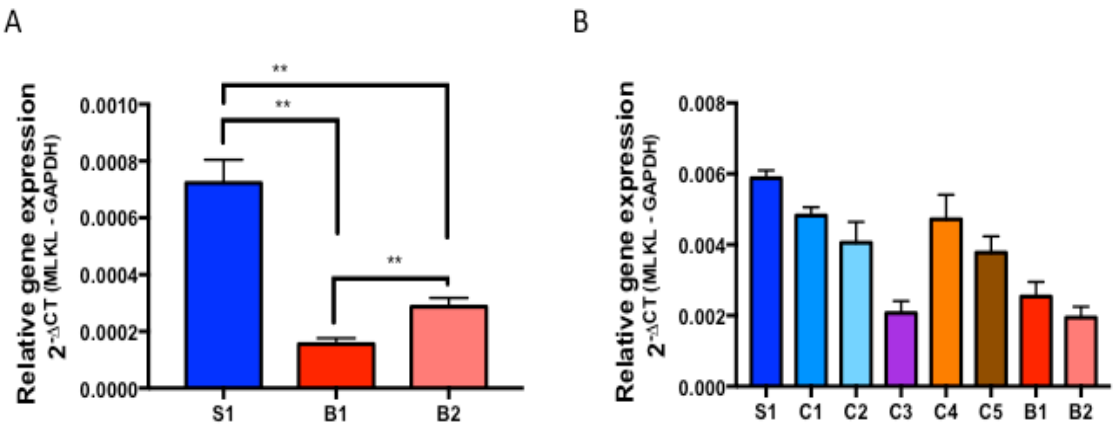


Figure 5.4. Quantification of MLKL mRNA expression by qPCR. A. Relative MLKL mRNA expression in cultured fibroblasts of the siblings normalised to GAPDH expression. Each data point was carried out in triplicate. n = 5. Paired t-test. **B.** Relative MLKL mRNA expression in freshly isolated PBMCs of the siblings and 5 non-affected male donors (C1-C5) analysed in triplicates and normalised to GAPDH. RNA was extracted from the same PBMC samples analysed by western blotting in Figure 5.1.

This observation posed the question of whether or not this reduction was an effect of the variant in *MLKL* (rs561839347) or whether *MLKL* expression in B1 and B2 is within the normal range. It was not possible to obtain a panel of cultured fibroblasts from unaffected individuals, so we aimed to characterise the MLKL mRNA

expression in PBMCs using the same male control donors (C1-C5) as described in Figure 5.1. MLKL mRNA in PBMCs of B1 and B2 showed a trend toward a lower expression compared to unaffected control individuals (Figure 5.4 B). However, in one control (C3), we measured a level of MLKL mRNA expression that was very similar to B2, which suggests that lower MLKL mRNA levels in the brothers is unlikely to solely explain the absence of protein, as MLKL is detectable in C3 (Figure 5.1). These observations would altogether indicate that the absence of MLKL might be due to a post-transcriptional mechanism.

Whilst fibroblasts could only be obtained from a single female, S1, the differences in MLKL mRNA levels between S1 and the brothers could be due to a trend towards higher MLKL expression in females compared to males, which has not been previously investigated. To address whether potential gender-specific differences in MLKL expression may exist, MLKL mRNA data in transformed fibroblasts from men and women in the GTEX database were extracted and compared (107). It is important to note that the database quantifies mRNA as transcripts per million, which is not directly comparable to MLKL mRNA expression data measured by qPCR as shown above. Nevertheless, no difference in MLKL mRNA expression in transformed fibroblasts is observable between men and women (Figure 5.5).

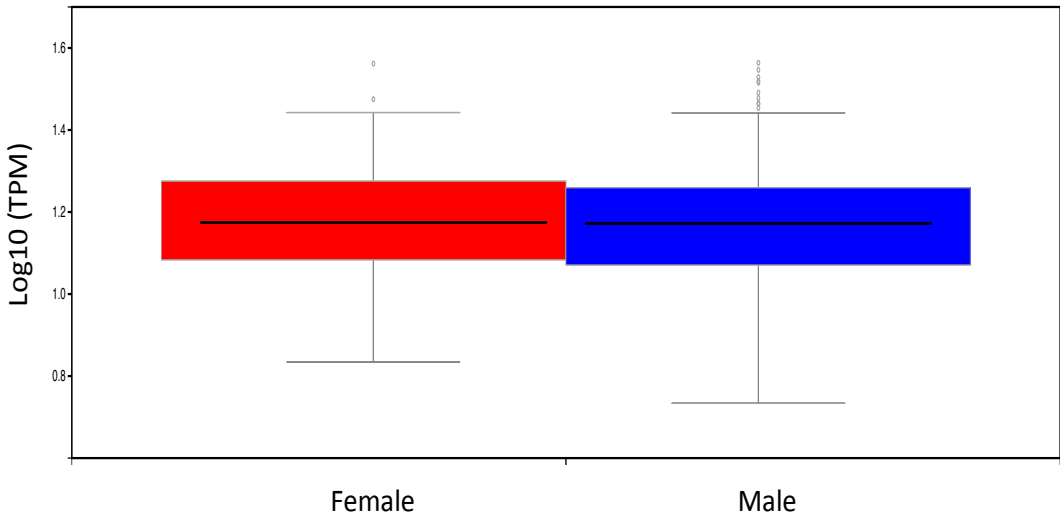


Figure 5.5. No difference in MLKL mRNA expression between men and women in transformed fibroblasts. MLKL mRNA expression data extracted from GTEX database showing transcripts per million (TPM). Red: Female n = 121, TPM median 14.890. Blue: Male, n = 222, TPM median 14.805.

5.2.5 No MLKL protein expression in patients despite IFNγ-mediated mRNA upregulation

Despite the observed variability in MLKL mRNA in the PBMCs among all donors, it could not be completely ruled out that low MLKL mRNA expression in B1 and B2 could at least partly contribute to the observed lack of MLKL protein. The expression of MLKL can be increased by interferon-γ (IFNγ) stimulation, which is in keeping with the described role of MLKL in anti-viral immunity as described in Chapter 1 (108). As the *MLKL* promoter is reported to be sensitive to IFNγ stimulation, this cytokine was used to explore whether MLKL expression in the fibroblasts of the family could be increased with the aim of further elucidating the underlying reason for the observed lack of MLKL protein expression in B1 and B2.

S1 fibroblasts were initially used to verify the effect of IFNγ stimulation on MLKL mRNA expression. Using a range of concentrations of IFNγ (5, 30 and 100 ng/ml) one could observe an increased amount of MLKL mRNA by qPCR after 24 h, as shown in Figure 5.6A. The MLKL mRNA expression was comparable across the range of concentration used, which might indicate that the cytokine-dependent upregulation was saturated at 5 ng/ml of IFNγ. Using this lower concentration of IFNγ on B1 and B2 fibroblasts one could also observe an 6 to 9-fold increase in the level of MLKL mRNA, respectively, as shown in Figure 5.6B.

These results indicated that the *MLKL* promoter in B1 and B2 was intact and was not substantially affected by the *MLKL* rs561839347 variant. Although there was an increase in MLKL expression in the patients, which was not dissimilar to the relative increase in MLKL in the sister (5-fold upregulation), the MLKL mRNA levels in B1 and B2 upon stimulation with IFNγ only reached the approximate levels of MLKL mRNA observed in the SI unstimulated cells.

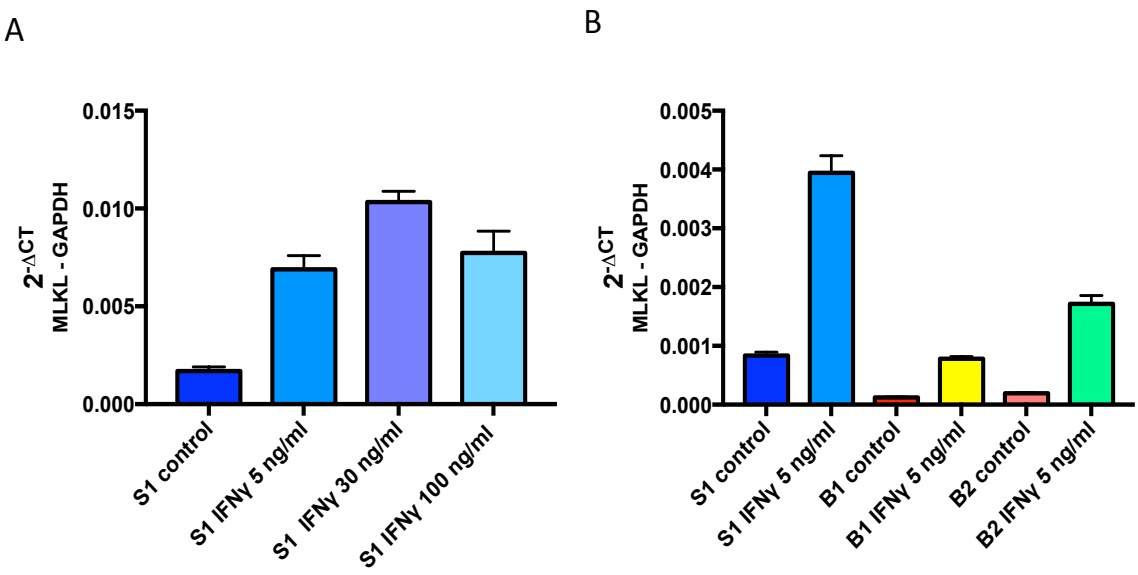


Figure 5.6. MLKL mRNA is inducible by IFNγ. A: MLKL mRNA expression in fibroblasts of S1 stimulated with indicated concentrations of IFNγ. **B:** IFNγ stimulation of family fibroblasts using 5 ng/ml. Cells were harvested after 24-hours. Each data point was carried out in triplicates. Error bars indicate SEM.

To verify the effect of MLKL induction of IFNγ at the protein level, fibroblasts were stimulated with IFNγ at same concentrations and harvested 24 and 48 hours post stimulation. B2 fibroblasts were chosen to examine the impact of (rs561839347) in this experimental setting as B2 fibroblasts were consistently showing higher MLKL mRNA levels compared to B1, which would maximise the chances of detecting MLKL 369 protein.

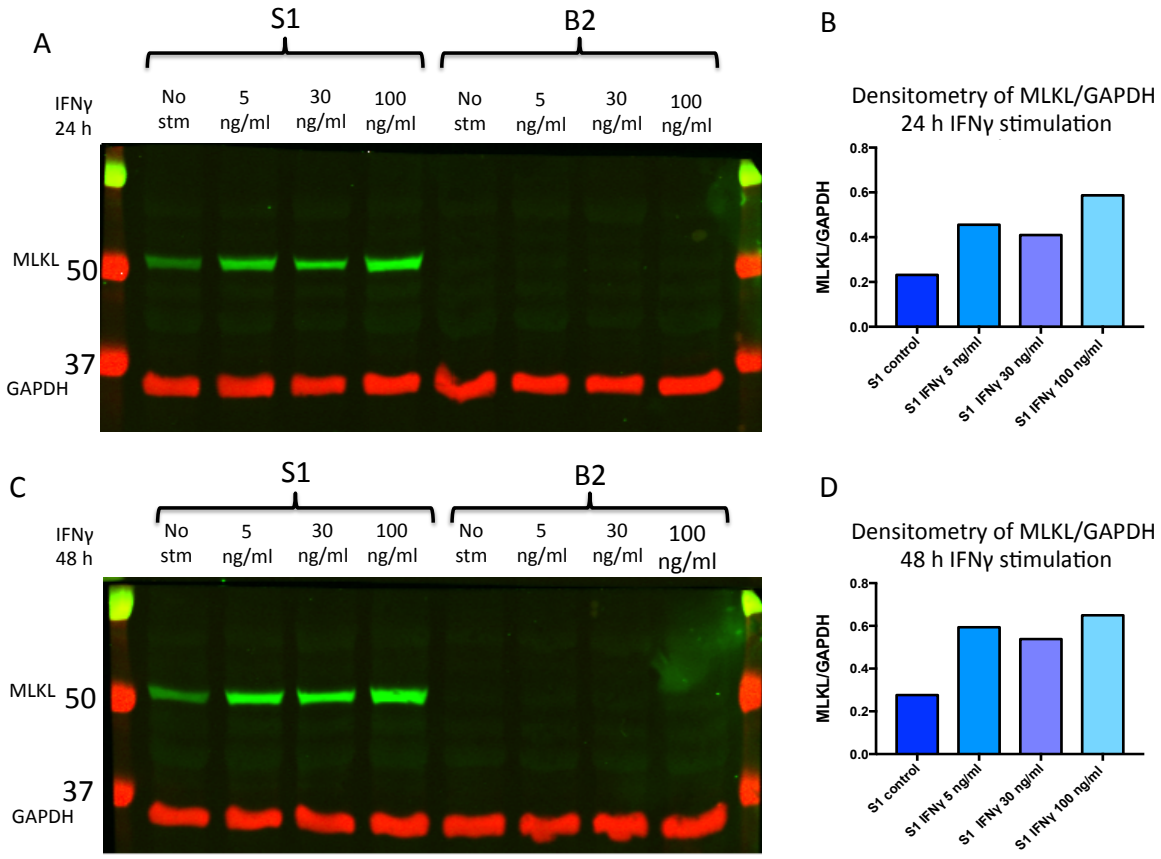


Figure 5.7. Stimulating MLKL expression in family fibroblast. A. Western blot analysis of S1 and B2 fibroblast upon IFNγ stimulation. **B.** Densitometry of MLKL expression shown in A, normalised to GAPDH expression of S1, 24 hours post IFNγ stimulation. **C.** Western blot analysis of S1 and B2 fibroblast upon IFNγ stimulation. **D.** Densitometry of MLKL expression shown in C, normalised to GAPDH expression of S1, 48 hours post IFNγ stimulation. 300.000 cells loaded per lane. Band intensity was quantified using Li-Cor software and analysed in GraphPad Prism.

IFNγ stimulation caused a 2-3-fold increase in the expression of MLKL at the protein level as detected in S1, with no strong difference between the two time-points assayed (Figure 5.7A+B). However, no detectable MLKL expression could be observed in B2 using this range of IFNγ stimulations and time points. Interestingly, a trend towards slightly increased MLKL expression of S1 fibroblasts with increasing IFNγ concentrations was noted at 24 hours (Figure 5.7A). This was unanticipated

given that the increased S1 MLKL mRNA levels seemed to plateau using IFNγ concentrations between 5 and 100 ng/ml (Figure 5.6A). To further confirm a complete absence of MLKL 369 protein in B2, as well as B1, a maximal cytokine concentration of IFNγ 1000 ng/ml for 24 h was used and lysates of S1, B1 and B2 were analysed on a single gel. No MLKL 369 band in B1 or B2 lysates could be detected as shown in Figure 5.8A.

These findings could indicate that the lack of MLKL expression in B1 and B2 is due to MLKL 369 exerting a pro-necroptotic effect to the fibroblasts expressing the protein, which would imply that the fibroblasts would undergo necroptosis before being detected in a western blot. This possible effect could be assayed using the commercially available MLKL inhibitor NSA, analogues to the results shown in Chapter 4 (Figure 4.10A). Another possibility could be that MLKL 369 is unstable, which would cause it to be degraded by proteasomal activity. To address these possibilities experimentally, S1 and B1 fibroblasts were stimulated with IFNγ in the presence of NSA or proteasome inhibitor MG-132. Again a clear effect of IFNγ stimulation was observed in S1, but no indication of MLKL 369 expression was observed in the lysates of B1, as shown in figure 5.8B.

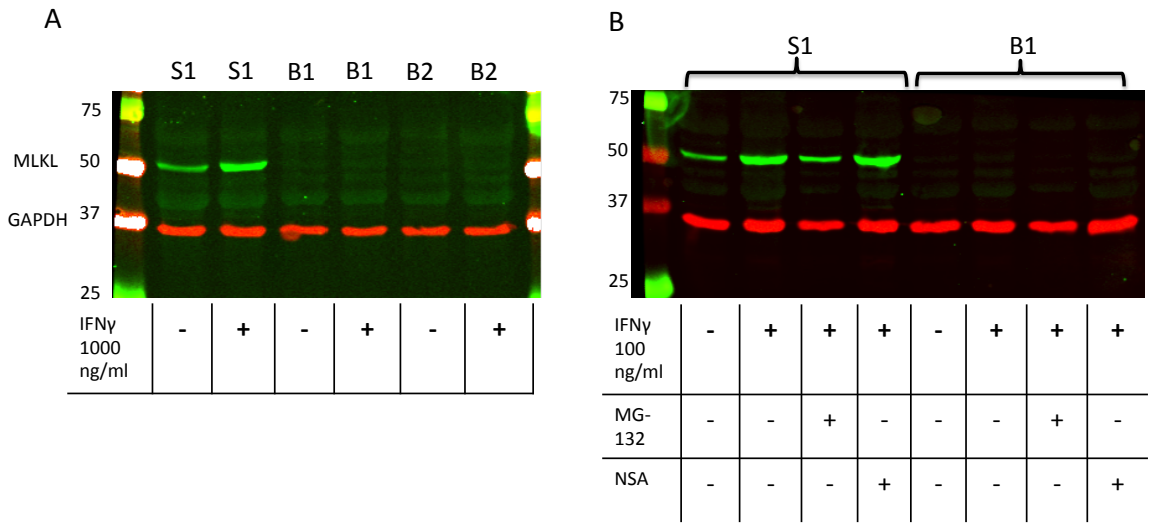


Figure 5.8. MLKL 369 is not detectable in protein lysates of B1 and B2. A. Family fibroblasts stimulated with 1000 ng/ml IFNγ and harvested after 24 h. **B.** S1 and B1 fibroblasts stimulated with IFNγ in the presence of MLKL-inhibitor (NSA) 2 µM or proteasome-inhibitor MG-132, 25 µM.

5.2.6 Assaying the effect of the *MLKL 369* variant on cell death

The data shown thus far demonstrated that B1 and B2 do not express detectable levels of MLKL protein in fibroblasts or PBMCs at baseline. Nor was it possible to stimulate the expression of MLKL to detectable levels, even though the promoter is sensitive to induction by IFNγ. However, if MLKL 369 causes increased cell death then an apparent lack of the protein could be secondary, resulting from the loss of MLKL 369-expressing cells, which would therefore not be detectable by western blotting. One would thus hypothesise that if this is the case then IFNγ stimulation would cause increased cell death in B1 and B2 fibroblasts, but not necessarily in S1 fibroblasts. IFNγ stimulation (5 ng/ml) in combination with the pan-caspase inhibitor z-VAD (50 µM) that blocks apoptosis has been shown to induce necroptosis in mouse embryonic fibroblasts (MEF) (193, 194) via the JAK/STAT1

pathway - at least in part due to the increase in MLKL expression. zVAD inactivates caspase-8, which allows for the induction of RIPK1-RIPK3 necrosome formation that in turn activates MLKL and prevents the activation of apoptosis. The Incucyte live imaging system was used to monitor cell death over 90 hours upon stimulation as shown in Figure 5.9. The fibroblasts of B1, B2 and S1 showed no obvious differences in baseline cell death through time, which was low (<1% at all time points) (Figure 5.9A), and blocking apoptosis alone through zVAD at 50μM did not substantially increase cell death by necroptosis (Figure 5.9B). Stimulation with IFNγ 5 ng/ml and IFNγ 5 ng/ml with zVAD marginally increased cell death to around 1%, (Figure 5.9 C and D). Increasing IFNγ to 30 ng/ml lowered the degree of cell death to <1%, which may reflect pro-survival signalling of IFNγ via NF-kappa B. (Figure 5.9E +F).

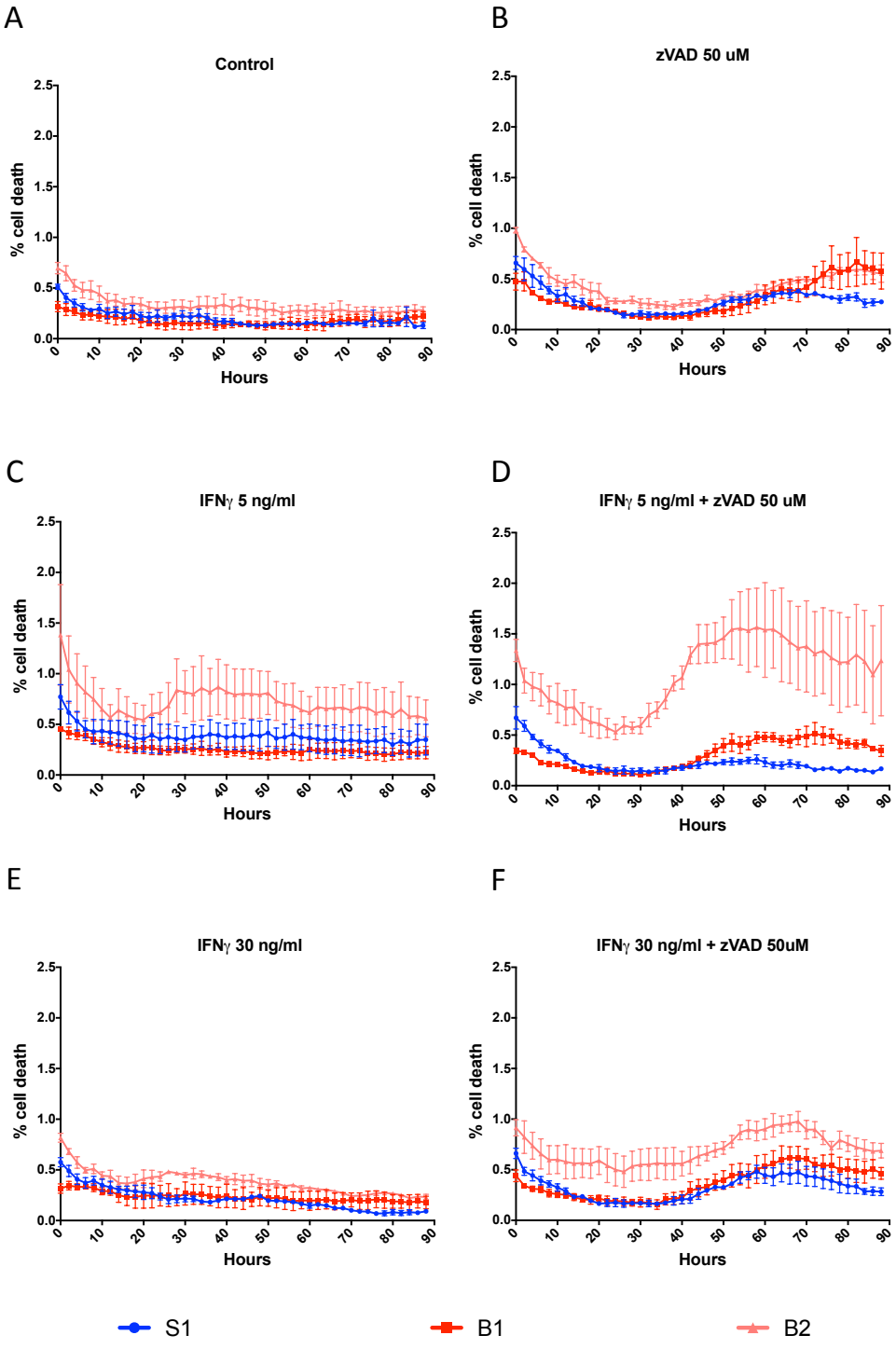


Figure 5.9. Assaying cell death in family fibroblasts upon stimulation of necroptosis. A: Non-stimulated family fibroblasts. **B:** zVAD 50μM. **C:** Stimulation with IFNγ 5ng/ml. **D:** Stimulation with IFNγ 5ng/ml and zVAD 50μM. **E:** Stimulation with IFNγ 30ng/ml. **F:** Stimulation with IFNγ 30ng/ml and zVAD 50μM. Each data point carried out in triplicate wells. Error bars indicate SEM.

The very low level of necroptosis in B1 and B2, taken together with the absence of MLKL protein could suggest that the lack of protein is not due to an increased loss of MLKL 369-expressing cells. Notably, necroptosis was also very low in the S1 fibroblasts, perhaps suggesting a tighter control of the necroptosis machinery or lower expression of its mediators in primary human fibroblasts compared to the MEFs described in the literature (9).

RIPK3 is a central molecule in programmed cell death that orchestrates the induction of caspase-8 dependent apoptosis, via the recruitment of RIPK1 and FADD (195, 196), and necroptosis by phosphorylation of MLKL at aa 357/358(92). Transduction of RIPK3 into human fibroblasts has previously been shown to sensitise primary fibroblasts to necroptosis (95). As the RIPK3 phosphorylation site in MLKL 369 would theoretically be intact, increased RIPK3 could potentially help to mediate necroptosis in the patients if their MLKL expression is below the detection limit, but is not negligible. RIPK3 transduction was validated in fibroblasts of S1 by western blotting, in which a band around 57 kDa could be observed in the lysates of transduced cells (Figure 5.10A). Exposing the blot at a higher gain intensity also revealed that human primary fibroblasts do express a lower level of endogenous RIPK3 as shown in Figure 5.10B. Figure 5.10C-H shows the effect of RIPK3 transduction on cell death in S1, B1 and B2 fibroblasts measured over the course of 90 hours. To facilitate RIPK3 transduction, the medium was supplemented with 8 μg/ml of polybrene, which did not affect viability (Figure 5.10D).

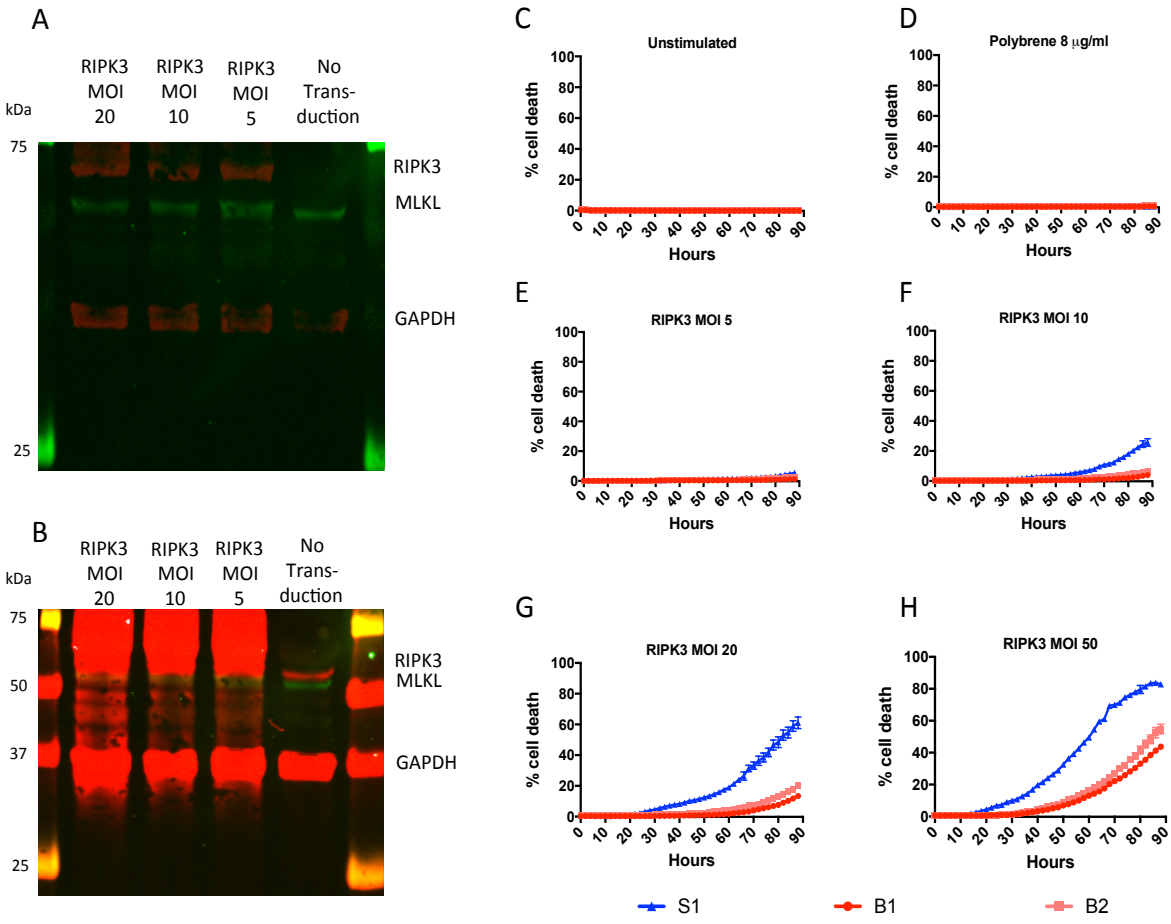


Figure 5.10 RIPK3 transduction of family fibroblasts. A. Western blot of RIPK3 transduced S1 fibroblasts 3 days post transduction. RIPK3 is visible around 60 kDa. **B**: Same western blot as shown in A visualised at higher gain intensity. Endogenous RIPK3 is visible around 57 kDa in non-transduced S1 fibroblasts (far right). **C-H:** Cell death in S1, B1 and B2 fibroblasts measured by Incucyte after RIPK3 transduction using MOI of 5 to 50. Each data point is the mean of triplicate wells. Error bars indicate SEM.

RIPK3 transduction had the expected effect of causing increased levels of cell death in a dosage dependent manner using MOI of 5, 10, 20 and 50. In S1, RIPK3 MOI 5 resulted in cell death of approximately 5 % of cells at 90 hours, which increased to 20%, 60% and 80% cell death using MOI of 10, 20 and 50, respectively. At RIPK3 MOI 50, the cell death curve began to plateau around 80 hours post transduction. The fibroblasts of B1 and B2 showed substantially lower degrees of cell death

compared to S1 across the four different RIPK3 MOI concentrations tested. Maximal percentages of cell death in B1 and B2 only reached roughly 5%, 13% and 40% using MOI of 10, 20 and 50, respectively.

It is important to note that the cell death observed in S1 upon RIPK3 transduction, most likely reflects activation of necroptosis, as well as apoptosis, because RIPK3 has the capacity to orchestrate both forms of programmed cell death. The reduced cell death observed for B1 and B2 is probably due to MLKL not being expressed at baseline, which would imply that the observed cell death in B1 and B2 reflects apoptosis. However, the capacity of IFNγ to stimulate the expression of MLKL 369 at the mRNA level could imply that the combination of RIPK3 and IFNγ induced MLKL 369 expression would have an additive effect on cell death in the cells of B1 and B2 by inducing necroptosis. To test this hypothesis the cells were transduced with RIPK3 in the presence of IFNγ 5 ng/ml and zVAD 50μM. A fourth primary fibroblast line (F1) was purchased from ATCC to serve as an additional positive control a long with S1.

As shown in Figure 5.11A, the transduction of RIPK3 enabled an efficient sensitisation to cell death, which began to affect the fibroblast viability approximately 40 hours after transduction. The effect was most pronounced in S1 and F1, for which roughly 30% of cells had undergone cell death at the end of the experiment, whereas only around 10% of B1 and B2 cells were Cytotox red-positive at this point. Adding IFNγ to the culture medium seemed to potentiate the effect of RIPK3 by increasing the degree of cell death in S1 and F1 to approximately 50% of

cells, whereas one could only observe a marginal increase in cell death in B1 and B2 to roughly 15% (Figure 5.11B). The difference in cell death between the control and patient fibroblasts was significant (P= 0.0155 - <0.0001). zVAD 50μM effectively blocked apoptosis during the course of the experiment, as indicated by the absence of cell death in B1 and B2, despite being stimulated with RIPK3 as demonstrated in Figure 5.11C, 5.11D and Figure 5.12. These results indicated that the observed cell death under this condition is a product of necroptosis. Interestingly, in the absence of IFNγ, F1 showed marginally higher degree of cell death upon overexpression of RIPK3 and administration of zVAD compared to S1. This difference likely relates to a higher baseline expression of MLKL in F1 compared to S1, as shown in Figure 5.13. Figure 5.11D shows the condition of directed necroptosis induction using RIPK3, zVAD and IFNγ, which demonstrate that the cells of B1 and B2 are not able to undergo necroptosis. 50% and 70% of cells of F1 and S1 fibroblasts, respectively, underwent cell death with this condition, which was significantly higher than B1 and B2 in which approximately 4% of cells were dead at the end of the experiment. No significant difference was observed between B1 and B2 at any time point.

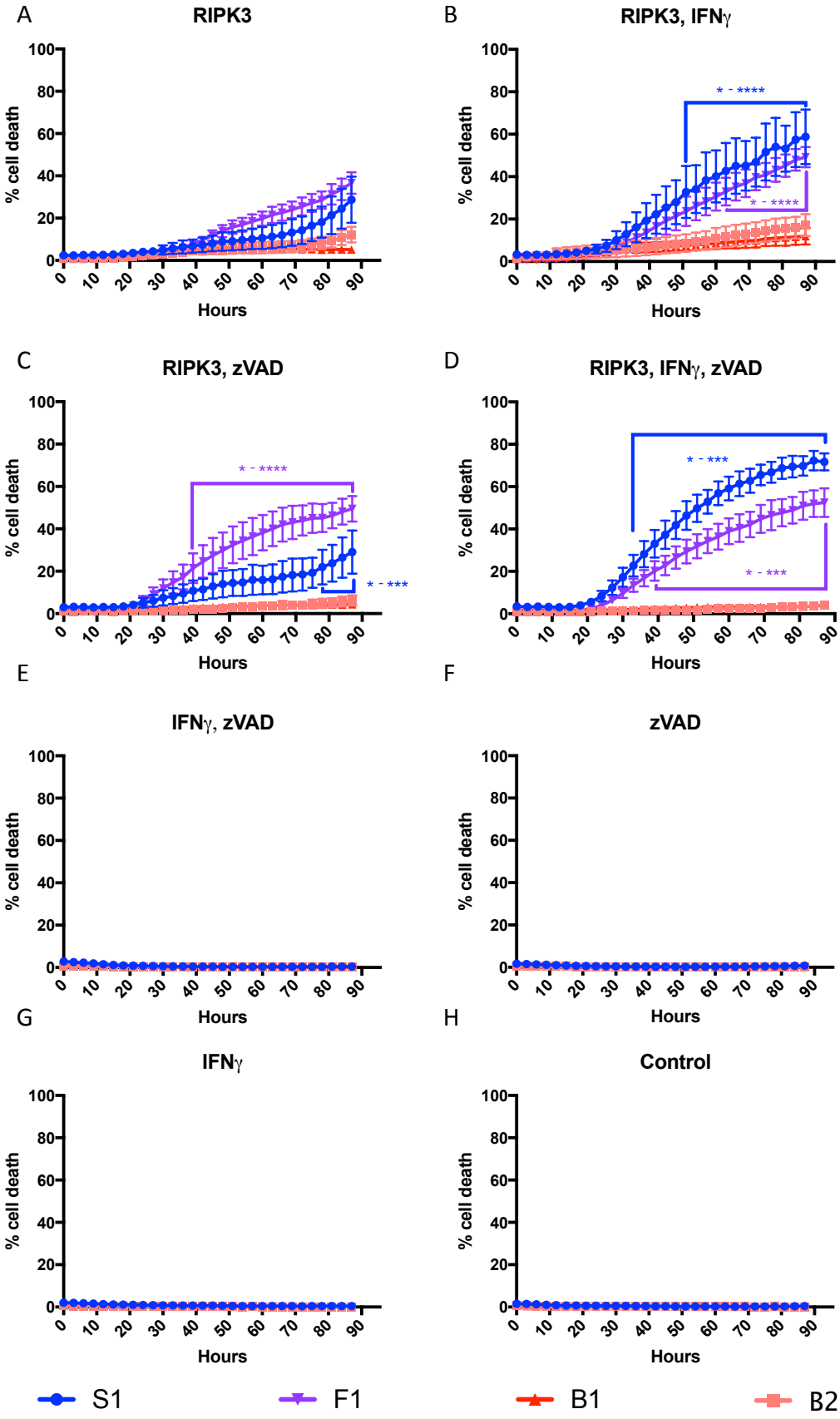

A
RIPK3
B
RIPK3, IFNγ
C
RIPK3, zVAD
D
RIPK3, IFNγ, zVAD
E
IFNγ, zVAD
F
zVAD
G
IFNγ
H
Control
% cell death
Hours
* - ****
* - ***
S1
F1
B1
B2

Figure 5.11 B1 and B2 cannot undergo necroptosis. Cell death analysis by incucyte of RIPK3 transduced fibroblasts in the presence or absence of zVAD 50 μM and IFNγ 5 ng/ml as indicated. **A.** RIPK3. **B.** RIPK3 and IFNγ 5 ng/ml. **C.** RIPK3 and zVAD 50 μM. **D.** RIPK3, IFNγ 5 ng/ml and zVAD 50 μM **E.** IFNγ 5 ng/ml and zVAD 50 μM. **F.** zVAD 50 μM. **G.** IFNγ 5 ng/ml **H.** Control. Error bars denote SEM of 4 independent experiments. Each data point in individual experiments was carried out in triplicate. * (purple) indicate significant difference between F1 and B1/B2. * (blue) indicate significant difference between S1 and B1/B2. Two-way ANOVA. * $P <$ 0.05 ** $P < 0.001$, *** $P = 0.0001$, **** $P < 0.0001$.

This marked difference between patient and control cells is also demonstrated in Figure 5.12 showing representative images of all fibroblast lines at 87 hours with RIPK3, IFNγ and zVAD condition.

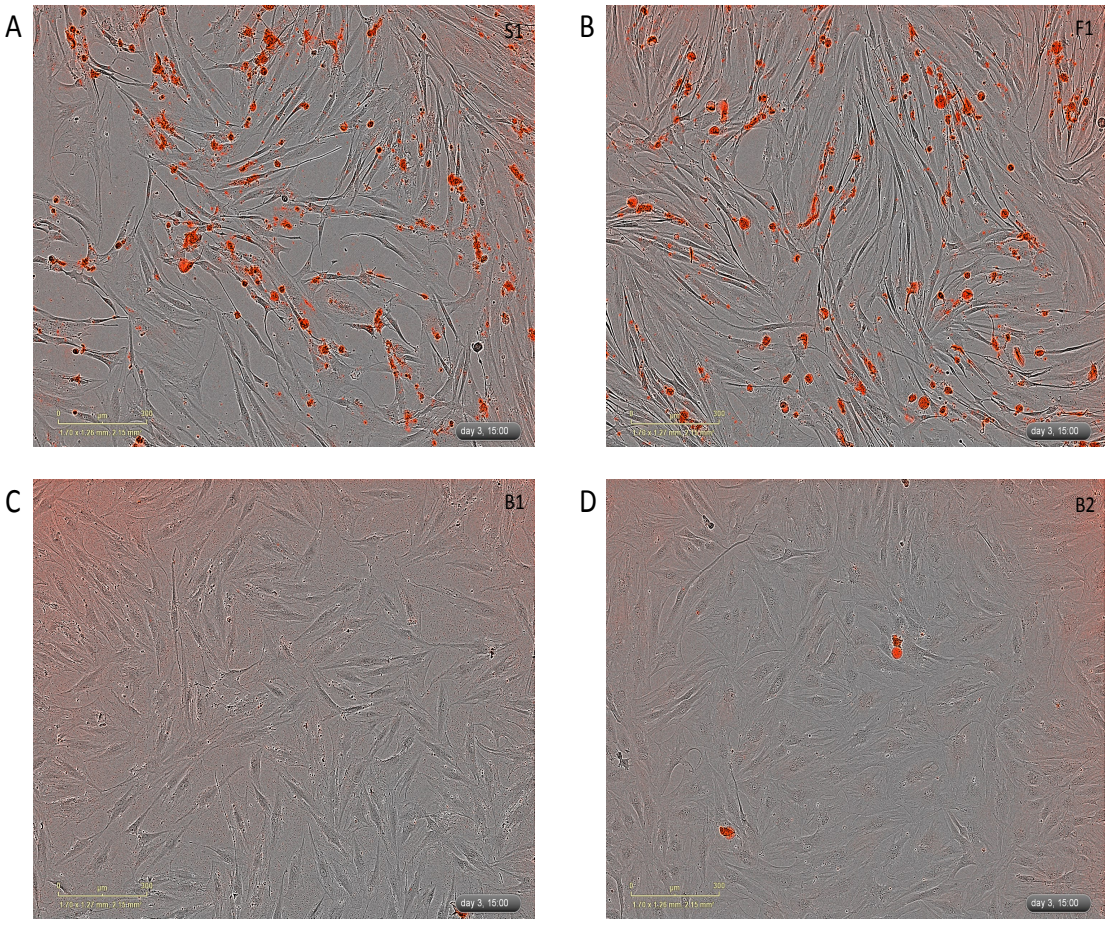


Figure 5.12. Live cell imaging of family fibroblasts upon induction of necroptosis. Representative images of incucyte analysis of donor fibroblasts at 87 hours post RIPK3 transduction (MOI 10), IFNγ 5 ng/ml and zVAD 50μM. **A:** S1. **B:** F1.

C: B1 and **D:** B2. Cytotox red nuclei indicate dead cells. Scale denotes 300 µm. The percentage cell death was measured by quantifying Cytotox red-positive cells at a given time point. This measure was then normalised to the total amount of cells in each well, measured by lysing all cells using 0.5% Triton-X 100 at 90 hours post stimulation.

5.2.7 Exploring effects of *MLKL* (rs561839347) on non-necroptotic functions

The western blot and cell death analysis had thus demonstrated that B1 and B2 do not express MLKL and the cells are therefore not capable of undergoing necroptosis. These results implied that the complete absence of MLKL in the brothers could also affect other cellular functions that MLKL is thought to be involved in and which are unrelated to its role in as the critical mediator of necroptosis. As described in Chapter 1, MLKL was recently shown by Yoon *et al*. 2017 (106) to have a house-keeping function by regulating endosomal recycling of cytokines, specifically TNF. Upon binding of TNF to TNFR1 on the cell surface, the ligand-receptor complex undergoes endocytosis, a process whereby MLKL was shown to associate with the endosome and facilitate the transport of the ligand-receptor complex to lysosomes. Lack of MLKL in cell lines therefore delayed the degradation of the TNF/TNFR1, which resulted in signalling augmentation of genes susceptible to TNF stimulation. This effect of MLKL was investigated by measuring the cellular degradation of biotinylated TNF in MLKL silenced (siRNA transfection) MEFs. The cells were exposed to TNF-biotin for 30 min on ice, which temporarily halts all enzymatic activity and allows TNF-biotin to bind the TNF receptor. Subsequently, the cells were incubated at 37 °C for 0.5 h, 1 h and 2h and analysed by western blotting. Figure 5.13A shows the results of this experimental setup using the primary fibroblasts of the family and F1. In the process of characterising the TNF pathway in

the primary fibroblasts, we also found that the fibroblasts express TNFR1 as well as TNFR2, as shown in Figure 5.13B. Having two upstream receptors of the same ligand complicated the analysis, as MLKL may not affect both receptor-dependent pathways of TNF degradation and recycling. Biotinylated TNF could be observed at the expected size of 17kDa. To account for potential differences in surface binding of TNF between donors, the band intensity TNF at time points 0.5 h, 1h and 2h was normalised to the 0 h time point. Across four independent experiments a trend towards a lowering of signal intensity with increasing time could be observed, reflecting time- and temperature-dependent degradation of TNF-biotin. However, no significant difference in TNF-biotin levels could be detected between the MLKL-expressing fibroblasts of S1 and F1, and the MLKL-deficient fibroblasts of B1 and B2 (Figure 5.13C). There is therefore no evidence to suggest that a lack of MLKL affects the recycling of TNF in cultured human fibroblasts.

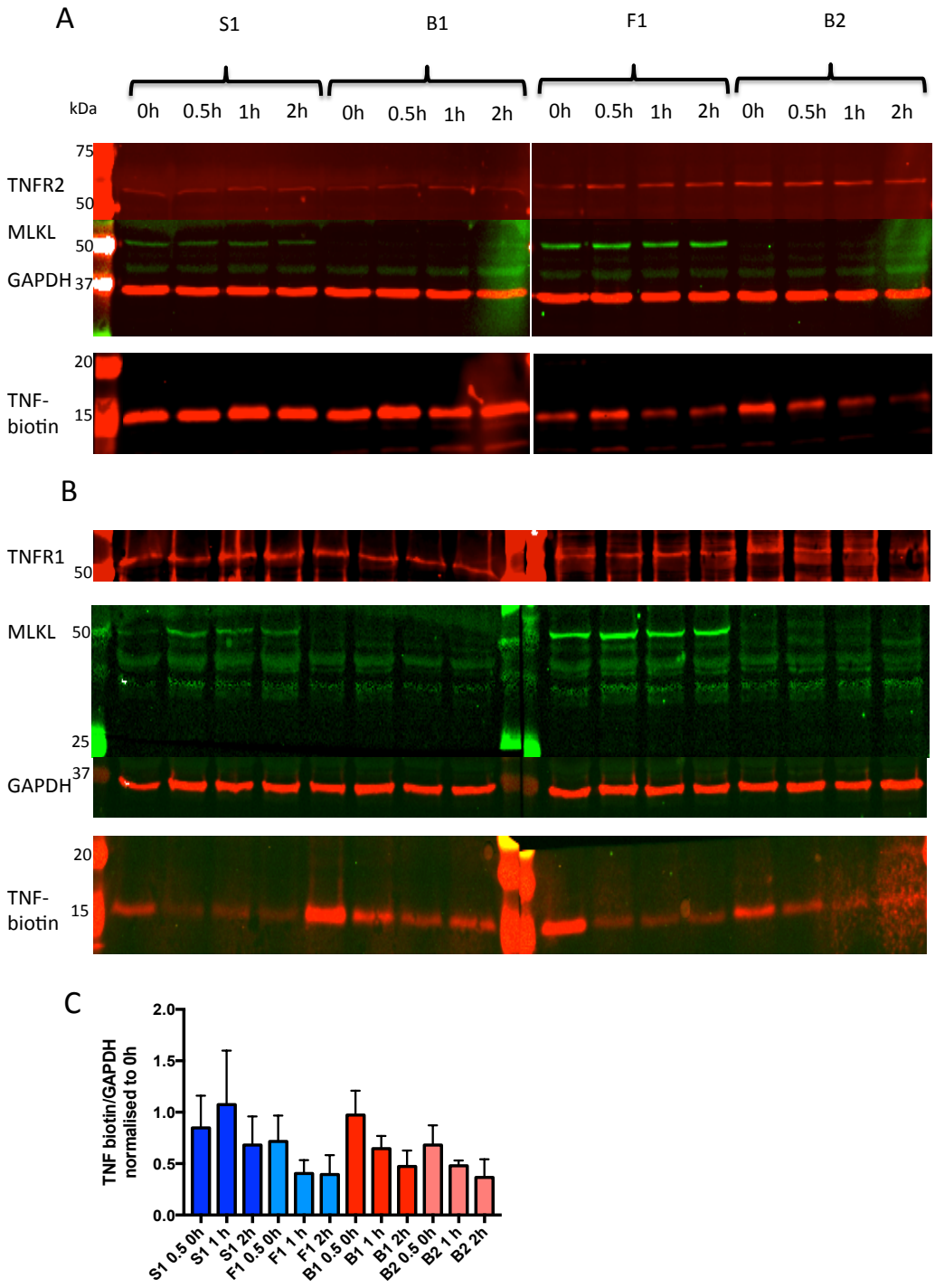


Figure 5.13. Assaying the impact of MLKL deficiency on TNF recycling. A: Western blot of TNF-biotin metabolised in the fibroblasts of S1, B1, F1 and B2 at indicated time points. Top row shows expression of TNFR2 **B**. Analogous experiment as in A showing the expression of TNFR1 in top row. **C** Diagram depicting relative reduction in band intensity with time as normalised to 0 hour time point in each donor. Band intensity was quantified using Li-Cor software. n =4. Error bars indicate SEM.

5.3 Discussion

The aim of this chapter was to examine the effect of the *MLKL* variant (rs561839347) in primary cells of the two affected brothers and their unaffected sister, specifically looking at the impact on expression and implications for the capacity to induce necroptosis. The main finding of this work is that MLKL 369 is not expressed in PBMCs and cultured fibroblasts of the brothers. The immune subsets of the brothers were within the normal range of lymphocyte and monocyte frequencies, indicating that the absence of MLKL in PBMCs does not affect the development of immune cells. These results that are derived from human samples are thus in keeping with literature on *Mlkl* KO mice, demonstrating that MLKL is dispensable for immune cell development (100).

The promoter of *MLKL* is sensitive to IFNγ in the fibroblasts of S1, B1 and B2, which resulted in increased expression of MLKL protein in S1, but not in B1 and B2. These results indicate that the lack of MLKL expression in B1 and B2 is due to a defect at the post-transcriptional level. The efforts to prevent protein degradation using MG-132 and MLKL induced necroptosis using NSA did not enable the detection of MLKL 369. One explanation for the lack of MLKL is that non-sense mediated decay (NMD) of the MLKL 369 mRNA transcript prevents protein synthesis. Also, the expression of MLKL mRNA in cultured fibroblasts of B1 and B2 was reduced to approximately one third of S1 (Figure 5.4A). This observation would support NMD as the most likely explanation, because such marked reductions in transcript levels have previously been reported of mutated transcripts susceptible to NMD (197). To test whether NMD is responsible for the observed reduction in MLKL 369 mRNA, one

could inhibit UPF1, which normally controls NMD(198), using lentiviral transduction of UPF1 shRNA or UPF1 siRNA transfection. Alternatively, pharmacological inhibitors of NMD are also available to use in cell culture (199). In both of these methodological approaches would one anticipate a significant increase of MLKL mRNA expression as measured by qPCR. The lack of MLKL in B1 and B2 could also be caused by transcriptional decay or translational stalling. The latter mechanism could potentially be assayed using affinity immunoprecipitation of the ribosomes.

The MLKL mRNA levels in the PBMCs showed the same pattern of reduced expression in B1 and B2 compared to S1 (Figure 5.4B). However, these data also demonstrated the variability in MLKL mRNA expression among unaffected individuals in PBMCs. One donor (C3) expressed a similarly low amount of MLKL mRNA compared to B1 and B2, even though MLKL protein was clearly detectable in the PBMCs of this individual using western blotting. These findings would suggest that there most likely is not a 1:1 relationship between MLKL mRNA expression and MLKL protein expression across individuals. It should also be noted that the data on MLKL mRNA and protein expression was derived from isolated PBMCs taken at a single time point from the affected and unaffected donors. As MLKL expression is affected by cytokine levels, as demonstrated for IFNγ for example, this variable factor must be taken into account when interpreting MLKL expression in PBMCs, as cytokine levels will naturally vary.

The absence of the MLKL 369 protein could either be due to loss of MLKL 369 expressing cells as the protein triggers necroptosis, or be due to a bona fide lack of MLKL 369 protein expression. To test these possibilities, the fibroblasts of the family were stimulated towards cell death (apoptosis and necroptosis) using RIPK3, IFNγ and zVAD. Stimulating the fibroblasts with IFNγ 5ng/ml and zVAD 50μM did not have a marked effect on the induction of cell death, even though this stimulus has previously been reported to induce necroptosis in MEFs. RIPK3 transduction effectively sensitised all fibroblasts lines to cell death. By adding the pan-caspase inhibitor zVAD 50μM to the medium, the cell death attributed to apoptosis could be effectively excluded, enabling the analysis of genotype-dependent effects on necroptosis. These data demonstrated that necroptosis does not occur in the fibroblasts of B1 and B2. The brothers are therefore effectively knockout for MLKL and consequently unable to execute necroptosis.

The complete lack of MLKL in the fibroblast of B1 and B2 did not cause detectable deficiencies in the ability to degrade biotinylated TNF, which has been reported by Yoon *et al*. 2017(106). This discrepancy could possibly reflect cell-specific differences.

5.4 Conclusions and future studies

From the studies in primary cells it became apparent at this point that the *MLKL* variant (rs561839347) prevents the expression of MLKL protein and the brothers are therefore deficient in the ability to induce necroptosis. The guidelines from the

American College of Medical Genetics and Genomics (171) would thus suggest a moderate to strong degree of evidence for the *MLKL* variant (rs561839347) to be pathogenic. The reports of heterozygous loss of function variants in *MLKL* in a cohort of Alzheimer's patients(130) further supported a pathogenic effect. However, the variant in *FA2H* also segregated with disease and a pathogenic effect of this variant could therefore not be ruled out. The functional studies designed to examine the *FA2H* variant using lipidomics are described in Chapter 6.

Chapter 6. The functional analysis of the FA2H F11 deletion and *in silico* analysis of the K55R substitution in *AP1S2*

6.1 Introduction

The FA2H F11del and AP1S2 K55R substitution segregated with disease in the family as described in Chapter 3 and the variants were therefore subject to investigation for potential pathogenicity in the brothers. In this chapter the variant is further explored *in vitro* to determine whether the deletion of the 11th amino acid of FA2H has any detrimental effect on its hydroxylase activity. The K55R substitution in *AP1S2* seemed to be benign based on the observation that only severe truncation of the protein or large deletions in the gene causes disease in the reported cases, whose clinical presentation also differed considerably from the brothers. Nevertheless, the *AP1S2* variant was explored further *in silico* in this chapter to model any potential effects on protein binding.

Based on the localisation of the FA2H F11 deletion in close proximity to the N-terminal cytochrome b5 domain, we aimed to assess whether the deletion would impact the ability of FA2H to transport electrons from NADH via the cytochrome b5 domain to the catalytic domain (183), which would alter the degree of hydroxylation in ceramide species. The question was approached using overexpression of FA2H mutated constructs in CHO-K1 cells followed by lipidomic analysis, as this method has previously been used in the context of functional investigation of HSP-associated *FA2H* variants.

To provide the experiment with relevant positive controls, we exploited the fact that reported variants in *FA2H* of HSP patients have been shown reduce FA2H hydroxylase activity by 40-60% either by using thin-layer chromatography (141) or liquid chromatography-tandem mass spectrometry (LC-MS/MS) (147). Figure 6.1 shows the structure of FA2H and the sites of disease-associated amino acid substitutions used as positive controls for reduced FA2H function in the experimental setup. As the L77R substitution affects the cytochrome b5 domain and the R235C substitution is located in the catalytic domain, each domain would be represented in the assay. Finally, the Y170X (146) variant that causes a truncation of the catalytic domain was included as an additional, and more extreme, positive control as this FA2H construct would not be expected to have any hydroxylase activity. The phenotypes of the patients harbouring the mentioned variants of FA2H L77R, FA2H R235C and FA2H 170 are described in Chapter 1, section 1.3.2.

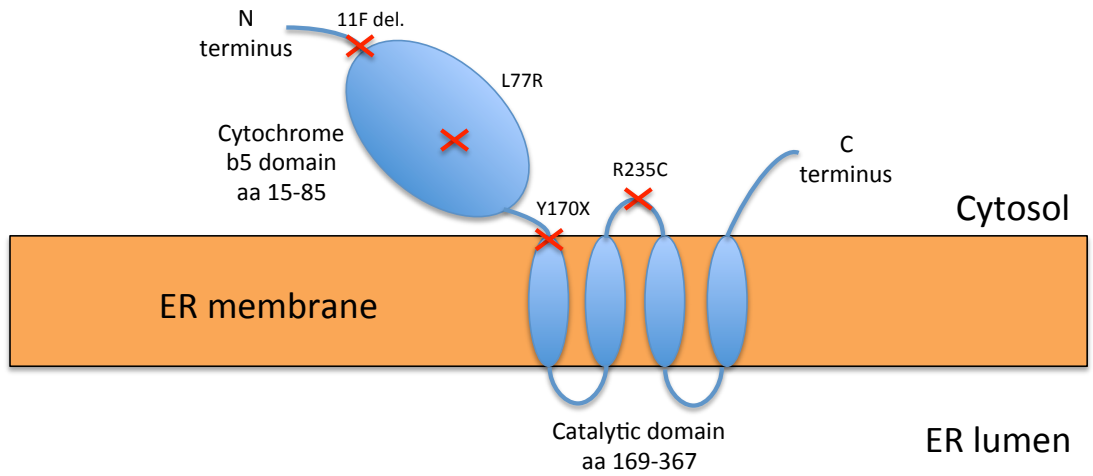


Figure 6.1. FA2H structure and site of amino acid alterations. Numbers indicate amino acid residue positions. Aa (amino acid), ER (endoplasmic reticulum). Adapted from Tonelli *et al*. (140).

6.2 Results FA2H

6.2.1 Validation of lentiviral FA2H transduction by flow cytometry and WB

Assaying the degree of hydroxylation using lipidomics was outside the capacity of the Fugger lab. Consequently, a collaboration with Professor Britta Brügger at the University of Heidelberg, Germany was set up to conduct the lipidomic analysis using LC-MS/MS on CHO-K1 cells expressing FA2H constructs prepared at the Fugger lab. The FA2H constructs were expressed in a 2nd generation lentiviral transduction system to ensure high expression efficiency. To avoid potential interference on FA2H hydroxylase activity from a large GFP tag we chose a plasmid (pSIN-CSGW-UbEm) expressing GFP in tandem with FA2H, which was used for viral titering and validation of expression as described in Chapter 2. The plasmids were expressed in CHO-K1 cells with a multiplicity of infection (MOI) of 20 to ensure saturation of expression. Figure 6.2 shows the expression of GFP measured by flow cytometry demonstrating 99.8-100% transduction efficiency across all FA2H constructs.

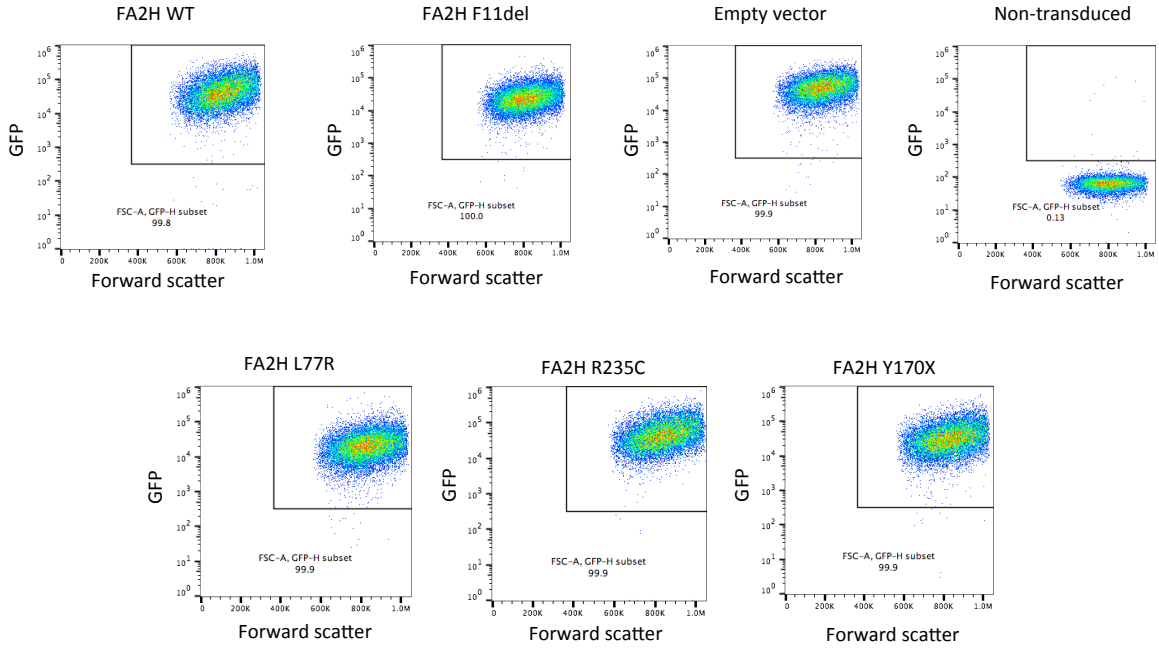


Figure 6.2. Verification of construct expression. Validation of FA2H transduction efficiency by flow cytometry using GFP expressed in tandem with FA2H.

To further validate the expression of FA2H, the transduced cells were subject to western blotting as shown in Figure 6.3. Using a monoclonal antibody against FA2H it was possible, as expected, to clearly identify FA2H around 42 kDa in cells expressing wildtype (WT) FA2H, as well as FA2H constructs harbouring single amino acid changes (FA2H F11del, FA2H R235C and FA2H L77R). Interestingly, there was a clearly reduced expression of FA2H Y170X, which may reflect instability of the protein due to the severe truncation.

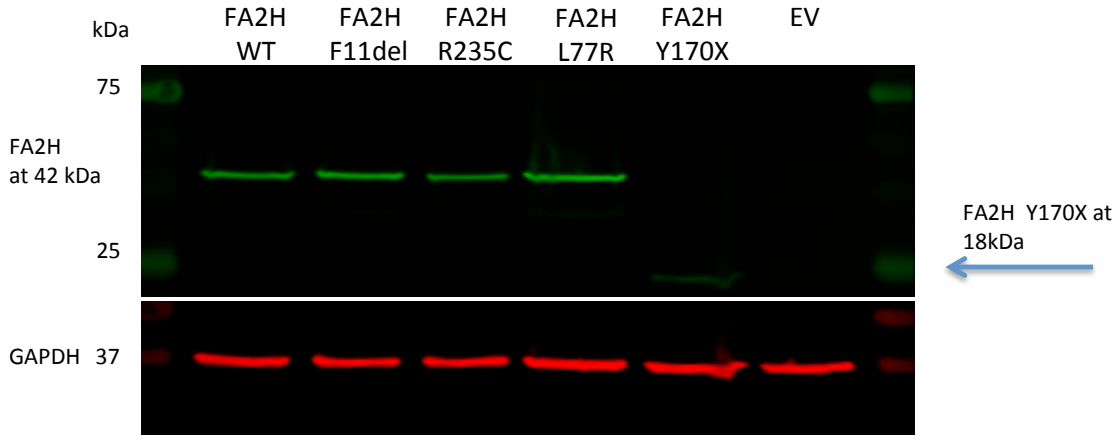


Figure 6.3. Western blot of CHO-K1 cell lysates 3 days post transduction of FA2H WT and FA2H mutant constructs. FA2H WT and FA2H mutant constructs (FA2H F11del, R235C and L77R) form stable protein, whereas FA2H Y170X is not stable.

6.2.2 FA2H enzyme activity analyses

The LC-MS/MS spectrum data of FA2H-transduced CHO K1 cell lysates were analysed in Heidelberg and identified a broad range of sphingolipids. Ceramides, hexosylceramides (which are the same as galactoceramides) (200), and sphingomyelin were the only sphingolipid species in which transduction of the stable FA2H constructs (FA2H WT, FA2H F11del, FA2H R235C and FA2H L77R) had a detectable effect of increased hydroxylation and they were therefore used for analysis. This observation indicated that fatty acids, which are the substrates of FA2H, were indeed incorporated into the expected lipid classes. Of the total amount of lipids, ceramides constituted approximately 0.2%, hexosylceramides 1.5% and sphingomyelin roughly 5%, with the remaining lipid species consisting primarily of cholesterol (23%), cholesterol esters (13%) and phosphatidylcholine (17 %) as shown in Figure 6.4.

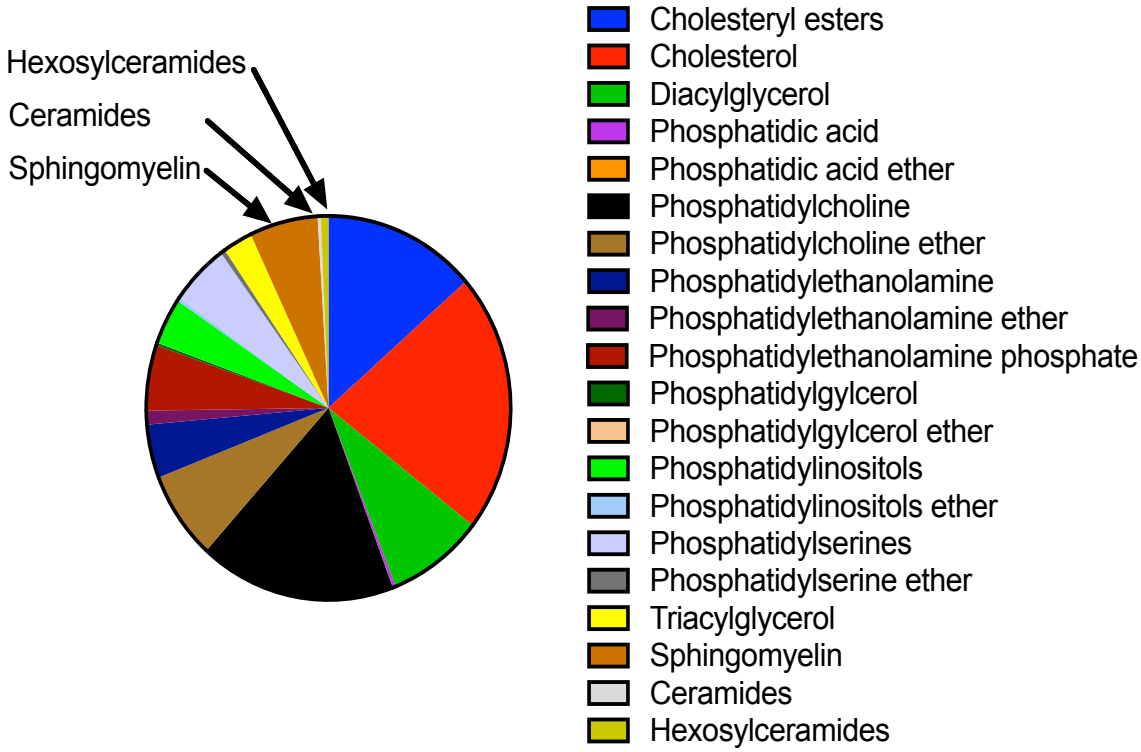


Figure 6.4. Lipid species isolated for analysis. Average percentages of lipid species isolated from CHO-K1 cells for LC-MS/MS analysis.

Figure 6.5 A-C shows the distribution in percentages of ceramides, hexosylceramides and sphingomyelin containing either 2,3 or 4 hydroxyl (OH) groups. Non-transduced cells contain ceramides, hexosylceramides and sphingomyelin primarily with 2 OH groups, whereas transduction with stable FA2H constructs (FA2H WT, FA2H F11del, FA2H R235C and FA2H L77R) increased the relative abundance of the sphingolipid species containing 3 and 4 OH groups (see Figure 1.8 for ceramide structure and OH groups). Sphingomyelin only contained 2 or 3 OH groups. Transduction of stable FA2H constructs caused a higher increase in the ratio of hydroxylated to non-hydroxylated ceramides and hexosylceramides compared to sphingomyelin. For example, FA2H WT transduced cells contained 1% 3 OH ceramides and 1 % non-hydroxylated (2 OH groups) (Figure 6.5A). For

hexosylceramides the increase was substantially higher with approximately 17% containing 3 OH groups upon FA2H WT transduction and 3% being non-hydroxylated (Figure 6.5B). In comparison, only about a third (20%) of sphingomyelin species were hydroxylated (3 OH) and 60% were non-hydroxylated (Figure 6.5C), which might reflect a higher tendency of ceramides and hexosylceramides to undergo hydroxylation or exist in a hydroxylated form.

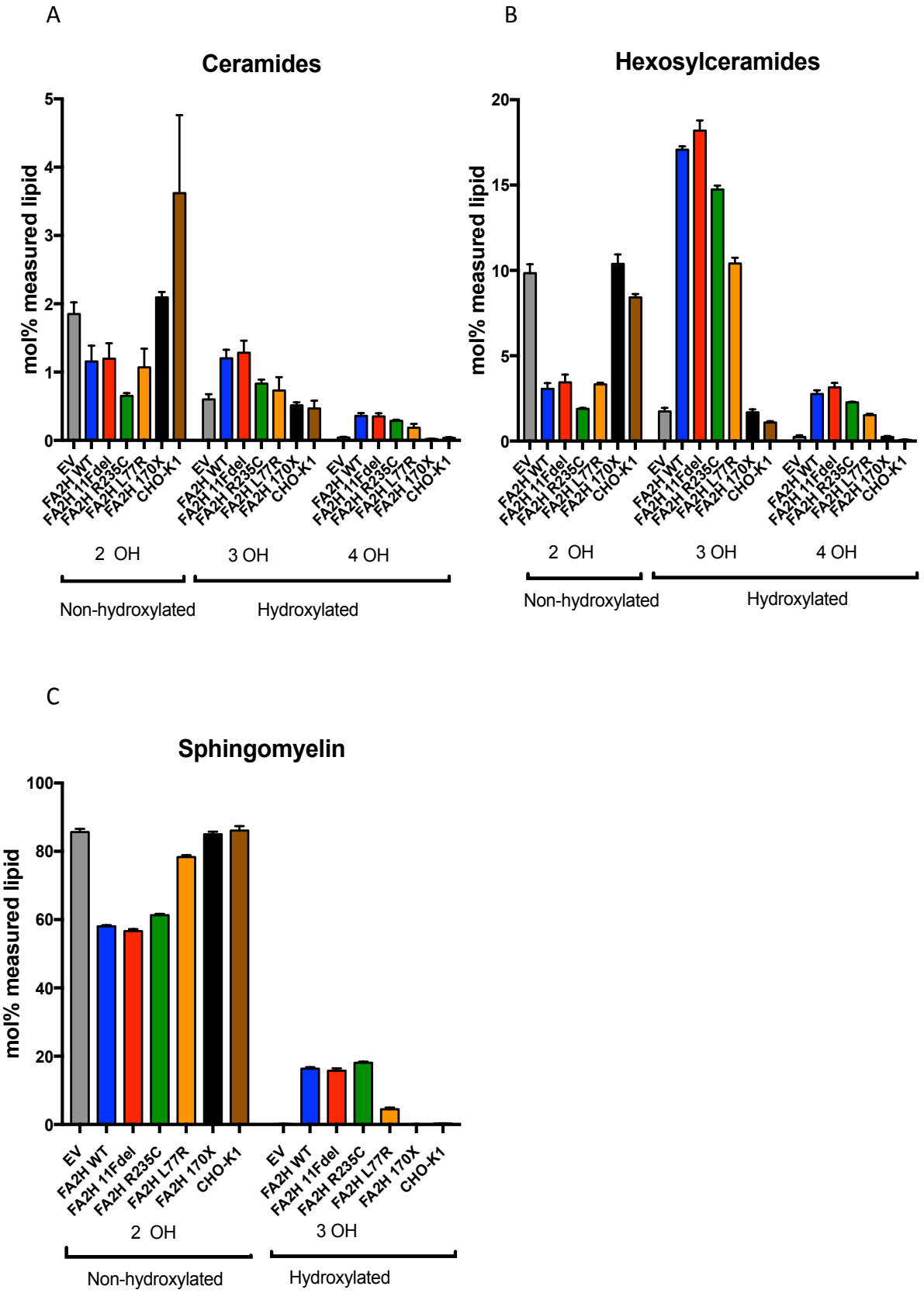

A
Ceramides
mol% measured lipid
EV
FA2H WT
FA2H 11Fdel
FA2H R235C
FA2H L77R
FA2H 170X
CHO-K1
2 OH
3 OH
4 OH
Non-hydroxylated
Hydroxylated
B
Hexosylceramides
mol% measured lipid
C
Sphingomyelin
mol% measured lipid

Figure 6.5. The relative abundance and hydroxylation of sphingolipid species upon expression of FA2H WT and FA2H mutant constructs. A-C. Relative abundance in molar (mol) % of hydroxylated ceramides, hexocylceramides and sphingomyelin, respectively, relative to the total amount of lipid species containing 2, 3 or 4 OH groups. Experiments carried out in duplicates. Error bars indicate ± SEM. n = 6.

To narrow down the analysis on potential FA2H genotype dependent differences in hydroxylation, the percentages of hydroxylated species (with variable chain length) containing 3 or 4 OH groups were added to provide a combined measure of hydroxylated species (3 and 4 OH group) relative to non-hydroxylated species (2 OH groups). Figure 6.6 A-C shows the relative degree of hydroxylation as a function of FA2H transduction in ceramides, hexosylceramide, and sphingomyelin, respectively. The degree of hydroxylation in ceramide species was not significantly different between FA2H WT and FA2H F11del transduced cells, in which approximately 1.5% of ceramides were hydroxylated, as shown in Figure 6.6 A. In contrast, cells expressing the control construct FA2H R235C and FA2H L77R showed a significantly reduced degree of hydroxylation of ceramides to about 1%. The degree of hydroxylation in FA2H Y170X expressing cells was comparable to empty vector expressing cells and non-transduced cells. This finding indicated that the FA2H Y170X construct, as expected, has no catalytic activity, which is most likely due to the truncation of the protein and the reduced expression as observed in Figure 6.3.

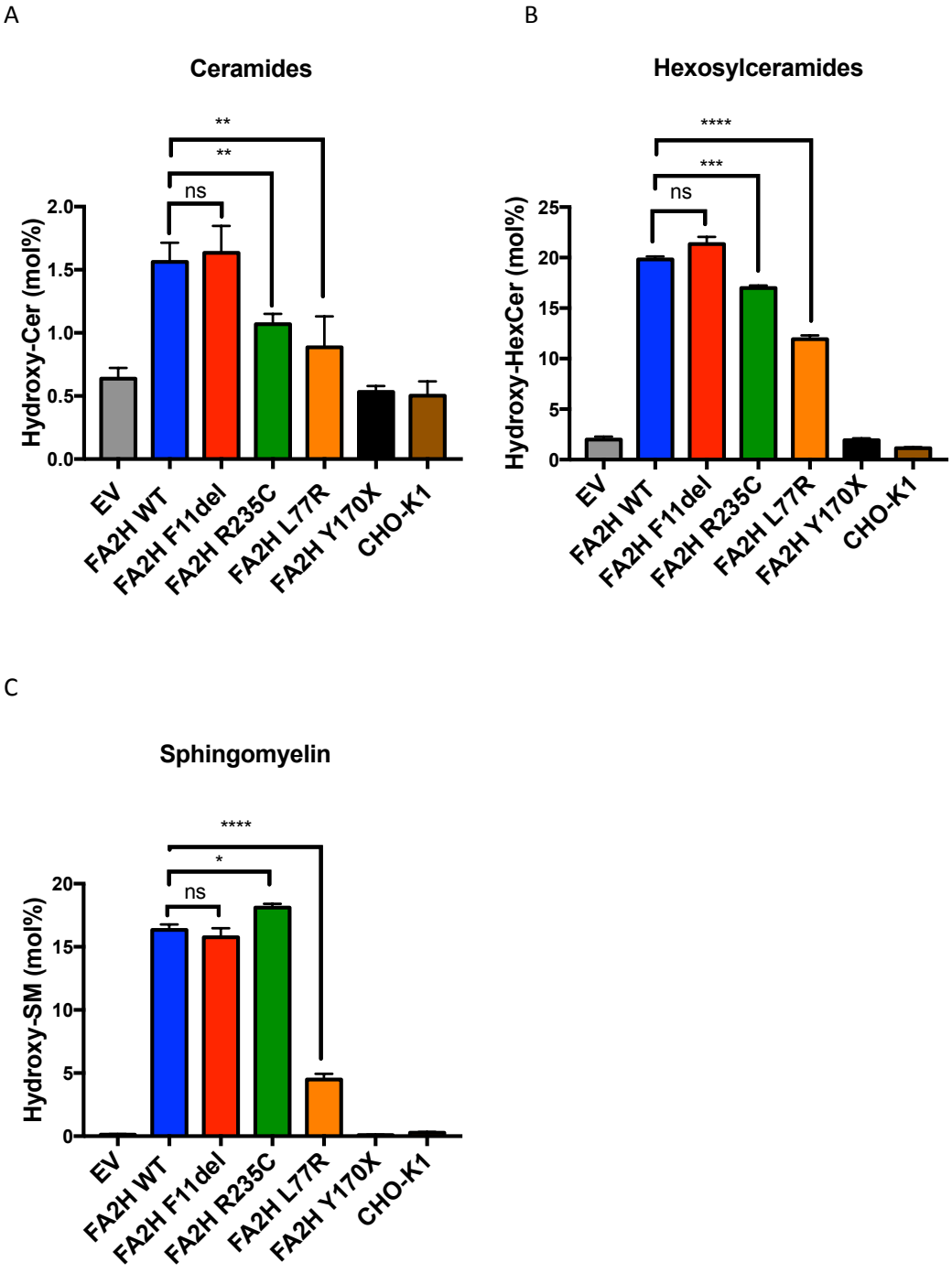


Figure 6.6. FA2H mediated hydroxylation of ceramides, hexosylceramides and sphingomyelin. Diagrams show the percentage of ceramides **(A)**, hexocylceramides **(B)** and sphingomyelin **(C)** species that were hydroxylated upon FA2H transduction relative to the total amount of lipid species containing 2, 3 or 4 OH groups. Error bars indicate ± SEM. n = 6. Paired t-test.

For hexosylceramide species (Figure 6.6 B), FA2H WT and FA2H F11del expression caused hydroxylation of approximately 20% of hexosylceramides and no significant genotype dependent difference could be detected. Similarly to ceramides, the FA2H R235C and FA2H L77R expressing cells were shown to contain significantly reduced levels of hydroxylated hexosylceramides (≈16% and 10%, respectively) compared to FA2H WT.

The FA2H F11del expression resulted in approximately 15% of sphingomyelin species being hydroxylated, which was not significantly different from sphingomyelin hydroxylation in FA2H WT expressing cells (Figure 6.6 C). Sphingomyelin in the FA2H R235C expressing cells was marginally increased in hydroxylation, which contradicted the results of hydroxylation of this control construct in hexosylceramides and ceramides. In contrast, FA2H L77R expressing cells only contained approximately 4% hydroxylatated sphingomyelin species, which was significantly lower compared to FA2H WT.

6.2.3 In silico analysis of FA2H F11del variant

The computational predictor algorithm PROVEAN (201) is based on alignment analysis of the variant and normal protein sequence homologs. Using this tool, the FA2H F11del variant was given a PROVEAN score of -1.305, indicating a neutral effect of the variant. Independent of this DPhil project, a clinical genetic analysis of the brothers was carried out by the company Centogene AG in 2014 in order to investigate whether HSP could be confirmed genetically. The FA2H variant was detected in this analysis, but it was not deemed to be pathogenic. CentoGene AG

therefore concluded that a diagnosis of autosomal recessive spastic paraplegia could not be genetically confirmed. The *in silico* analyses thus supported the functional analysis using LS-MS/MS suggesting that the FA2H F11del is benign.

6.3 *In silico* characterisation of K55R substitution in AP1S2

The variant in *AP1S2* identified in the brothers is a substitution of A to G at base pair 164 causing a K55R substitution, both positively charged amino acids with a pKa of 10.67 and 12.10, respectively. *In silico* analysis of the *AP1S2* variant using polyphen-2(168) resulted in a score of 0.642 indicating a possibly damaging effect, based on the degree of protein sequence conservation across species. Moreover, the lysine and arginine residues encoded by the common and rare alleles, respectively, have similar biochemical properties in that both are hydrophilic and have positively charged side chains - further suggesting that any effects on protein function would likely be subtle.

AP1S2 encodes the σ1b subunit of the AP-1 complex as described in Chapter 1. σ1b knock out mice are indeed viable, but suffer from reduced synaptic vesicle recycling, as well as impaired spatial memory and lipodystrophy (158) (157), phenotypic characteristics not shared by the brothers. These observations suggested that the substitution does not affect protein stability, as that would lead to protein loss and thus to a phenotype that would resemble the patients with childhood onset X-linked mental retardation due to truncations of AP1S2 and possibly the σ1b -/- mice. These considerations led to the hypothesis that any functional impact of the K55R variant might relate to protein binding. A computational analysis was therefore conducted

using the publically available crystal structures of the AP complexes from The Protein Databank Website (176) to model the effect of the variant.

σ1 subunits in AP complexes contain conserved amino acids that bind dileucine motifs with the sequence: (DE)XXXL(LI) (D, aspartate; E, glutamate; L, leucine; I, isoleucine and X is any amino acid). These dileucine motifs are present on numerous transmembranous proteins, such as ion channels and receptors that are destined for transport within the cell, as described in Chapter 1 section 1.4. The amino acid residues on σ subunits involved in dileucine motif binding have been characterised in detail for AP-2 based on co-crystallisation of the *Mus musculus* AP-2 complex with the RM (phosphoS) QIKRLLSE (Q peptide) peptide from the human T-cell surface antigen CD4 (RSCB PDB number: 2JKR (2.98 Ångstöm resolution)) (202). The amino acid residues (marked by black boxes in Figure 6.7: R15, Y62, A63, L65, V88, N92, V92, E100, L103) form a hydrophobic pocket on σ2 that allows the binding of the dileucine motif on the Q peptide. With the exception of N92 and L103, the residues interacting are conserved across the σ subunits.

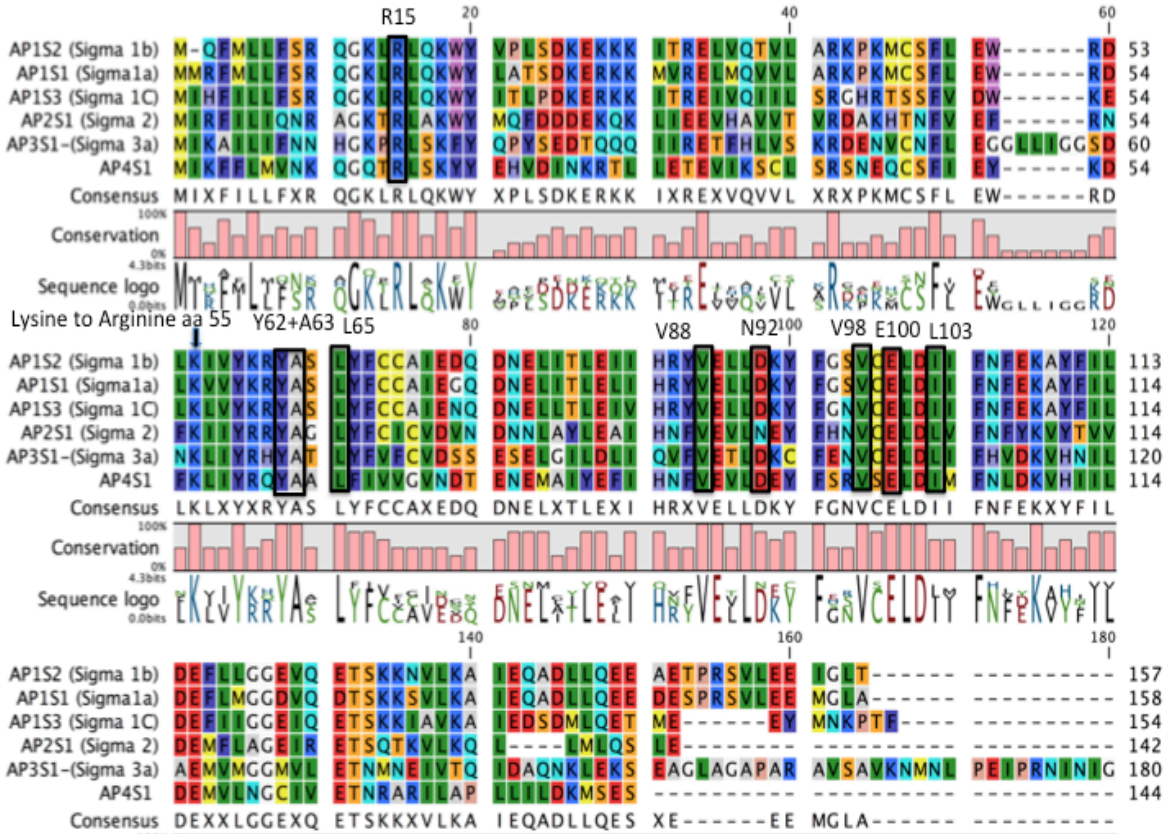


Figure 6.7. Alignment and conservation of human σ subunits in AP complexes 1-4. Conserved residues that interact with the Q-peptide are marked in black boxes.

To visualise the corresponding site of the hydrophobic pocket that binds dileucine residues in the AP-1 complex and the spatial relation to K55, the Pymol software was used to analyse the AP-1 complex co-crystallised with Arf1 (ADP-ribosylation factor 1) from Ren *et al*. 2013 (156) (PDB accession number 4hmy, 7 Ångstöm resolution). In this structure the third isoform σ1c encoded by *AP1S3* (human) was used. The lysine residue in σ1c is homologous to the K55 residue in σ1b is shown in purple in Figure 6.8A and enlarged in 6.8B. In Figure 6.8C and 6.8D the hydrophobic pocket is shown in orange on the opposite side of the subunit. The crystal structure analysis thus reveals that the K55 residue is relatively exposed, but spatially present on the direct opposite side of the hydrophobic dileucine binding residues. Based on this image it seems unlikely that the K55R substitution of the brothers would

interfere with the ability of the σ1b subunit to bind dileucine motifs on peptides and thus sorting of cargo proteins.

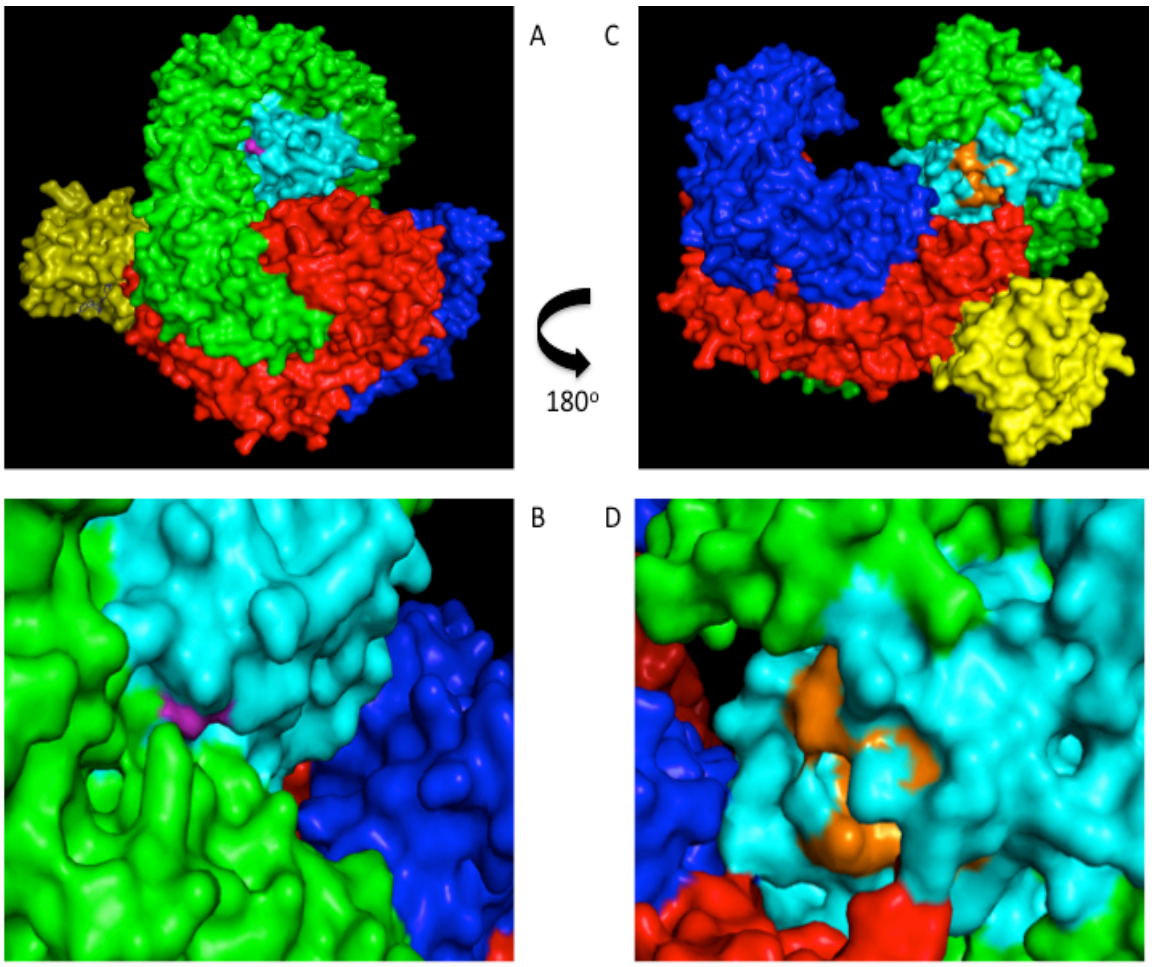


Figure. 6.8. AP-1 complex with Arf1 (PDB 4hmy). Green: γ-subunit. Red: β1-subunit. Blue: μ-subunit. Cyan: σ1c-subunit. Yellow: Arf1. Purple: Mutated K55R aa residue. Orange: dileucine binding residues (R15, Y62, A63, L65, V88, N92, V92, E100, L103) that binds peptides containing dileucine motifs.

To further explore the relative location of the K55 residue and dileucine binding residues on the σ1 subunit, we also considered a co-crystallisation of the AP-1 complex with BST2 (Bone marrow stromal antigen 2, antiviral restriction factor) and protein u (Vpu) encoded by HIV-1 (203) (PDB number 4p6z, 3 Ångström resolution). Human σ1a was used as the σ-subunit in this crystal structure.

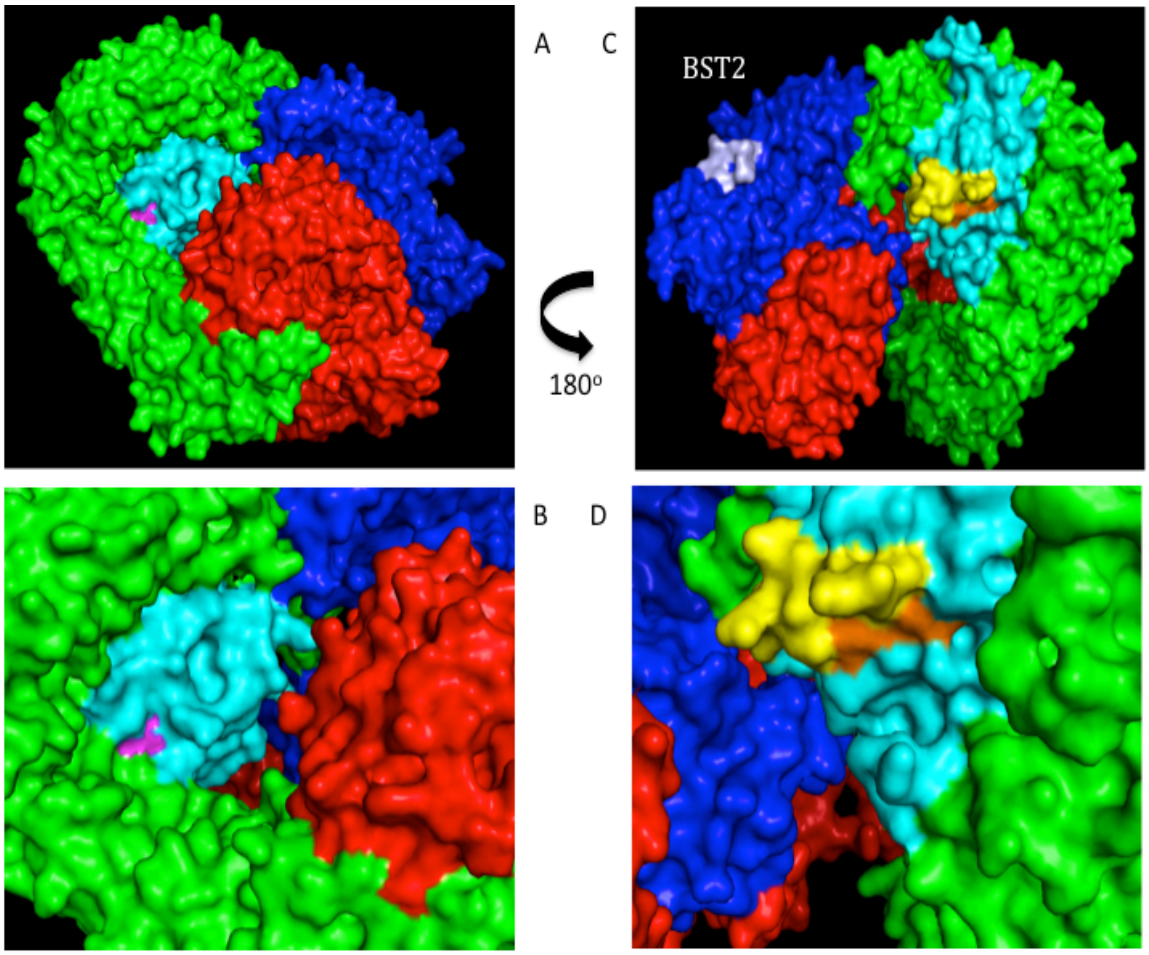


Figure 6.9. AP-1 complex with BST2 and Vpu (PDB 4p6z). Green: γ-subunit. Red: β1-subunit. Blue: μ-subunit. Cyan: σ1a-subunit. Purple: Mutated K55R aa residue. Orange: dileucine binding sites. Yellow: Vpu Pale blue: BST2.

Similar to the previous crystallisation, the K55 residue seems to be located in a pocket (Purple) on the σ1a subunit as shown in Figure 6.9A and enlarged in Figure 6.9B. Rotating the complex 180 degrees, the Vpu protein shown in yellow was found, as expected, in close proximity to the hydrophobic dileucine binding residues labelled in orange. Analogous to the findings of the 4hmy structure, this co-crystallisation demonstrated that the K55 residue and the dileucine binding site are at opposing sides of the σ1 subunit.

6.4 Discussion

6.4.1 Discussion on FA2H lipidomics

The LC-MS/MS measurements of hydroxylation of hexosylceramides, ceramides and sphingomyelin in FA2H-transduced cells suggested that the FA2H F11del expressed in the brothers does not affect the hydroxylating activity of the enzyme. FA2H constructs containing the HSP-associated amino acid substitutions (R235C and L77R) functioned as positive controls as they have previously been shown to reduce ceramide hydroxylation. The experiment demonstrated that FA2H R235C and FA2H L77R significantly decreased the ceramide and hexosylceramide hydroxylation, indicating that these variants indeed cause a reduction in FA2H enzymatic activity, which further supports the pathogenic effect of these variants in HSP. The similarity in the pattern of hydroxylation of ceramides and hexosylceramides most likely reflects that these lipids are biochemically closely linked as they are only separated by one enzyme, galactosyltransferase, which functions downstream of FA2H.

The method was based on CHO-K1 transduction followed by lipidomic assaying as it is the most established method to explore the effect of disease-associated *FA2H* variants. The lentiviral transduction ensured ≥ 99.8 % transduction efficiency as measured 3 days post transduction. As the CHO-K1 cells were transduced with a MOI of 20, the protein synthesis machinery of the cells was therefore at saturation. The differences observed are therefore not likely to reflect differences in protein expression but rather differences in FA2H activity in keeping with quantified GFP

expression of FA2H constructs (Figure 6.2) and western blot analysis of FA2H expression (Figure 6.3).

The increase in hydroxylation of sphingomyelin in FA2H R235C expressing cells was unanticipated, given that that FA2H L77R expression caused a reduced degree of hydroxylation. It should be noted, however, that the effects of the FA2H R235C variant on sphingomyelin hydroxylation has not previously been investigated, nor has any of the other known disease associated FA2H variants been assayed for the effects on spingomyelin hydroxylation, as fatty acids in ceramides are the described target for FA2H. Nonetheless, one could observe sphingomyelin hydroxylation upon FA2H overexpression using LS-MS/MS, which is a novel finding. It is possible that the variant may somehow have changed the affinity of the hydroxylated ceramides for export to the Golgi apparatus, where it would be further modified to sphingomyelin and thus cause an enrichment of the hydroxylated form of sphingomyelin, though this option remains speculative. This possibility could potentially be explored using immunogold labelling of sphingomyelin and ceramide species as this technique has previously been used to delineate cellular location and metabolism of these lipid species (204).

In summary, there is currently no experimental evidence to support an effect of the FA2H 11Fdel variant on fatty acid hydroxylation, in keeping with the PROVEAN *in silico* analysis and Centogene AG report suggesting no effect of the variant. The data would, however, support the current understanding that FA2H hydroxylation of ceramide species is reduced in HSP patients with *FA2H* variants as the method

detected reduced hydroxylation of ceramides upon FA2H R235C and FA2G L77R expression.

However, it is still unresolved how reduced hydroxylation of ceramides would cause HSP. One possibility is that reduced FA2H activity causes compromised plasma membrane integrity due to decreased levels of intermolecular hydrogens bonds. A more complicated explanation for the observed disease association is that lack of hydroxylation perturbs the formation of ceramide-enriched platforms in the cell membrane, which are important for receptor clustering (205). Ceramides have been shown to have a complex role in the regulation of apoptosis, in which it has a pro-apoptotic function by facilitating TNF signalling (206).

6.4.2 Discussion on AP1S2 *in silico* analysis

The *in silico* analysis based on species conservation using polyphen-2 indicated that the K55R variant in *AP1S2* is possibly damaging. However, based on the analysis of two independent crystal structures, the K55 residue was found to be located distant to the dileucine binding site used for the protein sorting during transport of clathrin coated vesicles. The crystal structure analyses therefore indicated that the K55R substitution of the brothers, most likely does not affect the binding and sorting of cargo proteins. These results added another layer of evidence to suggest that the variant in *AP1S2* does not affect protein function.

Collectively, the population data, the phenotype of the brothers being very different from patients and mice deficient in AP1S2 and the crystal structure analysis,

suggested that the substitution in AP1S2 is benign. It is, nevertheless, important to underscore that the *in silico* analysis is not suitable to estimate potential subtle effects of the K55R substitution on AP1S2 function, which could theoretically have affected the disease course of the brothers. The involvement of AP1S2 in the neuronal metabolism and the association of loss of function variants in *AP1S2* to Pettigrew syndrome emphasizes the relevance of the AP1S2 K55R variant as a possible contributing factor in the disease of the brothers.

To explore possible effects of the K55R substitution in AP1S2 *in vitro*, immunoprecipitation of core subunits in the AP-1 complex could be used to explore whether the K55R substitution exerts a pathogenic effect by affecting the stability of the AP-1 complex. As described in Jain et al (159), it is possible to incorporate transgenic 1σ constructs into the endogenous AP-1 complex of HeLa cells. Alternatively, it is also a possibility that the K55R substitution has subtle effects on the ability of the AP-1 complex to bind interaction partners that are destined for transport. To assay this possibility, one could exploit the fact that the AP-1 complex interacts with the copper transporter ATP7B (159), and stain for this protein in the IP lysate. However, the lack of known disease associated missense variants in *AP1S2* posses a difficulty in the experimental setup of the assay, as no positive control variants can be used in the experiment. It is therefore potentially hard to estimate the sensitivity of the assay, which needs to be taken into account.

Chapter 7. Discussion

7.1 Summary of results

This DPhil project aims to investigate and describe the genetic and clinical characteristics of two brothers, who over the course of 30 years developed a severe progressive neurodegenerative disease. The disease in both brothers is clinically characterised by slowly progressive, asymmetrical paresis of the lower limbs (initially presenting in the left side) with spasticity, cerebellar ataxia, dysarthria, seizures and mental impairment, reflecting severe atrophy of the cerebrum, cerebellum and brainstem as demonstrated by MRI. They were originally diagnosed with PPMS in 1985 (brother B1, at that time aged 19 years) and 1990 (brother B2, aged 30 years). The diagnosis of B1 was based on the clinical presentation, and it was supported by isolated oligoclonal band positivity and bilaterally affected visual evoked potentials. The diagnosis of MS was in accordance with the Poser criteria used at the time. B2 was also diagnosed clinically, essentially based on the clinical resemblance to B1. Since the time of diagnosis, the disease in both patients has developed in a manner not typical for PPMS. The most important difference is the absence of sensory symptoms. Moreover, the fasciculations observed in B1 in 2017 are inconsistent with PPMS, as they are indicative of peripheral neurodegeneration. At the time of diagnosis MRI scans were not conducted and it is thus unknown if the patients would have fulfilled the McDonald criteria for the diagnosis of MS (30). The MRI conducted in 2013 showed no evidence of significant white matter lesions in either brother, however, there is no literature describing what a typical MRI of the CNS would show 30 years after a diagnosis of PPMS. Overall, the collected clinical data would in hindsight suggest that PPMS is not the appropriate diagnosis.

Clinically it can be argued that the phenotypic presentation of the brothers would be more suggestive of a complex form of HSP, which is a more heterogeneous diagnostic category of neurodegenerative diseases. However, the presence of oligoclonal bands in the CSF and fasciculations are usually not a part of the clinical picture in HSP. The described clinical phenotype is thus suggestive of a neurodegenerative spectrum disorder that clinically overlaps with PPMS, HSP and ALS. In this context it is worth noting that multiple cases of patients fulfilling the diagnostic for MS as well as HSP have been described (78, 79, 207), underscoring the phenotypic overlap between these diseases that evidently poses a diagnostic challenge to clinicians. These nosographic considerations aside, the disease in the patients under study is, in phenotypic terms, initially characterized by progressive, global atrophy of the central nervous system, and, later in the course of disease, possibly also by involvement of the peripheral nervous system (PNS). The severe atrophy causes a clinical phenotype of a neurodegenerative spectrum disorder.

The atypical clinical course of the brothers was the main reason for conducting WGS through the WGS 500 program, designed to assess the diagnostic utility of WGS. WGS enabled an unbiased approach to the identification of rare variants with a potentially strong impact on disease. The bioinformatics analysis was conducted based on the hypothesis that any causative or contributing genetic variants would show an autosomal recessive, a compound heterozygous or an X-bound inheritance pattern. The described variants in *MLKL*, *FA2H* and *AP1S2* were all found to segregate with disease. The phenotype of the brothers, as well as the bioinformatical analysis and computational modelling of the K55R substitution in AP1S2 shown in

Chapter 6, suggested that the missense variant in *AP1S2* is benign (171). The haplotype on chromosome 16 containing the *FA2H* F11 del and the *MLKL* variant (rs561839347), for which the brothers are homozygous, consequently became the prime object of investigation. The variants in either gene could potentially contribute to the phenotype of the brothers, since other variants in these genes have been implicated in neurodegenerative diseases. As mentioned in Chapter 1, missense variants in *FA2H* are linked to HSP (SPG35) (141), heterozygous loss-of-function variants in *MLKL* have been linked to Alzheimer's disease (130), and heterozygous deletions spanning both genes have been linked to autism spectrum disorders (150).

From this perspective, the *FA2H* F11del appeared to be a strong candidate to explain the disease in our patients. According to ACMG guidelines (171), however, phenotypic resemblance with the known spectrum of clinical features does not by itself provide decisive support for claiming pathogenicity. The variant is novel as it does not exist in the gnomAD database and could thus be a private variant only found in this family. As *FA2H* F11del is located immediately outside the cytochrome b5 domain of FA2H, it was unclear whether it would have any detrimental impact on protein function. This question could not be answered using computational modelling, but only in an experimental setting. The lipidomic assay of the *FA2H* F11del in CHO-K1 cell lysates, described in the results section of Chapter 6, detected no significant impact of the *FA2H* F11del variant, as compared to FA2H WT, on the degree of FA2H-mediated ceramide hydroxylation. This observation suggested that the *FA2H* F11del variant is in fact benign, which is consistent with results of

PROVEAN *in silico* analysis of the variant as well as the CentoGene report on the family described in Chapter 6. Consequently, there is no formal evidence that could confirm a diagnosis of autosomal recessive spastic paraplegia.

In contrast, we can show that the *MLKL* 369 variant (rs561839347) severely impacts the MLKL protein. The initial approach using transfection of MLKL into HEK293 cells, demonstrated that upon expression of the MLKL variant protein, the lack of a functional pseudokinase domain in the truncated MLKL 369 led to increased cell death, consistent with the known auto inhibitory function of the MLKL pseudokinase domain (92). Thanks to the generous decision of the family to provide primary cells in the form of PBMCs and skin fibroblasts, it became possible to study the effect of rs561839347 homozygosity *ex vivo.* Using these cells, whereby MLKL expression is under the control of its endogenous promoter as opposed to being over-expressed in a transfection system, it was demonstrated that rs561839347 homozygosity leads to an absence of MLKL protein. This inability of the brothers to express MLKL was shown to cause deficiency in the capability to execute necroptosis, as demonstrated in Chapter 5. The experiments conducted on primary cells thus demonstrated that the effect of the *MLKL* variant (rs561839347) on necroptosis was the opposite of what was concluded based on the results in cell lines, in which expression of MLKL 369 was shown to increase cell death due to lack of a functional pseudokinase domain. Of the two methodological approaches to the same question on the effect of *MLKL* variant (rs561839347), it would seem reasonable that the data derived from primary cells is more likely to reflect the physiological conditions and therefore constitutes a stronger degree of evidence.

The absence of MLKL in the brothers most likely reflects NMD of the MLKL 369 mRNA transcript, as MLKL mRNA levels in the brothers' fibroblasts were approximately three fold lower than observed in S1 fibroblasts as demonstrated in Chapter 5. The magnitude of decrease in mutant mRNA is expected when the transcript is susceptible to NMD (197). Indeed, expression of MLKL 369 would be detrimental to cell viability as demonstrated in Chapter 4. These observations combined with the association of heterozygous loss-of-function variants in Alzheimer's patients (130) would be supportive of a pathogenic effect of the *MLKL* 369 variant (rs561839347) (171).

7.2 Limitations of the study

The functional assay of the *FA2H* F11del variant was conducted *in vitro* and showed that the variant does not affect FA2H hydroxylase function. It is possible, however, that the variant could exert subtle effects on the biochemical or clinical phenotype over longer time periods, indeed decades in this case, which cannot be detected in *in vitro* experiments. One way to capture any long-term subtle effects of the variant could be analysis of the variant *in vivo* using a mouse model. Animal experimentation has its own limitations, of course, and, given that the brothers developed disease in adulthood, is it unclear when, if ever, one could expect neurological symptoms to appear in mice carrying the homozygous *FA2H* F11del variant.

Finally, it is possible that environmental factors have also had an effect on the disease course of the brothers, even though their patient history does not contain information about any unusual environmental exposures.

7.3 Interpreting WGS findings

Despite the strong similarity of the disease course in the two brothers, it is worth noting that there is an 11-year difference in disease onset, a difference that cannot be explained by any of the variants in *MLKL, FA2H* or *AP1S2.* None of the identified variants in question can therefore entirely account for the course of disease in these two patients, which would imply that other genetic and/or environmental factors are influencing the individual impact of each variant.

As such the WGS of this family exemplifies how the technology requires the researcher/clinician to consider that any genetic variant will exert its effect on the phenotype in concert with the genetic background of the individual. The use of WGS thus stresses the need of the clinician/researcher to think in terms of the whole genome, i.e. in principle to consider the entirety of genetic contributions to disease (with the exception of epigenetic factors). This way of thinking is quite different from understanding the results of single gene or gene-panel approaches. WGS is especially relevant in cases of rare diseases in pedigrees with multiple affected members across generations with a clear mode of inheritance, in which it is unclear which gene might be affected. In this context, the strength of WGS lies in its capacity to identify rare variants, and even de novo variants, with a previously unknown impact on the phenotype.

The results of the WGS and the functional studies of the brothers have helped to elucidate possible biological mechanisms of disease pathogenicity, which will be discussed below. It is worth noting, however, that WGS as a diagnostic tool did not provide a definitive clarification of the diagnosis of the brothers, which was one of the aims of WGS500 program (18). This finding was, however, not too surprising given previous studies of the clinical utility of next-generation sequencing. For example, Yang *et al*. showed that whole exome sequencing (WES) is able to identify a clear pathogenic variant in only 25% of cases with a phenotype suggesting genetic aetiology, which is nevertheless higher than the average success rate of single gene or gene panel approaches (208). Other studies have reported diagnostic success rates of up to 40% (209). The variable diagnostic success rate indicates that despite the comprehensive guidelines of ACMG, it remains a challenge to determine the effect of rare genetic variants on clinical phenotype and translate these finding into the clinical setting, as exemplified by the family investigated in this thesis. Notwithstanding these difficulties, WGS (or WES) is often hailed as an important technique towards the path to personalised medicine, which is further promoted by the decline in the cost of WGS (210). One can argue that stringent adherence to the clinical guidelines of ACMG (171) on the interpretation of genetic variants identified by next-generation sequencing selects for variants with strong effects on the clinical phenotype, with the aim of identifying a single heritable component that can explain the disease. This approach can be necessary in a clinical setting in which it is necessary to provide a diagnosis that can have prognostic and therapeutic implications.

However, to understand the heritability of a disease it may be necessary to consider that the effect of rare variants might not be an "all or nothing" effect, as the variants in question may also exert a more moderate effect on the phenotype. Recognising that there are often varying levels of evidence to support pathogenicity of a variant, it is has been underscored by leading experts in the field that definitive assignment of disease causality is often impossible as the variants in question by definition are rare (170), and consequently, few patients will harbour the variants that are suspected of being pathogenic. Accordingly, it is often more appropriate when considering disease associated variants identified by WGS or WES to discuss the collected body of evidence to suggest that a variant is implicated in disease or not.

This distinction is particularly relevant when considering late onset diseases, in which the studied variant does not affect the reproductive fitness of the individual. In this situation the variant in question would be subject to a lower degree of evolutionary selection, which, when the inheritance is recessive, may lead to higher allele frequencies of up to 1% (211). With respect to the brothers, the *MLKL* variant (rs561839347) has not affected the reproductive fitness of the brothers, as B2 has fathered two non-affected children. Furthermore, as the brothers have inherited the identical haplotype on chromosome 16, harbouring the *MLKL* variant, from each parent, the parents must have had a common ancestor who would obviously have been homozygous. This further substantiates that reproductive fitness is not affected. It is therefore not surprising that the allele frequency of *MLKL* variant (rs561839347) is approximately 0.2%. These results based on allele frequency would thus suggest that *MLKL* loss of function variants, such as the *MLKL* variant

(rs561839347) in the brothers and the *MLKL* variant (c. C142T, p.Q48X) observed in patients with Alzheimer's patients(130), exert a slowly progressive effect over decades, which would consequently not affect reproduction.

However, the variable disease phenotype associated with *MLKL* deficiency and the difference in the age of disease onset in the brothers harbouring the same *MLKL* variant could also suggest that other environmental and genetic factors could modify the effect of MLKL deficiency. As previously mentioned do *Mlkl* KO mice not develop neurodegenerative disease spontaneously, which could also imply that environmental and time dependent effects are necessary to observe a detectable effect on disease development. As the phenotype and age of the three individuals carrying the homozygous *MLKL* variant (rs561839347) registered in the gnomAD database is not known, it is difficult to dissect the importance of this information. In theory, the individuals can either be: 1) non-affected by the variant and remain unaffected, 2) be non-affected but later develop disease depending on other genetic variants or environmental exposures and 3) be affected by a neurodegenerative disease.

The observation of heterozygous *MLKL* loss-of-function variants (c. C142T, p.Q48X) in patients with late-onset Alzheimer's disease could also indicate that the degree of MLKL deficiency, determined by having either one or two dysfunctional alleles affects the relative risk and severity of neurodegeneration. This concept of a gene dosage dependent mechanism would be consistent with the fact that the brothers are affected by global atrophy of the CNS, seemingly with a strong impact on motor

neuron function, whereas Alzheimer's patients most often only suffer a slow decline in mental status. In this context it is also worth noting that the disease onset of the brothers happened considerably earlier than most patients with Alzheimer's disease. The fact that the parents of the brothers were heterozygous for the *MLKL* variant (rs561839347) and yet did not develop a neurodegenerative disease could suggest that, either the Alzheimer associated MLKL variant (c. C142T, p.Q48X) is more detrimental than the (rs561839347) variant, or additional environmental and genetic factor are influencing the development of Alzheimer's disease.

7.4 Which cells of the CNS are affected by the identified variants?

MLKL is normally expressed at low levels in multiple cell types of the CNS and loss of function variants in *MLKL* will therefore most likely also affect multiple cell types of the of the CNS. MLKL activity caused by increased RIPK1 activity has, however, been shown to primarily affect neurons and oligodendrocytes in animal models of ALS (122). Likewise, if the *FA2H* F11del variant exerts a subtle and non-detectable effect on the neurodegenerative phenotype of the brothers, it would be expected that multiple cell types would be affected, as observed in *FA2H* KO mice (137). In contrast, AP1S2 has only been implicated in neuronal metabolism. The presented data suggests that the variant in *MLKL* is the most likely candidate to explain the neurodegenerative phenotype of the brothers, which implies that the pathogenic effect of the loss of function variant might exert its effect across multiple cells types of the CNS. This interpretation is consistent with the phenotype and MRI of the brothers demonstrating global atrophy and no signs of a particular cell population being affected.

7.5 Implications of MLKL deficiency

As mentioned above, *MLKL* is currently not a gene in which variants are known to cause a defined spectrum of disorders and the gene is therefore not subject to common gene panel testing in patients being studied for genetic disease. The discovery of the disease-associated variant in *MLKL* was therefore a novel finding that was made possible by the use of WGS. The homozygous *MLKL* variant (rs561839347) in the brothers prevents expression of MLKL, as demonstrated in primary fibroblasts and PBMCs, and necroptosis can therefore not occur. To the author's knowledge, no patients have previously been described with complete deficiency of MLKL.

Genetic variants in genes regulating programmed cell death, such as *casp8* in apoptosis, are normally not tolerated, because apoptosis plays an important role during embryogenesis(101). MLKL is not involved in murine embryogenesis, since newborn *Mlkl* KO mice are viable and show no defects. The literature currently provides no formal evidence to confirm that necroptosis, as with mice, is not involved in human embryogenesis. However, the fact that the brothers were not affected by disease before adulthood strongly supports the idea that necroptosis is a form of programmed cell death that in humans plays a physiological role after birth.

The necroptotic machinery has been shown to become activated in a broad range of diseases, including disease of the CNS, most notably MS (112), ALS (122), Niemann-Pick's disease (115), and Alzheimer's disease (113), as described in Chapter 1. Despite the very different aetiologies of these diseases, the literature would suggest

that they share necroptosis as a downstream process that is initiated in neurons (Alzheimer's disease and Niemann-Pick's disease) or in oligodendrocytes (ALS and MS) during the pathophysiological process. Observations such as these suggest that necroptosis is a contributing factor to neuronal and oligodendrocytic loss, and they have therefore sparked the search for pharmacological inhibitors of necroptosis. The data are compatible with another interpretation, however. The results could also suggest a more fundamental, beneficial mechanism, whereby the CNS responds to disease by clearing damaged and dying cells. In support of this interpretation is the recent observation of *MLKL* heterozygous loss-of-function variants in patients with Alzheimer's patients(130). This finding contradicts the more established interpretation that necroptosis is a detrimental and pathogenic mechanism that should be targeted for inhibition in Alzheimer's disease (113).

Clearance of dead and dying cells is crucial for the maintenance of tissue homeostasis in metazoans (212). Apoptotic cells normally release chemokines to the extracellular environment as so-called "find me" signals, and express the phospholipid, phosphatidylserine, on the cell surface as a so-called "eat me" signal. These signals recruit phagocytes, such as macrophages, which ingest the cell or other materials destined for phagocytosis. Perturbations of these cellular processes have been associated with a broad range of diseases including MS, autoimmune uveitis, ulcerative colitis and systemic lupus erythematosus (SLE) (213). It has been described, for example, that defective clearance of apoptotic cells can lead to the accumulation of cellular remnants that induce autoimmunity and chronic inflammation in SLE (214). Similarly, apoptotic cells have been shown to accumulate

in the brains of patients with Alzheimer's disease (215), which has been attributed to defective activation of phagocytes, such as microglia and astrocytes, due to reduced expression of the glycoprotein Mfge8 (milk fat globule-epidermal growth factor-like-factor VIII). This molecule is normally expressed on the cell surface of phagocytes where it binds phosphatidylserine on the cell surface of apoptotic cells in the CNS (216).

As in apoptosis, necroptosis also results in the exposure of phosphatidylserine on the cell surface, as demonstrated in the results section of Chapter 4 by Annexin V staining of MLKL transfected HEK293 cells. This effect of necroptosis will most likely also occur in the CNS in the course of development of MS, ALS and Alzheimer´s diseases and enable the recruitment of microglia to sites of tissue injury. As demonstrated in Chapter 5, our patients cannot initiate necroptosis, and their cells in the CNS would therefore be expected to be less able to express phosphatidylserine and recruit microglia.

It is theoretically possible that apoptosis could compensate for the lack of necroptosis initiation in our patients. However, the cell death analysis of the family fibroblasts shown in Figure 5.10 and Figure 5.11A and B, in which necroptosis and apoptosis were induced by RIPK3 transduction, demonstrated that the fibroblasts of B1 and B2 are less prone to cell death compared to fibroblasts of F1 and S1. These data therefore do not support the notion that the brothers are able to compensate for the lack of necroptosis by inducing apoptosis. Inability to initiate necroptosis and relative inability to clear dying cells could lead to accumulation of cellular

remnants, such as immunogenic nuclear antigens (217), in tissues and the initiation of an autoimmune response. It is uncertain what the nature of such an autoimmune response would be, but this interpretation of the data and the literature would be consistent with the detection of oligoclonal bands in the CSF of B1 at the time of diagnosis.

These questions of necroptosis-dependent cellular clearance in the CNS could potentially be approached using *Mlkl* KO mice. However, the experiment would be complicated by the fact that the disease in our patients began when they were adult and has since then evolved over 3 decades. *Mlkl* KO mice have not been described to display spontaneous neurological deficits, and it is therefore unclear whether one could expect to observe any effects in the CNS over the lifespan of a mouse. As described above it is possible that other genetic and/or environmental modifiers are required to develop MLKL dependent disease and it is currently unclear what these modifiers might be. It is therefore unlikely that it would be possible to recapitulate all phenotypic characteristics of the brothers in a mouse model. To test whether MLKL dependent clearance is important for cellular homeostasis in the CNS, one option is to intercross *MLKL* KO mice with mouse models of ageing, such as *Cisd2 -/-* mice, which develop early onset degeneration of the central and peripheral nervous system (218).

One complicating factor is that the role of necroptosis could be different in mice and humans, given that *Mlkl* KO mice display increased disease severity and mortality due to infections, which is not the case in the brothers. These potential species

dependent differences are further supported by the fact that the necroptotic cellular machinery is not very well conserved across the animal kingdom. Carnivores and metatheria, for example, do not express MLKL (129).

Induced pluripotent stem cells (IPSc) have previously been informative in the research of the molecular mechanisms driving neurodegenerative diseases (219). IPSc derived from the family fibroblasts could thus potentially be used to study MLKL dependent cellular effects in a more relevant CNS cell type. However, as MLKL is ubiquitously expressed, it is at present unclear which CNS cell type/types would be involved in the disease, and it is therefore uncertain which cell type one would differentiate the IPSc into. The MRI scans are in this context not informative with respect to pin pointing any cell type specific effects. These cell specific considerations aside; the presented interpretation of the MLKL data and the literature described above would suggest that MLKL deficiency confers disease due to defective clearance of dying cells. Accordingly any IPSc culture system (neuronal or oligodendroglial) would probably have to be studied in a co-culture system with macrophages or microglia.

If the family and brothers would be willing to provide consent for a post-mortem histological examination of the CNS of the brothers, it would potentially be possible to study the downstream effects of MLKL deficiency in the CNS. The immunohistochemical analysis should include a general characterisation of neurons, oligodendrocytes, astrocytes, microglia and infiltrating immune cells, as well as markers for apoptosis (for example cleaved caspase-3). Based on this analysis one

could get a clearer picture of the pathological mechanisms of disease and could thus initiate further experiments accordingly.

In order to further explore whether MLKL and necroptosis deficiency is implicated in neurodegeneration, it would currently be informative to screen patients with neurodegenerative disease for variants in *MLKL* and its immediate upstream and downstream regulators. Given the spectrum of different phenotypes of patients with *MLKL* variants (Alzheimer's disease, Autism spectrum disorders and the patients described in this thesis), it would be necessary to include a broad range of neurodegenerative disorders. Patients with HSP, ALS, FTD and Alzheimer's disease, as well as patients with neurodegenerative spectrum disorders would be most appropriate.

7.6 Why would MLKL deficiency affect the CNS and not other organs?

Given the ubiquitous expression of MLKL, it is at this point unclear why MLKL deficiency in Alzheimer's patients and the brothers seems only to affect the nervous system. In this context it is worth noting that ALS patients with variants in *OPTN* that cause increased necroptosis via activation of RIPK1, do not have symptoms of other organ malfunction. Similarly, were no other clinical symptoms reported in the Alzheimer's patient with the MLKL loss of function variant (c. C142T, p.Q48X) (130). These observations would suggest that the CNS and PNS are more reliant on a very tight regulation of necroptosis than other tissues and organs. Indeed, cells in the CNS and PNS are not replenished to the same extent as in other organs, and it is therefore possible that perturbations of the necroptosis machinery caused by

genetic variants would lead to a greater loss of cells over time.

7.7 Why do the brothers not have increased susceptibility to infections?

Since the discovery of necroptosis and MLKL as the prime mediator of necroptosis in 2012 (81), much research has focused on the role of necroptosis in immunity. Viruses (e.g. HSV-1 and CMV) and bacteria (e.g. *E. coli*) have evolved mechanisms to counteract necroptosis by inhibiting the function of RIPK3 and MLKL (94, 95, 98). *In vivo* studies have thus shown that *Mlkl* KO mice are less able to withstand infection with S*taphylococcus aureus* and suffer from higher rates of sepsis-induced lethality compared to wildtype littermates (99). Our two patients have been immobilised (wheelchair-bound) since the beginning of 2000, and one could have anticipated that they would be at higher risk of developing pneumonia. However, the brothers are not overtly susceptible to infections based on the clinical records from the hospital and GP. It is important to note that the mouse experiments have been performed under very controlled settings where a strong and specific challenge has been provided. One explanation for this apparent difference between humans and mice with respect to MLKL-dependent bacterial clearance could be that the infectious load of bacteria used in disease mouse models is higher than the level of exposure for the brothers over time. Alternatively, the data would suggest that humans are less immunologically reliant on necroptosis with respect to the clearance of microbes in comparison to mice.

With respect to viral infections, it is unlikely that the brothers have not been exposed to HSV-1 and CMV during their lifetime. Based on the reported ability of

HSV-1 and CMV to counteract necroptosis, one would expect that the brothers would be prone to a severe, or potentially lethal, disease course following these viral infections. The lack of exacerbated viral infections in the brothers could reflect that other redundant mechanisms of viral clearance compensate for the lack of necroptosis. Alternatively, the *in vitro* and mouse results obtained on the counteractive mechanisms of HSV-1 and CMV to necroptosis are not directly translatable to the human setting. Regardless of these possibilities, what remains is that the clinical profile of the brothers indicates that MLKL deficiency does not give rise to an overt pathophysiological immune phenotype.

7.8 MLKL as a therapeutic target

In addition to the above mentioned reports of necroptosis in neurological diseases, necroptosis has also been implicated in a broad range of other conditions, including autoimmune hepatitis (108), cardiac ischaemia (110), pancreatitis (100) and atherosclerosis. Briefly, in atherosclerosis phosphorylated MLKL (activated MLKL) has been shown to be present in the atherosclerotic lesions of coronary arteries, and RIPK3 and MLKL gene expression has been demonstrated to be upregulated in the carotid plaques of patients with atherosclerosis (109). This study and others (188) argue that necroptosis (MLKL) should therefore be targeted therapeutically in order to prevent necrotic core formation and promote plaque stability in atherosclerotic diseases. Given the high worldwide prevalence of atherosclerotic coronary and cerebral artery disease, the market for MLKL inhibitors as part of the treatment of atherosclerosis could be very large. The current body of evidence to suggest that necroptosis is pathogenic in these diseases has therefore given rise to the proposal

that MLKL is a “druggable” target. Indeed, a new MLKL inhibitor (TC13172) was recently reported, for example, to be a more powerful inhibitor of MLKL than necrosulfonamide, which today is the most commonly used and commercially available MLKL-inhibitor (190).

The studies reported in this thesis suggest three points of interest for any discussion of the use of MLKL inhibitors for human therapy:

1. The complete absence of functional MLKL in the brothers does not appear to render the patients more susceptible to infections. This would otherwise be a reasonable concern given the current published literature on the function of MLKL in the immune system. From this point of view, the studies reported here provide some assurance that treating patients with MLKL inhibitors would, in this respect, be safe and not lead to infections.

2. On the other hand, our studies show that deficiency of MLKL is implicated in a serious, chronic neurodegenerative disease. This is supported by a recently reported study of *MLKL* heterozygous loss of function variants conferring susceptibility to Alzheimer’s disease (130). Treatment with MLKL inhibitors, especially if it is long-term, as would be the case in inhibition or prevention of atherosclerosis, could therefore involve substantial risk of neurological side effects that would likely be undetectable during the course of randomized clinical trials of less than 10 years of duration. The side effects would most likely originate from tissue injury in the CNS, rather than the PNS.

3. MLKL inhibitors for clinical use should be approached with caution. If it is possible to develop a MLKL inhibitor that reliably does not cross the blood-brain barrier and the blood-nerve barrier, it could be safe, perhaps, to inhibit the function of MLKL.

7.9 Future studies summary

To further explore how dysregulated necroptosis causes neurodegenerative disease and the implications for necroptosis as a drugable target, it would first and foremost be informative to identify additional patients or families with variants in the necroptosis pathway. This work could be approached using whole genome or exome sequencing of patients and families with neurodegenerative disorders, as well as matching platforms. Secondly, it would be useful to intercross *MLKL* KO mice with other disease models, such as mouse models of ageing to investigate *in* vivo mechanisms of dysregulated necroptosis. Third, to explain the lack of MLKL in B1 and B2, it would be interesting to inhibit UPF1 to test whether NMD prevents the expression of MLKL. Finally, with respect to the genetic analysis of these brothers, it would be valuable to further assay any subtle effects of the K55R variants *in vitro,* as described in Chapter 6.

7.10 General conclusions

WGS enables the identification of rare variants and the analysis of their influence on disease. The clinical genetics approach to variant interpretation promoted by ACMG (171) considers the varying degrees of evidence to suggest that a variant is pathogenic or benign, based on allele frequency, bioinformatics, segregation with

disease, computational and functional studies. As the diagnosis can have prognostic and therapeutic implications for the patient, it is necessary to apply relatively strict principles to the interpretation of the variant. From a research point of view, it is important to acknowledge that rare variants can also exert more subtle effects. With respect to the brothers, it is impossible to completely rule out subtle effects over time of the variants in *FA2H* and *AP1S2* segregating with disease. The experimental and computational evidence presented in Chapter 6 would, however, suggest a benign effect of these variants.

The identification of the *MLKL* variant (rs561839347) in the brothers exemplified the power of WGS in finding a new gene that is implicated in human disease. To the author´s knowledge, this is the first report that implicates a homozygous loss of function variant in *MLKL* in a neurodegenerative disease. The clinical phenotype is characterised by progressive, asymmetrical paresis of the lower limbs with spasticity, cerebellar ataxia, dysarthria, seizures, mental impairment, late stage fasciculations and oligoclonal band positivity. In hindsight, the clinical findings are neither consistent with a diagnosis of PPMS, nor do they fit the typical clinical picture of FA2H associated HSP. The recent report of heterozygous loss of function variants in *MLKL* conferring susceptibility to late onset Alzheimer's disease (130) would suggest that MLKL deficiency is implicated in a spectrum of neurodegenerative phenotypes. It is consequently likely that our patients suffer from a neurodegenerative spectrum disorder. Genetic variants in *MLKL* should therefore be considered in the diagnostic work-up of patients with hereditary neurodegenerative disease.

Functional studies demonstrated that rs561839347 homozygosity prevents expression of MLKL and necroptosis, suggesting that absence or deficiency of a functional necroptosis pathway is detrimental to the CNS. In addition, the fact that the brothers do not show an increased susceptibility to infections is an observation that stands in marked contrast to the reports on infection severity in *Mlkl* KO mice. This discrepancy between mice and humans has significant implications for the physiological understanding of necroptosis.

The mechanisms by which necroptosis deficiency causes neurodegeneration remain to be fully elucidated. However, accumulation of dying cells due to deficiency in cellular clearance is a known disease mechanism in Alzheimer's disease and SLE, which supports the concept that perturbation of cell death regulation is pathogenic. Whilst studies show evidence of active necroptosis in the CNS of a spectrum of neurological diseases (most notably MS (112), ALS (122), Niemann-Pick's disease (115), and Alzheimer's disease (113)), this necroptotic activation might not always be a pathogenic mechanism, but could constitute a more physiological, protective mechanism. The results presented in this thesis thus demonstrate that the *MLKL* variant (rs561839347) exerts a detrimental effect on protein function and possibly a neurodegenerative effect. These findings suggest that the current plans for therapeutic application of MLKL-inhibitors for a range of diseases should be approached with caution, as MLKL-inhibitors may in the long-term result in serious damage to the CNS.

References

1. Group GBDNDC. Global, regional, and national burden of neurological disorders during 1990-2015: a systematic analysis for the Global Burden of Disease Study 2015. Lancet Neurol. 2017;16(11):877-97.

2. Bertram L, Tanzi RE. The genetic epidemiology of neurodegenerative disease. J Clin Invest. 2005;115(6):1449-57.

3. Citron M, Oltersdorf T, Haass C, McConlogue L, Hung AY, Seubert P, et al. Mutation of the beta-amyloid precursor protein in familial Alzheimer's disease increases beta-protein production. Nature. 1992;360(6405):672-4.

4. Polymeropoulos MH, Lavedan C, Leroy E, Ide SE, Dehejia A, Dutra A, et al. Mutation in the alpha-synuclein gene identified in families with Parkinson's disease. Science. 1997;276(5321):2045-7.

5. Freischmidt A, Wieland T, Richter B, Ruf W, Schaeffer V, Muller K, et al. Haploinsufficiency of TBK1 causes familial ALS and fronto-temporal dementia. Nat Neurosci. 2015;18(5):631-6.

6. Klein CJ, Wu Y, Duan X, Middha S, Dawson BD, Kocher JP, et al. Novel SOD1 mutation discovered in atypical ALS by whole exome sequencing. J Neurol Neurosurg Psychiatry. 2013;84(8):943-4.

7. Manolio TA, Collins FS, Cox NJ, Goldstein DB, Hindorff LA, Hunter DJ, et al. Finding the missing heritability of complex diseases. Nature. 2009;461(7265):747-53.

8. Tsuji S. Genetics of neurodegenerative diseases: insights from high-throughput resequencing. Hum Mol Genet. 2010;19(R1):R65-70.

9. International Schizophrenia C. Rare chromosomal deletions and duplications increase risk of schizophrenia. Nature. 2008;455(7210):237-41.

10. Helbig I, Mefford HC, Sharp AJ, Guipponi M, Fichera M, Franke A, et al. 15q13.3 microdeletions increase risk of idiopathic generalized epilepsy. Nat Genet. 2009;41(2):160-2.

11. Weisfeld-Adams JD, Katz Sand IB, Honce JM, Lublin FD. Differential diagnosis of Mendelian and mitochondrial disorders in patients with suspected multiple sclerosis. Brain. 2015;138(Pt 3):517-39.

12. Homann OR, Misura K, Lamas E, Sandrock RW, Nelson P, McDonough SI, et al. Whole-genome sequencing in multiplex families with psychoses reveals mutations in the SHANK2 and SMARCA1 genes segregating with illness. Mol Psychiatry. 2016;21(12):1690-5.

13. Satake W, Nakabayashi Y, Mizuta I, Hirota Y, Ito C, Kubo M, et al. Genome-wide association study identifies common variants at four loci as genetic risk factors for Parkinson's disease. Nat Genet. 2009;41(12):1303-7.

14. Kathiresan S, Willer CJ, Peloso GM, Demissie S, Musunuru K, Schadt EE, et al. Common variants at 30 loci contribute to polygenic dyslipidemia. Nat Genet. 2009;41(1):56-65.

15. Hobbs HH, Brown MS, Goldstein JL. Molecular genetics of the LDL receptor gene in familial hypercholesterolemia. Hum Mutat. 1992;1(6):445-66.

16. Benjannet S, Rhainds D, Hamelin J, Nassoury N, Seidah NG. The proprotein convertase (PC) PCSK9 is inactivated by furin and/or PC5/6A: functional consequences of natural mutations and post-translational modifications. J Biol Chem. 2006;281(41):30561-72.

17. Brown MS, Goldstein JL. A receptor-mediated pathway for cholesterol homeostasis. Science. 1986;232(4746):34-47.

18. Taylor JC, Martin HC, Lise S, Broxholme J, Cazier JB, Rimmer A, et al. Factors influencing success of clinical genome sequencing across a broad spectrum of disorders. Nat Genet. 2015;47(7):717-26.

19. Compston A, Coles A. Multiple sclerosis. Lancet. 2008;372(9648):1502-17.

20. Kingwell E, Marriott JJ, Jette N, Pringsheim T, Makhani N, Morrow SA, et al. Incidence and prevalence of multiple sclerosis in Europe: a systematic review. BMC Neurol. 2013;13:128.

21. Reich DS, Lucchinetti CF, Calabresi PA. Multiple Sclerosis. N Engl J Med. 2018;378(2):169-80.

22. Belbasis L, Bellou V, Evangelou E, Ioannidis JP, Tzoulaki I. Environmental risk factors and multiple sclerosis: an umbrella review of systematic reviews and meta-analyses. Lancet Neurol. 2015;14(3):263-73.

23. Miller DH, Leary SM. Primary-progressive multiple sclerosis. Lancet Neurol. 2007;6(10):903-12.

24. Camp SJ, Stevenson VL, Thompson AJ, Miller DH, Borras C, Auriacombe S, et al. Cognitive function in primary progressive and transitional progressive multiple sclerosis: a controlled study with MRI correlates. Brain. 1999;122 (Pt 7):1341-8.

25. Kurtzke JF. Rating neurologic impairment in multiple sclerosis: an expanded disability status scale (EDSS). Neurology. 1983;33(11):1444-52.

26. Tremlett H, Paty D, Devonshire V. The natural history of primary progressive MS in British Columbia, Canada. Neurology. 2005;65(12):1919-23.

27. Correale J, Gaitan MI, Ysrraelit MC, Fiol MP. Progressive multiple sclerosis: from pathogenic mechanisms to treatment. Brain. 2017;140(3):527-46.

28. Ingle GT, Sastre-Garriga J, Miller DH, Thompson AJ. Is inflammation important in early PPMS? a longitudinal MRI study. J Neurol Neurosurg Psychiatry. 2005;76(9):1255-8.

29. Sastre-Garriga J, Ingle GT, Chard DT, Cercignani M, Ramio-Torrenta L, Miller DH, et al. Grey and white matter volume changes in early primary progressive multiple sclerosis: a longitudinal study. Brain. 2005;128(Pt 6):1454-60.

30. Thompson AJ, Banwell BL, Barkhof F, Carroll WM, Coetzee T, Comi G, et al. Diagnosis of multiple sclerosis: 2017 revisions of the McDonald criteria. Lancet Neurol. 2018;17(2):162-73.

31. Solomon AJ, Klein EP, Bourdette D. "Undiagnosing" multiple sclerosis: the challenge of misdiagnosis in MS. Neurology. 2012;78(24):1986-91.

32. Warshawsky I, Rudick RA, Staugaitis SM, Natowicz MR. Primary progressive multiple sclerosis as a phenotype of a PLP1 gene mutation. Ann Neurol. 2005;58(3):470-3.

33. Harding AE, Sweeney MG, Miller DH, Mumford CJ, Kellar-Wood H, Menard D, et al. Occurrence of a multiple sclerosis-like illness in women who have a Leber's hereditary optic neuropathy mitochondrial DNA mutation. Brain. 1992;115 (Pt 4):979-89.

34. Vennegoor A, van Rossum JA, Polman CH, Wattjes MP, Killestein J. Longitudinal JCV serology in multiple sclerosis patients preceding natalizumab-associated progressive multifocal leukoencephalopathy. Mult Scler. 2015;21(12):1600-3.

35. Calabresi PA. Advances in multiple sclerosis: from reduced relapses to remedies. Lancet Neurol. 2018;17(1):10-2.

36. Montalban X, Hauser SL, Kappos L, Arnold DL, Bar-Or A, Comi G, et al. Ocrelizumab versus Placebo in Primary Progressive Multiple Sclerosis. N Engl J Med. 2017;376(3):209-20.

37. Lucchinetti C, Bruck W. The pathology of primary progressive multiple sclerosis. Mult Scler. 2004;10 Suppl 1:S23-30.

38. Venken K, Hellings N, Broekmans T, Hensen K, Rummens JL, Stinissen P. Natural naive CD4+CD25+CD127low regulatory T cell (Treg) development and function are disturbed in multiple sclerosis patients: recovery of memory Treg homeostasis during disease progression. J Immunol. 2008;180(9):6411-20.

39. Frischer JM, Bramow S, Dal-Bianco A, Lucchinetti CF, Rauschka H, Schmidbauer M, et al. The relation between inflammation and neurodegeneration in multiple sclerosis brains. Brain. 2009;132(Pt 5):1175-89.

40. Chard DT, Brex PA, Ciccarelli O, Griffin CM, Parker GJ, Dalton C, et al. The longitudinal relation between brain lesion load and atrophy in multiple sclerosis: a 14 year follow up study. J Neurol Neurosurg Psychiatry. 2003;74(11):1551-4.

41. Friese MA, Schattling B, Fugger L. Mechanisms of neurodegeneration and axonal dysfunction in multiple sclerosis. Nat Rev Neurol. 2014;10(4):225-38.

42. DeLuca GC, Williams K, Evangelou N, Ebers GC, Esiri MM. The contribution of demyelination to axonal loss in multiple sclerosis. Brain. 2006;129(Pt 6):1507-16.

43. Tam RC, Traboulsee A, Riddehough A, Li DK. Improving the clinical correlation of multiple sclerosis black hole volume change by paired-scan analysis. Neuroimage Clin. 2012;1(1):29-36.

44. Popescu BF, Lucchinetti CF. Pathology of demyelinating diseases. Annu Rev Pathol. 2012;7:185-217.

45. Choi SR, Howell OW, Carassiti D, Magliozzi R, Gveric D, Muraro PA, et al. Meningeal inflammation plays a role in the pathology of primary progressive multiple sclerosis. Brain. 2012;135(Pt 10):2925-37.

46. Fischer MT, Sharma R, Lim JL, Haider L, Frischer JM, Drexhage J, et al. NADPH oxidase expression in active multiple sclerosis lesions in relation to oxidative tissue damage and mitochondrial injury. Brain. 2012;135(Pt 3):886-99.

47. Craner MJ, Newcombe J, Black JA, Hartle C, Cuzner ML, Waxman SG. Molecular changes in neurons in multiple sclerosis: altered axonal expression of Nav1.2 and Nav1.6 sodium channels and Na+/Ca2+ exchanger. Proc Natl Acad Sci U S A. 2004;101(21):8168-73.

48. Friese MA, Craner MJ, Etzensperger R, Vergo S, Wemmie JA, Welsh MJ, et al. Acid-sensing ion channel-1 contributes to axonal degeneration in autoimmune inflammation of the central nervous system. Nat Med. 2007;13(12):1483-9.

49. Vergo S, Craner MJ, Etzensperger R, Attfield K, Friese MA, Newcombe J, et al. Acid-sensing ion channel 1 is involved in both axonal injury and demyelination in multiple sclerosis and its animal model. Brain. 2011;134(Pt 2):571-84.

50. Eichhorst H. Über infantile und hereditäre multiple Sklerose. Wirchows Arch f path Anat 1896;146:173-92.

51. O'Gorman C, Lin R, Stankovich J, Broadley SA. Modelling genetic susceptibility to multiple sclerosis with family data. Neuroepidemiology. 2013;40(1):1-12.

52. Hensiek AE, Seaman SR, Barcellos LF, Oturai A, Eraksoi M, Cocco E, et al. Familial effects on the clinical course of multiple sclerosis. Neurology. 2007;68(5):376-83.

53. International Multiple Sclerosis Genetics C, Wellcome Trust Case Control C, Sawcer S, Hellenthal G, Pirinen M, Spencer CC, et al. Genetic risk and a primary role for cell-mediated immune mechanisms in multiple sclerosis. Nature. 2011;476(7359):214-9.

54. Moutsianas L, Jostins L, Beecham AH, Dilthey AT, Xifara DK, Ban M, et al. Class II HLA interactions modulate genetic risk for multiple sclerosis. Nat Genet. 2015;47(10):1107-13.

55. International Multiple Sclerosis Genetics C, Beecham AH, Patsopoulos NA, Xifara DK, Davis MF, Kemppinen A, et al. Analysis of immune-related loci identifies 48 new susceptibility variants for multiple sclerosis. Nat Genet. 2013;45(11):1353-60.

56. International Multiple Sclerosis Genetics C, Hafler DA, Compston A, Sawcer S, Lander ES, Daly MJ, et al. Risk alleles for multiple sclerosis identified by a genomewide study. N Engl J Med. 2007;357(9):851-62.

57. Dendrou CA, Cortes A, Shipman L, Evans HG, Attfield KE, Jostins L, et al. Resolving TYK2 locus genotype-to-phenotype differences in autoimmunity. Sci Transl Med. 2016;8(363):363ra149.

58. Gregory AP, Dendrou CA, Attfield KE, Haghikia A, Xifara DK, Butter F, et al. TNF receptor 1 genetic risk mirrors outcome of anti-TNF therapy in multiple sclerosis. Nature. 2012;488(7412):508-11.

59. Dendrou CA, Fugger L, Friese MA. Immunopathology of multiple sclerosis. Nat Rev Immunol. 2015;15(9):545-58.

60. Sawcer S, Franklin RJ, Ban M. Multiple sclerosis genetics. Lancet Neurol. 2014;13(7):700-9.

61. Bashinskaya VV, Kulakova OG, Boyko AN, Favorov AV, Favorova OO. A review of genome-wide association studies for multiple sclerosis: classical and hypothesis-driven approaches. Hum Genet. 2015;134(11-12):1143-62.

62. Gudbjartsson DF, Helgason H, Gudjonsson SA, Zink F, Oddson A, Gylfason A, et al. Large-scale whole-genome sequencing of the Icelandic population. Nat Genet. 2015;47(5):435-44.

63. Kallio SP, Jakkula E, Purcell S, Suvela M, Koivisto K, Tienari PJ, et al. Use of a genetic isolate to identify rare disease variants: C7 on 5p associated with MS. Hum Mol Genet. 2009;18(9):1670-83.

64. Sanna S, Pitzalis M, Zoledziewska M, Zara I, Sidore C, Murru R, et al. Variants within the immunoregulatory CBLB gene are associated with multiple sclerosis. Nat Genet. 2010;42(6):495-7.

65. Novarino G, Fenstermaker AG, Zaki MS, Hofree M, Silhavy JL, Heiberg AD, et al. Exome sequencing links corticospinal motor neuron disease to common neurodegenerative disorders. Science. 2014;343(6170):506-11.

66. McDermott C, White K, Bushby K, Shaw P. Hereditary spastic paraparesis: a review of new developments. J Neurol Neurosurg Psychiatry. 2000;69(2):150-60.

67. Fink JK. Hereditary Spastic Paraplegia Overview. 2000 Aug 15 [Updated 2014 Feb 6]. GeneReviews® [Internet] Seattle (WA): . 2014;University of Washington, Seattle; 1993-2018. .

68. https://omim.org/phenotypicSeries/PS303350.

69. Musumeci O, Bassi MT, Mazzeo A, Grandis M, Crimella C, Martinuzzi A, et al. A novel mutation in KIF5A gene causing hereditary spastic paraplegia with axonal neuropathy. Neurol Sci. 2011;32(4):665-8.

70. O'Donnell JP, Byrnes LJ, Cooley RB, Sondermann H. A hereditary spastic paraplegia-associated atlastin variant exhibits defective allosteric coupling in the catalytic core. J Biol Chem. 2018;293(2):687-700.

71. Hansen JJ, Durr A, Cournu-Rebeix I, Georgopoulos C, Ang D, Nielsen MN, et al. Hereditary spastic paraplegia SPG13 is associated with a mutation in the gene encoding the mitochondrial chaperonin Hsp60. Am J Hum Genet. 2002;70(5):1328-32.

72. Orthmann-Murphy JL, Salsano E, Abrams CK, Bizzi A, Uziel G, Freidin MM, et al. Hereditary spastic paraplegia is a novel phenotype for GJA12/GJC2 mutations. Brain. 2009;132(Pt 2):426-38.

73. Minase G, Miyatake S, Nabatame S, Arai H, Koshimizu E, Mizuguchi T, et al. An atypical case of SPG56/CYP2U1-related spastic paraplegia presenting with delayed myelination. J Hum Genet. 2017;62(11):997-1000.

74. Fink JK. Hereditary spastic paraplegia: clinico-pathologic features and emerging molecular mechanisms. Acta Neuropathol. 2013;126(3):307-28.

75. Kuru S, Sakai M, Konagaya M, Yoshida M, Hashizume Y. Autopsy case of hereditary spastic paraplegia with thin corpus callosum showing severe gliosis in the cerebral white matter. Neuropathology. 2005;25(4):346-52.

76. Hourani R, El-Hajj T, Barada WH, Hourani M, Yamout BI. MR imaging findings in autosomal recessive hereditary spastic paraplegia. AJNR Am J Neuroradiol. 2009;30(5):936-40.

77. Hensiek A, Kirker S, Reid E. Diagnosis, investigation and management of hereditary spastic paraplegias in the era of next-generation sequencing. J Neurol. 2015;262(7):1601-12.

78. Mead SH, Proukakis C, Wood N, Crosby AH, Plant GT, Warner TT. A large family with hereditary spastic paraparesis due to a frame shift mutation of the spastin (SPG4) gene: association with multiple sclerosis in two affected siblings and epilepsy in other affected family members. J Neurol Neurosurg Psychiatry. 2001;71(6):788-91.

79. Yazici I, Yildirim N, Zorlu Y. The coexistence of multiple sclerosis and hereditary spastic paraparesis in a patient. Neurol Int. 2013;5(2):17-9.

80. DeLuca GC, Ramagopalan SV, Cader MZ, Dyment DA, Herrera BM, Orton S, et al. The role of hereditary spastic paraplegia related genes in multiple sclerosis. A study of disease susceptibility and clinical outcome. J Neurol. 2007;254(9):1221-6.

81. Sun L, Wang H, Wang Z, He S, Chen S, Liao D, et al. Mixed lineage kinase domain-like protein mediates necrosis signaling downstream of RIP3 kinase. Cell. 2012;148(1-2):213-27.

82. Weinlich R, Oberst A, Beere HM, Green DR. Necroptosis in development, inflammation and disease. Nat Rev Mol Cell Biol. 2017;18(2):127-36.

83. Pasparakis M, Vandenabeele P. Necroptosis and its role in inflammation. Nature. 2015;517(7534):311-20.

84. Vanden Berghe T, Linkermann A, Jouan-Lanhouet S, Walczak H, Vandenabeele P. Regulated necrosis: the expanding network of non-apoptotic cell death pathways. Nat Rev Mol Cell Biol. 2014;15(2):135-47.

85. Silke J, Rickard JA, Gerlic M. The diverse role of RIP kinases in necroptosis and inflammation. Nat Immunol. 2015;16(7):689-97.

86. Cai Z, Jitkaew S, Zhao J, Chiang HC, Choksi S, Liu J, et al. Plasma membrane translocation of trimerized MLKL protein is required for TNF-induced necroptosis. Nat Cell Biol. 2014;16(1):55-65.

87. Chen X, Li W, Ren J, Huang D, He WT, Song Y, et al. Translocation of mixed lineage kinase domain-like protein to plasma membrane leads to necrotic cell death. Cell Res. 2014;24(1):105-21.

88. Su L, Quade B, Wang H, Sun L, Wang X, Rizo J. A plug release mechanism for membrane permeation by MLKL. Structure. 2014;22(10):1489-500.

89. Vandenabeele P, Riquet F, Cappe B. Necroptosis: (Last) Message in a Bubble. Immunity. 2017;47(1):1-3.

90. Murphy JM, Czabotar PE, Hildebrand JM, Lucet IS, Zhang JG, Alvarez-Diaz S, et al. The pseudokinase MLKL mediates necroptosis via a molecular switch mechanism. Immunity. 2013;39(3):443-53.

91. Quarato G, Guy CS, Grace CR, Llambi F, Nourse A, Rodriguez DA, et al. Sequential Engagement of Distinct MLKL Phosphatidylinositol-Binding Sites Executes Necroptosis. Mol Cell. 2016;61(4):589-601.

92. Hildebrand JM, Tanzer MC, Lucet IS, Young SN, Spall SK, Sharma P, et al. Activation of the pseudokinase MLKL unleashes the four-helix bundle domain to induce membrane localization and necroptotic cell death. Proc Natl Acad Sci U S A. 2014;111(42):15072-7.

93. Wang X, Li Y, Liu S, Yu X, Li L, Shi C, et al. Direct activation of RIP3/MLKL-dependent necrosis by herpes simplex virus 1 (HSV-1) protein ICP6 triggers host antiviral defense. Proc Natl Acad Sci U S A. 2014;111(43):15438-43.

94. Guo H, Omoto S, Harris PA, Finger JN, Bertin J, Gough PJ, et al. Herpes simplex virus suppresses necroptosis in human cells. Cell host & microbe. 2015;17(2):243-51.

95. Omoto S, Guo H, Talekar GR, Roback L, Kaiser WJ, Mocarski ES. Suppression of RIP3-dependent necroptosis by human cytomegalovirus. J Biol Chem. 2015;290(18):11635-48.

96. Mocarski ES, Upton JW, Kaiser WJ. Viral infection and the evolution of caspase 8-regulated apoptotic and necrotic death pathways. Nat Rev Immunol. 2011;12(2):79-88.

97. Kaiser WJ, Upton JW, Mocarski ES. Viral modulation of programmed necrosis. Curr Opin Virol. 2013;3(3):296-306.

98. Pearson JS, Giogha C, Muhlen S, Nachbur U, Pham CL, Zhang Y, et al. EspL is a bacterial cysteine protease effector that cleaves RHIM proteins to block necroptosis and inflammation. Nat Microbiol. 2017;2:16258.

99. Kitur K, Wachtel S, Brown A, Wickersham M, Paulino F, Penaloza HF, et al. Necroptosis Promotes Staphylococcus aureus Clearance by Inhibiting Excessive Inflammatory Signaling. Cell reports. 2016;16(8):2219-30.

100. Wu J, Huang Z, Ren J, Zhang Z, He P, Li Y, et al. Mlkl knockout mice demonstrate the indispensable role of Mlkl in necroptosis. Cell Res. 2013;23(8):994-1006.

101. Kaiser WJ, Upton JW, Long AB, Livingston-Rosanoff D, Daley-Bauer LP, Hakem R, et al. RIP3 mediates the embryonic lethality of caspase-8-deficient mice. Nature. 2011;471(7338):368-72.

102. Conos SA, Chen KW, De Nardo D, Hara H, Whitehead L, Nunez G, et al. Active MLKL triggers the NLRP3 inflammasome in a cell-intrinsic manner. Proc Natl Acad Sci U S A. 2017.

103. Takahashi N, Vereecke L, Bertrand MJ, Duprez L, Berger SB, Divert T, et al. RIPK1 ensures intestinal homeostasis by protecting the epithelium against apoptosis. Nature. 2014;513(7516):95-9.

104. Dannappel M, Vlantis K, Kumari S, Polykratis A, Kim C, Wachsmuth L, et al. RIPK1 maintains epithelial homeostasis by inhibiting apoptosis and necroptosis. Nature. 2014;513(7516):90-4.

105. Gong YN, Guy C, Olauson H, Becker JU, Yang M, Fitzgerald P, et al. ESCRT-III Acts Downstream of MLKL to Regulate Necroptotic Cell Death and Its Consequences. Cell. 2017;169(2):286-300 e16.

106. Yoon S, Kovalenko A, Bogdanov K, Wallach D. MLKL, the Protein that Mediates Necroptosis, Also Regulates Endosomal Trafficking and Extracellular Vesicle Generation. Immunity. 2017;47(1):51-65 e7.

107. Consortium GT, Laboratory DA, Coordinating Center -Analysis Working G, Statistical Methods groups-Analysis Working G, Enhancing Gg, Fund NIHC, et al. Genetic effects on gene expression across human tissues. Nature. 2017;550(7675):204-13.

108. Gunther C, He GW, Kremer AE, Murphy JM, Petrie EJ, Amann K, et al. The pseudokinase MLKL mediates programmed hepatocellular necrosis independently of RIPK3 during hepatitis. J Clin Invest. 2016;126(11):4346-60.

109. Karunakaran D, Geoffrion M, Wei L, Gan W, Richards L, Shangari P, et al. Targeting macrophage necroptosis for therapeutic and diagnostic interventions in atherosclerosis. Sci Adv. 2016;2(7):e1600224.

110. Koshinuma S, Miyamae M, Kaneda K, Kotani J, Figueredo VM. Combination of necroptosis and apoptosis inhibition enhances cardioprotection against myocardial ischemia-reperfusion injury. J Anesth. 2014;28(2):235-41.

111. Degterev A, Huang Z, Boyce M, Li Y, Jagtap P, Mizushima N, et al. Chemical inhibitor of nonapoptotic cell death with therapeutic potential for ischemic brain injury. Nat Chem Biol. 2005;1(2):112-9.

112. Ofengeim D, Ito Y, Najafov A, Zhang Y, Shan B, DeWitt JP, et al. Activation of necroptosis in multiple sclerosis. Cell reports. 2015;10(11):1836-49.

113. Caccamo A, Branca C, Piras IS, Ferreira E, Huentelman MJ, Liang WS, et al. Necroptosis activation in Alzheimer's disease. Nat Neurosci. 2017;20(9):1236-46.

114. Vitner EB, Salomon R, Farfel-Becker T, Meshcheriakova A, Ali M, Klein AD, et al. RIPK3 as a potential therapeutic target for Gaucher's disease. Nat Med. 2014;20(2):204-8.

115. Cougnoux A, Cluzeau C, Mitra S, Li R, Williams I, Burkert K, et al. Necroptosis in Niemann-Pick disease, type C1: a potential therapeutic target. Cell Death Dis. 2016;7:e2147.

116. Zhu S, Zhang Y, Bai G, Li H. Necrostatin-1 ameliorates symptoms in R6/2 transgenic mouse model of Huntington's disease. Cell Death Dis. 2011;2:e115.

117. Re DB, Le Verche V, Yu C, Amoroso MW, Politi KA, Phani S, et al. Necroptosis drives motor neuron death in models of both sporadic and familial ALS. Neuron. 2014;81(5):1001-8.

118. Trichonas G, Murakami Y, Thanos A, Morizane Y, Kayama M, Debouck CM, et al. Receptor interacting protein kinases mediate retinal detachment-induced photoreceptor necrosis and compensate for inhibition of apoptosis. Proc Natl Acad Sci U S A. 2010;107(50):21695-700.

119. Liu M, Wu W, Li H, Li S, Huang LT, Yang YQ, et al. Necroptosis, a novel type of programmed cell death, contributes to early neural cells damage after spinal cord injury in adult mice. J Spinal Cord Med. 2015;38(6):745-53.

120. Qu Y, Shi J, Tang Y, Zhao F, Li S, Meng J, et al. MLKL inhibition attenuates hypoxia-ischemia induced neuronal damage in developing brain. Exp Neurol. 2016;279:223-31.

121. Bian P, Zheng X, Wei L, Ye C, Fan H, Cai Y, et al. MLKL Mediated Necroptosis Accelerates JEV-Induced Neuroinflammation in Mice. Front Microbiol. 2017;8:303.

122. Ito Y, Ofengeim D, Najafov A, Das S, Saberi S, Li Y, et al. RIPK1 mediates axonal degeneration by promoting inflammation and necroptosis in ALS. Science. 2016;353(6299):603-8.

123. Slowicka K, Vereecke L, van Loo G. Cellular Functions of Optineurin in Health and Disease. Trends Immunol. 2016;37(9):621-33.

124. Ayaki T, Ito H, Komure O, Kamada M, Nakamura M, Wate R, et al. Multiple Proteinopathies in Familial ALS Cases With Optineurin Mutations. J Neuropathol Exp Neurol. 2018;77(2):128-38.

125. Li F, Xie X, Wang Y, Liu J, Cheng X, Guo Y, et al. Structural insights into the interaction and disease mechanism of neurodegenerative disease-associated optineurin and TBK1 proteins. Nature communications. 2016;7:12708.

126. Skibinski G, Parkinson NJ, Brown JM, Chakrabarti L, Lloyd SL, Hummerich H, et al. Mutations in the endosomal ESCRTIII-complex subunit CHMP2B in frontotemporal dementia. Nat Genet. 2005;37(8):806-8.

127. Cox LE, Ferraiuolo L, Goodall EF, Heath PR, Higginbottom A, Mortiboys H, et al. Mutations in CHMP2B in lower motor neuron predominant amyotrophic lateral sclerosis (ALS). PLoS One. 2010;5(3):e9872.

128. Cho Y, McQuade T, Zhang H, Zhang J, Chan FK. RIP1-dependent and independent effects of necrostatin-1 in necrosis and T cell activation. PLoS One. 2011;6(8):e23209.

129. Dondelinger Y, Hulpiau P, Saeys Y, Bertrand MJ, Vandenabeele P. An evolutionary perspective on the necroptotic pathway. Trends Cell Biol. 2016;26(10):721-32.

130. Wang B, Bao S, Zhang Z, Zhou X, Wang J, Fan Y, et al. A rare variant in MLKL confers susceptibility to ApoE varepsilon4-negative Alzheimer's disease in Hong Kong Chinese population. Neurobiol Aging. 2018;68:160 e1- e7.

131. Eckhardt M, Yaghootfam A, Fewou SN, Zoller I, Gieselmann V. A mammalian fatty acid hydroxylase responsible for the formation of alpha-hydroxylated galactosylceramide in myelin. Biochem J. 2005;388(Pt 1):245-54.

132. Hama H. Fatty acid 2-Hydroxylation in mammalian sphingolipid biology. Biochim Biophys Acta. 2010;1801(4):405-14.

133. Hannun YA, Obeid LM. Principles of bioactive lipid signalling: lessons from sphingolipids. Nat Rev Mol Cell Biol. 2008;9(2):139-50.

134. Alderson NL, Maldonado EN, Kern MJ, Bhat NR, Hama H. FA2H-dependent fatty acid 2-hydroxylation in postnatal mouse brain. J Lipid Res. 2006;47(12):2772-80.

135. Aggarwal S, Yurlova L, Simons M. Central nervous system myelin: structure, synthesis and assembly. Trends Cell Biol. 2011;21(10):585-93.

136. Hoshi M, Williams M, Kishimoto Y. Characterization of brain cerebrosides at early stages of development in the rat. J Neurochem. 1973;21(3):709-12.

137. Potter KA, Kern MJ, Fullbright G, Bielawski J, Scherer SS, Yum SW, et al. Central nervous system dysfunction in a mouse model of FA2H deficiency. Glia. 2011;59(7):1009-21.

138. Edvardson S, Hama H, Shaag A, Gomori JM, Berger I, Soffer D, et al. Mutations in the fatty acid 2-hydroxylase gene are associated with leukodystrophy with spastic paraparesis and dystonia. Am J Hum Genet. 2008;83(5):643-8.

139. Alderson NL, Rembiesa BM, Walla MD, Bielawska A, Bielawski J, Hama H. The human FA2H gene encodes a fatty acid 2-hydroxylase. J Biol Chem. 2004;279(47):48562-8.

140. Tonelli A, D'Angelo MG, Arrigoni F, Brighina E, Arnoldi A, Citterio A, et al. Atypical adult onset complicated spastic paraparesis with thin corpus callosum in two patients carrying a novel FA2H mutation. Eur J Neurol. 2012;19(11):e127-9.

141. Dick KJ, Eckhardt M, Paisan-Ruiz C, Alshehhi AA, Proukakis C, Sibtain NA, et al. Mutation of FA2H underlies a complicated form of hereditary spastic paraplegia (SPG35). Hum Mutat. 2010;31(4):E1251-60.

142. Kruer MC, Paisan-Ruiz C, Boddaert N, Yoon MY, Hama H, Gregory A, et al. Defective FA2H leads to a novel form of neurodegeneration with brain iron accumulation (NBIA). Ann Neurol. 2010;68(5):611-8.

143. Garone C, Pippucci T, Cordelli DM, Zuntini R, Castegnaro G, Marconi C, et al. FA2H-related disorders: a novel c.270+3A>T splice-site mutation leads to a complex neurodegenerative phenotype. Dev Med Child Neurol. 2011;53(10):958-61.

144. Rupps R, Hukin J, Balicki M, Mercimek-Mahmutoglu S, Rolfs A, Dias C. Novel Mutations in FA2H-Associated Neurodegeneration: An Underrecognized Condition? J Child Neurol. 2013;28(11):1500-4.

145. Zaki MS, Selim L, Mansour L, Mahmoud IG, Fenstermaker AG, Gabriel SB, et al. Mutations in FA2H in three Arab families with a clinical spectrum of neurodegeneration and hereditary spastic paraparesis. Clin Genet. 2015;88(1):95-7.

146. Donkervoort S, Dastgir J, Hu Y, Zein WM, Marks H, Blackstone C, et al. Phenotypic variability of a likely FA2H founder mutation in a family with complicated hereditary spastic paraplegia. Clin Genet. 2014;85(4):393-5.

147. Liao X, Luo Y, Zhan Z, Du J, Hu Z, Wang J, et al. SPG35 contributes to the second common subtype of AR-HSP in China: frequency analysis and functional characterization of FA2H gene mutations. Clin Genet. 2015;87(1):85-9.

148. Pierson TM, Simeonov DR, Sincan M, Adams DA, Markello T, Golas G, et al. Exome sequencing and SNP analysis detect novel compound heterozygosity in fatty acid hydroxylase-associated neurodegeneration. Eur J Hum Genet. 2012;20(4):476-9.

149. Uchida Y, Hama H, Alderson NL, Douangpanya S, Wang Y, Crumrine DA, et al. Fatty acid 2-hydroxylase, encoded by FA2H, accounts for differentiation-associated increase in 2-OH ceramides during keratinocyte differentiation. J Biol Chem. 2007;282(18):13211-9.

150. Scheid I, Maruani A, Huguet G, Leblond CS, Nygren G, Anckarsater H, et al. Heterozygous FA2H mutations in autism spectrum disorders. BMC Med Genet. 2013;14:124.

151. Vu TH, Coccaro EF, Eichler EE, Girirajan S. Genomic architecture of aggression: rare copy number variants in intermittent explosive disorder. Am J Med Genet B Neuropsychiatr Genet. 2011;156B(7):808-16.

152. Mattera R, Boehm M, Chaudhuri R, Prabhu Y, Bonifacino JS. Conservation and diversification of dileucine signal recognition by adaptor protein (AP) complex variants. J Biol Chem. 2011;286(3):2022-30.

153. Canagarajah BJ, Ren X, Bonifacino JS, Hurley JH. The clathrin adaptor complexes as a paradigm for membrane-associated allostery. Protein Sci. 2013;22(5):517-29.

154. Paczkowski JE, Richardson BC, Fromme JC. Cargo adaptors: structures illuminate mechanisms regulating vesicle biogenesis. Trends Cell Biol. 2015;25(7):408-16.

155. Janvier K, Kato Y, Boehm M, Rose JR, Martina JA, Kim BY, et al. Recognition of dileucine-based sorting signals from HIV-1 Nef and LIMP-II by the AP-1 gamma-sigma1 and AP-3 delta-sigma3 hemicomplexes. J Cell Biol. 2003;163(6):1281-90.

156. Ren X, Farias GG, Canagarajah BJ, Bonifacino JS, Hurley JH. Structural basis for recruitment and activation of the AP-1 clathrin adaptor complex by Arf1. Cell. 2013;152(4):755-67.

157. Glyvuk N, Tsytsyura Y, Geumann C, D'Hooge R, Huve J, Kratzke M, et al. AP-1/sigma1B-adaptin mediates endosomal synaptic vesicle recycling, learning and memory. EMBO J. 2010;29(8):1318-30.

158. Baltes J, Larsen JV, Radhakrishnan K, Geumann C, Kratzke M, Petersen CM, et al. sigma1B adaptin regulates adipogenesis by mediating the sorting of sortilin in adipose tissue. J Cell Sci. 2014;127(Pt 16):3477-87.

159. Jain S, Farias GG, Bonifacino JS. Polarized sorting of the copper transporter ATP7B in neurons mediated by recognition of a dileucine signal by AP-1. Mol Biol Cell. 2015;26(2):218-28.

160. Tarpey PS, Stevens C, Teague J, Edkins S, O'Meara S, Avis T, et al. Mutations in the gene encoding the Sigma 2 subunit of the adaptor protein 1 complex, AP1S2, cause X-linked mental retardation. Am J Hum Genet. 2006;79(6):1119-24.

161. Cacciagli P, Desvignes JP, Girard N, Delepine M, Zelenika D, Lathrop M, et al. AP1S2 is mutated in X-linked Dandy-Walker malformation with intellectual disability, basal ganglia disease and seizures (Pettigrew syndrome). Eur J Hum Genet. 2014;22(3):363-8.

162. Ballarati L, Cereda A, Caselli R, Maitz S, Russo S, Selicorni A, et al. Deletion of the AP1S2 gene in a child with psychomotor delay and hypotonia. Eur J Med Genet. 2012;55(2):124-7.

163. Turner G, Gedeon A, Kerr B, Bennett R, Mulley J, Partington M. Syndromic form of X-linked mental retardation with marked hypotonia in early life, severe mental handicap, and difficult adult behavior maps to Xp22. Am J Med Genet A. 2003;117A(3):245-50.

164. Carpenter NJ, Brown WT, Qu Y, Keenan KL. Regional localization of a nonspecific X-linked mental retardation gene (MRX59) to Xp21.2-p22.2. Am J Med Genet. 1999;85(3):266-70.

165. Saillour Y, Zanni G, Des Portes V, Heron D, Guibaud L, Iba-Zizen MT, et al. Mutations in the AP1S2 gene encoding the sigma 2 subunit of the adaptor protein 1 complex are associated with syndromic X-linked mental retardation with hydrocephalus and calcifications in basal ganglia. J Med Genet. 2007;44(11):739-44.

166. Biesecker LG, Green RC. Diagnostic clinical genome and exome sequencing. N Engl J Med. 2014;370(25):2418-25.

167. Eilbeck K, Quinlan A, Yandell M. Settling the score: variant prioritization and Mendelian disease. Nat Rev Genet. 2017;18(10):599-612.

168. Adzhubei IA, Schmidt S, Peshkin L, Ramensky VE, Gerasimova A, Bork P, et al. A method and server for predicting damaging missense mutations. Nat Methods. 2010;7(4):248-9.

169. Lek M, Karczewski KJ, Minikel EV, Samocha KE, Banks E, Fennell T, et al. Analysis of protein-coding genetic variation in 60,706 humans. Nature. 2016;536(7616):285-91.

170. MacArthur DG, Manolio TA, Dimmock DP, Rehm HL, Shendure J, Abecasis GR, et al. Guidelines for investigating causality of sequence variants in human disease. Nature. 2014;508(7497):469-76.

171. Richards S, Aziz N, Bale S, Bick D, Das S, Gastier-Foster J, et al. Standards and guidelines for the interpretation of sequence variants: a joint consensus recommendation of the American College of Medical Genetics and Genomics and the Association for Molecular Pathology. Genet Med. 2015;17(5):405-24.

172. Thomas M, Boname JM, Field S, Nejentsev S, Salio M, Cerundolo V, et al. Down-regulation of NKG2D and NKp80 ligands by Kaposi's sarcoma-associated herpesvirus K5 protects against NK cell cytotoxicity. Proc Natl Acad Sci U S A. 2008;105(5):1656-61.

173. Demaison C, Parsley K, Brouns G, Scherr M, Battmer K, Kinnon C, et al. High-level transduction and gene expression in hematopoietic repopulating cells using a human immunodeficiency [correction of imunodeficiency] virus type 1-based lentiviral vector containing an internal spleen focus forming virus promoter. Hum Gene Ther. 2002;13(7):803-13.

174. Schrodinger, LLC. The PyMOL Molecular Graphics System, Version 1.8. 2015.

175. The UniProt C. UniProt: the universal protein knowledgebase. Nucleic Acids Res. 2017;45(D1):D158-D69.

176. Berman HM, Battistuz T, Bhat TN, Bluhm WF, Bourne PE, Burkhardt K, et al. The Protein Data Bank. Acta Crystallogr D Biol Crystallogr. 2002;58(Pt 6 No 1):899-907.

177. Flicek P, Amode MR, Barrell D, Beal K, Billis K, Brent S, et al. Ensembl 2014. Nucleic Acids Res. 2014;42(Database issue):D749-55.

178. Maelfait J, Liverpool L, Bridgeman A, Ragan KB, Upton JW, Rehwinkel J. Sensing of viral and endogenous RNA by ZBP1/DAI induces necroptosis. EMBO J. 2017;36(17):2529-43.

179. Poser CM, Brinar VV. Diagnostic criteria for multiple sclerosis: an historical review. Clin Neurol Neurosurg. 2004;106(3):147-58.

180. Ribbons KA, McElduff P, Boz C, Trojano M, Izquierdo G, Duquette P, et al. Male Sex Is Independently Associated with Faster Disability Accumulation in Relapse-Onset MS but Not in Primary Progressive MS. PLoS One. 2015;10(6):e0122686.

181. Polman CH, Reingold SC, Banwell B, Clanet M, Cohen JA, Filippi M, et al. Diagnostic criteria for multiple sclerosis: 2010 revisions to the McDonald criteria. Ann Neurol. 2011;69(2):292-302.

182. Exome Aggregation Consortium (ExAC), Cambridge, MA 2015 [Available from: (URL: http://exac.broadinstitute.org).

183. Zhu G, Koszelak-Rosenblum M, Connelly SM, Dumont ME, Malkowski MG. The Crystal Structure of an Integral Membrane Fatty Acid alpha-Hydroxylase. J Biol Chem. 2015;290(50):29820-33.

184. Zhao J, Jitkaew S, Cai Z, Choksi S, Li Q, Luo J, et al. Mixed lineage kinase domain-like is a key receptor interacting protein 3 downstream component of TNF-induced necrosis. Proc Natl Acad Sci U S A. 2012;109(14):5322-7.

185. Yoon S, Bogdanov K, Kovalenko A, Wallach D. Necroptosis is preceded by nuclear translocation of the signaling proteins that induce it. Cell Death Differ. 2015.

186. Parkinson N, Ince PG, Smith MO, Highley R, Skibinski G, Andersen PM, et al. ALS phenotypes with mutations in CHMP2B (charged multivesicular body protein 2B). Neurology. 2006;67(6):1074-7.

187. Li HF, Wu ZY. Genotype-phenotype correlations of amyotrophic lateral sclerosis. Transl Neurodegener. 2016;5:3.

188. Coornaert I, Hofmans S, Devisscher L, Augustyns K, Van Der Veken P, De Meyer GRY, et al. Novel drug discovery strategies for atherosclerosis that target necrosis and necroptosis. Expert Opin Drug Discov. 2018:1-12.

189. Ma B, Marcotte D, Paramasivam M, Michelsen K, Wang T, Bertolotti-Ciarlet A, et al. ATP-Competitive MLKL Binders Have No Functional Impact on Necroptosis. PLoS One. 2016;11(11):e0165983.

190. Yan B, Liu L, Huang S, Ren Y, Wang H, Yao Z, et al. Discovery of a new class of highly potent necroptosis inhibitors targeting the mixed lineage kinase domain-like protein. Chem Commun (Camb). 2017;53(26):3637-40.

191. Zerbino DR, Achuthan P, Akanni W, Amode MR, Barrell D, Bhai J, et al. Ensembl 2018. Nucleic Acids Res. 2018;46(D1):D754-D61.

192. Ch'en IL, Tsau JS, Molkentin JD, Komatsu M, Hedrick SM. Mechanisms of necroptosis in T cells. J Exp Med. 2011;208(4):633-41.

193. Thapa RJ, Basagoudanavar SH, Nogusa S, Irrinki K, Mallilankaraman K, Slifker MJ, et al. NF-kappaB protects cells from gamma interferon-induced RIP1-dependent necroptosis. Mol Cell Biol. 2011;31(14):2934-46.

194. Thapa RJ, Nogusa S, Chen P, Maki JL, Lerro A, Andrake M, et al. Interferon-induced RIP1/RIP3-mediated necrosis requires PKR and is licensed by FADD and caspases. Proc Natl Acad Sci U S A. 2013;110(33):E3109-18.

195. Nogusa S, Thapa RJ, Dillon CP, Liedmann S, Oguin TH, 3rd, Ingram JP, et al. RIPK3 Activates Parallel Pathways of MLKL-Driven Necroptosis and FADD-Mediated Apoptosis to Protect against Influenza A Virus. Cell host & microbe. 2016;20(1):13-24.

196. Orozco S, Oberst A. RIPK3 in cell death and inflammation: the good, the bad, and the ugly. Immunol Rev. 2017;277(1):102-12.

197. Baker M, Mackenzie IR, Pickering-Brown SM, Gass J, Rademakers R, Lindholm C, et al. Mutations in progranulin cause tau-negative frontotemporal dementia linked to chromosome 17. Nature. 2006;442(7105):916-9.

198. Lykke-Andersen S, Jensen TH. Nonsense-mediated mRNA decay: an intricate machinery that shapes transcriptomes. Nat Rev Mol Cell Biol. 2015;16(11):665-77.

199. Martin L, Grigoryan A, Wang D, Wang J, Breda L, Rivella S, et al. Identification and characterization of small molecules that inhibit nonsense-mediated RNA decay and suppress nonsense p53 mutations. Cancer Res. 2014;74(11):3104-13.

200. Zama K, Hayashi Y, Ito S, Hirabayashi Y, Inoue T, Ohno K, et al. Simultaneous quantification of glucosylceramide and galactosylceramide by normal-phase HPLC using O-phtalaldehyde derivatives prepared with sphingolipid ceramide N-deacylase. Glycobiology. 2009;19(7):767-75.

201. Choi Y, Sims GE, Murphy S, Miller JR, Chan AP. Predicting the functional effect of amino acid substitutions and indels. PLoS One. 2012;7(10):e46688.

202. Kelly BT, McCoy AJ, Spate K, Miller SE, Evans PR, Honing S, et al. A structural explanation for the binding of endocytic dileucine motifs by the AP2 complex. Nature. 2008;456(7224):976-79.

203. Jia X, Weber E, Tokarev A, Lewinski M, Rizk M, Suarez M, et al. Structural basis of HIV-1 Vpu-mediated BST2 antagonism via hijacking of the clathrin adaptor protein complex 1. Elife. 2014;3:e02362.

204. Vielhaber G, Pfeiffer S, Brade L, Lindner B, Goldmann T, Vollmer E, et al. Localization of ceramide and glucosylceramide in human epidermis by immunogold electron microscopy. J Invest Dermatol. 2001;117(5):1126-36.

205. Mencarelli C, Martinez-Martinez P. Ceramide function in the brain: when a slight tilt is enough. Cell Mol Life Sci. 2013;70(2):181-203.

206. Obeid LM, Linardic CM, Karolak LA, Hannun YA. Programmed cell death induced by ceramide. Science. 1993;259(5102):1769-71.

207. Gorman MP, Golomb MR, Walsh LE, Hobson GM, Garbern JY, Kinkel RP, et al. Steroid-responsive neurologic relapses in a child with a proteolipid protein-1 mutation. Neurology. 2007;68(16):1305-7.

208. Yang Y, Muzny DM, Reid JG, Bainbridge MN, Willis A, Ward PA, et al. Clinical whole-exome sequencing for the diagnosis of mendelian disorders. N Engl J Med. 2013;369(16):1502-11.

209. Sawyer SL, Hartley T, Dyment DA, Beaulieu CL, Schwartzentruber J, Smith A, et al. Utility of whole-exome sequencing for those near the end of the diagnostic odyssey: time to address gaps in care. Clin Genet. 2016;89(3):275-84.

210. Schwarze K, Buchanan J, Taylor JC, Wordsworth S. Are whole-exome and whole-genome sequencing approaches cost-effective? A systematic review of the literature. Genet Med. 2018;00:1-9.

211. Gibson G. Rare and common variants: twenty arguments. Nat Rev Genet. 2012;13(2):135-45.

212. Henson PM, Hume DA. Apoptotic cell removal in development and tissue homeostasis. Trends Immunol. 2006;27(5):244-50.

213. Green DR, Oguin TH, Martinez J. The clearance of dying cells: table for two. Cell Death Differ. 2016;23(6):915-26.

214. Munoz LE, Lauber K, Schiller M, Manfredi AA, Herrmann M. The role of defective clearance of apoptotic cells in systemic autoimmunity. Nat Rev Rheumatol. 2010;6(5):280-9.

215. Sokolowski JD, Mandell JW. Phagocytic clearance in neurodegeneration. Am J Pathol. 2011;178(4):1416-28.

216. Boddaert J, Kinugawa K, Lambert JC, Boukhtouche F, Zoll J, Merval R, et al. Evidence of a role for lactadherin in Alzheimer's disease. Am J Pathol. 2007;170(3):921-9.

217. Baumann I, Kolowos W, Voll RE, Manger B, Gaipl U, Neuhuber WL, et al. Impaired uptake of apoptotic cells into tingible body macrophages in germinal centers of patients with systemic lupus erythematosus. Arthritis Rheum. 2002;46(1):191-201.

218. Chen YF, Kao CH, Chen YT, Wang CH, Wu CY, Tsai CY, et al. Cisd2 deficiency drives premature aging and causes mitochondria-mediated defects in mice. Genes Dev. 2009;23(10):1183-94.

219. Zhang Y, Schmid B, Nikolaisen NK, Rasmussen MA, Aldana BI, Agger M, et al. Patient iPSC-Derived Neurons for Disease Modeling of Frontotemporal Dementia with Mutation in CHMP2B. Stem Cell Reports. 2017;8(3):648-58.